LIFE CYCLE ASSESSMENT AND OPTIMIZATION OF CARBON DIOXIDE MITIGATION AND REMOVAL TECHNOLOGIES

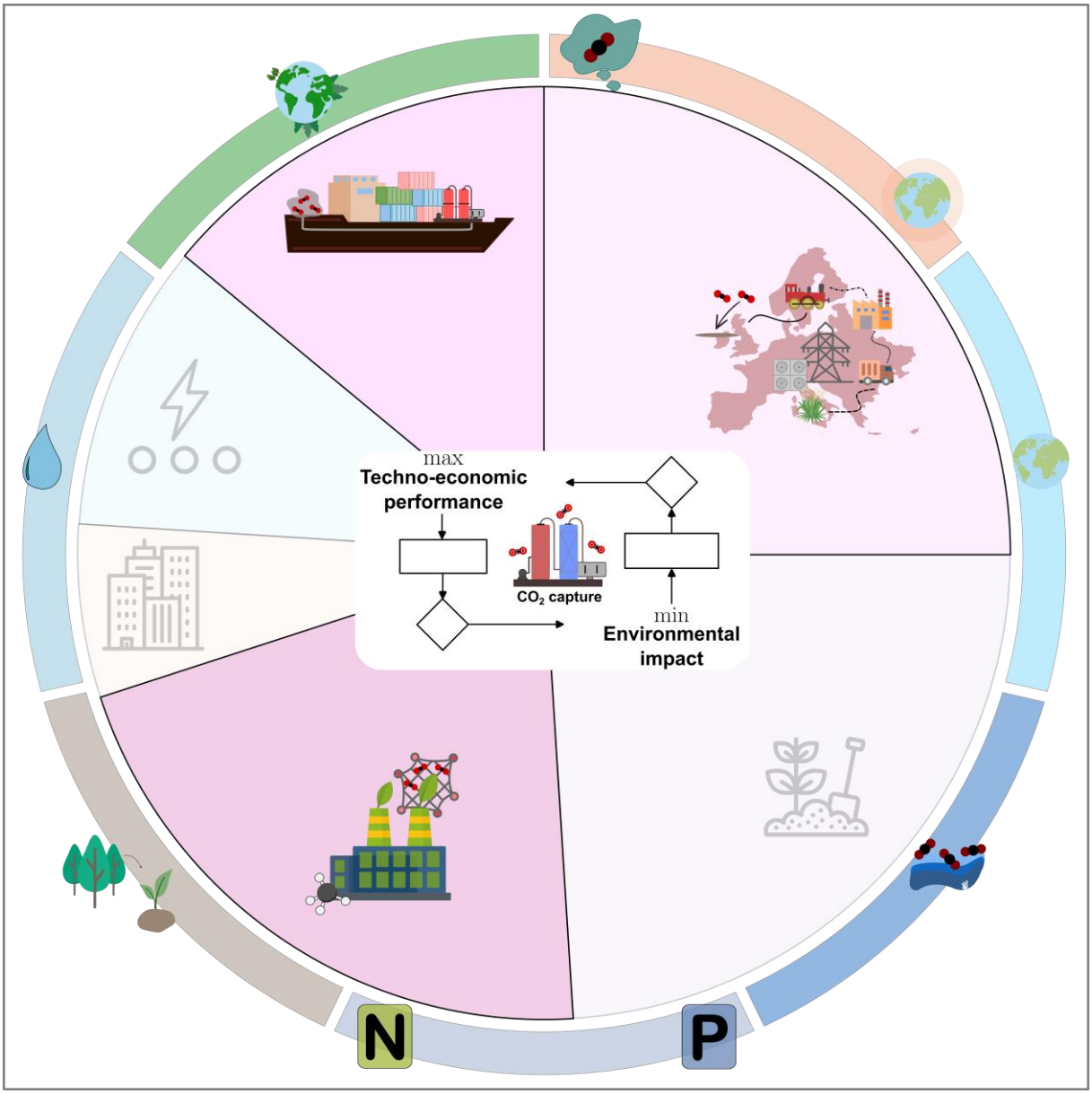

Valentina Negri

DISS. ETH NO. 29582

2023

DISS. ETH NO. 29582

LIFE CYCLE ASSESSMENT AND OPTIMIZATION OF CARBON DIOXIDE MITIGATION AND REMOVAL TECHNOLOGIES

A thesis submitted to attain the degree of

DOCTOR OF SCIENCES of ETH ZURICH
(Dr. sc. ETH Zurich)

presented by

VALENTINA NEGRI

MSc ETH PE, ETH Zurich

born on 19.03.1995

accepted on the recommendation of

Prof. Dr. Gonzalo Guillén-Gosálbez, examiner
Prof. Dr. Ignacio E. Grossmann, co-examiner
Prof. Dr. André Bardow, co-examiner

2023

Afoot and light-hearted I take to the open road,

Healthy, free, the world before me,

The long brown path before me leading me wherever I choose.

Henceforth I ask not good-fortune, I myself am good-fortune,

Henceforth I whimper no more, postpone no more, need nothing,

Done with indoor complaints, libraries, querulous criticisms,

Strong and content I travel the open road.

W. Whitman, 1856, Song of the Open Road

Acknowledgments

This thesis only reflects a part of the amazing journey that my Ph.D. has been. Here they go all the publications, and successful findings, leaving out the struggles and fun moments that cannot be reported in a scientific journal.

First and foremost, I am very grateful to Gonzalo for making this journey possible and guiding me through it, but also for your patience, enthusiasm, wide knowledge, and encouragement during these years. Not only I learned about process modeling, optimization and environmental assessment, but also how to take advantage of critical remarks as a chance to be more open-minded and courteous, implementing improvements to my work.
I had the opportunity to participate in many conferences, develop soft skills – which I discovered to be as valuable as the technical ones- and spend some time with my colleagues and new friends.
All in all, four years passed really fast, diving into carbon capture while touching upon many different areas and applying various tools. And I enjoyed them a lot.

I am also very grateful for the opportunity to visit Carnegie Mellon University. And there, to Prof. Ignacio Grossmann for welcoming me into his group. I really enjoyed our collaboration and was inspired by you as a researcher and person.
My time in Pittsburgh has also been a really good occasion to explore another little bit of North America, discover a good friendship from house-sharing, and bond with many brilliant and fun colleagues overseas.

I want to thank my collaborators as well for the interesting and enriching projects we worked on together. I have learned a lot from your suggestions and expert comments. These experiences reminded me how much I like interacting with different backgrounds and personalities.
I also want to thank my students for teaching me more than what I think I taught them. It was an incredible experience to be able to collaborate with Sebastian, Matteo, Valentin, and all the students from the lectures.

Additionally, my Ph.D. would not have been the same great experience without the support of the SuperLabers, among whom I found really good friends. I have many nice memories with you in Boston, Japan, Korea, London, and Phoenix. I was also lucky to be among the pioneers

of the group, helping shape it and seeing it grow. During these years, I realized the enormous potential that this group has, and I can only wish my colleagues all the best. I hope to keep in touch with you.

Certainly, I was not alone during this journey. Many people accompanied me all along. Do not take it personally if your name does not appear in this section. I only have a limited space to express my gratitude to all of you.
To all my friends in Zurich, in Italy, and those spread across the rest of Europe and America: I am grateful to have you in my life.

Thank you to the FAIL! team for the motivation and passion that each one of you transmits. It is exciting to be part of such an inspiring group.
To Richard. Thank you for being like a mentor to me and a really dear close friend.

Giulia, Silvia, ed Elia: voi meritate molto più di una dedica per avermi su/opportata ogni giorno e ascoltato ogni mio infinito audio messaggio riguardo quotidiane vicissitudini in questi anni. Grazie di cuore per esserci sempre.

Ai miei genitori. Grazie per il vostro sostegno ed affetto. Questo traguardo è stato possibile grazie a voi.

A mio fratello Alessandro, da cui continuo sempre ad imparare per migliorarmi.

A David. No podría estar más feliz de cruzar esta meta a tu lado y más sabiendo que ahora se nos abren muchos nuevos caminos.

Valentina Negri
Zurich, Switzerland
October 2023

Abstract

In response to the pressing challenge of climate change, this doctoral thesis explores diverse strategies in Sustainable Process Systems Engineering to advance carbon capture and removal technologies. With the aim of curbing greenhouse gas emissions and eventually reaching net negative emissions, this thesis consists of six interconnected research studies that tackle CO_2 emissions of the most contributing economic sectors, namely transportation, industrial processes, and heating in particular, and power. The works span different temporal and spatial scales, all together contributing practical tools and valuable insights into the technical, economic and environmental aspects of carbon capture, complemented by machine learning and process optimization.

This thesis starts with an analysis focused on the conventional absorption-based carbon capture technology aimed at simplifying its modeling. Traditional models involving complex systems with carbon capture processes based on first principles can be computationally costly and challenging to use, particularly when the user faces convergence issues. To overcome these limitations, we propose an innovative approach using symbolic regression. We derive simple, interpretable correlations by applying this technique to rigorous process simulations. These analytical expressions streamline the process modeling task and enhance the accessibility of process models for experimental researchers. By employing synthetic data from two CO_2 capture processes, we successfully identify accurate and simplified equations for key variables dictating the process's economic and environmental performance. These models can then be used to study the relation between independent and dependent process variables or benchmark innovative technologies without relying on process simulators.

Moving to the application of carbon capture to the transportation sector and recognizing the increasing concern about maritime emissions, we assess how a conventional chemical absorption-based CO_2 capture plant retrofitted on-board cargo vessels can reduce the freight shipping industry’s direct emissions. A comprehensive assessment of its technical and economic feasibility highlights the potential of this alternative solution. Indeed, a 94% capture rate is achieved at 85 $\$_{2019}$/tonne CO_2, displacing 7% of the cargo on a mass basis. Then, we analyze the carbon footprint and perform an absolute sustainability assessment based on the planetary boundaries framework. The results show that on-board CO_2 capture significantly reduces direct emissions. In particular, it decreases the carbon footprint of the business as usual

by half, outperforming an alternative scenario that captures the same amount of CO_2 using direct air capture. Additionally, the configuration proposed does not transgress the safe operating space of any Earth's system. Therefore, this research highlights the attractiveness of on-board capture for decarbonizing cargo shipping in the short term while alternative carbon-free fuels and infrastructure are under development.

Next, we investigate the potential of carbon capture in the context of the industrial heating sector, which is also highly critical regarding climate change. Intending to provide energy security and curb greenhouse gas emissions, we explore biomethane production from five biomass feedstocks using thermal gasification followed by a CO_2 capture stage in the European Union and the United Kingdom. Rigorous process modeling demonstrates the technical feasibility and economic competitiveness of biomethane production, which meets the quality requirements for grid feed-in. Based on regional biomass availability and process efficiency, we identify the biomethane production potential in each country. A cradle-to-gate life cycle assessment analysis reveals that biomethane can remove up to 0.33 Gt CO_2 if the syngas produced during the gasification is treated in a conventional CO_2 capture plant before being converted into methane. However, burden-shifting toward other environmental categories, such as land use and freshwater ecotoxicity, occurs. Our findings suggest that an optimized blend of natural gas and biomethane should be explored to minimize environmental burden across all Earth's systems.

Then, the urgency of achieving the ambitious climate change targets by the end of the century drives us to explore the potential of combining carbon capture with bioenergy production, known as bioenergy with carbon capture and storage in the power sector. This technology is a reliable and clean energy source capable of providing negative emissions, which plays a crucial role in global carbon removal strategies. Therefore, we evaluate the implications of large-scale bioenergy with carbon capture and storage supply chains in the European Union and the United Kingdom, emphasizing the importance of cooperation among the countries to meet given carbon removal targets. Considering regional biomass availability and land use constraints, we optimize the system's total cost and three selected environmental indicators. Within the given constraints, the system is able to reach net negative carbon emissions on a cradle-to-grave basis. Additionally, the analysis highlights trade-offs between cost optimization and environmental impact minimization, providing valuable insights into the hotspots of the supply chain.

Lastly, we expand the scope of the previous research further to explore the synergies between selected carbon removal technologies and the power sector. The former include bioenergy and direct air capture with CO_2 storage, while the latter consists of dispatchable and non-dispatchable technologies. We investigate the optimal design of integrated carbon removal and power generation systems under uncertainty in electricity demand. A multi-stage stochastic programming model is proposed, and a tailored decomposition approach is developed to reduce its computational time. The latter allows us to explore various scenarios of carbon removal targets and assess the corresponding impact within a regional context in the European Union and the United Kingdom. We identify an optimal combination of technologies and bioenergy to achieve significant net CO_2 removal from the atmosphere while satisfying the energy demand. Our findings emphasize the importance of accounting for uncertainty and the consequent model complexity that needs to be tackled in planning optimal carbon removal and energy systems.

In summary, this doctoral thesis is a comprehensive contribution of valuable insights and tools into carbon capture and removal strategies for a sustainable future to decarbonize the sectors most contributing to CO_2 emissions, namely transportation and industrial processes focusing on heating and power. Through process modeling, feasibility studies and environmental assessments within regionalized analyses, this research offers insights and practical solutions, including surrogate models and optimization frameworks, in addition to a novel decomposition algorithm. The findings presented herein aim to support policymakers, researchers, and industries in the pursuit of mitigating climate change impacts and facilitating the transition toward a low-carbon economy.

Riassunto

In risposta alle sfide poste dal cambiamento climatico, la presente tesi di dottorato esplora diverse strategie nel campo dell'ingegneria di processo sostenibile per lo sviluppo di tecnologie che catturano e rimuovono l'anidride carbonica dall'atmosfera. Con lo scopo di ridurre le emissioni di gas serra e al fine di raggiungere un bilancio negativo delle emissioni, questa tesi presenta sei studi interconnessi, per contrastare le emissioni di CO_2 nei settori a maggior impatto. Ciascuno di questi si estende su una scala spazio-temporale diversa e tutti assieme forniscono strumenti e considerazioni rilevanti sotto i profili tecnici, economici e ambientali della cattura del carbonio, in aggiunta a "machine learning" e ottimizzazione.

Questa tesi si apre con un'analisi sul processo convenzionale di cattura del carbonio che si basa sull'assorbimento con lo scopo di semplificarne la modellazione. I modelli tradizionali che coinvolgono sistemi complessi di cattura del carbonio sono basati su modelli ad equazioni rigorosi che possono risultare dispendiosi sotto il profilo computazionale e in generale difficili da usare, specialmente quando sorgono problemi di convergenza. Per aggirare queste limitazioni, abbiamo proposto un approccio innovativo basato sulla regressione simbolica. Applicando questa tecnica a rigorose simulazioni di processo, sono state sviluppate semplici correlazioni che risultano facilmente interpretabili. Queste equazioni analitiche facilitano inoltre la modellazione di processo e provvedono ad un più ampio accesso ai modelli per ricercatori sperimentali. Utilizzando dati derivati da due simulazioni di processi di cattura della CO_2, sono state identificate con successo equazioni accurate e semplici per alcune delle variabili che influenzano la prestazione economica e ambientale dei processi. Questi modelli possono poi essere usati per studiare le relazioni tra variabili dipendenti e indipendenti o per paragonare tecnologie emergenti senza dover ricorrere all'aiuto di simulatori di processo.

Volendo applicare il processo di cattura del carbonio al settore del trasporto, riconosciuta la rilevanza crescente delle emissioni nel settore navale, lo studio valuta come un impianto convenzionale di cattura della CO_2 ad assorbimento, installato a bordo di navi mercantili da carico, possa ridurre le emissioni dirette nel settore del trasporto merci. Una valutazione complessiva della fattibilità tecnica e delle conseguenze economiche evidenzia il potenziale di questa soluzione alternativa. Si ottiene infatti un tasso di cattura del 94% a 85 $\$_{2019}$/tonn di CO_2, rimuovendo il 7% del carico in massa. Viene poi analizzata l'impronta di carbonio ed eseguita una valutazione della sostenibilità assoluta basata sui c.d. "planetary boundaries". I

risultati mostrano che un sistema di cattura della CO_2 a bordo riduce significativamente le emissioni dirette. In particolare, riduce della metà l'impronta di carbonio rispetto allo stato attuale, e con un risultato migliore rispetto ad uno scenario che cattura la stessa quantità di CO_2 tramite cattura diretta dall'aria. Inoltre, la configurazione proposta non viola alcun "planetary boundary". Pertanto, questo lavoro mette in evidenza un interessante sistema di cattura a bordo per la decarbonizzazione del trasporto marittimo nel breve termine, mentre sono in fase di sviluppo combustibili e infrastrutture alternativi a basse o zero emissioni di anidride carbonica.

Successivamente, si investiga il potenziale del processo di cattura del carbonio nel contesto del settore industriale, un altro settore critico per il riscaldamento globale. Con l'obiettivo di fornire una fonte sicura di energia e ridurre le emissioni di gas serra, lo studio esplora il processo di produzione di biometano da cinque risorse di biomassa utilizzando la gassificazione termica della biomassa e conseguente cattura della CO_2 nell'Unione Europea e nel Regno Unito. Per dimostrare la fattibilità tecnica e la competitività economica della produzione di biometano che soddisfa i requisiti di qualità per l'immissione diretta nei gasdotti, viene sviluppato un modello dettagliato del processo. Sulla base della disponibilità regionale della biomassa e dell'efficienza del processo, si identifica il potenziale di produzione di biometano in ciascun paese. Un'analisi di valutazione del ciclo di vita completo rivela che il biometano può rimuovere fino a 0.33 Gtonn di CO_2 se si effettua la cattura della CO_2 prima che il gas prodotto durante la gassificazione termica sia convertito in metano. Tuttavia, si verifica un peggioramento della prestazione ambientale in altre categorie ambientali, come ad esempio l'utilizzo del terreno ed ecotossicità dell'acqua. Questi risultati suggeriscono che una miscela di gas naturale e biometano deve essere utilizzata per ridurre al minimo l'impatto ambientale in tutti gli indicatori.

L'urgenza di raggiungere gli obiettivi posti per far fronte al cambiamento climatico entro la fine di questo secolo ci spinge ad esplorare il potenziale della cattura del carbonio combinata con la produzione di bioenergia, nota come bioenergia con cattura e stoccaggio del carbonio, nel settore energetico. Questa tecnologia è una fonte di energia affidabile e pulita in grado di fornire emissioni negative e svolge un ruolo cruciale nelle strategie globali di rimozione del carbonio dall'atmosfera. Qui viene valutato il potenziale della bioenergia con cattura e stoccaggio del carbonio su larga scala nell'Unione Europea e nel Regno Unito, sottolineando l'importanza della cooperazione tra i paesi per raggiungere determinati obiettivi di rimozione del carbonio dall'atmosfera. Considerando la disponibilità regionale della biomassa e i vincoli

di utilizzo del terreno, si ottimizza il costo totale del sistema e tre indicatori ambientali. Entro i limiti stabiliti, il sistema è in grado di raggiungere emissioni nette negative di carbonio su tutto il ciclo di vita. Inoltre, l'analisi evidenzia il compromesso tra ottimizzazione dei costi e minimizzazione dell'impatto ambientale, fornendo preziose informazioni sui punti critici della catena del processo.

Infine, il presente studio espande ulteriormente l'ambito della precedente ricerca per esplorare sinergie tra le tecnologie di rimozione del carbonio e il settore energetico. Il primo comprende la bioenergia e la cattura diretta dell'aria con stoccaggio di CO_2, mentre il secondo comprende tecnologie di produzione di energia elettrica sia a fonte stabile che intermittente. Viene analizzata la progettazione ottimale di sistemi integrati di rimozione del carbonio e di generazione di energia considerando incerta la domanda di elettricità in ciascun paese. Viene quindi proposto un approccio con un modello stocastico multistadio e conseguentemente sviluppato un algoritmo di decomposizione su misura per ridurre il tempo computazionale di soluzione del problema. Quest'ultimo consente di esplorare vari scenari di obiettivi di rimozione del carbonio e valutarne l'impatto in un contesto regionale nell'Unione Europea e nel Regno Unito. Identifichiamo una combinazione ottimale di tecnologie e bioenergia per ottenere una significativa rimozione netta di CO_2 dall'atmosfera soddisfando al tempo stesso la domanda energetica. I nostri risultati evidenziano l'importanza di tenere conto dell'incertezza e della conseguente complessità del modello che deve essere affrontata per ottenere sistemi di rimozione del carbonio e produzione di energia ottimali.

In sintesi, questa tesi di dottorato rappresenta un contributo completo e fornisce informazioni utili per la cattura e rimozione del carbonio per un futuro sostenibile per decarbonizzare settori che contribuiscono maggiormente alle emissioni di CO_2, cioè trasporto, processi industriali ed energia. Attraverso la modellazione dei processi e un'analisi della loro fattibilità, le valutazioni ambientali e le analisi regionali, questo lavoro offre soluzioni pratiche, modelli surrogati e di ottimizzazione, oltre a un nuovo algoritmo di decomposizione. I risultati presentati nei capitoli successivi mirano a supportare politici, ricercatori e industrie nel tentativo di mitigare gli impatti dei cambiamenti climatici e facilitare la transizione verso un'economia a basse emissioni di carbonio.

Table of Contents

List of Figures

List of Tables

Chapter 1

Introduction

1.1 Research background and state-of-the-art

The Paris Agreement, stipulated in 2015, represents a critical milestone in global efforts to combat climate change. Intending to limit the temperature increase to 1.5 degrees Celsius (°C) above pre-industrial levels, the Agreement serves as a catalyst for implementing climate action plans[1]. However, despite a plethora of technological approaches, the level of greenhouse gas emissions (GHGs) remains at a record high[2]. Furthermore, even after the COVID-19 pandemic that drastically slowed down the global economy with a consequent unprecedented decline of emissions in recent years[3], emissions are now on the rise again. This underlines the urgent need to accelerate emission reduction efforts and, at the same time, emphasizes the insufficiency of emissions reduction alone in meeting the ambitious goals outlined in the Agreement[4]. In particular, in 2019, direct emissions accounted for 59 Gt of carbon dioxide (CO2) equivalent, of which CO2 contributed 74%. Among the major economic sectors, transportation, industrial heating, and power generation accounted for more than 60% of the total CO_2[5].

In this framework, carbon capture and storage (CCS) has emerged as an effective solution for mitigating anthropogenic emissions, also at a large scale[6]. Many technologies encompassing a range of capture methods are currently available. They vary from those in the early stage of laboratory testing to commercially viable applications and are usually categorized based on their technology readiness level (TRL). Among these, chemical absorption using aqueous amine solutions has proven to be the most mature technology, having been employed for decades in the removal of CO_2 from natural gas (sweetening process[7]). Despite their effectiveness, CCS technologies require extensive infrastructures to capture, transport and store CO_2, either in countries with available storage capacity or by building a network for CO_2 transportation to exploit the overall global potential collaboratively.

Having learned from the sweetening process, carbon capture technologies have been applied to various other concentrated sources of CO_2, such as combustion, gasification and exhaust emissions. Therefore, they are particularly effective in reducing the emissions at point sources of highly carbon-intensive industrial sectors such as iron, steel, cement, and petrochemicals production[8]. However, given the high TRL of this technology, recent forecasts also indicate the potential for on-board capture systems to be implemented in the heavy-duty transportation sector, where emissions are captured while the vehicles are in motion. Membranes and adsorption systems are being explored for truck applications[9], while conventional amine-based CO_2 capture is being considered for future scenarios in the shipping industry[10]. Preliminary

technical studies have already assessed the feasibility of retrofitting this technology on board vessels[11], while the wide environmental implications have not been explored yet.

While CCS plays a crucial role in emissions reduction, there is a need for additional technologies to remove GHGs from the atmosphere. Carbon dioxide removal (CDR) has become a key approach to achieving the long-term objectives outlined in the Intergovernmental Panel on Climate Change (IPCC) Special Report on Global Warming of 1.5 °C[4]. CDR technologies shift the focus from reducing or completely avoiding emissions to lowering the atmospheric concentration of CO_2 compared to present levels. These technologies, which combine CCS with other practices, often referred to as carbon sinks, aim to achieve a net negative emissions balance[12]. The amount of CO_2 to be removed, known as CDR targets, can be determined based on optimal cost pathways[13] or equity principles[14] and can be achieved cooperatively or at a single country level, if feasible. However, it is important to emphasize that this shift in focus does not diminish the significance of other mitigation strategies: decarbonization efforts must still be accelerated[15].

Several negative emissions technologies and practices (NETPs) arise as capable of delivering CDR[16]. Among them, afforestation and reforestation (AR) and bioenergy combined with carbon capture and storage (BECCS) emerge as particularly attractive choices[17–19]. Some NETPs have been recently incorporated into the Integrated Assessment Models (IAMs), which represent the human interaction with the natural system[18] and can combine economic, environmental and societal aspects in the scenario analyses. In almost all assessments run by IAMs, the results point to BECCS as an up-and-coming pivotal technology of choice[15,20,21] to be integrated in the power system. Differently, only a few IAMs include direct air carbon capture and storage (DACCS) in the portfolio of CDR options[22]. However, the accessibility and transparency of IAM assumptions and models are often limited[23], requiring the development of additional models to explore NETPs networks in more depth to ensure meeting the climate goals sustainably.

Special focus should be placed on the European Union (EU), presently one of the biggest emitters on a global scale[24]. At the same time, based on its proven leadership in international climate legislation[25–27], its role in the future deployment and application of CDR technologies is essential. However, conflicting political and economic goals of the EU member states have hindered technological integration, contrary to initial forecasts[25,26]. Indeed, nowadays, economic feasibility still remains a significant barrier to large-scale deployment of NETPs, as

decisions are predominantly driven by economic considerations[28,29]. Nonetheless, to favor the deployment of NETPs, a comprehensive analysis should include economic and environmental indicators.

Specifically regarding BECCS and DACCS, process modeling and optimization are necessary for their rigorous technical assessment. However, studies are still scarce, even more so when considering standard life cycle assessment (LCA) and planetary boundaries (PBs) frameworks for the environmental assessment, and particularly in the context of the EU. While economic perspectives have been explored for BECCS[30–32], and a few studies have considered major environmental metrics like carbon and water footprint[33], a comprehensive analysis incorporating the full range of environmental indicators is necessary to avoid burden-shifting. This phenomenon occurs when an environmental problem, usually climate change, is mitigated by worsening another[34]. Large-scale deployment of BECCS has been shown to exceed core PBs such as freshwater use and biosphere integrity within the PBs framework[35], but the level of detail in existing models is insufficient to draw definitive conclusions or assess regional implications in the EU. On the other hand, the impact of DACCS on the PBs still remains to be exhaustively explored. While models to assess the benefits of BECCS and DACCS in single countries' energy sectors, such as the UK[36–38], are numerous, only a few studies focus on the interplay of these technologies in the context of the EU, particularly in relation to the power sector, with which they display strong links[39]. Here, uncertainties are often overlooked despite their significance. Indeed, considering variability in the energy system electricity demand and NETPs technology learning curves[33] might be decisive factors for the optimal deployment of these CDR options. Other uncertain parameters, such as land and CO_2 storage availability, might be crucial as well.

Lastly, net negative emissions can also be achieved through different biomass-based processes complemented by CCS, which can be evaluated using process simulation to identify technical challenges and energy-intensive steps. Therefore, innovative routes that replace current fossil-based fuels and energy products contributing to CO_2 removal during biomass growth have been explored. Following the recent Russia-Ukraine war, which led to disruptions in the natural gas supply[40] and consequent volatility of the natural gas market prices, the EU Members were urged to step up the transition from fossil to renewable resources. Notably, natural gas can be produced from bioresources, e.g., different types of biomass, with the same quality as the conventional fossil one, therefore contributing to decarbonization efforts. Thus, the available biomass potential should be sustainably exploited to increase the EU energy security and

mitigate climate change, leveraging already commercially available options, i.e., anaerobic digestion followed by upgrading, while gradually increasing the share of biomethane production from gasification[41].

In light of the above, this thesis contributes to advancing our understanding of CO_2 mitigation and removal by integrating CCS and NETPS into the countries' climate agenda to tackle CO_2 emissions from major contributing sectors. By conducting process modeling, optimization, and environmental assessments, we provide valuable insights into the technical feasibility, economic and environmental implications, and uncertainties associated with the standalone carbon capture technology and its role within BECCS and DACCS. Such knowledge will contribute to informed decision-making and the development of effective strategies to address climate change within the EU and beyond.

1.2 Goals and objectives of this thesis

This doctoral thesis investigates the technical, economic and environmental feasibility of CCS and its role within selected NETPs, with a particular focus on the EU[1] context in the economic sectors that contribute the most to global CO_2 emissions. Additionally, the research addresses the uncertainties associated with these systems, offering valuable insights and advancements in the field of Sustainable Process Systems Engineering regarding CCS.

We start with a rigorous evaluation of the economic and environmental drivers of the standalone carbon capture technology. In particular, we aim at providing simple tools that can be used for economic and environmental analyses by everyone, independently of process modeling expertise, which can result particularly attractive for experimental researchers. From a broader perspective, this study aims to support achieving a deeper understanding of the factors influencing the viability and sustainability of CCS projects when integrated into larger chemical processes.

Subsequently, this thesis explores the application of carbon capture technologies within complex systems to reduce the emissions from hard-to-abate point sources. Notably, at first, the focus is placed on two critical sectors: heavy-duty maritime transport and industrial heating. By integrating CCS into these systems, we seek to evaluate the associated technical and economic implications. Simultaneously, these scenarios provide CO_2 mitigation and removal, respectively.

Building upon the knowledge gained from the evaluation of carbon capture technology as a standalone solution, in this thesis, we then investigate a network of integrated technologies and practices that leverage CO_2 capture in the power system. This network includes well-established technologies such as BECCS and DACCS. These technologies are already integrated into the IAMs and hold significant potential for large-scale carbon removal. An optimization model is developed to optimize the deployment and configuration of this technology network. This model, which adheres to LCA principles, enables a comprehensive evaluation of both the cost and environmental impact of the technology network. By adopting a life cycle optimization (LCO) approach, we can identify the optimal pathway and corresponding configuration that minimize both the technology network's total cost and

[1] In this thesis we refer to the EU before Brexit; therefore, including the United Kingdom.

environmental footprint. Environmental performance assessment relies on standard LCA metrics.

Lastly, the research addresses uncertainties in the electricity demand across EU countries for the optimal deployment of NETPs within the regional power system. Given the computational challenges posed by the size of this problem, a tailored decomposition algorithm is developed to expedite its solution process without compromising solution quality, i.e., reaching the same solution as the starting problem.

In summary, this doctoral thesis provides significant contributions to the field of Sustainable Process Systems Engineering and tackles many of its future scopes[42]. By presenting a thorough evaluation of the carbon capture technology, studying its integration into specific systems, and the optimization of a technology network, this research offers tools and valuable insights for a sustainable energy transition. Additionally, it provides a comprehensive framework to understand the challenges and opportunities associated with large-scale implementation of NETPs. Finally, it aims to inform decision-makers and contribute to the development of strategies for a sustainable net negative carbon future.

This work aims to address the challenges and gaps discussed above and highlighted in Section 1.1. The overall objective is to develop tools and perform analyses to improve our understanding of the role of carbon capture in combating climate change. This overarching objective can be broken down into the following sub-objectives:

1 Develop simplified interpretable equations for key variables dictating the CO_2 capture process economic and environmental performance, which can be employed by any user to gain insights into the process without requiring process simulation expertise.

2 Evaluate the economic, technical, and environmental feasibility of an interim solution for low-carbon shipping using the state-of-the-art CO_2 capture technology, namely chemical absorption, on-board cargo ships.

3 Assess the potential of biomethane production from gasification with carbon capture and storage in the EU through a regionalized framework, considering local constraints on feedstock availability to provide energy security and combat climate change.

4 Develop a detailed model of a BECCS supply chain on a multi-regional level in the EU to perform a comprehensive environmental analysis and identify critical hotspots in the supply chain.

5 Investigate the synergies between the EU power system and selected NETPs. In particular,
   5.1 Develop a model that integrates negative emission technologies within regionalized power systems and the uncertainty in the energy demand to understand the synergies.
   5.2 Develop a tailored decomposition algorithm to reduce the computational time to solve the problem more efficiently.

1.3 Software and methods

In this thesis, various tools and analyses were integrated, as depicted in Figure 1.1, to answer the research questions posed in the previous section, bringing together process modeling and simulation, optimization, and environmental assessment.

At the process level, below the mega meter scale, process simulation plays a pivotal role, employing software packages such as Aspen Plus, Aspen HYSYS, and Aspen Absorption[43]. The selection of a particular software package depends on the specific requirements of the study. For instance, Aspen HYSYS is primarily employed for general complex systems involving distillation steps, while Aspen Absorption is utilized for the evaluation of absorptive processes. Leveraging the capabilities of these process simulators enables the accurate calculation of mass and energy balances of large and nonlinear systems. Furthermore, the utilization of Aspen Energy Analyzer facilitates rigorous heat integration by determining the full system's heat exchanger network. In scenarios where an approximate energy analysis suffices, a composite curve is generated using the Python programming language[44]. This approach assumes perfect heat integration, resulting in the minimal consumption of utilities.
Additionally, at the centimeter to meter scale, the Bayesian Machine Scientist (BMS)[45] has been employed for symbolic regression and, in particular, to identify closed-form analytical expressions that represent a set of given data accurately. The BMS determines the models from the observed data by exploring the space of possible mathematical expressions using a Markov Chain Monte Carlo Algorithm.

When moving to supply chain design, at a scale of megameters and larger, mathematical modeling and optimization are performed using the General Algebraic Modeling System (GAMS)[46]. The intrinsic advantages of GAMS lie in its simplicity and efficiency, allowing for the formulation of complex models in a concise manner. GAMS provides a versatile framework that seamlessly interfaces with optimization solvers, enabling an efficient solution to the problems at hand.

All the processes described at different spatial scales span across a large temporal scale based on the scope of each analysis. Each chapter represented in Figure 1.1 is represented on the temporal scale according to the timeline of the study. For example, in Chapter 2, we evaluate a carbon capture system on-board cargo vessels that travel for a week. Consequently, the icon is placed at the week level on the temporal scale.

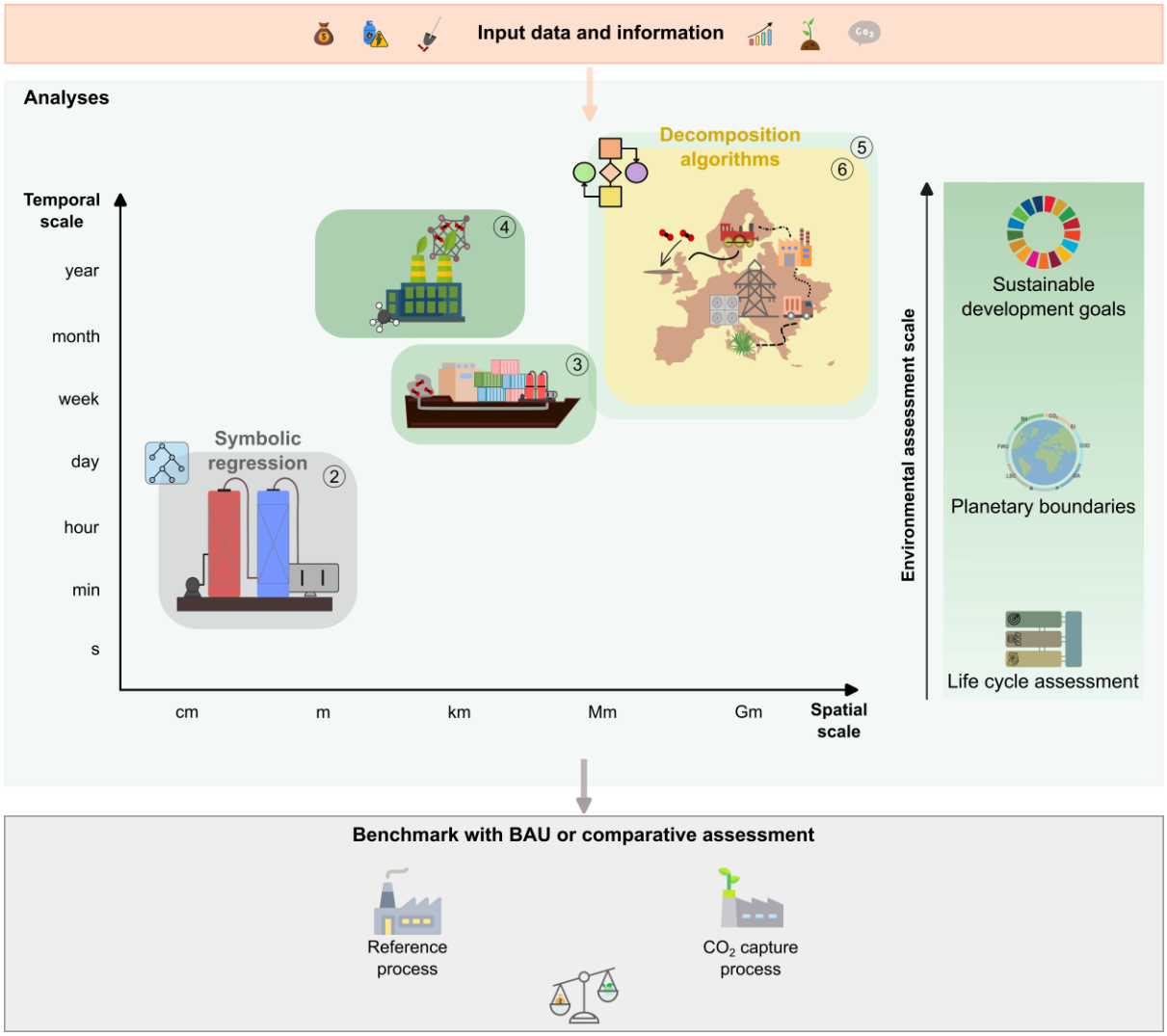

Figure 1.1: Overview of analyses and tools presented in this thesis. We first gather the input data and all necessary information for each research question, including technical, economic and environmental parameters. The studies carried out in each chapter (indicated by the circled number) span different temporal and spatial scales. Process simulation is employed to analyze processes at a spatial scale smaller than Mm, with the temporal scope of the analyses ranging from minutes to years. Chapter 2 is focused on the smallest engineering scale, where we only consider the conventional carbon capture and storage technology. Chapter 3 also involves modeling a capture process on-board cargo ships, and then the results are extrapolated for a week trip. Finally, in Chapter 4 we assess a biomethane production process, considering production targets in 2030. Mathematical modeling and optimization are used for larger scales involving the planning of supply chains and energy systems, such as those in Chapter 5 and 6. respectively. Additional tools such as symbolic regression are used in Chapter 2 to produce surrogate models, and decomposition algorithms are developed to speed up the computational time in Chapter 6. Complementing the previous analyses, environmental assessment is performed at different scales, from the conventional life cycle assessment to the planetary boundaries framework, which can be linked to the Sustainable development goals. Lastly, several alternatives can be compared with a reference process such as the business as usual scenario or among each other.

In parallel to Process Systems Engineering approaches, environmental assessment is performed. It constitutes a crucial aspect of this thesis and is carried out using two fundamental frameworks. The first framework employed is standard LCA, a widely accepted methodology for evaluating the environmental impact of products or processes throughout their entire life

cycle. The LCA adheres to the requirements and guidelines outlined in the ISO standards 14040 and 14044[47]. This methodology is well suited for comparative analyses of two products or processes with identical functional units. Initially, the SimaPro[48] interface was used for conducting LCA, followed by the adoption of Brightway2[49], a Python-based LCA platform that offers enhanced flexibility and customization. The background system takes data from the Ecoinvent database[50], while the foreground is based on our own calculations and process simulations. The selected Life Cycle Impact Assessment (LCIA) methods comprise Recipe 2016[51] and the Environmental Footprint (EF) method[52]. Recipe 2016 includes a comprehensive set of indicators at mid-point and end-point levels, whereas the EF method focuses solely on mid-points.

In addition to LCA, the PBs framework is employed to conduct absolute environmental assessments. This framework outlines global ecological thresholds that must not be surpassed[53,54], serving as a robust reference for evaluating the environmental sustainability of processes or systems. Lastly, a recent publication[55] that links nine PBs to five Sustainable Development Goals[56] based on the EF method and updated LANCA[57] method offers the broadest framework for environmental analyses.

Complementing the previous tools, Python is employed for comprehensive data analysis and symbolic regression, exploiting its extensive libraries and robust analytical capabilities.

The application of these integrated tools extends to a wide array of challenging problems addressed in this thesis, ranging from carbon capture and storage to the heavy-duty transportation sector. This research aims to provide solid insights and innovative solutions to address engineering and environmental concerns through the synergistic use of process modeling, simulation, optimization, and environmental assessment.

1.4 Thesis Outline

The previous sections provided a general introduction of the background, research questions and methods. An exhaustive literature review and a detailed explanation of the methods employed are found in each chapter of this thesis, summarized below.

Chapter 2: Bayesian symbolic learning to build analytical correlations from rigorous process simulations: Application to CO_2 capture technologies

Process modeling has become a fundamental tool to guide experimental work. Unfortunately, process models based on first principles can be expensive to develop and evaluate, and hard to use, particularly when convergence issues arise. This work proves that Bayesian symbolic learning can be applied to derive simple closed-form expressions from rigorous process simulations, streamlining the process modeling task and making process models more accessible to experimental groups. Compared to conventional surrogate models, our approach provides analytical expressions that are easier to communicate and manipulate algebraically to get insights into the process. We apply this method to synthetic data obtained from two basic CO_2 capture processes simulated in Aspen HYSYS, identifying accurate simplified interpretable equations for key variables dictating the process economic and environmental performance. We then use these expressions to analyze the process variables' elasticities and benchmark an emerging CO_2 capture process against the BAU.

Chapter 3: Navigating within the safe operating space with carbon capture on board

Despite the global pandemic affecting human and cargo transportation recently, the emissions of the maritime sector are projected to keep growing steadily. The International Maritime Organization focused on boosting the fleets' efficiency to improve their environmental performance, while more sustainable fuels are currently under investigation. Here we assess the economic, technical and environmental feasibility of an interim solution for low-carbon shipping using state-of-the-art CO_2 capture technology, namely chemical absorption, on board cargo ships. We compute the carbon footprint of this alternative and perform an absolute sustainability study based on seven planetary boundaries. Our results show that the capture on-board scenario can achieve 94 % efficiency on the net CO_2 emissions at 85 \$/tCO_2 while substantially reducing impacts on core planetary boundaries (relative to the business as usual) and outperforming a direct air capture scenario in global warming and all planetary boundaries, except nitrogen flow. Hence, capture on board seems an appealing solution to decarbonize

shipping in the short term while alternative carbon free fuels and related infrastructure are developed and deployed.

Chapter 4: Harnessing biomethane from thermal gasification with CCS for enhanced energy security and GHG emissions reduction in the EU

Given the current international landscape, natural gas supply has been gaining importance in the political and climate agenda of the European Union Members. We build a rigorous process model to produce biomethane from different biomass feedstocks using thermal gasification. We show that the process is technically feasible, with biomethane production meeting the quality required for grid feed-in, and economically competitive. A cradle-to-gate life cycle assessment shows that a significant reduction in global warming leads to burden-shifting in other environmental categories, such as land use and freshwater ecotoxicity. The analysis is carried out for the average European activities and then regionalized to provide insights regarding the biomethane production potential in each of the EU-27 countries and the UK. An analysis of the availability of biomass in the EU shows that biomethane has the potential to substitute current volatile natural gas imports while providing 0.33 Gt of net CO_2 removal on a cradle-to-gate basis.

Chapter 5: Life cycle optimization of BECCS supply chains in the European Union

Carbon dioxide removal options have been identified as key to achieving the climate change target laid out in the 2015 Paris Agreement. Bioenergy with carbon capture and storage (BECCS) is particularly attractive because it can provide negative emissions and is a reliable energy source. We explore the complexity of the infrastructures involved in realizing a large-scale system and the sequestration potential of bioenergy in Europe. Starting from a minimum cost scenario, we develop cost-optimal solutions that minimize the environmental impact of the overall BECCS supply chain according to the life cycle impact assessment methodology. Our analysis is based on cooperation among the 28 countries of the European Union (as of 2018) to achieve a global carbon removal target. Given regional biomass and marginal land availability inputs and a carbon removal target of 0.61 $GtCO_2$/year, the minimum-cost scenario provides negative emissions, with an overall cost of 140 Eur/MWh of bioelectricity generated or 117 Eur/tCO_2 removed, without considering revenues from selling the electricity produced. On the other hand, minimizing environmental impacts increased costs by 45% relative to the first scenario but improved the environmental performance by 23%.

Chapter 6: A tailored decomposition approach for optimization under uncertainty of carbon removal technologies in the EU power system

The broad portfolio of technologies delivering negative emissions calls for integrated analyses to explore the synergies between them and the power sector, with which they display strong links. These analyses, encompassing carbon removal and power generation, should be conducted at a regional level, considering system uncertainties, assessing local benefits and the impact on carbon removal potential. This study investigates how uncertainty in electricity demand affects the optimal design of integrated carbon removal and power generation systems using multistage stochastic programming. Given the model complexity, we propose a tailored decomposition approach that reduces the computational time by 90%, enabling insights into various European scenarios. We find that a combination of conventional technologies and biomass could satisfy the electricity demand with up to 9 Gt of net CO_2 removal from the atmosphere. Omitting uncertainties leads to an underestimation of the total cost and the selection of different technologies that might lead to suboptimal performance.

Chapter 7: Conclusions

Chapter 7 concludes this thesis by offering a critical assessment of the work presented, summarizing the key contributions, accomplishments, and findings, and exploring potential paths for future research.

Scientific publications produced from this dissertation and oral presentations are also listed in this chapter.

Chapter 2

Bayesian symbolic learning to build analytical correlations from rigorous process simulations: Application to CO_2 capture technologies[2]

[2] Published as V. Negri, D. Vázquez, M. Sales-Pardo, R. Guimerà and G. Guillén-Gosálbez, *Bayesian symbolic learning to build analytical correlations from rigorous process simulations: Application to CO_2 capture technologies*, ACS Omega, 2022, 7, 45, 41147–41164

2.1 Introduction

In the current emissions reduction scenario and transition toward a greener energy system, sustainable technology development has become key in every industrial sector. Nonetheless, the diffusion and application of new technologies is a lengthy process requiring multiple intermediate steps [58,59]: from the early conceptualization and planning phase to laboratory testing, pilot scale, and industrial operation. Moreover, every step requires specific experimental and modeling skills and tools in the quest for more sustainable technologies.

Standard Process Systems Engineering (PSE) tools and, more recently, also machine learning (ML) methods are being used at different stages of such technology development process to assist in the transition from laboratory to pilot or industrial scale. Notably, a critical step for scientists at the early development stage is to compare the performance of a novel technology relative to the business as usual (BAU). Information on emerging and established technologies might not always be readily available, making it necessary to generate in silico data using modeling tools to ensure meaningful comparisons. In this context, experimentalists often collaborate with modeling experts to conduct techno-economic assessments of competing technologies. These analyses might be challenging and time-consuming, particularly when process simulations need to be developed from scratch and/or lead to convergence issues. In this context, simple closed-form mathematical expressions describing the technologies' performance could simplify preliminary techno-economic and environmental assessments during the early stages of technology development, avoiding the need for complex simulations. Besides being easier to develop and use compared to rigorous simulations, such equations could also be employed for simplifying the optimization of the original processes, feasibility analysis and hybrid modeling.

Among the wide range of emerging technologies under investigation, here we focus on carbon dioxide (CO_2) capture technologies. This technology, which is expected to play a significant role in meeting the Paris agreement goals [60,61], has been the focus of intense modeling efforts. Applications of CO_2 capture technologies include flue gas treatment (e.g., pre- or post-combustion [62]), process streams purification, e.g., natural gas sweetening [63], and CO_2 removal from the atmosphere, e.g., direct air carbon capture and storage (DACCS) [64]. Among all the available options for CO_2 capture, post-combustion chemical absorption using amine-based solvents, historically developed to remove CO_2 and hydrogen sulfides from natural gas [65–67], is considered the most mature technology. Despite its high technology readiness level, chemical

absorption still leads to significant energy requirements due to the solvent regeneration step [68]. Consequently, novel solvents [69], hybrid configurations [70] and new technologies aiming at reducing energy consumption are under investigation [71,72].

Peters and co-workers carried out a techno-economic analysis to compare chemical absorption with membranes technologies for a natural gas sweetening process using Aspen HYSYS [7]. Two different inlet gases were tested, and the processes were optimized to reduce capital costs. The results showed that absorption leads to higher purity in the vented and sold gases (at the expense of higher capital costs). Other studies have also used Aspen HYSYS to optimize the CO_2 capture cost considering multiple configurations based on membranes, i.e., number of stages and recycle streams [73,74]. Hasan and co-authors [75] modeled and optimized a flue gas dehydration and CO_2 capture process based on absorption and membranes. They conclude that the CO_2 composition and gas flow rate dictate the most suitable technology. Other works modeled separations of CO_2/N_2 mixtures based on membranes to minimize the membrane area and energy consumption [76]. Hybrid configurations of membranes and cryogenic processes were also investigated, which improved the energy consumption compared to monoethanolamine (MEA) absorption for flue gas mixtures with CO_2 content by 12 to 25% [77]. The number of publications in this area (over 7000 on hybrid CO_2 capture technologies in the last decade, 16% of them about membrane-based processes [78]) highlights the scientific community's great interest in alternative, more sustainable technologies. Standalone cryogenic separation of CO_2 from flue gas [79] and hydrate-based gas separation[80] have also been studied, showing promising results in terms of energy consumption.

Traditionally, techno-economic assessments of these and other chemical technologies have been based on first-principles models. Aspen Plus, Aspen HYSYS and gPROMS are examples of simulation tools based on mass and energy balances, transfer phenomena and thermodynamic equations widespread in the modeling and optimization of chemical processes and energy systems. However, the advent of ML algorithms has opened new avenues for data-driven process modeling. Artificial neural networks (ANN), Gaussian processes and random forest, among others, are increasingly being used in process modeling [81–84], mostly to simulate complex unit operations hard to model based on first principles. For example, modeling bioreactors following complex kinetics is challenging and might be simplified using pure data-driven or hybrid models [85–88]. These approaches lead to mathematical models that often provide good approximations for time-constrained applications but are hard to interpret due to the

absence of closed analytical expressions. Additionally, the ability to extrapolate is usually minimal.

Analytical expressions can be explicitly obtained from data using symbolic regression, an application of genetic programming where the algorithm is trained to solve high-level problems combining simple functions [89]. Later, the expressions can be manipulated algebraically, differentiated, and more easily interpreted to generate valuable insights into the underlying principles governing the phenomena observed. As discussed in more detail later in this chapter, standard symbolic regression approaches rely on symbolic regression trees, i.e., superstructures of mathematical expressions, which can be coupled with optimization algorithms to find the best possible models. These representations can be optimized using either deterministic or stochastic optimizers. Deterministic methods guarantee convergence to a local solution or even to the global optimum within an epsilon tolerance[90]. In contrast, stochastic methods need to be run for an infinite time to guarantee global optimality, yet they tend to lead to lower CPU times to provide a satisfactory solution.

The pioneering ALAMO algorithm (automated learning of algebraic models for optimization) emerged in the PSE literature to address the symbolic regression problem using mixed-integer linear programming (MILP) [91]. This work was enlarged in scope to include *a priori* physical knowledge [92] and applied to a range of chemical reaction problems [93]. The main limitation of ALAMO stems from the use of a finite number of basis functions. This assumption constrains the search space drastically, eventually hindering the algorithm's ability to reproduce the data precisely. Cozad and Sahinidis overcame this shortcoming by formulating an elegant mixed-integer nonlinear programming (MINLP) model for symbolic regression that can be solved with deterministic optimization methods like the nonlinear branch and bound and outer approximation algorithms [94]. Moreover, deterministic global optimizers (e.g., BARON) can also be applied to this MINLP to compute rigorous bounds on the minimum error that could be attained in the best possible regression model in the symbolic tree [89].

To the best of our knowledge, the first studies that aimed at identifying interdependencies of process variables in CO_2 capture and storage (CCS**)** systems are from Rao et al.[95] and Zhou et al.[96] by employing response surface methodology and multiple-regression technique, respectively. Zhou and co-workers later applied ANN and neuro-fuzzy modeling to the same set of pilot plant data[97]. The predictive accuracy of the models developed by Zhou et al. using the aforementioned techniques ranges between 70 and 99%[98]. Response surface methodology

has been used later in other works to retrieve technical and techno-economical equations from CCS process simulation data[99]. Focusing on examples that employ symbolic regression, a very recent application of ALAMO to post-combustion CO_2 capture using an MEA solvent was proposed by Danaci and co-authors [100], who provided the capture costs for a range of input conditions. This work is based on an accurate model of the system and it explores a wide spectrum of operating conditions. However, the algorithm is constrained to a set of potential simple basis function forms that restrict the search significantly. The works by Pascual-González et al. [101] and Miró et al. [102] also applied mixed-integer programming (MIP) to address symbolic regression problems constrained within the limits of a reduced set of canonical expressions. In addition, the generation of tree regression models has been investigated, where the size of a tree can be controlled to balance the model's accuracy and complexity [103]. Differently, Ferreira and co-workers applied Kaizen Programming to solve symbolic regression problems, obtaining multi-output models in a single run, which were tested experimentally[104]. Recently, an MINLP for symbolic regression successfully recovered the relationship between shear stress and shear rate for both Newtonian and non-Newtonian fluids and chemical reactions kinetic laws [105]. Ansari and colleagues investigated the relationship of the variables in computational fluid dynamics simulations combining artificial intelligence and symbolic regression using sure-independence screening and sparsifying operator [106,107]. Lastly, linear sparse regression techniques, such as LASSO or elastic nets, can be deployed as an alternative to MI(N)LP formulations. ALVEN [108] is a recent approach part of the SPA framework[109] based on these methods, which was explicitly designed for modeling manufacturing data. An exhaustive literature review of ML models in chemical engineering, comparing strengths and weaknesses of the previous cited approaches, was given by Dobbelaere et al. [110] and Schweidtmann et al. [111], while a methodological review of machine learning tool interpretability is presented by Otte[112].

Moving to stochastic symbolic regression, some of us introduced a Bayesian machine scientist (BMS) [45] for symbolic regression in a recent publication. Unlike genetic programming, this approach uses a Markov chain Monte Carlo (MCMC) algorithm and a principled performance metric, the description length, to find expressions representing a good balance between accuracy and model complexity. This approach proved to be more robust than other data-driven approaches also when data is scarce and noisy [45].

Lately, the BMS has been employed to identify energy consumption and pollution drivers in an automated way in the work by Vázquez et al., outperforming the well-established STIRPAT empirical method [113]. Similarly, the relationship among emissions and economic parameters was previously assessed using symbolic regression, automatic identification, and search methods[114,115].

Here, we apply this novel ML method based on symbolic regression to simplify the modeling of a CO_2 capture process, providing explicit equations that represent the interdependencies of variables of the whole system. Most of the existing models for CO_2 capture are based on first principles, and analytical expressions to streamline the calculations and enable more straightforward comparisons are missing[99], such as in the work of Danaci et al. [100] and Subraveti et al.[116]. From a survey of the literature as reported above, many applications of ML to PSE tackle very specific problems, often focusing on single process units or academic examples. Morgan and co-workers highlighted in their recent review that most of the applications of artificial intelligence or ML applied to CO_2 capture are about predicting physical properties, such as components' miscibility and solubility[117–119], rather than process performance[120], e.g., CO_2 storage efficiency[121]. Among the few studies that analyze the latter aspect, the majority employs ANN and similar conventional ML tools[122–124]. Bearing this in mind, we here apply the BMS to two CCS processes, generating closed-form expressions that provide key economic and environmental parameters considering the entire process for a range of feed conditions. In this first attempt, our results show that the BMS can be applied to identify simple analytical expressions that reproduce the process precisely and can easily be used to facilitate comparisons and carry out further in-depth analyses. Notably, these equations can be reworked or studied analytically using the concept of elasticity, borrowed from economics, to investigate the effect of the operating conditions on the process' performance, as shown at the end of this chapter. Our simplified equations could assist experimental scientists in benchmarking emerging CO_2 capture technologies, such as membranes, cryogenic separation or adsorption [6,125], in their early development stages. From a broader perspective, this work opens up new avenues to bridge the gap between modeling and experimental communities by simplifying the adoption of modeling tools by experimental groups and streamlining the modeling calculations. Moreover, our models can be applied to solve standard PSE problems, especially in the areas of surrogate-based process optimization, feasibility analysis and hybrid modeling, exploiting their analytical structure.

This chapter is structured as follows. In the next section, we state the problem and introduce the two CCS case studies. Later, the methods employed to solve it are presented. Then, the results are analyzed and discussed for both cases. Lastly, we show two possible applications of the obtained surrogate models and discuss their use in different PSE areas before the conclusions and outlook for future works.

2.2 Problem statement

Figure 2.1 outlines the overall methodology adopted here. In essence, we are interested in generating simple analytical equations from process simulation data, which experimentalists could use to evaluate their technologies. We consider a process simulation implemented in Aspen HYSYS, which we run iteratively to generate $|K|$ scenarios for different inlet conditions. This data shall then be used to build an analytical expression reproducing the model precisely, as explained later.

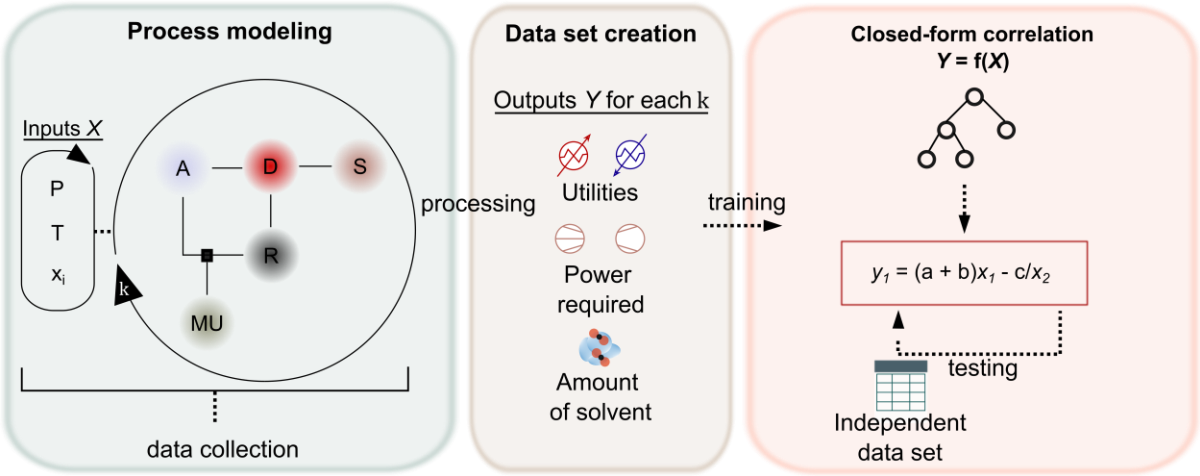

Figure 2.1: Sketch of the methodology adopted in this work. We first develop a process flowsheet, which is used to obtain data on key process variables Y linked to the economic and environmental performances from a set of inputs X (pressure (P), temperature (T), composition (xi)). Then, the data is processed to obtain a dataset used for the BMS algorithm training. Later, the equations derived from the data by the BMS are validated using an independently generated dataset. The flowsheet is here sketched in stages as absorption (A), desorption (D), CO_2 storage (S), recycle (R) and makeup (MU).

Let us consider a set of data points K, corresponding to experimental observations or generated in silico with a process model. These points are the basis for constructing the data-driven model. We classify the variables in the dataset as independent or dependent. The former refer to the degrees of freedom in the experimental setting (or process model), while the latter are obtained once the former are fixed, by either solving the process model or running the associated experiment. Let I denote the set of independent variables and J the set of dependent ones. The following notation is adopted: x_{ki} is the value of independent variable i in the

observed point k, while y_{kj} is the value of the dependent variable j in the same point. Therefore, the independent data takes the form of a matrix with dimension |K| x |I|, while the dependent data is represented by a matrix with dimension |K| x |J|.

The analysis aims to find analytical expressions of the form given in Eq. (2.1) that predict the output data (values of the dependent variables,$\tilde{y}_{kj}$) from the input data while minimizing the approximation error (e_k) and the risk of overfitting.

$$\tilde{y}_{kj} = f\left(x_{k1}, \dots, x_{ki}, \dots, x_{k|I|}\right) + e_k \quad \forall j \in J, k \in K \tag{2.1}$$

In Eq. (2.1), $f(x_{ki})$ is unknown, meaning that both the structure of the model and its parameters are to be learned from the data. Hence, three problems need to be solved simultaneously to find the best expressions. First, the features selection problem, i.e., identifying which independent variables are statistically relevant from the viewpoint of the dependent variables. The second problem is finding the model structure, i.e., identifying the best mathematical formulation to explain the data, which implies solving the previous task. Lastly, the third problem is the parameter estimation problem, i.e., finding the best model parameters for a given mathematical structure. We explain next how to solve these three problems simultaneously using the BMS.

2.3 Methods

2.3.1 Process models used for data generation

We consider the natural gas sweetening and flue gas treatment processes simulated in Aspen HYSYS V11 with the *Acid gas - chemical solvents* fluid package. The synthetic data generated is based on simulation results at steady-state. Appendix A provides more details about the assumptions and limitations of the model flowsheets.

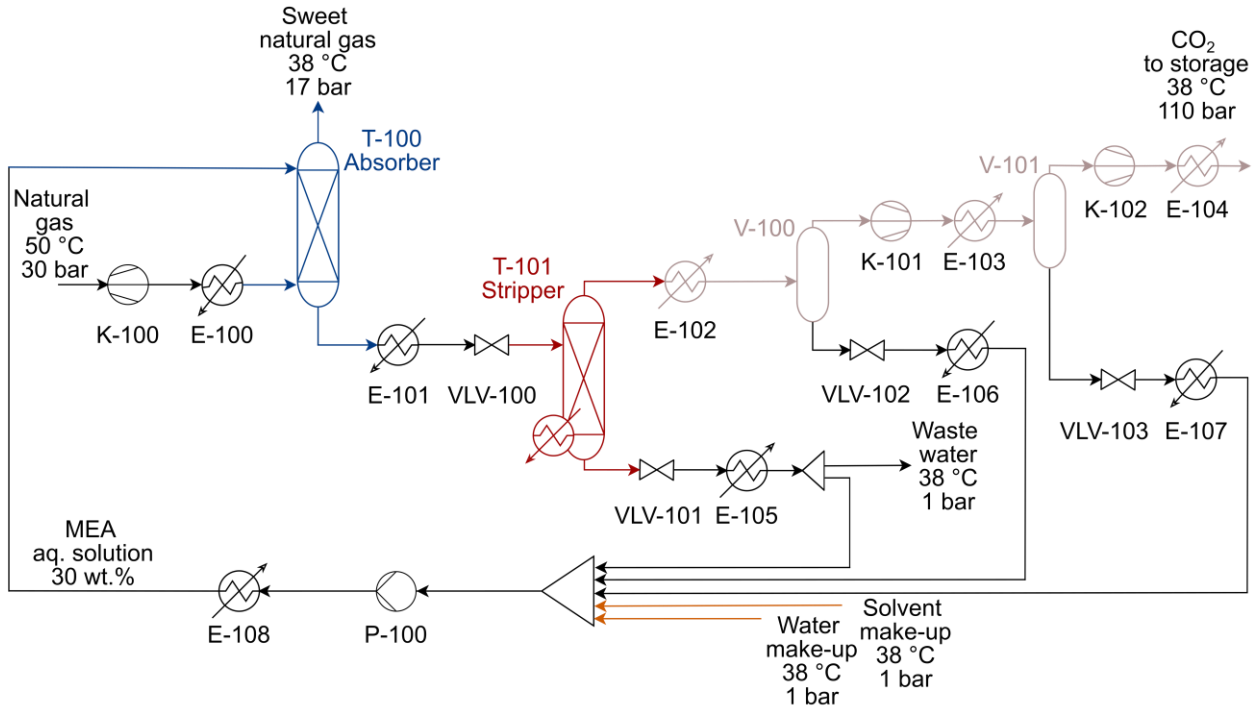

Figure 2.2: Natural gas sweetening process flow diagram**.** The process consists of an absorption stage (blue), desorption (red), CO_2 compression (sand) and recycle with solvent makeup (orange).

The first case study represented in Figure 2.2 refers to the sweetening of natural gas with CO_2 sequestration and storage. The process model considers a feed of sour natural gas, the absorption and desorption columns operating with an MEA aqueous solution, and the CO_2 compression stage. The natural gas (4986 kmol h^{-1}) is assumed a binary mixture of CH_4 and CO_2, 80% and 20% molar fraction (mol.), respectively, at 30 bar and 50°C. For simplicity, the presence of H_2S in the feed stream is neglected. We note that the flowsheet is based on published studies [7,126]. Sensitivity analyses were carried out to adjust the operating conditions for our case study, as explained in Appendix A.

The process operation is as follows. First, the natural gas pressure is decreased from 30 to 17 bar in an expander. Then, the stream is heated up to the absorber operating condition (50°C) and fed to the last stage, where the CO_2 is recovered. The sweet natural gas is obtained at the top at 99.6% mol. CH_4, meeting the standard required for pipeline injection and distribution. The CO_2-rich liquid stream is sent to the top of the stripper, where it is regenerated by CO_2 desorption with steam and subsequently recycled. The absorption and stripping columns operate at 17 and 11 bar, respectively, taking advantage of the inlet condition of the natural gas at high pressure. Indeed, in the first tower, a higher than atmospheric pressure favors the absorption of the CO_2, while in the second one, higher pressure is meant to lower the reboiler

duty, decreasing water evaporation, based on Schach et al. [127]. Both columns are designed with 12 stages and are packed with plastic material to avoid corrosion due to the CO_2-MEA mixture [128]. The stripper operates without a condenser, while the reboiler energy consumption is 5.4 MJ/kg CO_2 removed for 90% mol. CO_2 recovery. The lean load in the recycle is 0.053 mole CO_2/mole MEA. The CO_2-rich stream extracted at the top of the stripper is compressed to a supercritical state (110 bar and 38°C) for pipeline transportation and injection at a selected storage site (not considered in this work) with a purity of 99% mol. The MEA and water makeup maintain the solvent solution in the recycle at 30% wt. MEA at 38°C.

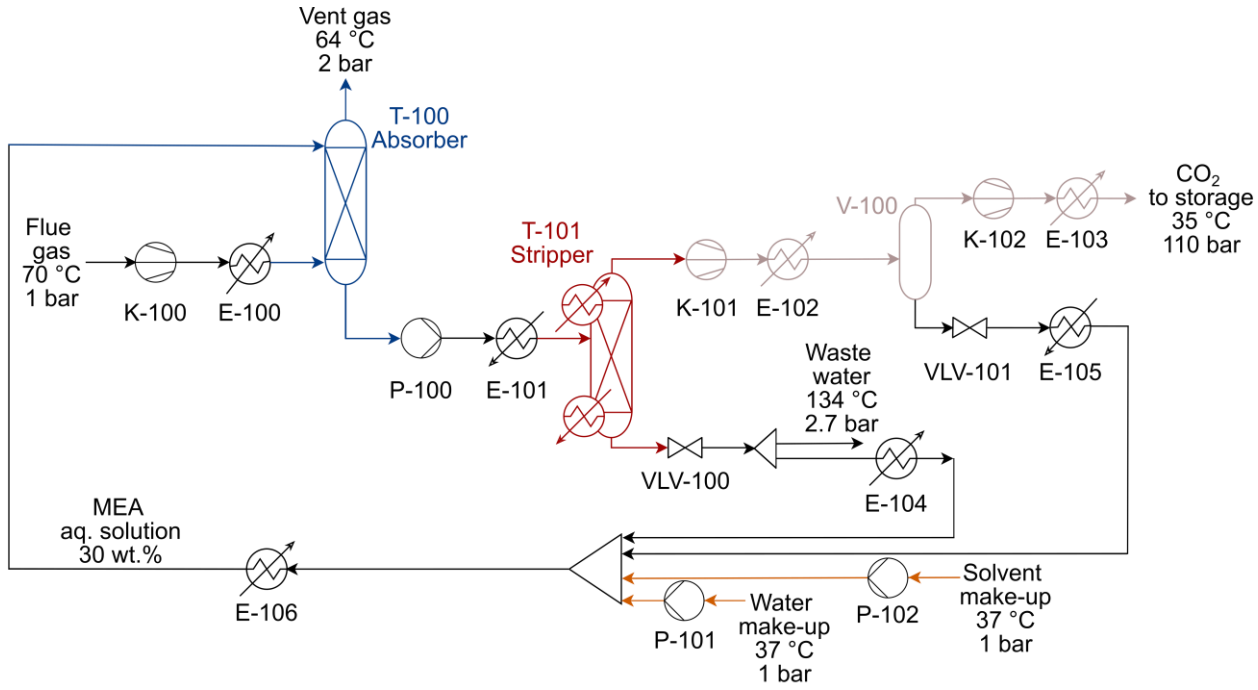

Figure 2.3: Flue gas treatment process flow diagram. The process consists of an absorption stage (blue), desorption (red), CO_2 compression (sand) and recycle with solvent makeup (yellow).

The second case study in Figure 2.3 investigates post-combustion CO_2 removal from a typical power plant flue gas. The flowsheet is based on similar studies [125,129–131] and adjusted with sensitivity analyses, described in Appendix A. The flue gas composition at the inlet can vary significantly depending on the power plant. This study focuses on flue gas in coal-fired power plants after the SO_2 scrubbing pre-treatment [132]. The process flowsheet can be divided into three main stages: absorption, desorption, and CO_2 compression.

The mixture of N_2, CO_2, O_2 and H_2O (1000 kmol h^{-1}) enters the post-combustion plant in Figure 2.3 at 1 bar and 70°C. The feed is compressed to 2 bar to overcome the column pressure drop and cooled down to 50°C. The CO_2 lean gas at the top contains 3% mol. CO_2. We highlight that an even lower CO_2 concentration can be achieved by increasing the amount of MEA and

consequently the reboiler duty, as discussed in Appendix A. The CO_2-rich solution leaving the bottom of the absorber is sent to the first stage of the stripper to separate the CO_2 using steam. The absorber and stripper columns operate under slight pressure at 2 and 5 bar to favor the absorption process and lower the reboiler duty, respectively, as done in the previous case study. The first tower has 17 stages and the second has 14. Both columns are packed with plastic material due to the corrosivity of the CO_2-MEA mixture. The energy consumption of the stripper is 2.7 MJ/kg CO_2 removed for a CO_2 loading of 0.052, in accordance with literature data [133]. The stripper operates under two design specifications: 90% mol. CO_2 recovery and 90% mol. CO_2 purity in the distillate. The CO_2-rich stream is compressed to supercritical conditions, at 110 bar and 38°C, prior to being transported and stored underground (not included in our analysis) with a purity of 99.6% mol. CO_2. The recycle stream is a 30 % wt. MEA aqueous solution at 37°C whose concentration is maintained constant with fresh water and MEA makeup.

In both case studies, we focus on predicting the cooling and heating utilities [kW], net power required [kW], and amount of MEA [kg/h] as output variables from the following input variables: feed pressure [bar], temperature [°C] and composition, and product composition. We hereafter refer to the product as the stream leaving at the top of the absorber in both examples. We note that the product composition in the absorber is a variable that depends on the amount of MEA in the recycle stream for a given inlet gas composition.

The values of the input variables to the process are obtained using Latin hypercube sampling (LHS), which returns the desired number of randomly distributed points for each independent variable in given intervals. We carry out the calculations of the absorber top product purity and amount of MEA in MATLAB. This method allows us to simplify the solution of the flowsheet reducing the number of loops to one (the recycle stream) and prevent dependencies between the variables MEA and product composition, while maintaining the number of degrees of freedom. More precisely, we define the variable MEA within an interval of interest using LHS and we run the process models to obtain a range of compositions of the absorber top product. Later, the composition is considered as an independent variable for the surrogate model.

In this regard, it is worth mentioning that, like other ML tools, the BMS has no physical knowledge about any of the two processes that are regarded as black box of which only inputs and outputs are relevant for building the simplified equations. The lack of information about physical and chemical laws that leads to poor interpretability of many black box models is a

well-known drawback of these tools and is extensively discussed in the literature[110,111], where the hybrid modeling approach is instead preferred[134]. However, here we claim that our approach, although it cannot be directly interpreted in terms of chemistry and physics first principles, offers a mathematical form that links input and output variables more intuitively than other ML algorithms previously published. Specifically, we argue that interpretability is a continuum rather than a binary feature, with simple, first-principle models at one end and very complex models with many parameters (such as state-of-the-art deep learning models) at the other end. Certainly, the models derived by the BMS are not directly relatable to first principles, but they are interpretable in many important regards. For example, they can be used directly to answer questions: How does property Y scale when property X tends to 0, or in the limit of large X? Or why are predictions of Y very large at some values of X? Or what is the derivative of Y with respect to X? In these important ways, the models proposed in this work are much closer to first-principle models than to deep learning models. Moreover, the prior used in the calculations could be modified to consider specific problem-related equations, e.g., from chemical engineering books. Lastly, we build the simplified equations from rigorous process simulations, so the model should ultimately capture the main trends dictated by the first principles.

The dependent variables we are interested in refer to the energy consumption of each process, which contributes most significantly to its economic and environmental performance. The utilities are calculated by computing the grand composite curves, assuming full heat integration (minimum utilities consumption), and that the utility requirements of the optimal heat exchanger network would approach the thermodynamic targets. The electricity consumption corresponds to the net power required to operate pumps and compressors, discounting the energy gained from the expander in the case of natural gas. The range of the sampling variables is defined based on the literature, as reported in Table 2.1. The feed composition in Table 2.1 is given for all the components but one, which is adjusted such that the sum of the components molar fractions is equal to one. Note that here we work under the strong assumption that the inlet conditions vary without any change in the design of the plant, assumed to be fixed. The assumptions and limitations of the models are reported in Appendix A.

In this work, we use a dataset for training and an independently generated set for validation. Firstly, we generated 1200 and 2500 scenarios in the natural gas and flue gas cases, respectively, out of which 1174 and 1245 converged in the simulation. More initial points were

run for the flue gas simulation to account for the increased complexity of the flowsheet, e.g., two more independent variables (two more components in the feed) and two design specifications for the stripper (CO_2 mol. purity and recovery). Out of the 2500 points, those that did not satisfy the conditions of 30% wt. MEA solution were discarded. This data was used to generate the models reported in Section 2.4. Then, the expressions were validated using additional points generated for the same ranges of input variables using LHS. The validation set includes 199 converged points for the natural gas sweetening and 195 for the flue gas treatment process, as reported in Section 2.4. We refer to Appendix A for the results of the training set.

Table 2.1. Independent and dependent variables with their respective ranges explored for the natural gas sweetening and flue gas treatment case studies. The product stream always refers to the stream leaving at the top of the absorber

	Independent variables	Lower bound	Upper bound		Dependent variables	Lower bound	Upper bound
Natural gas	x_1	Pressure [bar]	18	32	[74,126]	y_{MinCU} Minimum cooling utilities [kW]	64559.8	99100.6
	x_2	Temperature [°C]	35	50	[73,74,126]	y_{MinHU} Minimum heating utilities [kW]	63465.7	93289.2
	x_3	CO_2 mol. feed	0.2	0.3	[135]	$y_{NetPower}$ Net power required [kW]	1048.0	3267.4
	x_4	CH_4 mol. product	0.8786	0.9999	For pipeline injection CH_4 > 0.98% mol. [7,136]	$y_{AmountMEA}$ Amount of MEA [kg/h]	380000	550000
Flue gas	x_1	Pressure [bar]	1	2.8	[132,137]	y_{MinCU} Minimum cooling utilities [kW]	1737.1	4746.4
	x_2	Temperature [°C]	35	70	[129,131]	y_{MinHU} Minimum heating utilities [kW]	1168.6	4527.2
	x_3	CO_2 mol. feed	0.07	0.15	[132]	$y_{NetPower}$ Net power required [kW]	174.9	1484.1
	x_4	H_2O mol. feed	0.05	0.15	[132]	$y_{AmountMEA}$ Amount of MEA [kg/h]	12000	17000
	x_5	O_2 mol. feed	0.02	0.12	[132]			
	x_6	CO_2 mol. product	0.0228	0.1858	calculated			

2.3.2 Mathematical approach for symbolic regression

Typical symbolic regression methods combine three main ingredients: (i) a suitable representation of the problem based on symbolic trees; (ii) an appropriate objective function to drive the search; and (iii) an optimization engine to identify the best expressions. Although the BMS operates in slightly different terms (it samples models from the Bayesian posterior distribution and is not based on any MINLP formulation), it can also be cast into this scheme. The three ingredients are described in detail next.

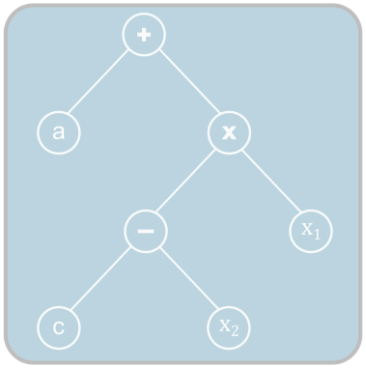

Figure 2.4: Example of a symbolic tree. The symbolic tree sketched represents the function $f(x) = a + (c - x_2)x_1$.

Closed-form mathematical expressions can be represented as trees: the internal nodes are simple mathematical operations (e.g., sum or exponential), while the leaves are variables and parameters, as represented in Figure 2.4.

Concerning the objective function, the BMS uses the description length (approximated as in Eq. (2.2) to select the best model. The description length is calculated from the Bayesian Information Criterion (BIC) reported in Eq. (2.3), which considers the number of model parameters, the sample size and the mean square error of the model (MSE, see Eq. (2.4), and the prior over expressions (*POE*). Note that the sample size is only considered for estimating the BIC of each model explored.

$$L \approx \frac{BIC}{2} - \log(POE) \tag{2.2}$$

$$BIC = p \cdot \log(|K|) + |K|[log(2\pi) + \log(MSE) + 1] \tag{2.3}$$

$$MSE = \frac{\sum_k (y_k - \tilde{y}_k)^2}{|K|} \quad (2.4)$$

In Eq. (2.3), p is the number of parameters of the learned model plus one. In Eq. (2.4), y_k is the real value observed of a generic variable i, while $\tilde{y}_k$ is the value predicted by the BMS for each point k.

Based on the symbolic tree representation above, an MCMC algorithm explores the space of all the possible mathematical expressions implementing three moves on the trees: i) node replacement, ii) root addition or removal, and iii) elementary tree replacement. Each of these moves affects the mathematical expressions differently, by introducing minor variations or significant changes in the structure, or causing the trees to shrink/grow. Alternatively, deterministic optimization methods could be used to explore the tree, e.g., by capitalizing on the MINLP formulation of Cozad and Sahinidis [89] coupled with a standard MINLP solution algorithm [94]. Finally, the BMS selects the most plausible model in an MCMC run, namely the one with the minimum description length.

The prior used in the description length calculations is the maximum entropy distribution consistent with a corpus of 4080 closed-form mathematical expressions retrieved from Wikipedia.

We apply the algorithm available in the online repository provided by the authors in a similar fashion as Žegklitz and Pošík[138] previously did to compare different ML tools, and we adjust only the number of MCMC steps. We refer to the original article [45] for further details regarding the BMS algorithm.

2.3.3. Mathematical implementation

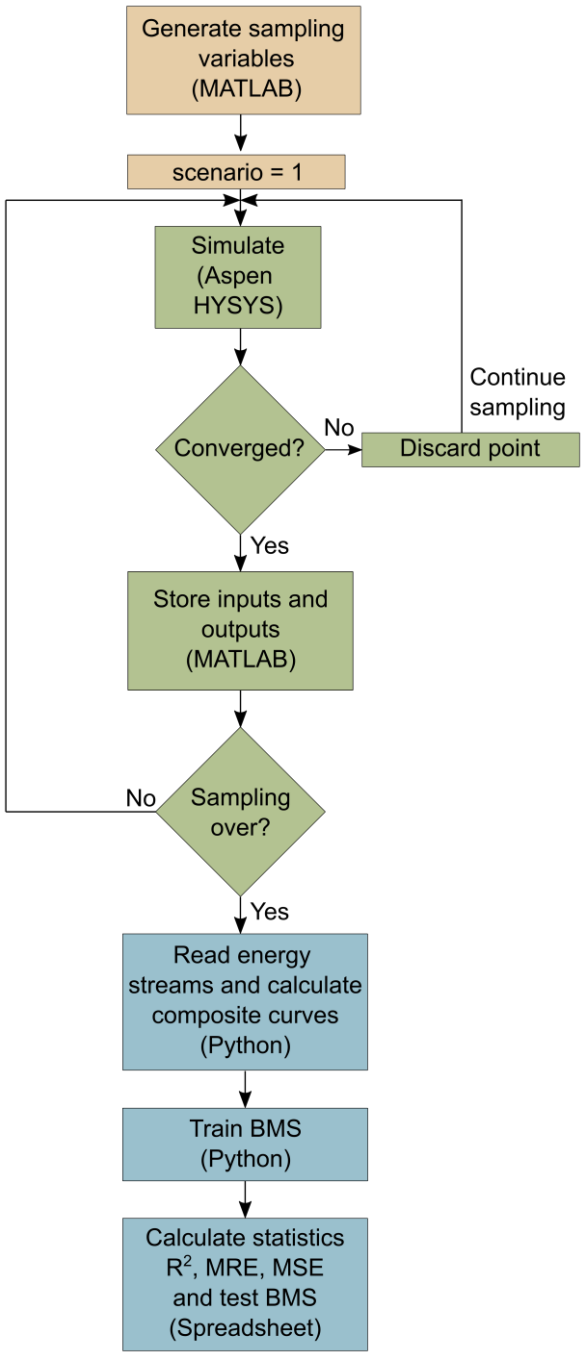

Figure 2.5: Outline of the procedure to obtain closed-form mathematical expressions. From the data sampling, through simulation and data processing, to the application of the BMS and model validation.

The inputs to the BMS include the training dataset (as small as 100 points [45]), the hyperparameters of the priors (given in [45] for a fixed number of independent variables and model parameters), and the number of MCMC steps.

The maximum number of parameters in an expression is fixed to twice the number of independent variables. This choice controls the size of the regression tree to avoid too large search spaces, which would lead to large CPU times. The number of steps has been chosen based on the coefficient of determination (R^2, described later) and description length obtained throughout the MCMC steps, reported in Appendix A. Notably, the description length tends to improve as iteration proceeds, often reaching a plateau after a sufficiently large number of steps, which is case-dependent. Here we generated the training and validation data by sampling process models. Therefore, the amount of data that can be obtained is in principle infinite, provided that the flowsheet converges. When dealing with an experimental setting, fewer points might be available as experiments are costly and time-consuming, and additional tools for the design of experiment might have to be coupled with the BMS[120,139]. To highlight the power of the BMS, we here report the results obtained at a relatively low number of MCMC steps to keep the computational time low.

The sampling was performed using MATLAB R2020a interfacing with Aspen HYSYS v11. Then, the outputs were processed in Python 3.8 using Numpy and Pandas and used to determine the values of the four dependent variables that dictate the operating costs. The BMS was trained using the Jupyter notebook code available online [45]. The algorithm returns one closed-form mathematical expression for each dependent variable of interest as a function of the independent variables and some parameters (multiple regression). Lastly, additional points were generated in the same interval of the training variables using LHS to validate the expressions. The methodology applied is summarized in Figure 2.5.

We computed some statistical metrics for each output model to assess the goodness of the model fit in both the training and validation steps. For regression models, the R^2 in Eq. (2.5) represents a measure of how well the regression predictions approximate the real data points on a convenient scale from 0% to 100%. Therefore, an R^2 of one indicates that the regression predictions fit the data perfectly.

$$R^2 = 1 - \frac{\sum_k (y_k - \tilde{y}_k)^2}{\sum_k (y_k - \bar{y})^2} \tag{2.5}$$

where y_k is the real value and $\tilde{y}_k$ the value predicted for each point k, and $\bar{y}$ is the average value.

Additionally, the mean relative error (MRE) in Eq. (2.6) measures the precision of the model. The MRE is calculated as the absolute value of the relative error between real and predicted data, normalized by the number of data points.

$$\mathrm{MRE} = \frac{abs\left(\frac{\sum_k (y_k - \tilde{y}_k)}{y_k}\right)}{|K|} \tag{2.6}$$

The elasticities can be calculated once $f(x)$ is obtained. They provide insight into the extent to which changes in the various inputs affect the process performance. Notably, elasticities quantify the proportionate change in a dependent variable y relative to a change in an independent variable x_i, keeping the other independent variables ($x_{j \neq i}$) and parameters constant. In Eq. (2.7), we report the generic formula employed to calculate the elasticity (E):

$$\mathrm{E} = \frac{\delta y}{\delta x}\,\frac{x}{y} \tag{2.7}$$

2.4. Results and discussion

2.4.1 Natural gas

We run the BMS for the data collected as described above, obtaining the closed-form mathematical expressions for the cooling (MinCU) and heating (MinHU) in Eqs. (2.8) and (2.9), respectively. The parameters (a) are available in Appendix A.

$$\mathrm{MinCU} = \left(a_0 \cdot \left(a_3 + \exp\left(a_2 \cdot \exp\left(\frac{x_4}{a_1}\right) + a_5^{x_4^{a_4}} + x_3\right)\right)\right)^{a1} \tag{2.8}$$

$$\mathrm{MinHU} = \left(\sinh\left(a_4^{x_4^{a_3}} \cdot x_4^{a_5} \cdot a_2^2\right) + a_0 \cdot \frac{x_3}{a_2 \cdot x_4}\right) \cdot a_1 + \left(\frac{a_0}{a_6 \cdot x_4}\right) + a_2 \tag{2.9}$$

As seen, the cooling and heating utilities equations only select two out of the four independent variables reported in Table 2.1: the concentration of CO_2 in the feed (x_3) and the CH_4 product purity (x_4). Notably, for a fixed input flow, these variables are strongly connected to the cooling needs in the CO_2 compression stage and heating requirements in the stripper reboiler, which represent a large percentage of the overall cooling and heating, respectively. In contrast, the

feed pressure and temperature almost do not influence the utilities consumption in the design reported in Figure 2.2, which is fixed in all the scenarios.

The net electricity consumption (Net power) is calculated as the duty required by compressors, pumps and expanders.

$$\text{Net power} = a_6 \cdot \left(a_0^{a_2 + x_3} + a_4 \cdot x_4 + x_1^{a_3} + \frac{a_6 + a_1}{a_5 + x_2}\right) \tag{2.10}$$

As expected, the expression reported in Eq. (2.10) relates Net power to all the independent variables: feed pressure (x_1) and temperature (x_2), the concentration of CO_2 (x_3) in the feed and the CH_4 product purity (x_4). The concentrations influence the duty of the CO_2 compressors and pumps for a fixed input flow, while the feed pressure and temperature determine how much power can be gained from the expansion.

Lastly, we find that the amount of solvent (Amount of MEA) required to achieve a specific product purity is proportional to the amount of CO_2 in the feed [140].

$$\begin{aligned}\text{Amount of MEA} &= a_0 \cdot a_3^{x_4} \cdot a_7 \cdot x_3 \\ &\cdot \left(\left(\frac{x_4}{a_2}\right)^{a_6}\right. \\ &+ \left.\left(a_4 \cdot x_4 + \frac{a_5 \cdot \tan\left(a_5 + x_4^{a_0}\right) \cdot (a_1 + 2 \cdot a_6 + x_4)}{x_3}\right)^2\right)\end{aligned} \tag{2.11}$$

Therefore, the amount of MEA in Eq. (2.11) is a function of the CO_2 molar fraction in the feed (x_3) and the CH_4 purity in the product (x_4). Consequently, the expression found by the BMS does not select the feed pressure and temperature.

The variable selection problem (or feature selection problem) is summarized in Table 2.2. Notably, the BMS identifies that feed pressure and temperature do not influence three out of the four dependent variables selected, while the CO_2 composition in the feed and the CH_4 product purity are included in all the expressions generated. All the closed-form mathematical expressions referring to the dependent variables in the natural gas flowsheet include fewer parameters than the maximum allowed, with the exception of the simplified equation predicting the MEA consumption. Eqs. (2.8) – (2.11) are quite compact and include elementary

operations, such as additions, multiplication, and exponentials. Trigonometric functions are also included in the case of MinHU and Amount of MEA.

Table 2.2.Summary of the features selection problem for the natural gas sweetening process. The dependent variables are listed per row, while the independent ones are reported in the columns with a one (if selected), and zero otherwise.

Independent/ dependent variables	**Feed pressure [bar]**	**Feed temperature [°C]**	**CO_2 mol. feed**	**CH_4 mol. product**
Min CU	0	0	1	1
Min HU	0	0	1	1
Net power	1	1	1	1
Amount of MEA	0	0	1	1

The data scatter around the regression line is shown in Figure 2.6 for each dependent variable (Eqs. (2.8) – (2.11)). The corresponding values of R^2, as well as MRE and MSE, are reported in Table.2.3.

The statistics indicate that the model for Net power shows the best match between observed and predicted data. This is shown in Figure 2.6 c), where the data of the validation set lies very close to the diagonal. Contrarily, MinCU shows the highest MRE and a slightly lower R^2 than the other variables, as shown by the broader distribution of the points on the diagonal in Figure 2.6 a). The scatter plots of MinHU and Amount of MEA show a predicted vs. observed data pattern between the previous two. The variable Amount of MEA is depicted in Figure 2.6 d). As seen, the data is distributed close to the regression line in the lower interval of values explored. However, it tends to scatter close to the upper bound of the variable.
It is also worth recalling that the utilities and power variables are processed data, i.e., they are not direct outputs of the simulation. Nevertheless, overall, the BMS is able to recover highly accurate models and identify the independent variables that physically influence the process, even when these have been processed.

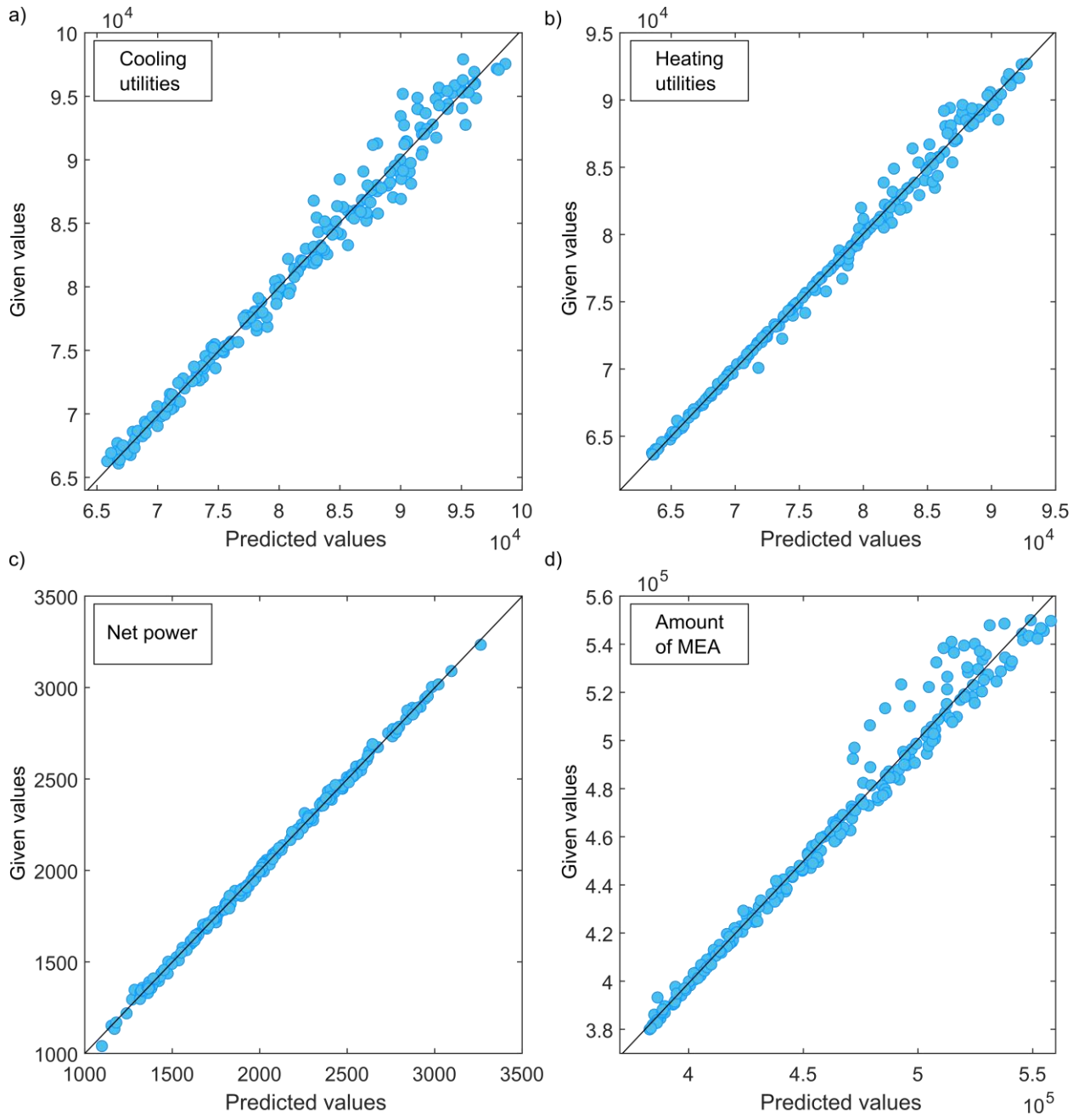

Figure 2.6: Given vs. predicted values correlation for the four output variables in the validation dataset of the natural gas sweetening process. a) cooling and b) heating utilities, c) net power and d) amount of MEA.

Table.2.3. Coefficient of determination (R^2), mean relative error (MRE) and mean square error (MSE) statistics for each output variable in the validation dataset of the natural gas sweetening process.

Case study	Variable	R^2	MRE	MSE
Natural gas	Min CU	0.9818	0.0103	1.50E+06
	Min HU	0.9921	0.0051	5.21E+05
	Net power	0.9986	0.0072	3.15E+02
	Amount of MEA	0.9922	0.0050	1.94E+07

2.4.2 Flue gas treatment

We repeat the analysis for the same outputs for the flue gas process, modifying the prior to consider six independent variables.

The minimum cooling (MinCU) utilities of the flue gas treatment process are found by the BMS to be a function of five independent variables reported in Table 2.1: feed pressure (x_1) and temperature (x_2), CO_2 (x_3) and O_2 (x_5) molar concentration in the feed, and CO_2 molar concentration in the product (x_6).

$$\mathrm{MinCU} = \left(\frac{x_3 + a_0 \cdot x_1}{x_2} + \left(a_2 + \frac{\left(x_3 + \frac{a_3 \cdot x_5 \cdot x_6}{x_5^{a_1}} \right) \cdot (a_5 + x_1)}{a_4 \cdot x_2} \right)^{a_2} \right)^4 \qquad (2.12)$$

In particular, feed pressure and temperature determine the amount of cooling necessary to reach the absorber operating conditions after the compression, while the CO_2 concentration in the feed and the remaining CO_2 in the product influence the cooling in the compression stage. The coolers in the CO_2 compression stage consume most of the total utilities reported in Eq. (2.12). For a fixed inlet flue gas stream, a change in the water concentration mainly affects the heating and the recycle streams, while the utility requirements of the cooler are negligible compared to the compression stage. Therefore, Eq. (2.12) omits water concentration (x_4). The expression obtained for MinCU is rather simple, as it only considers additions, multiplications and exponentials.

On the contrary, the total heating utility (MinHU) is a function of all six independent variables (Eq. (2.13)).

$$\begin{aligned}\text{MinHU} = \Bigg(& a_7 + x_2 + a_3 * (a_2 + x_4) \\ & \cdot \left(a_5 \cdot x_6 \cdot \exp(-x_3) + \frac{a_2 \cdot x_5 \cdot \left(a_1 \cdot (a_0 + x_2)\right)^{x_1}}{x_2} \right) \\ & + \frac{x_6 \cdot (a_4 + a_3 \cdot x_6 + a_6 \cdot x_5)}{x_3} \Bigg) / \cos(a_6 + x_5)\end{aligned} \tag{2.13}$$

The water content (x_4) in the feed stream is linked to the steam consumed by the reboiler of the stripper that regenerates the solvent. The amount of steam also depends on the CO_2 (x_3) and O_2 (x_5) feed concentration, and on the CO_2 concentration in the clean flue gas (x_6). We note that this expression is less compact than the previous ones and contains a trigonometric function. However, it can be simplified as follows. Parameter a_6 is quite large (5.6e+3), so the *cos()* function can be considered a constant that becomes zero for any value of x_5 (molar fraction between 0 and 1).

The net electricity consumption (Net power) in the flue gas treatment process accounts for the energy consumed by pumps and compressors.

$$\begin{aligned}\text{Net power} = \; & a_0 \cdot x_5 \\ & + \Bigg(a_6 \\ & + \left(x_5 + sinh\left(a_7 - x_1 \cdot cos(a_2) \cdot \left(x_6 + x_3^{cos(a_1 + x_6)} \right) \right) \right. \\ & \left. + \frac{a_3}{a_2 + x_2 + x_5 + a_4 \cdot x_2} + a_5 \cdot exp(a_7) \right)^{a_5} \Bigg)^4 / x_2^2\end{aligned} \tag{2.14}$$

In Eq. (2.14), Net power is expressed as a function of the feed pressure (x_1) and temperature (x_2), the CO_2 (x_3) and O_2 molar concentration in the feed (x_5), and the CO_2 molar concentration in the product (x_6). Like in Eq. (2.12), the concentration of water in the feed is omitted. The compressors contribute much more to the total energy consumed than the pumps, and the flow rate of the CO_2 mainly determines the compression duty.

Lastly, the closed-form expression of the amount of MEA (Amount of MEA) includes all the concentrations in the feed and the product (Eq. (2.15) because the stream composition dictates the amount of solvent needed.

$$\text{Amount of MEA} = \left(\frac{a_8 + \frac{a_8 + x_3}{a_9^{\frac{x_6}{2}}} + a_0 \cdot \left(x_5 + sin\left(a_7 \cdot x_6 + \frac{abs\left(a_1 \cdot x_3 \cdot (a_5 + x_5)\right)}{abs\left(a_5 + a_3 \cdot x_3^{a_4}\right)} \right) \right)}{a_2} \right)^{a_1} + a_6 \cdot x_4 \quad (2.15)$$

Once again, feed pressure and temperature are not linked to the amount of MEA required. The *abs()* function can be simplified because all the independent variables and parameters a_1 and a_5 are positive (see Appendix A). Conversely, a_4 is negative but $x_3^{a_4}$ is positive. Thus, the ratio of *abs()* functions can be calculated as the ratio of the arguments.

As observed, the simplified equation for the amount of MEA includes 10 parameters (out of the 12 allowed). A summary of the selection of the independent variable for each dependent one is reported in Table 2.4. At first glance, the expressions reported in Eqs. (2.12) – (2.15) seem more complex than in the previous case. However, the building blocks of the expressions are still very simple additions, multiplications, and some trigonometric and exponential functions. Although the second case considers two more independent variables and one more design specification, we can still obtain equations that fit the data with an R^2 value greater than 0.94 for three of the four variables, two above 0.99, as reported in Table 2.5. Even in the case of the minimum cooling utilities, the MRE remains below 8%. Our ultimate goal is to predict the economic and environmental performance, so estimating the cooling utilities with less accuracy is not an issue as their contribution to the overall performance is low.

Table 2.4. Summary of the features selection problem for the flue gas treatment process. The dependent variables are listed per row, while the independent ones are reported in the columns with a one (if selected), and zero otherwise.

Independent/ dependent variables	**Feed pressure [bar]**	**Feed temperature [°C]**	**CO_2 feed [mol.]**	**H_2O feed [mol.]**	**O_2 feed [mol.]**	**CO_2 product [mol.]**
Min CU	1	1	1	0	1	1
Min HU	1	1	1	1	1	1
Net power	1	1	1	0	1	1
Amount of MEA	0	0	1	1	1	1

The scatter plots in Figure 2.7 represent the goodness of fit for the four output variables in Eqs. (2.12) – (2.15) considering the data in the validation set. Once again, Net power is the variable that shows the best model performance (R^2 of 99.95%) and for which the data lies precisely on the regression line in Figure 2.7 c), while MinCU leads to the worst fit (R^2 of 45.06%) for the MCMC steps selected. The relationship between predicted and real values for MinCU shown in Figure 2.7 a) indicates that the model reproduces very well the data in the range 2500-3500, where it accumulates. However, some points are far from the regression line. We note that a low R^2 value not always implies that the model is unacceptable. If, for example, the variability of the data is low, the MRE will still probably be low (indeed, here is around 7%), and the model can still provide reliable predictions.

On the contrary, the model for MinHU improves compared to MinCU, while it still shows some data variability across the regression line. Finally, the data fit of Amount of MEA shows that the data is more aggregated along the diagonal, approaching the goodness of fit of Net power. The R^2, MRE and MSE values of the dependent variables are reported in Table 2.5.

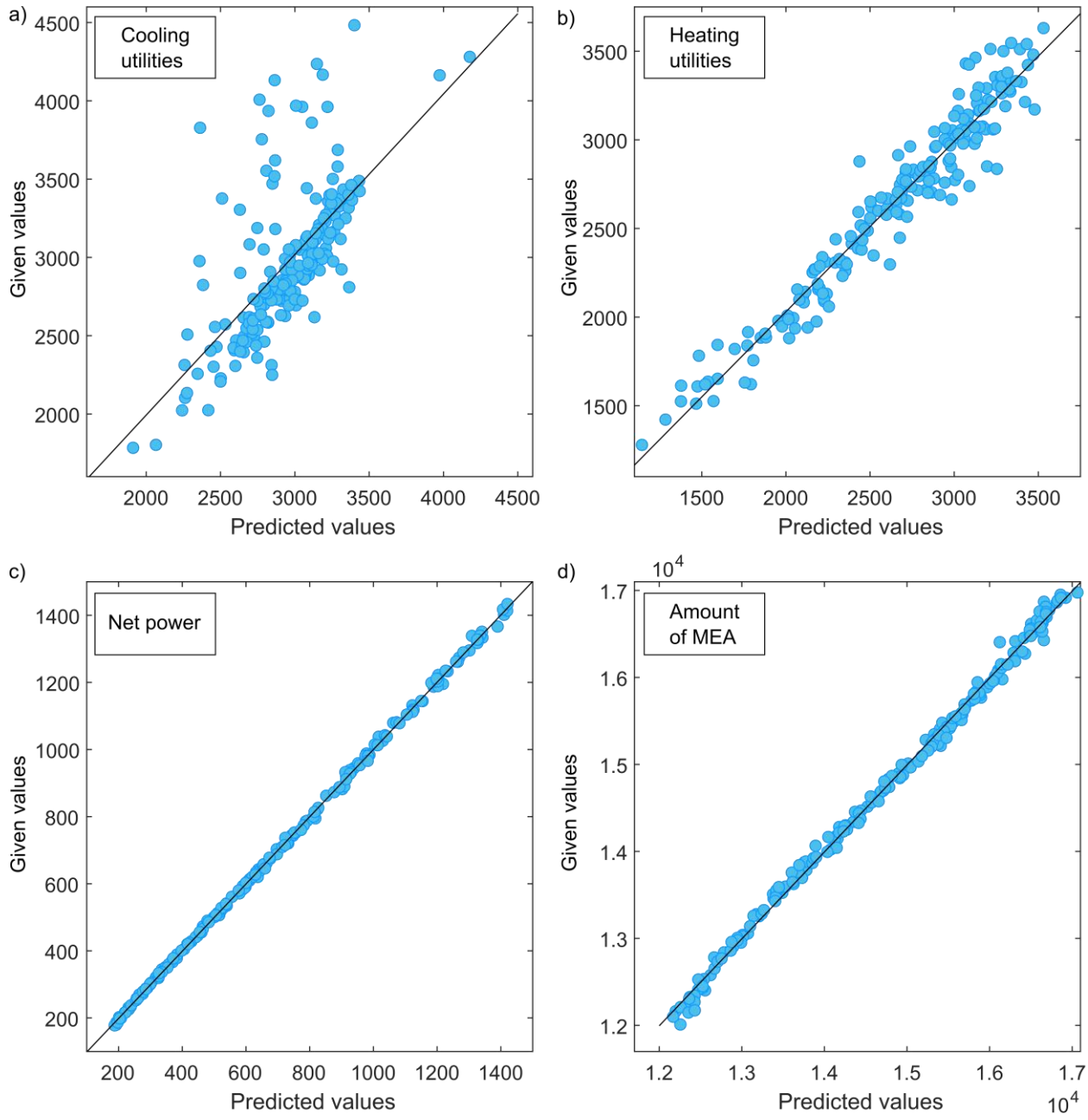

Figure 2.7: Given vs. predicted values correlation for the four output variables in the validation dataset of the flue gas treatment process. a) cooling and b) heating utilities, c) net power and d) amount of MEA.

Table 2.5. Coefficient of determination (R^2), mean relative error (MRE) and mean square error (MSE) statistics for each output variable in the validation dataset of the flue gas treatment process.

Case study	Variable	R^2	MRE	MSE
Flue gas	Min CU	0.4506	0.0744	1.22E+05
	Min HU	0.9405	0.0381	1.72E+04
	Net power	0.9995	0.0090	5.74E+01
	Amount of MEA	0.9965	0.0046	7.22E+03

The residual plots for each output variable of the two case studies can be found in Appendix A, where the training results and corresponding R^2, MRE and MSE values are also given. Additionally, the same dataset used to train the BMS was used to train an ANN with Bayesian regularization for both cases. The results are reported in Appendix A. The ANN models lead to an R^2 above 99%, both in the training and validation dataset. However, the obtained models are hardly interpretable, and hard to employ in further analyses such as those presented in the following sections.

2.5 Analytical application of the expressions

2.5.1 Analysis of the elasticities

The BMS has the advantage over other ML algorithms to provide closed-form mathematical expressions. In turn, these can be manipulated analytically, differentiated, or used in optimization frameworks to investigate the processes performance further or compare different alternatives. In this regard, we claim that our models are more interpretable than conventional black box tools and can be used to answer questions about the influence of each variable on the process as explained in Section 2.1.

In this section, we take a step forward to study the strength of the link between the independent variables selected to predict the minimum heating utilities (MinHU) and the value of this output variable. The choice of this variable is motivated by the high energy requirements of the absorption process, which can be ascribed almost entirely to the regeneration of the solvent (reboiler duty), ultimately dictating the economic and environmental performance. To carry out the calculations, we use Eq. (2.7) for each point of the training set, where y is the dependent variable chosen (MinHU) and x each independent variable y. We calculate the elasticities as described above for each x in all the points k and then plot the distribution of these values. From a practical viewpoint, the elasticities provide insight into the relationship of independent

and dependent variables. Although the analysis of the elasticities is still possible using other ML tools, the BMS allows for a more in-depth study of the change in a dependent variable as a result of an increment of an independent one. For example, it is possible to calculate the elasticity using ANN, but the result would be a numerical value and not an expression that can be manipulated further.

We provide in Figure 2.8 the histogram of the elasticities for the dependent variable MinHU in the natural gas sweetening process. Recall that the expression of this independent variable only includes two independent variables out of four: the CO_2 concentration in the feed (x_3) and the CH_4 product purity (x_4) (see Eq. (2.9). The mean of the CO_2 feed concentration elasticity is above 1 (subplot a)), representing a positive elastic relationship: for x% increase in the independent variable, the dependent variable increases by y%, where y>x, denoting a strong response in the output to changes in the input. The mean elasticity of the CH_4 product purity (subplot b)) is also positive elastic. However, the high value of the mean (620) is not representative of the majority of the points (median = 4.23). This behavior is due to the instability of the derivative, whose value skyrockets for x_4 above 0.999, which, however, does not influence the accuracy of the model itself. On the contrary, this provides an interesting insight into the physical model by implying that for purities above 0.999, which is infeasible to reach from a practical standpoint, the energy consumption required for an increment of the purity would be prohibitive.

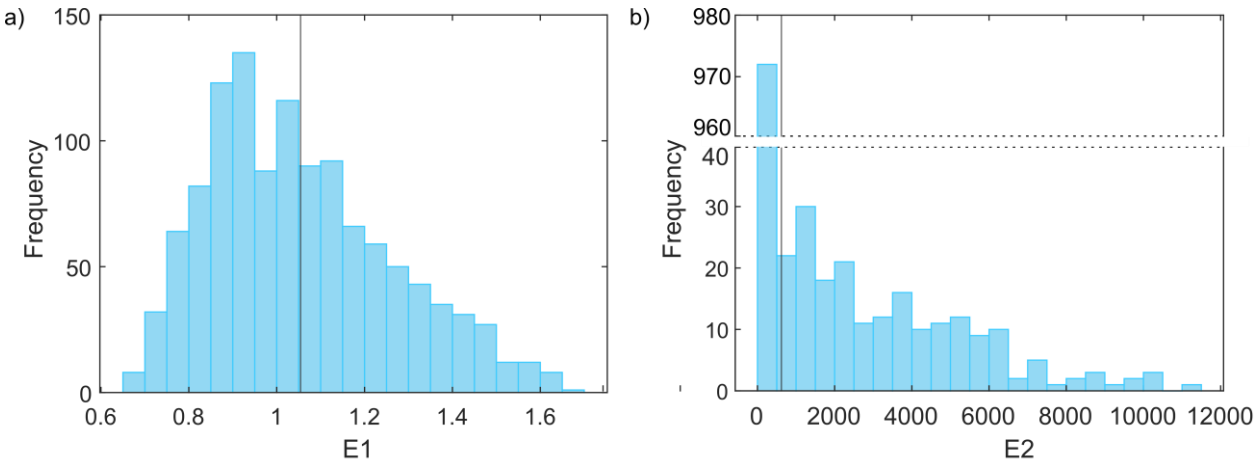

Figure 2.8: Elasticities of the natural gas dependent variables for $MinHU$ in the training dataset. a) E3 is the elasticity corresponding to the independent variable x_3 CO_2 concentration in the feed (mean = 1.0544), b) E4 to x_4 CH_4 product (mean = 620.6721).

Next, we analyze the elasticities of the minimum heating utilities of the flue gas process (Eq. (2.13). We recall that the dependent variable chosen is a function of all six independent variables whose histograms of elasticities are shown in Figure 2.9. The feed pressure (subplot

a)) shows a mean elasticity between 0 and 1, implying that the relationship is positive inelastic. An increase in the feed pressure (x_1) leads to higher heating utilities. On the contrary, the elasticity of the feed temperature (subplot b)) lies from -1 to 0, denoting a negative inelastic response. As expected, for an increase in the feed temperature (x_2), the minimum heating utilities decrease. The mean elasticity of the CO_2 feed concentration (x_3) is positive elastic (subplot c)), as its mean value is greater than 1. As said before, the reboiler duty, which is the most significant contribution to the total heating utilities, depends on the initial amount of CO_2. On the contrary, the concentration of water (subplot d)) in the feed shows a negative inelastic relationship with a mean value between 0 and -1. It is worth noting that the mean elasticity of water is -0.02, which shows that the influence of this variable is almost negligible for the dependent variable considered. We recall that water is not chosen in the simplified equation of the minimum cooling (Eq. (2.12). Increasing O_2 (subplot e)) increases, in turn, the energy consumption since the mean elasticity of x_4 is between 0 and 1 – positive inelastic. Finally, the elasticity of the CO_2 concentration (x_6) in the product stream at the top of the absorber (subplot f)) is smaller than -1, therefore indicating a negative elastic response, i.e., an increase in the CO_2 concentration of the product stream lowers the heating requirements.

Hence, the elasticities analysis clearly shows that the CO_2 concentration in the feed is the variable influencing the heating needs the most, as expected. Moreover, the effect of the water concentration is negligible, despite appearing in the simplified equation.

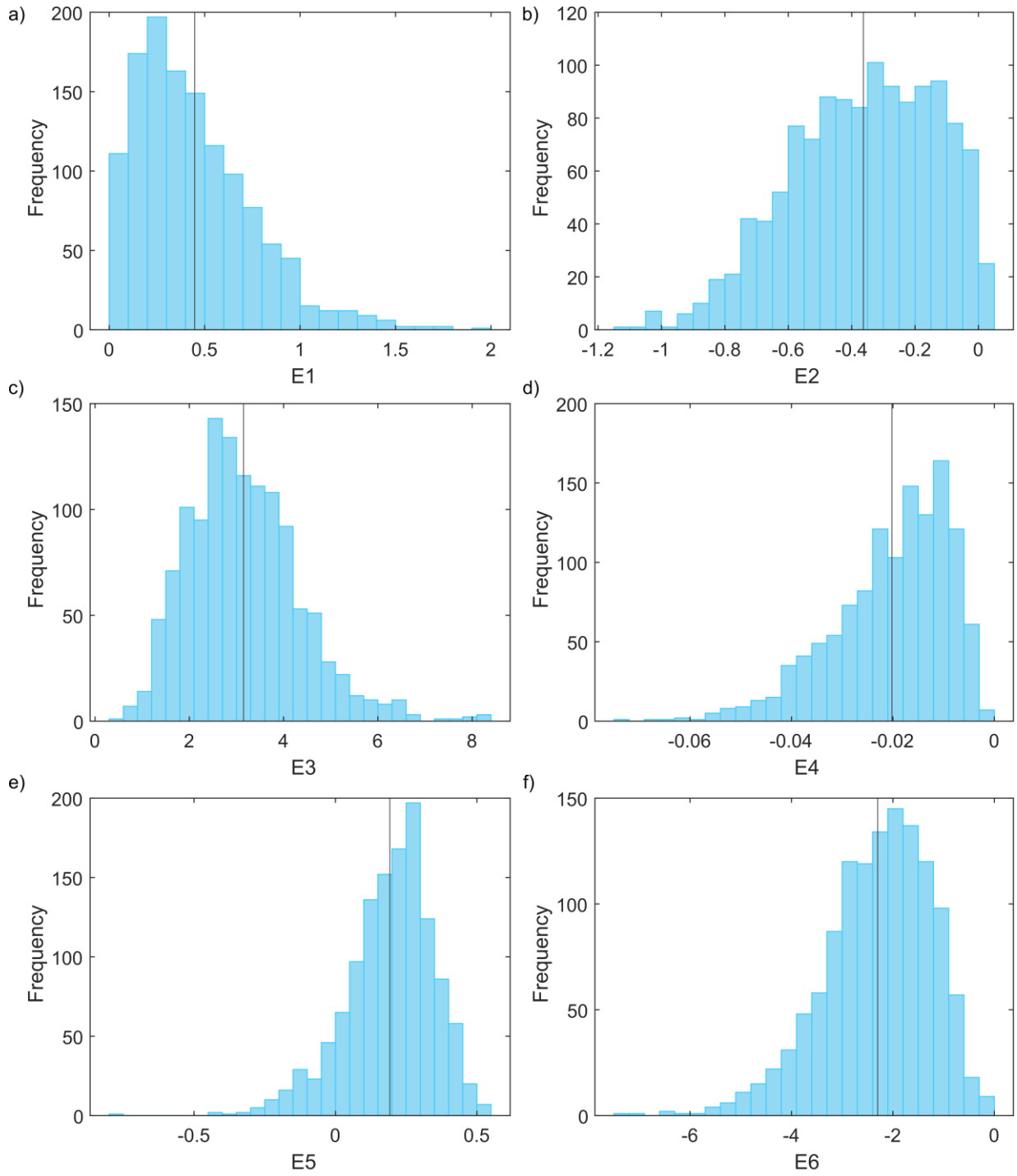

Figure 2.9: Elasticities of the flue gas dependent variables for $MinHU$ in the training dataset. a) E1 refers to the independent variable x_1 pressure (mean = 0.4475), b) E2 to x_2 temperature (mean = -0.3632), c) E3 to x_3 CO_2 mol. concentration in the feed (mean = 3.1495), d) E4 to x_4 water concentration in the feed (mean = -0.0202), e) E5 to x_5 O_2 concentration in the feed (mean = 0.1921) and f) E6 to x_6 CO_2 concentration in the product (mean = -2.3001).

2.5.2 Emerging technologies assessment

We next illustrate how the simplified equations could be used to benchmark emerging technologies. To this end, let us consider an alternative CO_2 capture technology still under development, namely the cryogenic CO_2 separation from flue gas based on the Stirling cooler system developed by Song and co-authors[79]. We shall compare the performance of the latter against that of the BAU using the expressions in Eqs. (2.8) – (2.15).

The authors provide the feed specifications and the cooling and electricity needs of the compressors, with and without heat integration. We analyze the case without heat integration for simplicity and determine the CO2 concentration (mol.) in the clean gas from the mass balance provided. The CO_2 concentration in the clean gas of the process developed by Song is 0.005 mol., which is below our lower bound 0.023 (Table 2.1) and, thus, falls outside the limits of our training set. We then calculate the minimum cooling [kW] required and the net electricity consumption [kW] using Eqs. (2.12) and (2.15) for both concentrations.

Moreover, since the input flow used by Song et al. is noticeably higher than in the case we explored here, we take the energy consumption per mass flow rate of the clean gas [kJ/kg]. In our process (Figure 2.3), the product is almost constant in all the scenarios analyzed. Nonetheless, we make predictions taking the maximum and minimum flow rate obtained from the sampling (which only differ by 13%, see Table A0.2 in Appendix A). The results are reported in Table 2.6 as the ratio between our dependent variables (subscript BAU) and the values of the Stirling process (subscript cry).

Table 2.6. Comparison of cooling and electricity requirements for the process by Song et al.[79] (*cry*) and our BAU (*BAU*). The values are calculated as the ratio of the processes' energy requirement: BAU/ cryogenic per absorber top product mass flow rate.

	Case I: without heat integration			
	$MinCU^{BAU}$/ $MinCU^{cry}$		**$Net\ power^{BAU}$ / $Net\ power^{cry}$**	
	Prod. low	Prod. high	Prod. low	Prod. high
CO_2 mol. in reference work [79] (0.5%)	2.19	1.91	1.17	1.02

Using the BMS models reported above, we conclude that the new process reduces energy consumption for the specific conditions analyzed, mainly owing to the lack of heating required. We note that our analysis here is just a simple example of an additional application of the BMS, and the conclusions we draw are based on the available data and assumptions. We point out that the extrapolation performed by using the equations for the CO_2 molar concentration outside

of the trained bounds leads to a relative error of 8.5% and 5% for the cooling and electricity ratios given in Table 2.6, respectively. We note that the simplified equation retrieved by the BMS for the cooling duty is the one affected by the poorest performance in predicting the data (R^2 of 45%).

2.6 Potential applications of the Bayesian machine scientist to process systems engineering problems

The models developed in this work aim to support experimentalists and guide their research in the quest for more sustainable technologies. For example, experimental groups could quickly benchmark their CO_2 separation technologies against standard MEA-based capture processes using simplified analytical methods without the need to carry out detailed simulations. This would allow them to identify critical hotspots in energy consumption or purity specifications. Moreover, the streamlined equations obtained with the BMS could find multiple applications in PSE, mostly in the areas of surrogate-based process optimization, flexibility analysis, and hybrid model building, as discussed next.

Surrogate-based optimization has recently emerged to overcome the challenges of simulation-based optimization, which attempts to optimize the decision variables in a detailed process simulation. In the latter, functions with an algebraic form or derivative information might be absent or too costly and noisy to evaluate[91]. Stochastic algorithms, such as genetic algorithms, can be employed in these cases, requiring numerous samplings and iterations[141]; alternatively, derivative-free algorithms can also be used[91]. Here, process flowsheet optimization is treated as a black box problem because process simulators commonly present intractable gradients[142]. In this context, the BMS could provide analytical surrogates that could be solved with state-of-the-art solvers using standard modeling systems. This would enable also the application of standard deterministic global optimization algorithms, which cannot be easily applied when dealing with ANNs and Gaussian processes (despite some recent work developed tailored deterministic global optimization algorithms for the said surrogates[143,144]).

This approach could find applications in refrigeration cycles[141], natural gas liquefaction[145], supply chain inventory system[146], carbon capture[147], process synthesis[148], pharmaceutical manufacturing industry[149], semi-batch bioprocesses[83], and biorefineries[150], to mention a few in chemical engineering design. On the other hand, the applications are not limited to technology benchmarking, as discussed below.

Our approach could also be used in the context of surrogate-based feasibility and flexibility analyses. The former addresses the question of whether a system can remain feasible within a given region of parameters values. In contrast, the latter computes the maximum deviation from the nominal conditions such that the system would still be feasible. Seminal works by Grossmann and co-workers proposed solution strategies[151] and especially a two-level optimization framework[152] to tackle these problems, which cannot be directly applied to black box problems that are not explicitly differentiable. Hence, analytical surrogates could enable the use of such algorithms based on bi-level optimization in a range of problems. Examples of applications include, but are not limited to, problems with black box constraints, computationally expensive models and non-convex feasible regions, particularly in pharmaceutical applications[153], planning, scheduling and control[154,155], or chromatography design[156].

Surrogate models can be further combined with an algebraic objective, material and energy balances to formulate algebraic optimization problems under the framework of hybrid modeling[91]. Hybrid models fill the gap linked to the lack of exact knowledge of the physical mechanisms of the process, allowing the user to specify part of the process through a data-driven model and requiring less data than pure black box models, particularly relevant in bioprocesses applications[157]. In this context, our approach could be used to build analytical hybrid models, where mechanistic equations would be combined with an analytical surrogate, leading to fully analytical formulations easier to handle. Moreover, it could also be used in tandem with deterministic global optimization algorithms for gray box models optimization, as presented by Boukouvala and Floudas[158]. Specifically, the BMS could help to approximate black box constraints, enabling the straightforward application of deterministic global optimization methods to hybrid models.

In particular, applications of ANNs coupled with black box optimization, which could benefit from analytical surrogates as those developed here, include process synthesis, flexibility analysis, and dynamic optimization, as reviewed by Tsay[159].

Overall, our approach has the advantage of providing an explicit mathematical form, which can be manipulated algebraically, differentiated, and integrated, alone or together with mechanistic equations, e.g., mass and energy balances in gray box models. Moreover, while interpretability is not a binary value, the results obtained from the BMS are more interpretable than those obtained from ANNs, or Gaussian processes.

2.7 Conclusions

In this chapter, we explored the application of machine learning to simplify the benchmarking of emerging technologies with a focus on carbon capture. We applied a Bayesian machine scientist algorithm to streamline the modeling of two basic processes for carbon dioxide removal, generating simple closed-form mathematical expressions of key variables dictating the economic and environmental performance of the whole system considered.

We found that it is possible to build highly accurate simplified process model equations in an automatic manner in relatively low computational time, which can then be used to compare alternative technologies and perform further numerical analyses. The statistics of the goodness of fit, namely the R-squared, mean relative error and mean square error, indicate that the best predictions correspond to the net power requirement, while the minimum cooling utilities are harder to predict. Nonetheless, the Bayesian machine scientist is able to find precise expressions even for those variables that are not directly an output of the simulations, such as process utilities and the net power consumption. It can also identify critical process variables that influence the dependent variables the most. Moreover, the number of steps for the Markov Chain Monte Carlo algorithm can be increased further to identify even better expressions.

An analysis of the elasticities was carried out to provide insights into how the process variables affect the technology performance. Moreover, the streamlined process equations were used to benchmark an emerging technology based on literature data with the standard amine capture process, finding that it could outperform the latter under the conditions and assumptions considered.

Overall, this study proved that advanced machine learning methods could be applied to automatically derive simplified process equations that can accurately predict the behavior of technologies in carbon capture applications and beyond. These simplified equations, in turn, can be used to analyze the influence of the independent variables on the overall performance and enable a direct comparison of emerging technologies without the need to run a process simulation in each comparative assessment sought.

This study represents a first proof of concept based on simple case studies, and future work should further explore how to control the shape and complexity of these expressions and include more specific a priori knowledge. Moreover, these simplified equations could also be applied to experimental and plant data and used for optimization purposes, i.e., in process

design, which could open new opportunities for developing machine learning-based optimization algorithms based on explicit symbolic equations.

2.A Nomenclature

Acronyms	
ALAMO	Automated learning of algebraic models for optimization
ANN	Artificial neural networks
BAU	Business as usual
BMS	Bayesian machine scientist
CCS	CO_2 capture and storage
CO_2	Carbon dioxide
DACCS	Direct air carbon capture and storage
E	Elasticity
LHS	Latin hypercube sampling
MCMC	Markov chain Monte Carlo
MEA	Monoethanolamine
MILP	Mixed-integer linear programming
MINLP	Mixed-integer nonlinear programming
MIP	Mixed-integer programming
ML	Machine learning
PSE	Process systems engineering

Sets, variables and parameters	
K	{k: set of training points}
I	{i: set of independent variables}
J	{j: set of dependent variables}
MinCU	Minimum cooling utilities [kW]
MinHU	Minimum heating utilities [kW]
Net power	Net power [kW]
Amount of MEA	Amount of MEA [kg/hr]
BIC	Bayesian Information Criterion
L	Description length
MRE	Mean relative error
MSE	Mean square error
POE	Prior over expressions

Chapter 3

Navigating within the safe operating space with carbon capture on-board[3]

[3] Published as V. Negri, M. A. Charalambous, J. D. Medrano-García, G. Guillén-Gosálbez, *Navigating within the safe operating space with carbon capture on board*, ACS Sustainable Chem. Eng. 2022, 10, 51, 17134–17142

3.1 Introduction

The reduction of the carbon intensity of rail, road, air and sea transport modes must be set as a priority to cope with the forecasted increase in the global population and consequent freight business, despite the remarkable decline of emissions resulting from the COVID-19 global pandemic[160–162]. Considering that roughly 80 % of the cargo is transported by sea, shipping is regarded as a very efficient and cost-effective way of moving goods[163]. Nonetheless, since it is still a sector almost entirely powered by fossil fuels, it contributed to roughly 3 % of global anthropogenic greenhouse gas (GHG) emissions in 2018[164].

Given the relatively low share of emissions compared to other economic sectors, decarbonization of ships was never a priority and not even explicitly mentioned in the Paris Agreement[165]. However, maritime emissions are projected to increase due to population growth, while the average lifetime of vessels is 25–40 years[166], implying that today's actions will have long-lasting effects[163]. Historically, attention has been paid to particulate matter (PM), sulfur and nitrogen oxides (SOx and NOx) emissions, which motivated the International Maritime Organization (IMO) to introduce stricter policies to limit the effects of these components[167] and increase the energy efficiency of marine activities[168–170]. Only recently, new initiatives and strategies have been proposed to tackle GHG emissions, with the European Union being at the forefront[171]. However, we are still far from reaching a scenario in line with a 50 % GHG emissions reduction target in 2050[172].

In addition to the IMO measures to increase ship efficiency, long-term sustainable solutions involve a substantial change in the current infrastructure and the manufacturing of new propulsion systems where low or zero-carbon fuels can be employed. Great interest has been expressed in liquefied natural gas (LNG), hydrogen (H_2), ammonia (NH_3) and methanol (MeOH)[167,173–175], which can be produced from sustainable biomass feedstock, solar energy or renewable electricity[10,176]. These alternative fuels, however, require compatible engines and large storage on-board, given their low volumetric energy density compared to heavy fuel oil (HFO)[177–179]. On the other hand, short-term solutions can be based on carbon dioxide (CO_2) capture, either at the source of emissions or from the atmosphere (*i.e.*, direct air capture, DAC[180]), while the new infrastructure is developed. CO_2 capture, often coupled with geological storage (CCS), is a mature technology[181] and a very efficient way of reducing direct emissions in industry and power plants[182]. Different configurations can be adopted, namely post-, oxy-, and pre-combustion, using physical or chemical adsorbents and absorbents[6]. Although carbon

capture on-board seems to represent a valid solution to tackle direct emissions in the short term and can be easily retrofitted on existing fleets, only a few studies were conducted on its technical and economic feasibility. Even more, a small number of those focused on deep-sea transportation, *e.g.*, container ships[11,183–186]. The concept was firstly proposed by Det Norske Veritas and Process Systems Enterprise in 2013 and was recently reviewed by Baroudi and co-workers[187]. In this context, the CO_2 captured from the exhaust gas must be stored on-board in liquid form until a port is reached, competing with the cargo for the available space and being potentially hazardous[188]. Therefore, for this solution, little changes in the infrastructure of the ships are required, as they only require CO_2 storage tanks on-board and extra energy for the CO_2 capture system.

The relevant studies of CO_2 capture on-board mentioned above lack an absolute sustainability assessment and a comparison with alternative CO_2 capture technologies. Specifically, one of the main shortcomings of current life cycle assessment (LCA) studies is the lack of thresholds to interpret the results globally. Recent works started to apply the planetary boundaries (PBs[54,189]), defining critical biophysical limits of the Earth, to the absolute sustainability assessment of industrial systems, including steel[190] and fuels[191] production. However, these studies are scarce and never evaluated the sustainability level of low-carbon technologies for shipping. In this work, we consider cargo carriers, which contribute to a relevant share of the maritime sector emissions (approximately 37 %[192]). We carry out the first comprehensive techno-economic and global environmental analysis of a state-of-the-art carbon capture plant on-board cargo vessels to reduce direct emissions, and we report the results for global warming (GW) and the PBs metrics. Additionally, we perform a comparative assessment with DAC and evaluate which option is most appealing in the short term compared to the business as usual scenario (BAU) until carbon-neutral fuels might eventually become competitive. Here, we consider a technical solution that can be implemented in the short term with few changes in the current fleet. Since some DAC facilities already exist, we provide the comparison with the carbon capture on-board as another valuable alternative that provides emissions reduction, although DAC technological readiness level is considerably lower. Finally, we also review and evaluate the different alternative fuels that could break into the market in the future.

3.2 Methods

3.2.1 Reference ship

We consider a reference ship that belongs to the liner shipping industry, therefore traveling fixed routes and distances[193], with the following characteristics. We assume a cargo ship of an average size of 8500 twenty-foot equivalent units (TEU)[194] powered by HFO in a conventional combustion engine. The emissions are calculated based on the rated speed of the ship[193] and the type of fuel (HFO)[195]. Here we assume that the engine was characterized and optimized at 26.5 knots, just above normal cruising speed[194]. Consequently, we consider a journey from the port of departure to the destination that lasts one week. As a reference for the reader, we report that the current route of the vessel GUDRUN MAERSK took four and half days from Tanjung Pelepas, Malaysia to Yantai port, China sailing at a speed of 18.5 knots, based on port calls data[196]. The exhaust gas composition analyzed in our case study is reported in Table B0.1 in Appendix B. We take into account CO_2, oxygen (O_2), nitrogen (N_2), water vapor, SOx and NOx, although combustion emissions can include more than 400 different compounds[187].

3.2.2 Process modeling and scenarios definition

Our study includes a detailed process modeling where we identify three necessary consecutive steps: exhaust gas cleaning, CO_2 capture and CO_2 liquefaction, which are interconnected in the energy analysis. The process is designed based on available data in the literature and further adapted to the final design of our case study by means of sensitivity analyses, as described in Appendix B. The process simulation is carried out in Aspen HYSYS v11.

The exhaust cleaning section includes the technology that is currently already on-board of ships for the reduction of SOx and NOx. This section has been included in our simulation to the best of our knowledge to perform the heat integration of the full process.

HFO is the most common and inexpensive fuel used in heavy maritime transport, and it comes with the downside of containing up to 4 % sulfur in its chemical composition[195], which leads to the production of SOx during its combustion. Additionally, due to the high temperatures achieved in the engine, NOx are also formed along with PM. To comply with current emission regulations, a cleaning system designed to remove PM, NOx and, depending on the fuel, SOx is mandatory in the current generation of ships. These pretreatment units are very similar, if not the same, as those found in standard coal power plants[197], and consist mainly of a trap for

PM, a selective catalytic reactor for NOx and a scrubber for SOx removal. In our study, we perform the pretreatment stage using the SNOX technology, which manages to remove 100 % of PM, 96 % of NOx and 94 % of SOx[198]. We refer to Figure 3.1 for the sketch of the process, while we report in Appendix B the simulation details such as temperatures of the streams and the reactions modeled.

The exhaust stream is first mixed with air that provides the O_2 necessary for the following steps. Then, the mixture enters the de-nitrification reactor (DeNOx) with NH_3, where NOx and SOx are converted into N_2 and sulfur trioxide (SO_3), respectively. Additionally, any unreacted NH_3 is also oxidized into N_2. The resulting mixture is cooled down to 200.0 °C at the temperature of the wet scrubber, and it is put into contact with water, thus forming sulfuric acid (H_2SO_4). We consider that H_2SO_4 is not stored due to safety and weight issues; hence, this process is operated in an open loop. Therefore, the H_2SO_4 stream is mixed with seawater, which alkalinity neutralizes the acid effectively[193] and is discharged into the ocean.

In our design, the scrubber installed on-board for the SOx reduction is also necessary to avoid a fast degradation of the solvent used in the CO_2 capture process[188]. We design a conventional[199] carbon capture plant that can be installed on-board by retrofitting the current ship architecture without significant changes. Compared to the commercially available alternatives, such as solid adsorbents or membranes, the advantages of this technology are the high technology readiness level and consequent know-how that leads to easy installation and high efficiency[200], at the expense of a considerable space reduction on-board due to the large scale system required. At this point, the exhaust gas that contains mainly CO_2 as impurity is first sent to a flash to separate the wastewater and then enters the absorption column on the bottom tray. An aqueous solution of monoethanolamine (MEA) 30 % wt. gets in contact with the gas from the top and it leaves at the bottom of the absorber as CO_2-rich solution. The CO_2-lean gas (CO_2 less than 1 % mol.) is vented to the atmosphere from the top. The solvent solution is circulating in a closed loop: from the absorber is sent to a second column where the CO_2 is desorbed by means of heat provided by the reboiler with a heat rate of 5.9 MJ/kg CO_2. The gaseous stream containing 90 % mol. of CO_2 leaves from the top to go to the refrigeration section. The MEA lean solution is recycled back to the absorber, with the addition of fresh solvent and water to keep it at the desired concentration due to losses in the system. The heat required by the reboiler, *i.e.*, medium pressure steam, is provided by a natural gas (NG) furnace installed on-board. The flue gas from the combustion in the furnace is mixed with the exhaust

stream from the engine and sent together to the absorber to capture the net CO_2 of the system. The CO_2-rich stream that leaves the stripper at 74.0 °C is stored on-board and transported until destination as refrigerated liquid, following common commercial practices[201]. We design a first refrigeration step that makes use of the NG required in the furnace. The amount of NG, however, is not sufficient to bring the CO_2 stream to the desired conditions. A refrigeration cycle with NH_3 adapted from the literature[202,203] is implemented in a closed loop to provide further cooling from −13.8 °C to the final temperature. The CO_2 stream is then stored in commercially available tanks at 22.0 bar and −16.6 °C[204] until the ship reaches the port where the CO_2 is unloaded and transported to suitable storage sites. We report the operating conditions of the equipment, such as the number of plates, pressure, design specifications, and the commercial tanks used in Appendix B.

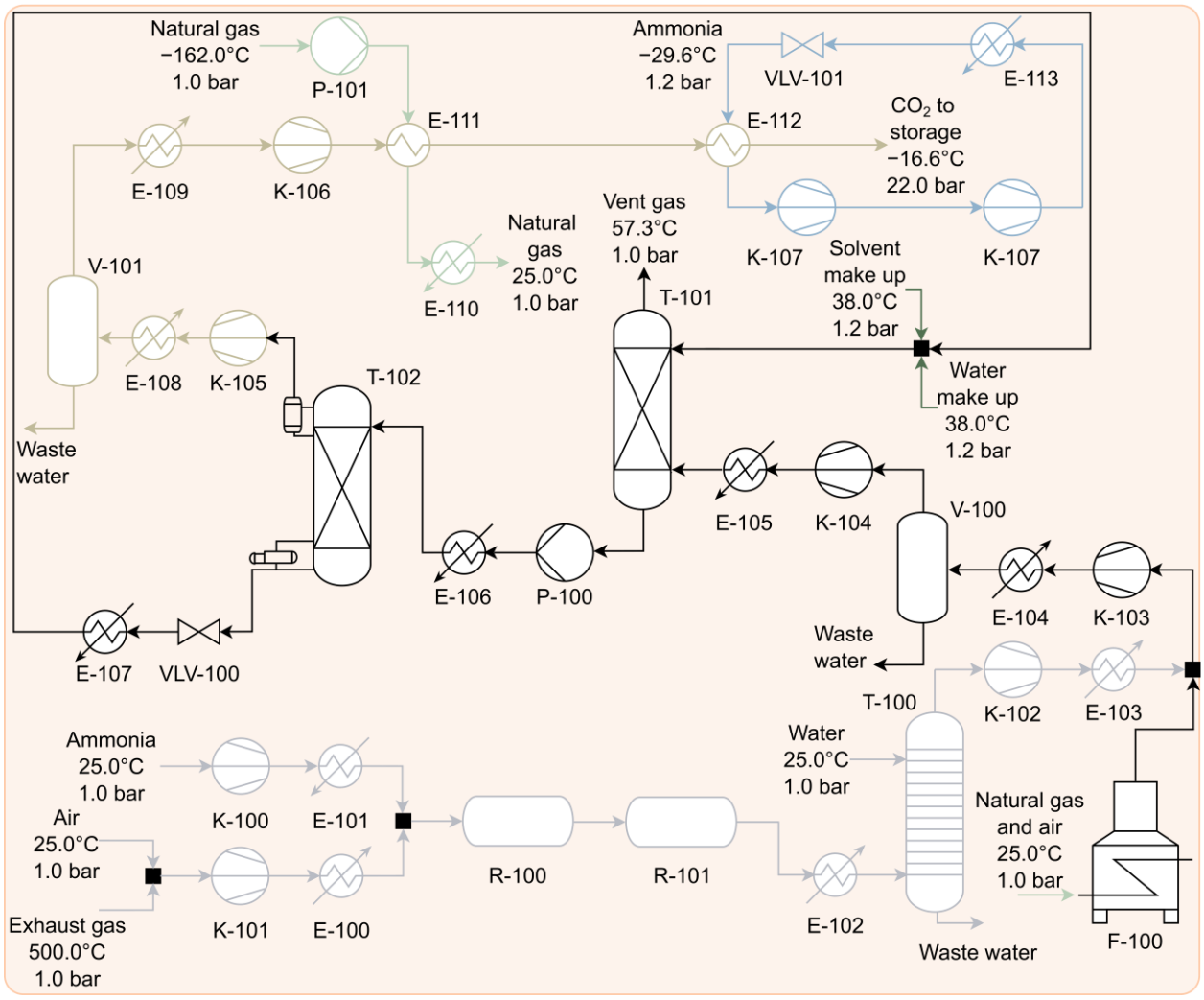

Figure 3.1: Process flowsheet of the retrofitted CO_2 capture plant. Three sections can be identified: pretreatment, carbon capture units, and refrigeration cycles for the storage of liquid CO_2 on-board.

In our analysis, we consider three scenarios sketched in Figure 3.2. We compare a retrofitted carbon capture plant on-board of container ships (capture on-board scenario) with the BAU, i.e., the current fleet of container ships (BAU scenario). Lastly, the capture on-board is assessed against an alternative carbon capture technology. We consider that DAC facilities powered by heating with NG and electricity are installed to capture the CO2 emissions from the BAU, with a 90 % efficiency[180] (BAU + DAC scenario). We impose that DAC achieves the same net CO2 removal as in the CO2 capture plant on-board to provide a fair comparison, meaning that the CO2 from the exhaust and the furnace captured by the plant on-board is equal to the CO2 from the air and the NG heating captured by DAC. Further details about the activities considered in the BAU and the DAC plant are provided below and in Appendix B.

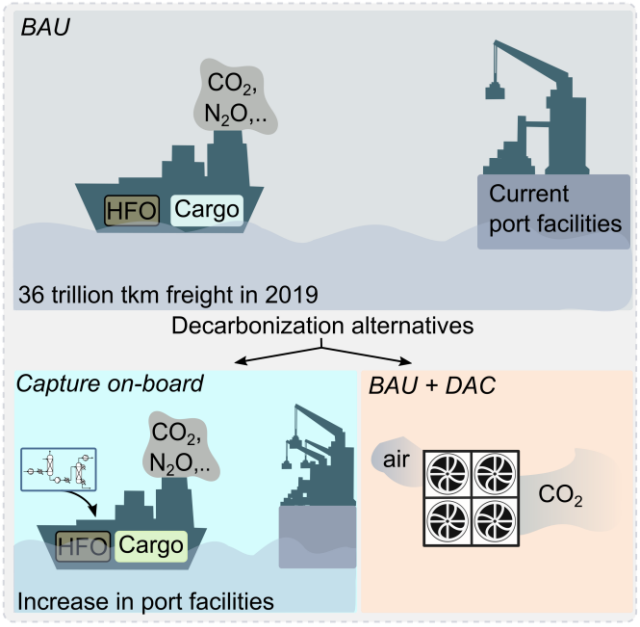

Figure 3.2: Scenarios considered in the study. BAU is represented at the top as the current scenario where the shipping industry operates without introducing any measure to mitigate direct emissions. The capture on board and BAU + DAC scenarios are represented in the bottom left and right, respectively. In these scenarios, the net CO2 captured is the same. The increase in the port facilities in the capture on board scenario corresponds to the displacement of the cargo and consequent increase in ships.

3.2.3 Feasibility and economic assessment

The first step to assess the feasibility of the retrofitted carbon capture plant before carrying out the economic and environmental analysis is to ensure that the equipment can be placed on-board. In their recent work, Stolz and co-workers based this assessment on the maximum permissible draught[176], while in our study we assume that the retrofitted plant displaces the current cargo in order to maintain the same total weight on the ship corresponding to 8500 TEU. We estimate the volume and the weight of the capture plant, consisting of the absorber,

stripper, furnace, pumps and compressors, flash units, heat exchangers, including NH_3, LNG, MEA and CO_2 storage tanks, based on the design of each equipment. The weight considers only the extra units needed for the CO_2 capture (*i.e.*, the scrubber for the SOx and NOx reduction is already present on-board of current vessels and, therefore, it is not accounted for). Then, we translate this information into equivalent TEU based on the standard dimensions of the latter[205] to obtain the cargo displacement on a volume basis. On the other hand, we compare the weight of the plant with the maximum cargo allowed on-board, which comes from the vessel dead weight tonnage subtracting the fuel, to calculate the cargo displacement on a mass basis. Since we impose that the final weight of the ship must be the same, the cargo that is displaced must be transported by additional ships with the same retrofitted CO_2 capture plant design. We calculate the increase in the number of ships traveling the same route and the consequent increase in the port facilities to accommodate the bigger fleet in the year. More information about the calculation of the cargo displacement is reported in Appendix B.

Given the large scale of the plant retrofitted on-board, the economic assessment is carried out based on the correlations and installation factors available in Towler and Sinnott[206]. We consider a shaft generator on-board that supplies the electricity to the additional components, *i.e.*, pumps and compressors, and a marine seawater desalination system that provides high-quality fresh water. Both technologies are already commercially available, *e.g.*, from Wärtsilä[207].

The calculations and a sketch of the technical feasibility are reported in Appendix B, together with the assumptions for the cost calculation.

3.2.4 Environmental assessment

The environmental analysis is carried out according to the LCA methodology following the ISO 14040/44 framework[208,209]. The goal is to assess the absolute environmental sustainability of the current cargo demand for container ships considering the environmental improvement of implementing CO_2 capture on-board or sequestering the same amount of CO_2 with DAC. The functional unit (FU) corresponds to the global annual tonne·kilometer (tkm) demand for container ships, estimated at 36 trillion tkm in 2019 by the International Energy Agency[192]. We adopt a well-to-propulsion scope following an attributional approach, meaning that average market data was used to model the system's inventory, but introducing changes to the existing product system. Therefore, the system boundaries include all the upstream activities, *i.e.*, HFO

production, utilities required for the capture on-board, and fuel combustion emissions in the engine. In the system boundaries of the scenarios assessed, we also consider the container ship manufacture and maintenance and the port facilities. A complete list of the activities used in the modeling of the environmental assessment is provided in Appendix B.

The life cycle inventory (LCI) phase is implemented in SimaPro v.9.2.0.2 using the Ecoinvent v3.5 database, combining data of the foreground and background system. The former includes information on the mass and energy flows from the process simulation that was developed. In the *BAU + DAC* scenario, the data is retrieved from Keith et al.[180], which is based on an existing commercial plant. The process is scaled to match the amount of CO_2 captured in the *capture on-board* scenario. The inventory of the *BAU* scenario is defined to meet the specifications of the reference ship used in the study, based on activities available in the Ecoinvent database[50].

During the life cycle impact assessment, we quantify the absolute environmental sustainability performance of the proposed decarbonization solutions and the *BAU* using seven PBs metrics. The PBs define limits of allowable human perturbation that, if surpassed, could threaten the Earth's stability; therefore, they delimit the safe operating space (SOS) in which humanity can operate. In order to quantify the impacts on the PBs, we use the characterization factors proposed by Ryberg et al.[210] and Galán-Martín et al.[211] that can convert the LCI elementary flows into impacts on the seven PBs. Additionally, we calculate the GW impact of the scenarios considered using the IPCC 2013 GWP 100a method.

In the life cycle interpretation phase, we analyze the relative impacts with respect to the full SOS (%). We clarify that an impact above 100 % indicates the transgression of the corresponding PB. We note that by using the full SOS we are not allocating a share of the PBs to the container ships industry. Consequently, during the result interpretation phase, each scenario should be carefully evaluated and regarded as sustainable only if the SOS occupied leaves sufficient space for additional economic activities, which all together should operate within the PBs.

3.3 Results and discussion

3.3.1 Technical and economic results

The retrofitted CO_2 capture plant on-board scenario is technically feasible and economically competitive compared to other carbon capture options, such as DAC or less mature technologies omitted in this analysis, *e.g.*, solid adsorbents[212]. The design described in Figure 3.1 has a net efficiency of 94 %, *i.e.*, considering the CO_2 from the exhaust gas and the furnace. The total cost of the additional equipment required on-board is 85 $\$_{2019}/tCO_2$, annualized considering 7446 hours per year based on an annual utilization factor of 0.85[213] and a 30 years lifetime of the units on the vessel, in agreement with literature results for conventional post-combustion capture applications at power plants[100]. The equipment needed to achieve 94 % capture of the net CO_2 emissions takes 7 % of the cargo on a mass basis and 4 % in volume for a week-long trip. The number of ships that fulfill the global tkm in 2019 featuring the new design proposed is calculated based on the nominal capacity of 8500 TEU. The increase in the number of vessels to transport the cargo displaced by the retrofitted plant on-board corresponds to 3 % of the current fleet in that year (weight and volume displacement of the cargo based on an average trip of a week). However, we estimate that for longer traveling times, such as four weeks, the displacement could be up to 25 and 12 % of the cargo in mass and volume, respectively, which would be economically unattractive.

The CO_2 sequestered is stored on-board in liquid form in commercial tanks until the ship reaches the port where it is unloaded and transported to suitable storage sites, *e.g.*, saline aquifers, via pipeline. We note that the transport of liquid CO_2 is a major safety concern due to its instability at the triple phase point[186]. However, at ambient pressure, gaseous CO_2 requires large space available on-board, which would make this option infeasible even for a week trip.

In the alternative scenario where CO_2 is captured using DAC, the energy requirement and the total cost are estimated from the literature. This technology currently is rated at a capture cost of 300 $\$/tCO_2$ for high temperature liquid sorbents[214] and 600 $\$/tCO_2$ for low temperature solid sorbents[215], with an estimated CO_2 levelized cost of 94 to 232 $\$/tCO_2$[180] for scaled-up systems, whose lower bound is already 10 % more expensive than our solution. However, even given the economic competitiveness of the capture on-board scenario, the capital investment should be supported by international policies and government incentives to build the network infrastructure for injecting the CO_2 underground.

Our solution relies on the geological sequestration of CO_2, whose elements, namely capture, transportation and injection technologies, are mature and commercially available for decades[212]. CCS projects are slowly spreading and increasing worldwide, with 27 operational projects for a total of 36.6 $MtCO_2$ stored per year as of 2021. CCS is part of various countries' strategy to fight global warming, benefiting from shared infrastructure (pipeline, storage wells)[216], and positively impacting international climate policies. While lessons about cost projections and storage safety have been learned, legal and regulatory frameworks have still to be put in place to remove social and political barriers, especially for complex projects[217]. Although the scenario proposed is a temporary solution to mitigate direct emissions, the capital investment realized to retrofit the carbon capture plant on-board and the required infrastructure could be used in the future for circular low-carbon fuels, such as MeOH.

3.3.2 Planetary boundaries

We assess the performance of the capture on-board scenario compared to the *BAU* and *BAU+DAC* on the SOS of the seven PBs considered. The results are displayed in Figure 3.3. Our analysis shows that the global demand for container ships occupies up to 13 % of the full SOS. The most significant impacts occur in the GHG-related PBs (atmospheric CO_2 concentration (CO_2), energy imbalance (EI), ocean acidification (OA), and biosphere integrity (BII)). Indeed, 13 % of the CO_2, 12 % of EI, 4 % of OA and 1 % of BII are consumed by the current container ships sector to fulfill the global tkm demand. The impact on the remaining PBs is negligible (<1 %). However, we stress that the full SOS should accommodate all economic sectors that together should not surpass the given limits to operate sustainably. For example, the current chemical sector already takes up 25 % of the CO_2 SOS[211], which adds to the 13 % of the cargo shipping industry, contributing to 38 % of the global SOS for the CO_2 control variable. Alternatively, part of the SOS could be allocated to the container ships following downscaling principles[218,219]. For example, this share could be defined based on the sector gross value added (GVA), considering that the overall ocean economy contributed to conservatively 3 % of the global GVA in 2010[220]. Based on the sector GVA, the SOS space allocated to cargo ships would be greatly reduced and hence transgressed.

Our analysis proves that the decarbonization options assessed can decrease the current pressure exerted by container ships on the Earth-system processes. More specifically, the *capture on-board* scenario proposed performs better than the *BAU* and *BAU+DAC* in all the GHG-related PBs. Notably, a decrease of 58 % can be achieved in the CO_2 concentration and OA,

57 % in EI and 48 % in BII PBs compared to the *BAU*. On the contrary, an 18-fold increase in the impacts is observed in the nitrogen flows (N) PB. Nonetheless, the impacts on the latter PBs remain negligible compared to the GHG-related ones. Finally, the *BAU+ DAC* scenario can decrease the impacts by 49 % in all the GHG -related PBs compared to the BAU, except BII that is decreased by 41 %. However, the impacts in N and freshwater use (FWU) PBs increase by two and almost five times, respectively, although they are still rather low compared to the impact in the carbon-related PBs. The remaining acronyms in Figure 3.3 are as follows: stratospheric ozone depletion (O3D), phosphorus flow (P) and land-system change (LSC).

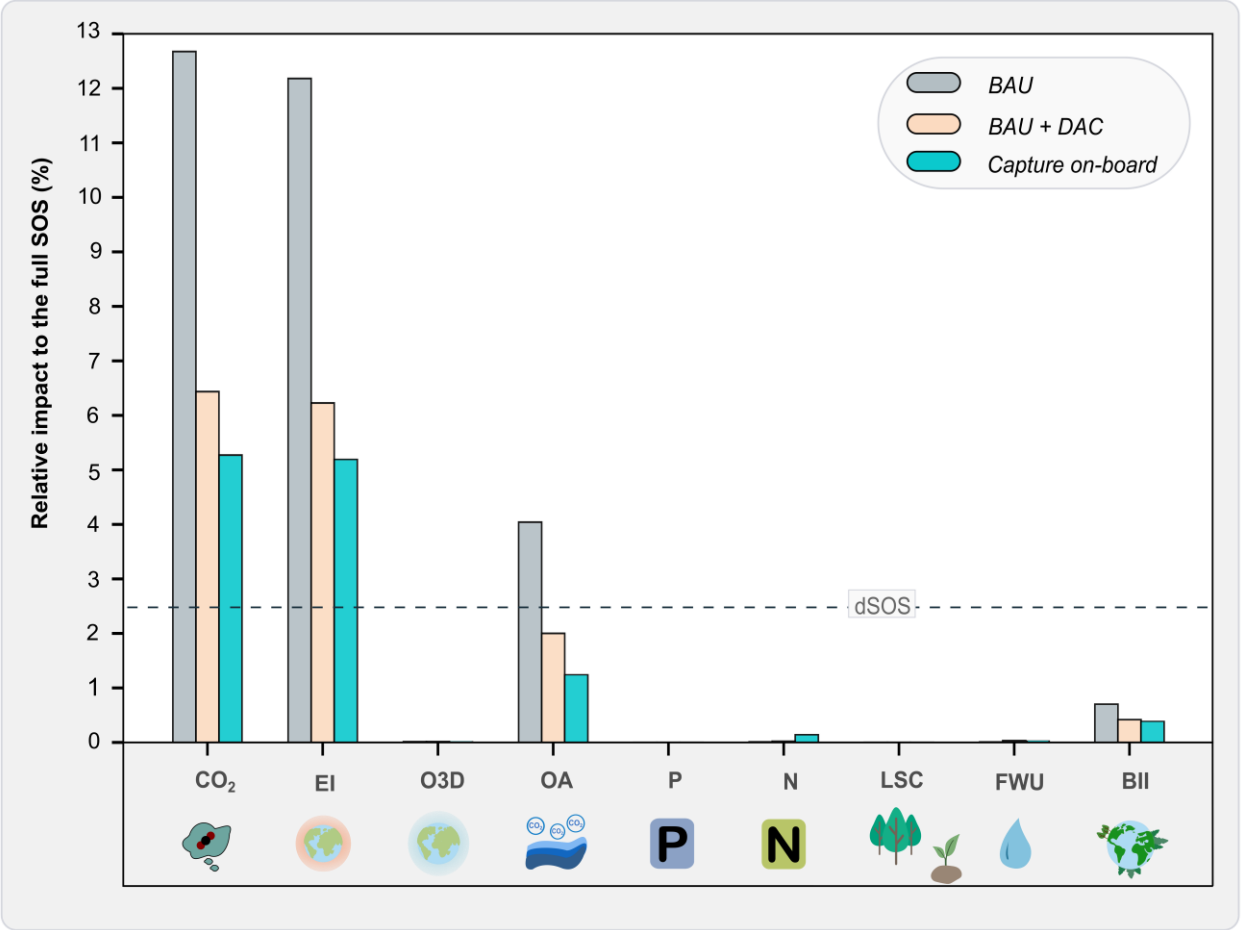

Figure 3.3: Scenarios performance on the PBs control variables. The impacts on the PBs most strongly connected to GHG emissions, namely CO_2 atmospheric concentration (CO_2), energy imbalance (EI), ocean acidification (OA) and biosphere integrity (BII) are the most significant in all the scenarios. dSOS represents the downscaled safe operating space, based on the contribution of the shipping sector to the global gross value added.

3.3.3 Global warming

We report in Figure 3.4 the impacts of the three scenarios on GW (kg $CO_{2\text{-eq}}$.), considering the activities common to both scenarios ('HFO', 'freight ship', 'port', 'combustion emissions', 'CO_2 storage'), those specific to the *capture on-board* scenario ('NG', 'MEA' and 'NH_3 added on-board'), and finally the ones in the *BAU+DAC* scenario ('CO_2 removed', NG ('NG DAC'), calcium carbonate ('$CaCO_3$ DAC'), 'water DAC' and 'electricity DAC'). CO_2 storage refers to the CO_2 transportation and injection underground.

We find that *Capture on-board* performs better overall ($1.71\ 10^{11}$ $kgCO_{2eq}$.) compared to the *BAU* ($3.53\ 10^{11}$ $kgCO_{2eq}$.) and *BAU + DAC* ($1.93\ 10^{11}$ $kgCO_{2eq}$.) scenario, leading to a reduction in GW by 52 % and 11 %, respectively. We note that in the *BAU* the impact from the combustion emissions corresponds to 66 % of the total, followed by the port facilities (20 %) due to electricity consumption and finally the HFO fuel (10 %). The *capture on-board* scenario tackles the largest contributor of the impacts, achieving an 86 % reduction in the combustion emissions compared to the *BAU*. However, implementing the captured on-board scenario requires an increased construction and operation of the port facilities, which takes up 43 % of the impacts, while the HFO contributes 21 %. The *BAU + DAC* scenario requires electricity and natural gas as utilities to operate the DAC unit causing 3-fold impact on GW compared to the energy inputs of the capture on-board scenario. Notably, capturing the emissions at point source is less energy intensive than from the air.

From Figure 3.4, it is evident that the impact of the port facilities is dominant in all the scenarios. Therefore, for further decarbonization efforts, renewable electricity should be considered to satisfy the requirement at the port facilities and zero or low carbon fuels should be considered for the propulsion of the vessel, as discussed next.

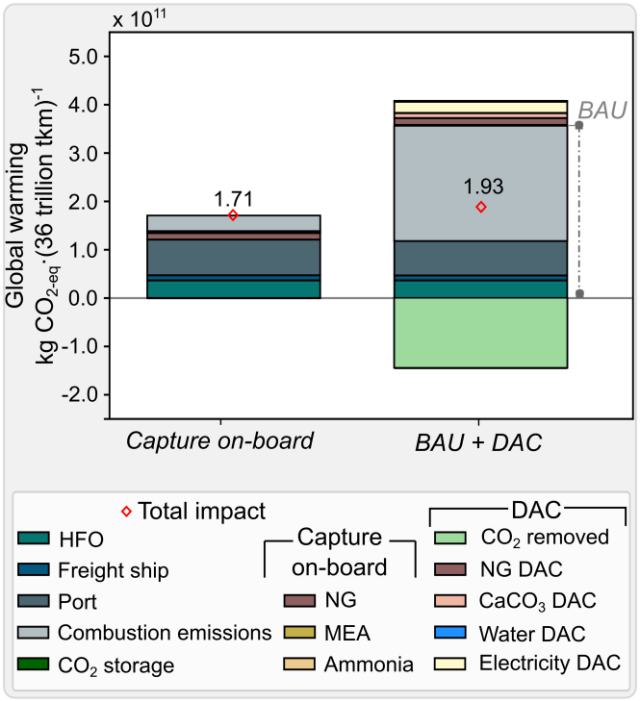

Figure 3.4: Global warming potential of the three scenarios considered. The capture on-board scenario performs best in global warming, outperforming the BAU and BAU + DAC scenarios by 52 % and 11 %, respectively.

3.4 Alternative fuels in the long-term solution

The carbon capture scenario proposed could enable the maritime sector to meet the 50 % GHG emissions reduction target in 2050 until more sustainable fuels are deployed and does not intend to be a long-term solution relying on fossil resources, *i.e.*, HFO. Among the fuels of interest currently under investigation in future fleets are liquid ones such as NH_3, MeOH, bio-based alternatives, and gaseous ones such as H_2 and (bio)NG. The production routes include CO_2 utilization, reformed NG with CCS and renewable electricity (electrofuels)[10]. Stolz and co-workers also considered the direct use of electricity in bulk cargo ships with Li-ion batteries, given their rapidly increasing energy density[176]. Despite a thorough techno-economic analysis of different options being carried out by these authors, alternative fuels should be analyzed from a life cycle perspective[221].

In particular, drop-in biofuels such as bio-MeOH, bio-dimethyl ether, or bio-oil have been assessed with prospective LCA[222,223] to consider technological improvements, electricity mixes changes and other socio-economic factors usually set constant in LCA assessments. In the works of Mukherjee et al. and Watanabe and co-authors, sustainable feedstock such as waste biomass or manure and forest residues was investigated in different processes, *e.g.*, gasification, anaerobic digestion, hydrothermal liquefaction or pyrolysis[222,223].

According to the literature, all the aforementioned alternative fuels will face technical challenges due to their characteristics, *e.g.*, toxicity, corrosiveness, low energy density leading to large storage on-board, and chemical composition, making them not suitable as drop-in at the moment[221,224,225]. Additionally, the switch to low- or zero-carbon fuels is hampered by the economic competitiveness of HFO and marine gas oil[223] and their current high share in the market (86 %[226]), and it will unlikely happen without a solid regulatory framework[10]. Furthermore, the maritime industry will compete for these fuels with other transportation sectors, namely land-based transport and aviation[223]. Although it is challenging to identify a clear winner among the many suitable candidates, NH_3 and MeOH may dominate the 2050 mix[10] if the infrastructure in place today is updated, although bio-based fuels might be preferred in the long run because they can be directly used in the current engines.

From the discussion above, it seems unrealistic to think that a complete replacement of the current fuels will happen instantly, and interim solutions such as the one proposed in our work will be pivotal. Additionally, carbon capture technologies are mature and the implementation on-board will not require considerable changes in the existing infrastructure, especially for ship owners. Moreover, we may implement CO_2 capture on-board today and switch from HFO to biomass-derived fuels in the future with the advancement of engines. In that case, we could even achieve negative emissions in the next generation of container fleets.

3.5 Conclusions

The application of carbon capture by chemical absorption using monoethanolamine solvents to cargo ship exhaust was analyzed from a technical, economic and environmental perspective. The scenario was assessed compared to the business as usual and the direct air capture technology. Our analysis proves that carbon capture on-board is a technically feasible and economically attractive solution to reduce the direct emissions from the cargo shipping industry at 85 $\$_{2019}/tCO_2$. The plant retrofitted on-board displaces 7 and 4 % of the freight on a mass and volume basis, respectively, which can be transported by additional ships with the same design. The solution proposed was assessed on seven planetary boundaries. The results show that it does not transgress the full safe operating space while halving the current pressure exerted by the business as usual on three core planetary boundaries. It also outperforms direct air capture, decreasing the carbon footprint of the current scenario by 52 %.

Overall, the solution proposed can be implemented in the short term with minor modifications to the current fleet until engines running on alternative fuels will be developed and will operate on newbuilds. In the long-term solution, low or zero carbon fuels such as biofuels or electrofuels should be employed where employing electric power is challenging, *e.g.*, for long-distance transportation. Moreover, a carbon negative scenario could also be achieved by retrofitting carbon capture on-board and deploying biomass-based fuels.

3.A Nomenclature

Acronyms	
BAU	Business as usual scenario
DAC	Direct air capture
DeNOx	De-nitrification reactor
FU	Functional unit
GHG	Greenhouse gas
GVA	Gross value added
GW	Global warming
IMO	International Maritime Organization
LCA	Life cycle assessment
LCI	Life cycle inventory
PBs	Planetary boundaries
PM	Particulate matter
SOS	Safe operating space
TEU	Twenty foot equivalent units
tkm	Tonne·kilometer

Chemicals	
CO_2	Carbon dioxide
H2	Hydrogen
H2SO4	Sulfuric acid
HFO	Heavy fuel oil
LNG	Liquefied natural gas
MEA	Monoethanolamine
MeOH	Methanol
N2	Nitrogen
NG	Natural gas
NH3	Ammonia
NOx	Nitrogen oxides
O2	Oxygen
SO3	Sulfur trioxide
SOx	Sulfur oxides

Planetary boundaries categories	
BII	Biosphere integrity
CO2	Climate change - atmospheric CO2 concentration
EI	Climate change - energy imbalance
FWU	Freshwater use
LSC	Land system change
N	Nitrogen flows
O3D	Stratospheric ozone depletion
OA	Ocean acidification
P	Phosphorus flow

Chapter 4

Harnessing biomethane from thermal gasification with CCS for enhanced energy security and GHG emissions reduction in the EU[4]

[4] Drafted for submission as V. Negri, S. H. Klukowksi, R. Istrate, A. Nandera and G. Guillén-Gosálbez

4.1 Introduction

The Russian invasion of Ukraine in February 2022 has emphasized the issue of the European Union's (EU) over-dependency on Russian natural gas. In 2021, the EU imported 83% of its natural gas, more than 45% of which came from Russia[227]. Within this context, the new geopolitical scenario has led to natural gas prices skyrocketing, exacerbating the economic crisis caused by the COVID-19 pandemic and resulting in a dramatic increase in electricity, heating and fuel prices weighing heavily on private consumers[228].

In March 2022, the EU Commission proposed REPowerEU, an action plan that focuses on incentivizing energy savings, boosting clean energy production, replacing natural gas in heating and power generation and promoting natural gas supply diversification[229]. Overall, REPowerEU is meant to completely phase-out the imports of Russian gas well before 2030. In the short term, the EU has drastically reduced gas imports from Russia by relying on other suppliers, such as Qatar and the United States (US)[227]. In the medium and long term, a more aggressive shift away from natural gas could be imperative to comply with climate policy targets[230,231]. In this challenging context, biomethane, a natural gas substitute produced from biomass, emerges as a promising alternative to help curbing greenhouse gas (GHG) emissions while enhancing energy security, i.e., alleviating the dependency of the EU on volatile fossil fuels imports, and mitigating the effects of current energy prices. Moreover, the potential of biomethane as a carbon dioxide removal (CDR) solution is particularly noteworthy if part of the carbon content of the biomass (i.e., the CO_2 that has been previously uptake from the atmosphere) is captured and permanently stored underground[232]. In light of its potential, the EU has established an ambitious goal of increasing biomethane production tenfold by 2030, reaching up to 35 billion normal cubic meters annually (bNcum)[229].

Biomethane is primarily produced via two routes: i) anaerobic digestion of biodegradable feedstocks to produce a biogas (a mixture of CO_2 and CH_4) which is upgraded to biomethane through the removal of the CO_2 (i.e., the biochemical route) and ii) thermal gasification of solid biomass coupled with subsequent methanation (i.e., thermochemical route)[41]. The biochemical route is a well-established technology with decades of deployment[233]. Meanwhile, gasification followed by methanation is an emerging technology which is gaining traction given its potential to produce biomethane at a larger scale[41]. Gasification uses solid biomass (e.g., woody feedstock and agricultural residues) which is broken down in a gasifier at high temperature and in the presence of oxygen and steam to produce syngas, a mixture of CO, H_2, CH_4, and other

gases[234]. After cleaning, the syngas undergoes the methanation stage, where the reaction between H_2 and CO produces biomethane. Before the syngas is converted into a higher value product in the methanation reactor, the CO_2 present in the syngas can be captured and stored underground, offering a unique CDR opportunity.

Previous studies have extensively analyzed the global and regional biomethane production potential via biomass gasification[41,235–237] as well as the process' economics, often using process simulations[238–246], while the literature on the potential environmental footprint is much more limited. Most environmental assessments have a rather narrow scope, often focusing on the life cycle GHG emissions of gasifying specific feedstocks (e.g., wood chips[247], lignocellulosic feedstock[248,249] and wheat straw[250]). Only a few studies have addressed the environmental implications of a large-scale deployment of thermochemical biomethane production, particularly concerning the climate change mitigation potential (e.g., in the US[237] and the Occitania region in France[251]). Notably, the possibility of coupling biomass gasification with carbon capture and storage (CCS) to deliver carbon-negative biomethane based on domestic resources remains largely overlooked in the literature.

Here we cover this knowledge gap by assessing the broad environmental implications of biomethane production via biomass gasification with CCS in the EU and United Kingdom (hereafter referred to as EU, before Brexit). We use a holistic framework that combines country-specific biomass availability with a detailed process simulation and the standardized life cycle assessment (LCA) methodology. Moreover, we also determine the optimal deployment of biomethane production that enables negative emissions without transgressing other critical environmental categories.

4.2 Results

4.2.1 Large biomethane potential in the EU

We first estimate the biomethane production potential via biomass gasification in the EU considering two biomass residues, namely wheat straw and forest, and three energy crops cultivated on marginal land, namely *Miscanthus*, willow and poplar according to the supply chain sketched in Figure 4.1. These five feedstocks account for the majority of the biomass available in the EU and do not compete for land with food production. By considering country-specific biomass availability and the process efficiency, we find that 151 billion normal cubic meters (bNcum)/year of biomethane could be produced cumulatively in the EU. Spain, Poland,

Germany, France and the United Kingdom provide 53% of the total biomethane production potential (Figure 4.2a). Spain, with 33.5 bNcum/year, has by far the largest potential, mainly due to the large availability of *Miscanthus* and poplar crops. Poland shows the second largest potential, equivalent to half of the Spain potential, i.e., 16 bNcum/year, and also mainly based on *Miscanthus* and poplar crops. Differently, Germany and France have a potential of roughly 12 and 11 bNcum/year, respectively, more than 50% and 35% of which comes from forest residues. Lastly, the United Kingdom has a biomethane potential of 9 bNcum/year almost split equally among the three investigated energy crops (*Miscanthus*, willow and poplar).

A previous study has reported a biomethane production potential via biomass thermal gasification of 67 bNcum/year by 2050[252]. However, this study omitted feedstocks cultivated on marginal land. According to our estimates, energy crops cultivated on marginal land may account for roughly 90% of the total biomethane potential. Overall, the estimated biomethane potential is similar to the volume of Russian gas imported by the EU in 2021, i.e., 155 bNcum[227], and substantially higher than the EU's target of 35 bNcum annually by 2030.

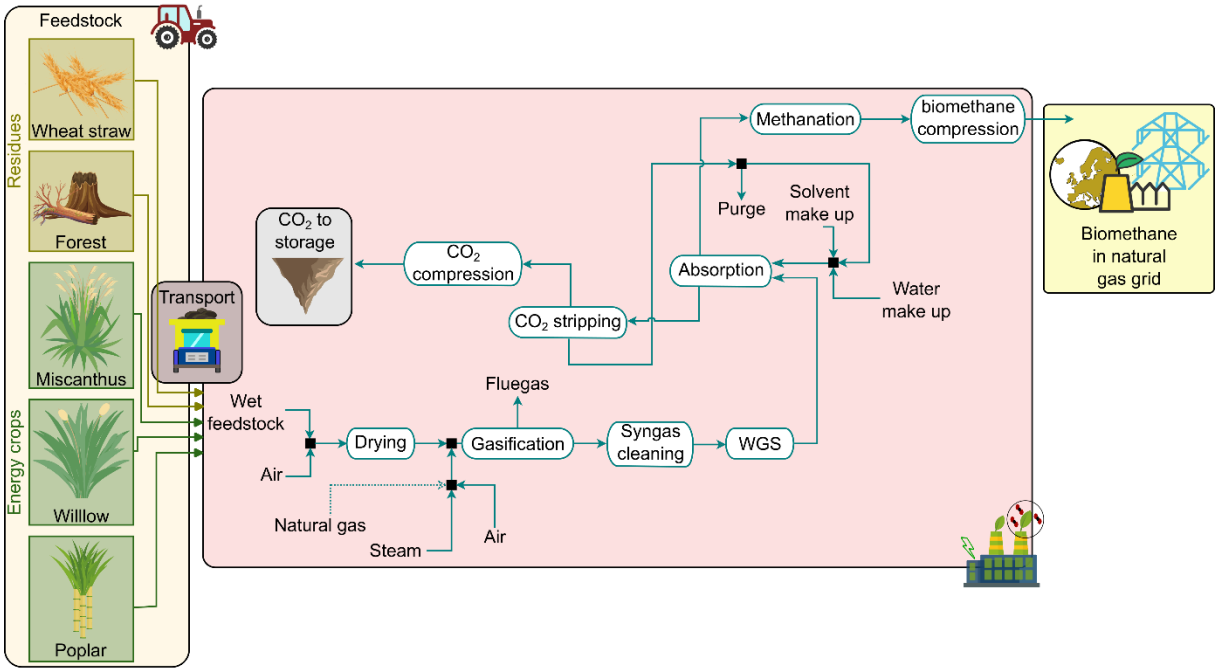

Figure 4.1: Biomethane routes explored. Biomethane for grid injection can be produced from five different feedstocks, two types of residues and three energy crops. The biomass is transported via truck to the processing plant, which consists of five steps. The final product has the same characteristics of the fossil natural gas and it is ready to be injected in the existing grid.

4.2.2 Biomethane can remove up to 0.33 Gt of $CO_{2\text{-eq}}$ in the EU

We next compute the carbon footprint of producing biomethane via biomass gasification with CCS in each country (Figure 4.2b). Notably, biomethane achieves net negative emissions on a cradle-to-gate basis across all the studied feedstocks and countries, compared to 0.4 kg CO_2-eq per Ncum of the business as usual (BAU). The carbon footprint of biomethane varies greatly across countries, i.e., from -3.3 kg $CO_{2\text{-eq}}$ in Sweden to -1.8 kg $CO_{2\text{-eq}}$ in Poland in the case of forest residues. This large variability is primarily due to the composition of the electricity mix in each country, as gasification and especially methanation are highly energy-intensive processes. Regarding feedstocks, wheat straw and forest residues show the lowest carbon footprint, as residues are assumed to be supplied burdens-free (i.e., zero emissions embodied from the cultivation stage[253,254]). More detailed analysis of the impacts of the energy crops cultivation stage can be found in Appendix C.

The negative carbon footprint indicates that the GHG emissions across the biomethane supply chain are lower than the amount of CO_2 uptake from the atmosphere via photosynthesis. After accounting for the hypothetical emissions from biomethane combustion, we find that a slightly negative carbon footprint would be achieved even on a cradle-to-grave basis, i.e., between - 0.009 and - 0.07 kg CO_2-eq/Ncum on average. This is possible because from the original carbon content of the biomass, more carbon is captured and stored underground than the one transferred into the biomethane.

Lastly, we determine the potential for curbing carbon emissions through the substitution of natural gas with biomethane in the EU (Figure 4.2c). Our results show that we can achieve a reduction in the global warming impact compared to the current scenario. If the total potential of 151 bNcum were supplied by BAU natural gas, the global warming impact would be 0.06 Gt $CO_{2\text{-eq}}$. By replacing 100% of the amount of natural gas with the potentially available biomethane, we achieve a maximum net removal of 0.33 Gt $CO_{2\text{-eq}}$.

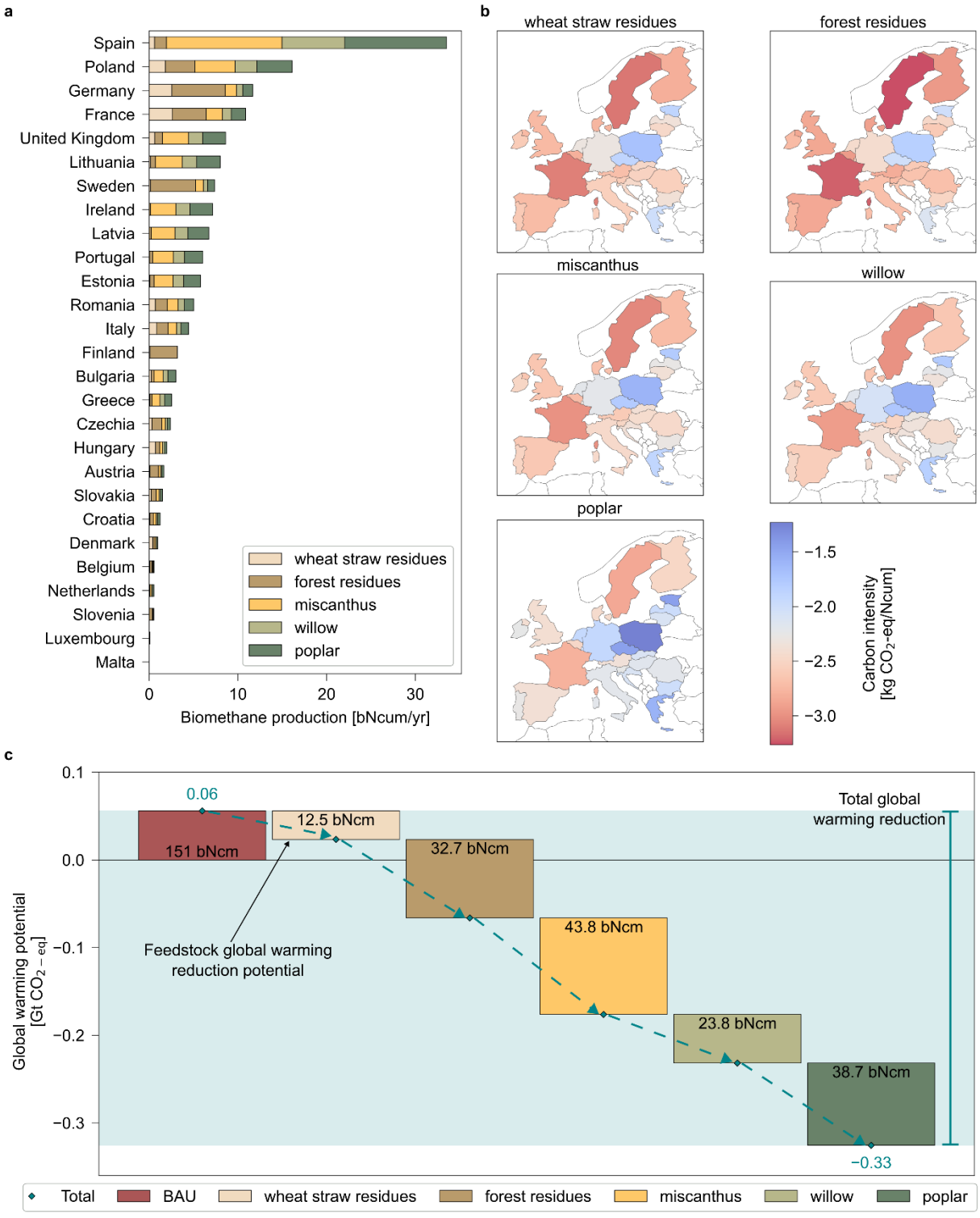

Figure 4.2: Potential and carbon footprint of biomethane production via biomass gasification with carbon capture and storage (CCS) in the EU. Subplot (**a**) shows the biomethane production potential in each EU country based on regional biomass availability. Subplot (**b**) represents the cradle-to-gate carbon footprint of biomethane production from each feedstock in each country. Subplot (**c**) shows the maximum global warming potential reduction based on the total biomass availability in the EU. The total global warming reduction is independent of the sequence by which BAU natural gas is replaced by biomethane. By exploiting the full biomethane potential, it is possible to achieve 0.33 Gt CO_2 removal on a cradle-to-gate basis.

4.2.3 Biomethane can shift burdens to 13 out of 15 impact categories

We next investigate the broader environmental implications of deploying biomethane at scale by studying impacts beyond climate change (Figure 4.3). We find that its large-scale deployment would shift burdens to other categories. Specifically, only 2 of the 15 Environmental Footprint and LANCA metrics investigated would improve, namely ozone depletion and non-renewable energy resources, while the rest would worsen, some of them quite substantially. In freshwater ecotoxicity, non-carcinogenic human toxicity and land use, a switch to biomethane would lead to impact values up to three orders of magnitude above the natural gas scenario. It is worth noting that the robustness of the impact categories varies widely, with ecotoxicity, human toxicity, resource depletion, and land and water use categories involving the highest level of uncertainty. While these impact categories are recommended by the European Commission's Environmental Footprint method, they should be applied with caution[255].

Figure 4.3: Environmental performance of biomethane production scenarios on non-climate change metrics relative to the BAU. The table shows the biomethane scenario impact over the impact of the BAU. A ratio lower than one means that biomethane has a lower impact than BAU. For ratios greater than 1, biomethane performs worse than the BAU. In the latter case, burden-shifting occurs, i.e., biomethane reduces global warming but worsens other categories.

Analyzing the breakdown of impacts (Figure C0.6, Appendix C), we note that among the human-related impacts, ecotoxicity freshwater is strongly linked to the process direct emissions and ash disposal, whose content is the highest in wheat straw. Similarly, ash disposal is the major responsible for the impacts on non-carcinogenic human toxicity, which is particularly relevant in the wheat straw scenario. Regarding the non-toxic categories, land use is affected by the cultivation stage of the energy crops on marginal land, being the worst in the case of willow production. This is not the case for the residues scenarios, whose impact on land use is mainly given by the feedstock transportation.

Overall, by looking at the breakdown of the impacts, we highlight that the ash content of the crops is a major concern in the biomethane process, followed by the crop cultivation stage. Other contributors to the impacts are the use of monoethanolamine solvent in the CO_2 capture plant and the electricity mix. Regarding the latter, we note that the impact may vary substantially depending on the location, as shown in Figure 4.2b.

Forest residues are an appealing choice among the feedstocks analyzed for biomethane production due to high process efficiency (Appendix C Table C0.17) and environmental performance. However, they are not the most abundant feedstock among the ones considered (Figure 4.2a), which makes it necessary to deploy a portfolio of different biomass types instead. Wheat straw, on the other hand, is characterized by low carbon content, which implies a low biomass to natural gas conversion. This low efficiency, however, leads to greater CO_2 removal potential for the same production capacity, as more feedstock is needed compared to other biomass types investigated. This comes with the downside of large amounts of ash due to the composition of the biomass, which has significant effects in all the toxicity-related categories. Among the energy crops investigated, poplar has the highest biomass-to-natural gas conversion (Appendix C Table C0.17) while showing the best environmental performance on critical indicators, e.g., ecotoxicity freshwater and land use, compared to other crops (Figure 4.3).

On a cradle-to-grave basis (Appendix C Figure C0.8), the impacts of the biomethane scenarios improve substantially, being at most up to two order of magnitude more than BAU and the majority of the categories being less than ten times the current scenario. The most critical indicators still remain ecotoxicity freshwater and land use.

4.2.4 An optimal natural gas blend could avoid significant burden-shifting

Our results show that biomethane has the potential to reduce global warming significantly (Figure 4.2c); however, burden-shifting takes place in almost all the non-climate change impact categories compared to the BAU (Figure 4.3). We contextualize these impacts considering some limits proposed in the literature[55] and regionalized to the EU. We find that only a subset of the 13 indicators transgressed are the most critical. Therefore, we can calculate the optimal potential that maximizes biomethane deployment without transgressing critical environmental categories by developing a linear programming optimization model described in Appendix C. Firstly, we calculate the maximum deployment of a natural gas blend (BAU and biomethane) to meet the EU industrial heat and power demand, restricted to 10 and 100 times transgression

(TF) of the current scenario (Figure 4.4 a). Our results show that in the first scenario, 86% of the total methane is supplied by conventional natural gas and the remaining by forest residues. When a higher level of transgression is allowed (TF100), only 56% of the total methane comes from fossil resources, complemented by wheat straw (10%) and forest residues (31%), and poplar.

The results computed for TF10 and TF100 only show the optimal portfolio of biomass feedstock that satisfies all the constraints. However, these results do not imply that the use of other biomass types is to be excluded. Therefore, we look at the maximum amount of the single feedstocks that can be deployed and still satisfies a BAU transgression of 10 and 100 times on non-climate change indicators (Figure 4.4b). We find that if BAU transgression is restricted to 10, only biomethane from forest residues is carbon negative, which could provide 7 tCO_2 removed. Even when 100 times transgression is allowed, none of the other scenarios leads to negative emissions, except forest residues, leading to 63 tCO_2 removed (Appendix C Table C0.18). Additionally, wheat straw residues and forest residues are fully deployed in the TF100 scenario. Land use is the limiting category for the deployment of the energy crops, as they worsen substantially the pressure on this indicator compared to BAU.

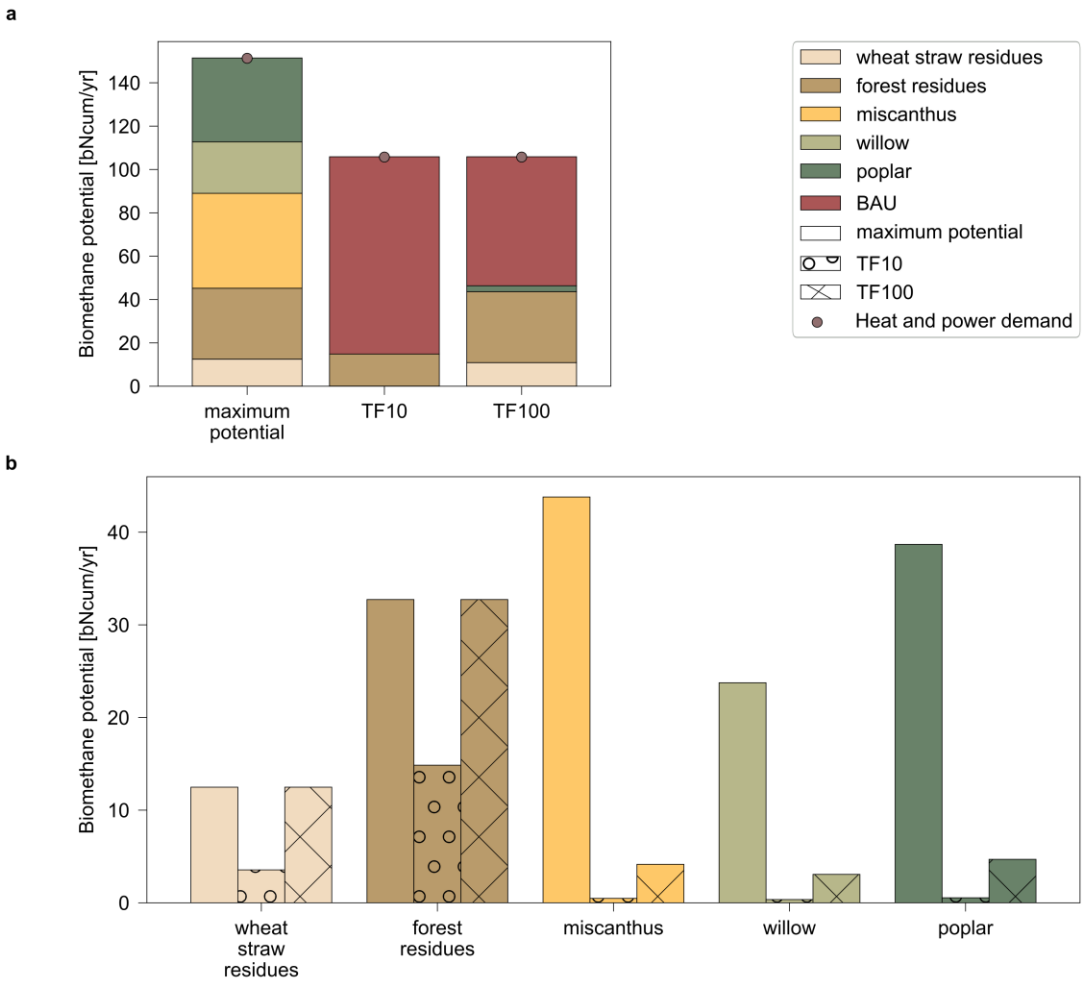

Figure 4.4: Optimal deployment of BAU natural gas and biomethane that avoids critical transgression on selected Environmental Footprint categories. Subplot (**a**) shows the maximum available potential of biomethane based on the total resources in the EU, compared to the natural gas blend that optimally meets the heat and power demand in the EU without transgressing the BAU more than 10 and 100 times (TF10 and TF100). Subplot (**b**) reports the maximum biomethane production per feedstock and the maximum amount that is possible to deploy without transgressing the BAU more than 10 and 100 times.

4.3 Discussion and conclusions

One of REPowerEU main goals is to provide a strategy to boost energy savings and renewable power generation. In this section, we discuss the potential applications of biomethane, while being aware that biomass is a finite resource, which many sectors are increasingly competing for, i.e., food, including manure food, transportation[41]. Indeed, biomass can be used to produce fuels or energy carriers such as hydrogen *via* syngas.

When biomass is employed to produce biomethane through thermal gasification with CCS, the substitute natural gas can be used directly as fuel, e.g., as a clean substitute to fossil fuels in road and sea transportation, for heat (domestic and industrial) and power production. Here, we

focus our discussion on industrial heating applications. Since the latter involves high temperature processes, it is a hard-to-decarbonize sector. Differently, low to medium temperature heat processes can be decarbonized through electrification, such as in the case of housing heating using heat pumps[234]. Therefore, we see clear potential for biomethane to play a key role in decarbonizing the industrial heating sector, replacing the conventional natural gas in boilers and furnaces. We foresee one competitor in decarbonizing high-temperature processes, which is the use of heat pumps powered by bioenergy with carbon capture and storage. However, given the current technology readiness level, we expect biomethane to produce roughly five times the amount of heat than heat pumps based on our calculations and assumptions.

Here we explored the environmental benefits of biomethane production *via* thermal gasification to tackle two main current concerns: energy security in the European Union and United Kingdom and climate change. Regarding the former, we estimated the maximum available potential of biomethane production from locally available feedstocks based on marginal land energy crops and residues considering sustainable removal rates. The amount of biomethane meeting grid feed-in quality resulted being of the same order of magnitude of Russian gas imports. This implies a potential to reduce the dependence of the European Union on volatile fossil fuels imports. Concerning the second issue, we have demonstrated that biomethane reduces greenhouse gas emissions, as it is a carbon-negative energy source on a cradle-to-gate basis, by removing up to 0.33 Gt $CO_{2\text{-eq}}$. However, biomethane production shifts the burden to 13 out of 15 environmental indicators considered compared to the business as usual scenario. Nonetheless, by computing optimal blends of conventional natural gas and biomethane it is possible to reduce the pressure on these indicators and still achieve carbon negative scenarios.

Chapter 5

Life cycle optimization of BECCS supply chains in the European Union[5]

[5] Published as V. Negri, Á. Galán-Martín, C. Pozo, M. Fajardy, D. M. Reiner, N. Mac Dowell and G. Guillén-Gosálbez, *Life cycle optimization of BECCS supply chains in the European Union*, Applied Energy, 2021, 298, 117252

5.1. Introduction

In 2015, 196 Parties agreed in the Paris Agreement to hold the temperature rise by 2100 to well below 2 °C while 'pursuing efforts' to limit temperatures to 1.5 °C above pre-industrial levels and finding a solution to the consequences of climate change[1].

Insufficient mitigation actions are maintaining record levels of world greenhouse gas (GHG) emissions, especially from fossil fuel combustion and cement production [256], such that existing commitments to reduce emissions will be insufficient to achieve the Paris climate goals[4], even accounting for the dramatic decline in emissions in 2020 resulting from the COVID-19 pandemic[162]. Most of the scenarios in the Intergovernmental Panel on Climate Change (IPCC) Special Report on Global Warming of 1.5°C identify carbon dioxide (CO_2) removal (CDR) as the key to achieving the ambitious long-term objective[4]. Unlike conventional mitigation technologies that reduce or avoid GHG release, CDR measures focus on CO_2 already present in the atmosphere and aim at reducing its concentration compared to its level today (i.e., providing a net negative emissions balance)[12]. However, CDR should not be used as a mitigation deterrent and decarbonization should still be accelerated[15], since the response of the carbon cycle to negative emissions remains uncertain and CDR measures may not be free of associated risks[257].

Several negative emissions technologies and practices (NETPs) may be capable of delivering CDR and have been included in the Integrated Assessment Models (IAMs). Among all possible NETPs, bioenergy with carbon capture and storage (BECCS) emerges as particularly appealing[15,18,21,258], as it delivers net negative emissions while providing sustainable and reliable energy. In essence, BECCS technologies involve a combination of bioenergy applications and carbon capture and storage (CCS). Fossil CO_2 is removed from the atmosphere by plants *via* photosynthesis and is fixed into biomass during its growth. The biomass is then processed and transported to be used as renewable feedstock and eventually converted into a set of valuable products such as electricity, biofuels or hydrogen [215,259–262]. Focusing on the application of BECCS to biopower, the biomass resources can either be combusted or gasified (alone or co-fired with coal). The CO_2 released during the process is then captured and sequestered permanently in geological reservoirs or materials (e.g., depleted gas fields or cement), thus potentially generating negative emissions over the life cycle[263]. This series of processes, together with the possibility of replacing fossil fuels with bioenergy, creates a net carbon sink[264].

There is proven evidence of the benefits of BECCS deployment physically removing CO_2 from the atmosphere, and the technology already shows a high maturity level that would make its integration into energy systems straightforward[265]. Despite these advantages, there are only five operating BECCS projects worldwide, storing a total of 0.85 Mt of CO_2 per year[6].

In a world where most policy decisions are economically driven, the main barrier for the large-scale deployment of BECCS is its economic feasibility [28,29]. Other concerns arise from the extensive land and water requirements of primary biomass, compromising the sustainability of biomass supply and potentially competing with food production[266] or causing biodiversity loss in natural environments, in addition to the need for substantial storage capacity for the CO_2[256],[6,20]. Furthermore, BECCS faces a lack of policy incentives[28,29] as well as socio-political challenges[267], especially when it comes to deciding who will deliver the CDR required to achieve the Paris goals[14].

The large-scale deployment of CDR measures seems inevitable, yet a few parties have explicitly mentioned their intention to deploy NETPs in their nationally determined contributions (NDCs)[25,26]. Given its historical leadership in international climate policy[25–27], the European Union (EU) is once more expected to play a key role in CDR policy design and deployment[25]. Targeted policy (such as the European Green Deal [268] and the Circular Economy Action Plan[269]) and investment plans should be developed to incentivize the deployment of NETPs such as BECCS, grounded on sound scientific analyses of its merits and potential drawbacks. Indeed, carbon taxes imposed by some countries in the EU as a penalty on CO_2 emissions will not be sufficient to achieve the Paris Agreement target and promote the large-scale deployment of CDR[270]. The EU could be one of the protagonists in meeting the 2 °C target, delivering a cumulative global CDR of 20 to 70 Gt CO_2 by 2100 using BECCS[13]. Additionally, environmental taxes cannot be applied to encourage the implementation of BECCS because the emissions due to biomass combustion are, in principle, carbon-neutral[271]. The necessary policies should be agreed upon by the individual Members of the EU, allowing each to consider national political and cultural differences as well as priorities[272]. This is a core concept already embedded in the NDCs of the Paris Agreement, which encourages Parties to reduce domestic emissions and adapt to the consequences of climate change, instead of imposing global measures[273].

Accordingly, in recent years BECCS has gained considerable attention in the scientific literature, focusing on the technological challenges and the climate impacts and only partially on the social and broader environmental effects.

A spatially explicit framework was developed to identify the main drivers of the optimal sizing of BECCS facilities[274]. This framework determined that economies of scale support centralized infrastructures and transportation for BECCS, and pretreatment and location have a small influence on costs. The effect of high and low efficiency BECCS power plants has also been investigated[275], leading to the conclusion that lower capital cost, lower efficiency plants outperform higher capital cost, higher efficiency ones, assuming that there is some revenue associated with the removal of CO_2.

In the context of the UK, several models have been published coupling BECCS with the power sector to meet the UK's emissions reduction target[276] or focusing on the potential of BECCS combined with DACCS to decarbonize the energy system while reducing the power generation investment costs[36]. An assessment of the water, land and carbon footprint, and embodied energy associated with the cultivation, transportation and conversion of biomass coupled with CCS has also been performed[33].

The value of collaboration and cooperation among the US, India, China, the EU and Brazil has been assessed deploying regional CDR targets and trading biomass and CDR credits[39]. The importance of yield, labor and electricity cost in determining the total cost has been highlighted as well. Lastly, BECCS has been assessed using the planetary boundaries (PB)[35] framework, finding that the CDR target can only be achieved if transgression of the boundaries is allowed, for the specific feedstock, infrastructure and region considered.

An extensive literature review on the topic of multi-objective biomass supply chain (SC) design[277] pointed out that global warming potential minimization is the most studied scenario, among the possible environmental and social objectives. In terms of social impact, a recent study looked at the impact of retrofitting coal plants to become BECCS plants with respect to job retention and creation in the US[278].

The majority of the works mentioned above aim to identify a cost-optimal solution, while almost always neglecting the environmental impacts or considering at most only a selection of climate indicators. Hence, the whole spectrum of implications of a multi-country BECCS SC on human health and the environment remains unclear.

To address this knowledge gap, this study provides a detailed optimization model of a BECCS SC in the EU that selects the optimal configuration to achieve a given global CDR target while simultaneously minimizing impacts on human health, ecosystems and resources. Following previous studies, human health can also be considered a social sustainability indicator to account for the years of life lost[37].

In the next section, the problem is defined and the input data are described. Next, the life cycle assessment (LCA) methodology used to calculate the SC's environmental performance is presented. The mathematical model is introduced in the fourth section, where the key equations are described. The results are conveyed and interpreted in the fifth section. Finally, the conclusions provide the reader with the main outcomes of the study and an outlook for future work.

5.2. Problem statement

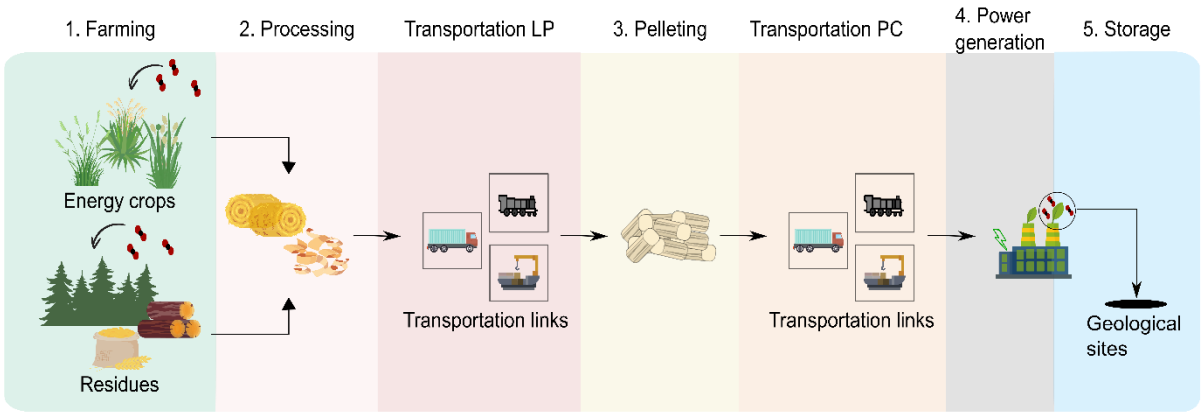

Figure 5.1: BECCS SC problem. The available biomass feedstock consists of a set of energy crops and residues that are harvested or collected and transformed into chips or bales. Then, they are transported to the pelleting stage by lorry, train, or ship. Later, the pellets are transported to the combustion site. Direct CO_2 emissions at the power plant are captured and transported *via* pipeline to a storage site (i.e., depleted hydrocarbon fields or saline formations). The colored background represents the "cradle-to-grave" system boundaries of the LCA analysis.

Our analysis is based on a five-echelons BECCS SC within the European Union (EU-28) linked by transportation, as shown in Figure 5.1. The region of interest (EU-28) is divided into its member states, each of them regarded as a potential location for farming, processing, pelleting, combustion and electricity production and CO_2 storage.

The objective of the optimization problem presented in this chapter is to determine the optimal configuration of the five-echelon BECCS SC to minimize costs and environmental impacts. Three environmental metrics have been chosen for this study, in order to carry out a holistic

analysis of a range of impacts using aggregated endpoint metrics of the ReCiPe 2016, which cover the full spectrum of environmental midpoint indicators. The decisions to be made include the location of the facilities, the transportation means, and the material and energy flows between the echelons.

The information available includes the costs per unit flow of each activity in the different regions and specific technical parameters for each stage, e.g., the combustion plant's efficiency and the amount of solvent needed for CO_2 capture. For each country, we consider the available marginal land, crop yield, residue abundance, and specific carbon content of each biomass feedstock. The distances between countries are also given, calculated for each transportation mean.

As an illustrative case, a global CDR target reported by Peters and Geden[13] is enforced to be met jointly by the EU-28 countries by 2100. This target is only one of many proposed over the last decade and was calculated based on cost-optimal scenarios from IAMs. In this study, we annualized the Peters and Geden target value linearly. We consider a cooperative system that allows for free shipment of biomass and CO_2 among the members.

5.3. Life cycle approach

The optimization model is based on LCA for both costs and impacts, and therefore follows a life cycle optimization (LCO) approach.

Goal and scope definition. We consider each particular activity to assess the entire network represented in Figure 5.1, from biomass growth to CO_2 storage underground, hence following a "cradle-to-grave" approach to sequester a minimum amount of CO_2. The system under study is divided into seven subsystems: farming, processing, transportation from farmland to processing, pelleting, transportation from processing to combustion, combustion with carbon sequestration and, lastly, transportation of CO_2 to the geological sites. The electricity generated is considered a sub-product of biomass combustion that cannot be exchanged among the countries.

Life cycle inventory (*LCI*). The inventory of data used in this study come from different sources. Secondary data for biomass growth, transportation, combustion and storage have been collected from previously published studies or calculated based on available data (when the

information was missing in the literature). The SC stages are modeled in SimaPro 9.0.0.48[279] using Ecoinvent v3.5[280] database activities.

*Life cycle impact assessmen*t (*LCIA)*. The impact categories selected are the three endpoints of the ReCiPe 2016 Hierarchist (H) method[51], which considers a time horizon of 100 years. These metrics correspond to the protection of human health, natural environment and resource scarcity, i.e., damage to human health (HH) [DALY], damage to ecosystem quality (ED) [Species.yr] and damage to mineral and fossil resource availability (RA) [USD_{2013}], respectively. LCIA provides environmental scores to facilitate the interpretation of the LCA results[281]. The categories selected in our work are particularly meaningful for BECCS, a land-based mitigation technology that consumes resources and competes with other human primary needs, e.g., food production.

Interpretation. The results interpretation is performed by analyzing the solutions provided by the optimization model integrating LCA principles.

5.4. Mathematical model and life cycle impacts

The model presented here, referred to as NETCOM (**N**egative **E**missions **T**echnologies **CO**operation **M**odel), provides a snapshot of the optimal BECCS SCs to meet a given CDR target in any given year rather than the best pathway to achieve the cumulative CDR target in 2100. NETCOM has been implemented in GAMS[46] 30.3.0 on an Intel 1.8 GHz machine and solved with CPLEX. The emission and environmental activities have been calculated in SimaPro 9.0.0.48[279], using Ecoinvent v3.5[280] and the ReCiPe 2016 Hierarchist (H) method. The mathematical model comprises techno-economic, environmental constraints and objective functions-related equations, with 1,121,041 variables and 1,077,348 equations in total.

The mathematical model reported hereunder and represented in Figure 5.2 only shows the life cycle impacts equations. The underlying mass and energy balances, as well as emission and cost equations, are reported in Appendix D.

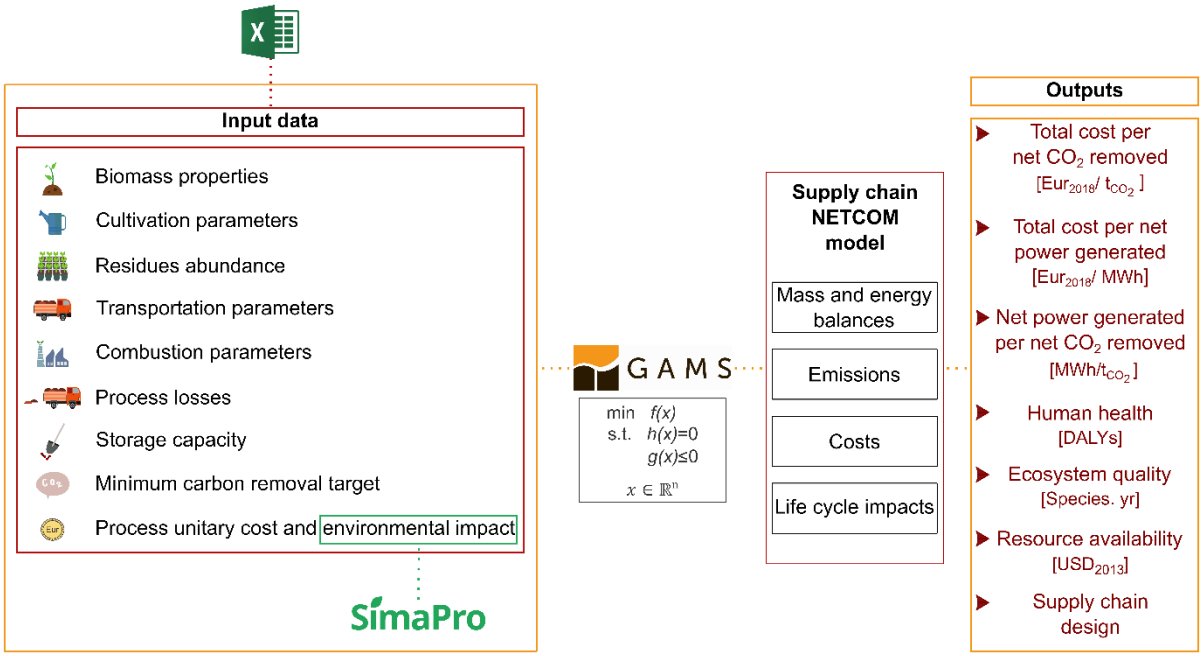

Figure 5.2: NETCOM optimization model. The output variables are computed in GAMS from the input data collected on a spreadsheet, either sourced from literature studies or calculated based on these or the Ecoinvent database in SimaPro. Mass and energy balances, emissions and cost equations are reported in Appendix D.

5.4.1 Biomass growth and cultivation stage

The cultivation stage entails two opposing contributions to the environmental impacts. On the one hand, Eq. (5.1) models the negative emissions, i.e., the CO_2 removed from the atmosphere during the biomass growth. Each activity-specific ecovector is retrieved from Ecoinvent accessed *via* SimaPro. Each ecovector (ECOVEC) includes the ReCiPe 2016 mid- and endpoint impacts of each stage of the SC per unit of stressor, following a hierarchist perspective. The ecovector ($\mathrm{ECOVEC}_{\mathrm{ibe}}^{\mathrm{grw}}$) contains the benefits deriving from the negative CO_2 emissions (em_{ib}^{grw}) at the mid- and endpoints for each biomass type b in country i. The gross negative impact is embedded in the variable $impact_{ibe}^{grw}$. In this process, the CO_2 is absorbed from the atmosphere and therefore contributes to bringing impacts down.

$$impact_{ibe}^{grw} = em_{ib}^{grw}\mathrm{ECOVEC}_{\mathrm{ibe}}^{\mathrm{grw}} \quad \forall i, b, e \tag{5.1}$$

The other -opposite- contributions of cultivation to the total damage are related to farming and include the impacts of the use of land, land-use change (LUC) and those associated with biomass losses. The impact of land use ($impact_{ibe}^{land}$) results from the use of fertilizers, pesticides and other farm inputs that are harmful to the environment. The $\mathrm{ECOVEC}_{\mathrm{ibe}}^{\mathrm{land}}$

parameter includes the impacts associated with these farm inputs, modeled from the FEAT database (Table D0.23) for the cultivation of 1 ha of $land_{ib}$ of each biomass feedstock of type energy crop (*EC*) (Eq. (5.2)).

$$impact_{ibe}^{land} = land_{ib}\mathrm{ECOVEC}_{\mathrm{ibe}}^{\mathrm{land}} \quad \forall i, b, e \in EC \tag{5.2}$$

At the cultivation stage, residues are assumed to have no impact and, consequently, the variable $impact_{ibe}^{land}$ is set to zero in Eq. (5.3). The amount of residues available in each country already assumes environmentally-compatible production[282]. Higher amounts of biomass utilized could indeed increase the pressure on the environment.

$$impact_{ibe}^{land} = 0 \quad \forall i, b, e \in RD \tag{5.3}$$

The losses occurring at the cultivation stage represent an additional impact source that needs to be considered. These impacts ($impact_{ibe}^{landloss}$) stem from the release of carbon from decayed biomass and they are calculated based on the land loss emissions ($em_{ib}^{landloss}$) and the corresponding ecovector ($\mathrm{ECOVEC}_{ibe}^{landloss}$). Once the CO_2 emissions have been calculated, the ecovector translates each ton of CO_2 released into the corresponding contribution to mid- and endpoints. Note that this is only applicable for the impact of energy crops (Eq. (5.4)) since residues are allocated no impact and therefore their impact ($impact_{ibe}^{landloss}$) is set to zero in Eq. (5.5).

$$impact_{ibe}^{landloss} = em_{ib}^{landloss}\,\mathrm{ECOVEC}_{ibe}^{landloss} \quad \forall i, b, e \in EC \tag{5.4}$$

$$impact_{ibe}^{landloss} = 0 \quad \forall i, b, e \in RD \tag{5.5}$$

Here we consider the effect of LUC on the environment due to the change of the purpose of the land, from marginal to agricultural land. It is calculated based on the amount of land used ($land_{ib}$) and the corresponding ecovector ($\mathrm{ECOVEC}_{\mathrm{ibe}}^{\mathrm{luc}}$), referred to 1 ha (Eq. (5.6)). LUC impact is usually negligible in the case of marginal land, while the activity chosen from Ecoinvent in SimaPro considers not only marginal land, but also different land types. Therefore, $impact_{ibe}^{luc}$ overestimates the true impact.

$$impact_{ibe}^{luc} = land_{ib}\,\mathrm{ECOVEC}_{\mathrm{ibe}}^{\mathrm{luc}} \quad \forall i, b, e \in EC \tag{5.6}$$

The impact of residues (biomass type of the set *RD*) for LUC $impact_{ibe}^{luc}$ is not considered, as shown in Eq. (5.7), because it is assumed that the impact of the cultivation stage is allocated to the original product.

$$impact_{ibe}^{luc} = 0 \quad \forall i, b, e \in RD \tag{5.7}$$

5.4.2 Processing into bales or chips

The biomass harvested is processed on the cultivation site into bales or chips. The activity of baling is retrieved from SimaPro as reported in Appendix D Table D0.22. It considers primarily machines, but also emissions to air and soil. The reference flow used for the calculation of the impact $impact_{ibe}^{bal}$ is 1 bale, equivalent to 160 kg of straw (Ecoinvent[280] from FAOSTAT data 2011). In Eq. (5.8) the conversion is already considered in $\mathrm{ECOVEC}_{\mathrm{ibe}}^{\mathrm{bal}}$ to calculate the impact of the number of bales produced $prod_{ib}^{bal}$ at mid- and endpoints.

$$impact_{ibe}^{bal} = prod_{ib}^{bal}\ \mathrm{ECOVEC}_{\mathrm{ibe}}^{\mathrm{bal}} \quad \forall i, b, e \tag{5.8}$$

As for the case of baling, the chipping activity is retrieved from Ecoinvent interfaced with SimaPro and reported in Table D0.22. $\mathrm{ECOVEC}_{\mathrm{ibe}}^{\mathrm{chip}}$ includes the contributions of machinery and electricity for the production of 1 t of chips. The environmental impact ($impact_{ibe}^{chip}$) is calculated based on the amount of chips produced $prod_{ib}^{chip}$ on a wet basis in Eq. (5.9).

$$impact_{ibe}^{chip} = prod_{ib}^{chip}\ \mathrm{ECOVEC}_{\mathrm{ibe}}^{\mathrm{chip}} \quad \forall i, b, e \tag{5.9}$$

The impacts of the losses of the baling and chipping processes are considered proportional to the direct emissions due to the decay of biomass losses occurring during baling ($em_{ib}^{balloss}$) and chipping ($em_{ib}^{chiploss}$). $\mathrm{ECOVEC}_{ibe}^{balloss}$ and $\mathrm{ECOVEC}_{ibe}^{chiploss}$ embed the impact of losses of 1 t of CO_2 and they are used to calculate $impact_{ibe}^{balloss}$ and $impact_{ibe}^{chiploss}$ in Eqs. (5.10) and (5.11) for baling and chipping, respectively.

$$impact_{ibe}^{balloss} = em_{ib}^{balloss}\mathrm{ECOVEC}_{ibe}^{balloss} \quad \forall i, b, e \tag{5.10}$$

$$impact_{ibe}^{chiploss} = em_{ib}^{chiploss}\ \mathrm{ECOVEC}_{ibe}^{chiploss} \quad \forall i, b, e \tag{5.11}$$

5.4.3 Transport from farmland to the processing site

Chips and bales are transported from the cultivation site to the pelleting plant for further processing. The transportation activity is retrieved from SimaPro (Appendix D), from which $\mathrm{ECOVEC}_{ibve}^{tlp}$ is calculated per tkm. The impact ($impact_{ii'be}^{tlp}$) in Eq. (5.12) depends on the amount of bales and chips transported ($tlp_{ii'bv}^{bal}$ or $tlp_{ii'bv}^{chip}$), the distance between the countries *i* and *i'* ($\mathrm{DIST}_{\mathrm{vii'}}$) and the correction factors for bales and chips ($\mathrm{CORF}_{\mathrm{v}}^{\mathrm{bal}}$ and $\mathrm{CORF}_{\mathrm{v}}^{\mathrm{chip}}$). The correction factors are used to relate the density of the biomass to the capacity of the transportation mean, as explained in Appendix D.

$$impact_{ii'be}^{tlp} = \sum_{v} (\mathrm{DIST}_{\mathrm{vii'}} \mathrm{ECOVEC}_{ibve}^{tlp} \Big(\mathrm{CORF}_{\mathrm{v}}^{\mathrm{bal}} tlp_{ii'bv}^{bal} + \mathrm{CORF}_{\mathrm{v}}^{\mathrm{chip}} tlp_{ii'bv}^{chip} \Big)) \quad \forall i, i', b, e \tag{5.12}$$

The losses of biomass that occur during transportation ($em_{ii'b}^{tlploss}$) are related to the impact of this activity $impact_{ii'be}^{tlploss}$ using the ecovector of impacts of losses at mid- and endpoints ($\mathrm{ECOVEC}_{ibe}^{tlploss}$) in Eq. (5.13).

$$impact_{ii'be}^{tlploss} = em_{ii'b}^{tlploss} \, \mathrm{ECOVEC}_{ibe}^{tlploss} \quad \forall i, i', b, e \tag{5.13}$$

5.4.4 Pelleting stage

Bales and chips are transported from the farmland to the pelleting stage, which is modeled in SimaPro (Table D0.22). The ecovector $\mathrm{ECOVEC}_{ibe}^{pro}$ includes the equipment used in the activity, in addition to water and production wastes to calculate the impact of 1 t of pellets at the mid- and endpoints (Eq. (5.14)). The total impact $impact_{ibe}^{pro}$ depends on the amount of pellets produced $pellet_{ib}^{pro}$, where here the parameter $\mathrm{ECOVEC}_{ibe}^{pro}$ already accounts for the transformation from dry basis (product output of Ecoinvent).

$$impact_{ibe}^{pro} = pellet_{ib}^{pro} \mathrm{ECOVEC}_{ibe}^{pro} \quad \forall i, b, e \tag{5.14}$$

The pelleting process also includes biomass losses which contribute to the total environmental impact. The impact of losses derived from processing the biomass into pellets ($impact_{ibe}^{proloss}$) is considered in Eq. (5.15) based on the emissions associated with the decay of biomass losses

produced at the pelleting stage ($em_{ib}^{proloss}$). The ecovector of the mid- and endpoints is of 1 t CO_2 ($\mathrm{ECOVEC}_{ibe}^{proloss}$) relates the pelleting direct emissions to the impacts.

$$impact_{ibe}^{proloss} = em_{ib}^{proloss}\ \mathrm{ECOVEC}_{ibe}^{proloss}\ \ \forall i, b, e \tag{5.15}$$

5.4.5 Transport from pelleting to the combustion plant

Once the biomass has been transformed into pellets, it is transported to the power plant to be combusted for electricity production. The activity used to model $impact_{ii'be}^{tpc}$ in Eq. (5.16) is the same as in Eq. (5.12). The impact is calculated based on the amount of pellets transported ($tpc_{ii'bv}^{pell}$), the distance between the countries $\mathrm{DIST}_{\mathrm{vii'}}$ and the relation between the density of the transportation mode and the one of the biomass ($\mathrm{CORF}_{\mathrm{v}}^{\mathrm{pell}}$).

$$impact_{ii'be}^{tpc} = \sum_{v} \mathrm{DIST}_{\mathrm{vii'}} \mathrm{CORF}_{\mathrm{v}}^{\mathrm{pell}} tpc_{ii'bv}^{pell}\ \mathrm{ECOVEC}_{ibve}^{tpc}\ \ \forall i, i', b, e \tag{5.16}$$

Eq. (5.17) relates the losses occurred during the transportation of the pellets ($em_{ii'b}^{tpcloss}$) to the impact $impact_{ii'be}^{tpcloss}$, based on the impacts at mid- and endpoint embedded in $\mathrm{ECOVEC}_{ibe}^{tpcloss}$.

$$impact_{ii'be}^{tpcloss} = em_{ii'b}^{tpcloss} \mathrm{ECOVEC}_{ibe}^{tpcloss}\ \ \forall i, i', b, e \tag{5.17}$$

5.4.6 Power generation

At the power generation plant, only direct CO_2 emissions are considered, while the infrastructure or the utilities and other emissions such as nitrogen oxides deriving from the combustion are omitted. In Eq. (5.18) the impacts of the direct emissions ($impact_{ibe}^{pow}$) are calculated based on the amount of CO_2 released into the atmosphere (what is not captured by the monoethanolamine (MEA) post-combustion unit). The ecovector of impacts at the mid- and endpoints embedded in $\mathrm{ECOVEC}_{ibe}^{pow}$ links the impacts to the direct emissions (em_{ib}^{pow}).

$$impact_{ibe}^{pow} = em_{ib}^{pow}\ \mathrm{ECOVEC}_{ibe}^{pow}\ \ \forall i, b, e \tag{5.18}$$

5.4.7 CO_2 transportation and storage

The impact of the CO_2 transportation $impact_{ii'e}^{p2s}$ in Eq. (5.19) has been modeled in Ecoinvent interfaced with SimaPro from the inventory proposed by Wildbolz[283] and it depends on the amount of CO_2 transported via pipeline $tCO2_{i'i}^{p2s}$ and the distance between the combustion plant and the storage site $\mathrm{DIST}_{ii'}^{\mathrm{pipe}}$. The mid- and endpoints per 1 tkm are calculated and included in $\mathrm{ECOVEC}_{ibe}^{p2s}$. The inventory of the activity used in SimaPro is reported in Table D0.22 in Appendix D.

$$impact_{ii'e}^{p2s} = \mathrm{DIST}_{ii'}^{\mathrm{totpipe}}\ tCO2_{i'i}^{p2s}\,\mathrm{ECOVEC}_{ie}^{p2s} \quad \forall i, i', e \tag{5.19}$$

As in the previous stage, the injection of CO_2 is modeled in SimaPro according to the inventories reported in Wildbolz[283] and the impact depends on the amount of CO_2 stored in each site $CO2_{i,g}^{site}$. The reference flow used to calculate the impact of the different storage sites $impact_{ibge}^{site}$ using the ecovector $\mathrm{ECOVEC}_{ibge}^{site}$ is 1 t CO_2 stored (see Eq. (5.20)).

$$impact_{ige}^{site} = CO2_{i,g}^{site}\,\mathrm{ECOVEC}_{ige}^{site} \quad \forall i, g, e \tag{5.20}$$

5.4.8 Global impact

$$\begin{aligned} imp_e = \sum_i \sum_b \big(& impact_{ibe}^{grw} + impact_{ibe}^{land} + impact_{ibe}^{luc} + impact_{ibe}^{chip} \\ & + impact_{ibe}^{bal} + impact_{ibe}^{landloss} + impact_{ibe}^{chiploss} + impact_{ibe}^{balloss} \big) \\ & + \sum_i \sum_b \sum_{i'} \Big(\big(impact_{ii'be}^{tlp} + impact_{ii'be}^{tlploss} \big) \mathrm{W} + \big(impact_{i'ibe}^{tlp} \\ & + impact_{ii'be}^{tlploss} \big)(1 - \mathrm{W}) \Big) + \sum_i \sum_b impact_{ibe}^{pro} \\ & + \sum_i \sum_b \sum_{i'} \big((impact_{ii'be}^{tpc} + impact_{ii'be}^{tpcloss})\mathrm{W} \ + (impact_{i'ibe}^{tpc} \\ & + impact_{ii'be}^{tpcloss})(1 - \mathrm{W}\ ) \big) + \sum_i \sum_b impact_{ibe}^{pow} \\ & + \sum_i \sum_{i'} \big(impact_{ii'e}^{t2s}\mathrm{W} \ + impact_{i'ie}^{t2s}(1 - \mathrm{W}\ ) \big) \\ & + \sum_i \sum_g impact_{ige}^{site} \qquad \forall e \in E \end{aligned} \tag{5.21}$$

The total environmental impact on the mid- and endpoints in each country *i* (imp_e) is calculated in Eq. (5.21), where W symbolizes the share of the impact between country *i* and *i'*.

5.4.9 Objective functions

We consider four objectives for the LCO problem detailed above, i.e., the total cost and the three endpoints of the ReCiPe 2016 (human health, ecosystems and resources). The total cost of the SCs ($gloco$) is calculated in Eq. (5.22), while the three different endpoint categories included in e - human health (hh), ecosystem quality (ed) and resource availability (ra) - are expressed in Eqs. (5.23) – (5.25).

$$gloco = \sum_i co_i \tag{5.22}$$

$$hh = imp_e \quad \forall e = \text{human health} \tag{5.23}$$

$$ed = imp_e \quad \forall e = \text{ecosystem quality} \tag{5.24}$$

$$ra = imp_e \quad \forall e = \text{resource availability} \tag{5.25}$$

For simplicity, we analyze only the single-objective solutions resulting from optimizing one separate objective at a time. To make these solutions comparable, the value of the net electricity produced by BECCS ($\text{NETELGEN}^{\text{mincost}}$), calculated for the minimum cost case has been fixed in the other solutions as an additional constraint (Eq. (5.26)).

$$\text{NETELGEN}^{\text{mincost}} = \sum_i (\sum_b (elgen_{ib}^{pow}) - elccs_i^{pow} - elcom_i^{pow}) \tag{5.26}$$

The optimization problem can, therefore, be expressed in compact form (Eq. (5.27)).

$$\begin{aligned} & min_x \quad \sum_{i \in I} \sum_{b \in B} c_{ib}^T x_{ib} \\ & s.t. \quad \sum_{i \in P} \sum_{b \in B} em_{ib} x_{ib} \leq TG \\ & \quad A_{ib} x_{ib} \leq a_{ib} \quad \forall i \in I, b \in B \\ & \quad x \in \mathbb{R} \end{aligned} \tag{5.27}$$

Here, the objective function changes for each scenario: the total cost in the first scenario (Eq. (5.22)), and the three environmental endpoints (Eq.(5.23)-(5.25)) in the others. The problem is subject to the constraints included in Appendix D, in addition to Eq. (5.26) for the environmental scenarios.

Since multiple SC configurations are possible in the case of a degenerative solution, for each environmental scenario the minimal cost solution is sought using an ε-constrained method. To this end, we first perform a LCO on one of the endpoints and, for the value obtained, we minimize the total cost of the SC. This is equivalent to ensuring these anchor points are strong Pareto in the bi-dimensional space of given endpoint-cost.

Note that the main purpose of the BECCS here is to deliver negative emissions, relegating electricity supply to a secondary consideration. Consequently, the model does not include environmental nor economic credits for the electricity produced in any of the scenarios analyzed, as the SC is not linked to the power sector. If considered, this would substantially decrease the total cost of the supply chain and have an impact on the three endpoints.

5.5. Results and discussion

5.5.1 Overview of the optimal scenarios

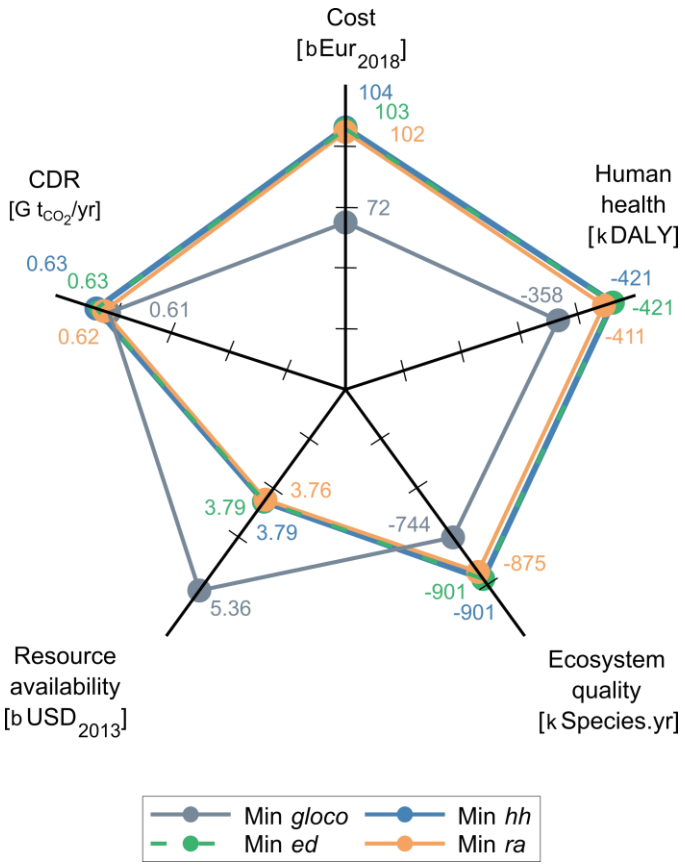

Figure 5.3: Overview of the four optimized scenarios. Each axis displays a variable of interest: cost [Eur_{2018}], net removal of carbon dioxide (t_{CO_2}), human health [DALY], ecosystem quality [Species.yr] and resource availability [USD_{2013}].

An overview of the four scenarios investigated and the values of the respective objective functions is shown in Figure 5.3, in addition to the net carbon dioxide removal [t_{CO_2}] for each of the extreme Pareto solutions to the problem. In the plot, the grey pentagon represents the solution to the first optimization problem: the minimization of the total cost of the SC. This case is taken as a baseline to analyze the performances of the other solutions in a second step, with a fixed net electricity production of 511 TWh, calculated according to Eq. (5.26). Figure 5.3 illustrates that the blue and the green pentagons, the minimum human health and minimum ecosystem quality scenario, respectively, nearly overlap, meaning that the two solutions present similar decisions provided by the optimization model. The total cost of these two solutions differs by only 0.5%, while both achieve a CDR of 0.63 G tCO_2. The distinction between the two scenarios is given by minor differences in the configuration of the SCs at the regional level, which will be explained in the next section. Lastly, the orange pentagon corresponds to the minimum resource availability solution.

The results indicate that BECCS provides credits for human health and ecosystem quality in all the scenarios analyzed, because they reach negative values, despite depleting resource availability, which is, in turn, a positive figure. Credits for human health can be interpreted as years of sickness that would be avoided or deaths potentially prevented, while for ecosystems quality they represent species whose extinction would be averted. These credits are the result of the CO_2 uptake, which is removed permanently. Compared to the minimum cost solution, an improvement in human health of 18% and a 21% reduction of ecosystem quality can be achieved at the expense of an increase in the total cost of almost 45%. Furthermore, a 30% decrease in impact on resource availability can be attained at an additional financial cost of 43%. These improvements are achieved by changing the configuration of the SC in the EU-28. While an increase in the total cost can be intuitively understood and easily compared among different scenarios, the improvement of deleterious impacts requires further explanation. Negative values of the environmental indicators (i.e., total emissions, human health, ecosystem quality or resource availability) imply that impacts are prevented. These negative values denote environmental credits that are beneficial to the environment, e.g., preventing human or species loss.

The target imposed on net carbon removal is an active constraint in the case of the minimum cost scenario, because of the trade-off between costs and environmental performance, i.e., removing more carbon leads to higher costs. By contrast, the environmental scenarios deliver

more CDR than required by the target (i.e., more than 0.61 $GtCO_2$/year removed). In the latter case, roughly the same amount of biomass is deployed and, therefore, the same amount of CO_2 is captured, owing to the electricity generation target, but the life cycle emissions are greatly reduced. This is because the minimization of the environmental objectives is driven by the CDR delivered: indeed, negative emissions signify that CO_2 is removed from the atmosphere and this is precisely one of the main stressors affecting both human health and ecosystem quality.

Table 5.1 shows the cost of the optimal SC design per net CO_2 removal for each scenario. The results reported consider the balance between negative (CO_2 uptake) and positive (direct and indirect) emissions, and the cost per net electricity produced, i.e., discounting the energy required for the CO_2 capture, regeneration of the solvent and the compression of CO_2. As seen, the economic performance per unit of CO_2 and electricity worsens substantially as we move from the minimum cost to the minimum impact solutions, yet the latter removes more CO_2 per unit of electricity generated.

The results obtained indicate that the BECCS SCs designed for the EU-28 based on a model of cooperation can deliver the CDR target imposed and simultaneously provide a secure and renewable source of electricity[21,199], which represents more than 70% of the 2018 electricity demand of the residential sector in the EU[284]. At a levelized cost of electricity of 124 Eur_{2018}/MWh[285] for biomass combustion technologies, the electricity produced could lead to a revenue of 63 billion Eur_{2018}, which represents more than 85% of the total cost in the minimum cost scenario SC.

In addition to the electricity production, bio-based fuels and heat will boost the reduction of transportation and processes carbon footprint if they will replace the current fossil-based options. Several models already identified that the deployment of BECCS in the bioenergy sector to be well above 50% already in 2050[55][286]. Additionally, it is expected that the costs reported in Table 5.1 will decrease considering the technology learning curve.

For comparative purposes, we report the impact of 511 TWh generated with the 2018 EU-28 power mix, assuming no CDR deployment. The electricity generation with conventional power mix leads to an impact on human health of 459 kDALY, on ecosystem quality of 1.09 kSpecies.yr and a depletion of resource availability of 13.1 $bUSD_{2013}$. In contrast, the same

electricity production *via* BECCS generates credits for human health and ecosystem quality, while the impact on resource availability is halved.

Table 5.1: Total cost of the BECCS SC per net ton of carbon dioxide removed and net electricity production for each scenario investigated. The net electricity generated per net removal is also calculated. The cost increases sharply when shifting from the minimum cost to the minimum impact solutions.

Scenario	Cost per net ton removed [Eur$_{2018}$/t_{CO_2}]	Cost per net MWh produced [Eur$_{2018}$/MWh]	Net MWh produced per net ton removed [MWh/t_{CO_2}]
Min $gloco$	117	140	0.84
Min hh	164	203	0.81
Min ed	163	202	0.81
Min ra	165	200	0.83

5.5.2 Breakdown of cost and emissions

The main share of the cost (Figure 5.4, subplot (a)) is at the combustion stage (60% of the total cost for the minimum cost solution). Additional critical stages are pelleting, transportation to the pelleting site and storage, which contribute more than 10% of the total cost. Indeed, pelleting and combustion are highly energy-intensive processes, while transportation requires fuels inputs, in addition to labor and maintenance. The effect of transportation is also higher in reaching the pelleting stage than between pelleting and the combustion plant because of the lower density of the biomass (note that during the pelleting stage the biomass is dried and therefore the density increases, in addition to the reduced volume).

The same trend can be observed in the breakdown of the total emissions in Figure 5.4, subplot (b). In this case, the emissions are linked to the activity's carbon intensity factor. Transportation, pelleting and combustion are the principal sources of positive emissions, with the chipping stage playing a significant role as well. In the case of transportation (making up about 30% of the positive emissions) the emissions are related to the fuel consumption, whereas the heat and electricity requirements for chipping and pelleting lead to positive emissions of 16% and 30%, respectively. It is worth noting again that the emissions at the combustion stage only include the share of CO_2 that is not captured by the MEA plant. However, the positive contributions are offset by the negative emissions of the biomass growth stage (CO_2 uptake) such that, the process is overall carbon negative (as indicated by the red star in Figure 5.4 (b)).

The results show that the three minimum impact solutions lead to very similar results in terms of total cost and emissions. These three solutions are forced to produce the same amount of net electricity (related to the amount of biomass combusted) and the same minimum CDR potential (also linked to the amount of biomass due to the CO_2 absorbed during growth). Only when minimizing the total cost do significant differences appear, which are driven by the asymmetric regionalized costs linked to purchasing power parity (PPP). Among other things, this leads to a higher contribution of transportation in the minimum cost scenario than in the minimum environmental impacts, as explained in the following section.

From Figure 5.4, we can conclude that technical improvements aimed at reducing costs and emissions should focus on the pelleting and combustion stages. Combining two or more SC echelons, e.g., pelleting the biomass right after the first biomass processing step in the same location, could help lower costs and impacts by removing the requirement for biomass transportation.

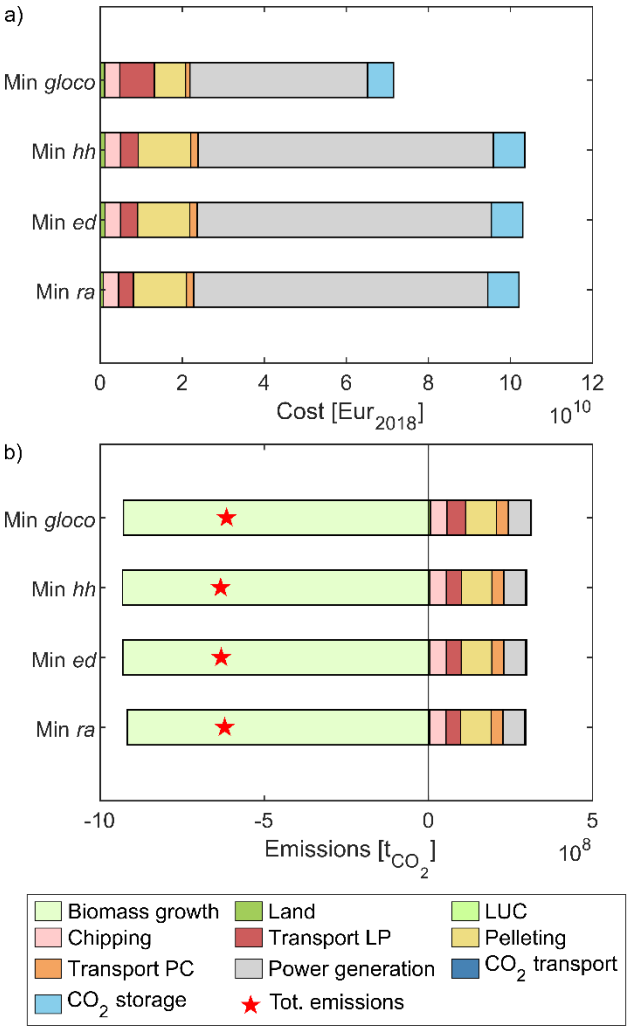

Figure 5.4: Breakdown of costs and emissions of the BECCS SCs for each scenario. Subplot a) shows the breakdown of the total cost, while subplot b) corresponds to the emissions breakdown. The stacked bar plots represent the contribution of each activity on the total cost and emission. LP = farmland to pelleting, PC = pelleting to combustion. The red star represents the net emissions value, which is negative in all four cases.

5.5.3 Life cycle assessment endpoints breakdown

Figure 5.5 shows the contributions of individual SC stages to the environmental endpoints, i.e., (a) minimum human health, (b) ecosystem quality and (c) resource availability.

In all the scenarios chipping, combustion and especially pelleting have the most significant positive impact per ton of biomass in all endpoint categories. The contribution of pelleting is conspicuously high due to the electricity and heat requirements to dry the biomass. Furthermore, CO_2 transportation and storage play a crucial role in the impact on resource availability because of the infrastructure and input materials needed[283]. Biomass transportation from land to pelleting plants substantially contributes to worsening the environmental performance of the SC due to the large distances between countries and the feedstock's low

density (accounted for in the correction factor $CORF_v$). On the other hand, the impacts of land usage and LUC are less relevant because of the extensive use of residues are assumed to have no impact. However, more land is cultivated in the minimum cost solution (1.95 Mha) than in the environmental scenarios (1.20-1.35 Mha), resulting in an impact of land in the latter equivalent to 60-70% of that of the minimum cost solution.

Figure 5.5 shows that the primary difference between the first scenario and the minimum impacts cases is a great reduction in the impact of transportation of the biomass from the land to the pelleting stage (LP). As a result of more decentralized SCs, the transportation occurs within the borders of each country, which results in shorter distances. This leads to a noticeable reduction of the impacts of transportation: e.g., transportation LP almost halves in the three minimum environmental impacts scenarios compared to the minimum cost scenario, from 82 kDALY to 45 kDALY on average. All the SCs consider the chipping of the biomass rather than baling because the former results in a lower impact. Similarly, transportation by train is preferred over lorry for land connections for the amount transported. Lastly, saline formations offer better environmental performance than coal seams or depleted hydrocarbon sites due to the smaller required drilling area [283].

Overall, BECCS can lead to negative endpoints in human health and ecosystem quality due to the uptake of carbon dioxide during biomass growth. Indeed, the main stressor of human health is CO_2, in addition to particulate formation. CO_2 is also the primary stressor of ecosystem quality, together with land use. Negative results in these two endpoints therefore imply that we can prevent the loss of years of life [DALYs] or species [Species.yr] by meeting the given CDR target.

While we present the aggregated environmental indicators here, we refer to Appendix D (Figure D0.1) for the breakdown of the midpoints of each optimal ReCiPe 2016 endpoint calculated.

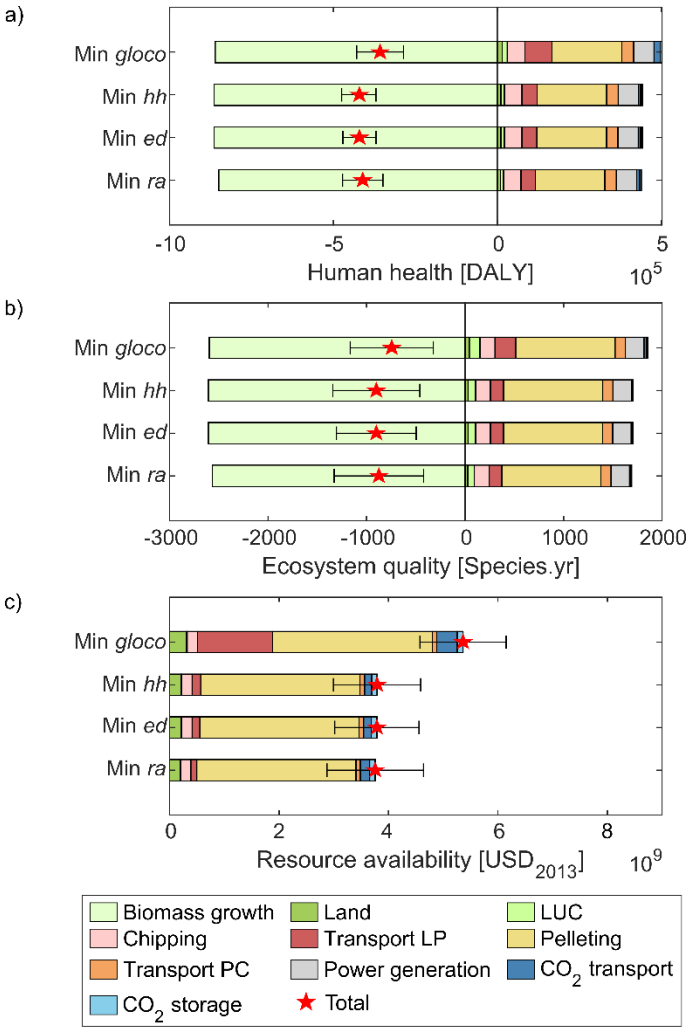

Figure 5.5: Breakdown of the three LCA endpoint solutions human health a), ecosystem quality b) and resource availability c) for each scenario. The stacked barplots represent the contribution of the individual activities on the total of each endpoint. LP = farmland to pelleting, PC = pelleting to combustion. The star represents the net effect on human health and ecosystem quality, negative in all cases. The error bars represent the uncertainty of the data calculated as the standard deviation of 1000 scenarios generated in SimaPro using Monte Carlo sampling. The limits of the error bars denote the worst- and best-case scenario of the total impact.

5.5.4 Regional implications

In all the optimal solutions, the CDR target is satisfied almost entirely by the residues feedstock. Residue availability is exploited in all scenarios, as it is assumed to have negligible costs and environmental impacts (the percentage of residues deployed in each scenario is reported in Appendix D, Figure D0.2). Only *Miscanthus* is selected among the available energy crops because of its higher yield [t_{wb}/ha/yr] in all the countries considered, as well as its high carbon content [%C in wet biomass]. Hence, more crops can be harvested and more CO_2 can be sequestered. At the next step, in all the studied scenarios, all the harvested biomass is converted into chips. In every case, every country is exporting biomass at a certain stage of the SC except Bulgaria, Poland and Romania, where indigenous biomass is harvested, processed, combusted and stored domestically. In the minimum total cost solution, these three countries are the only ones deploying a complete SC spanning from biomass harvest to CO_2 stored. This is because these countries offer the lowest processing costs per unit of biomass at each stage.

Minimization of the three environmental endpoints results in common modeling choices in the design of the SCs. The biomass feedstock consists of all the residues available and *Miscanthus* as the only energy crop harvested; biomass transportation occurs *via* train and ship; saline storage is the preferred option for CO_2 storage.

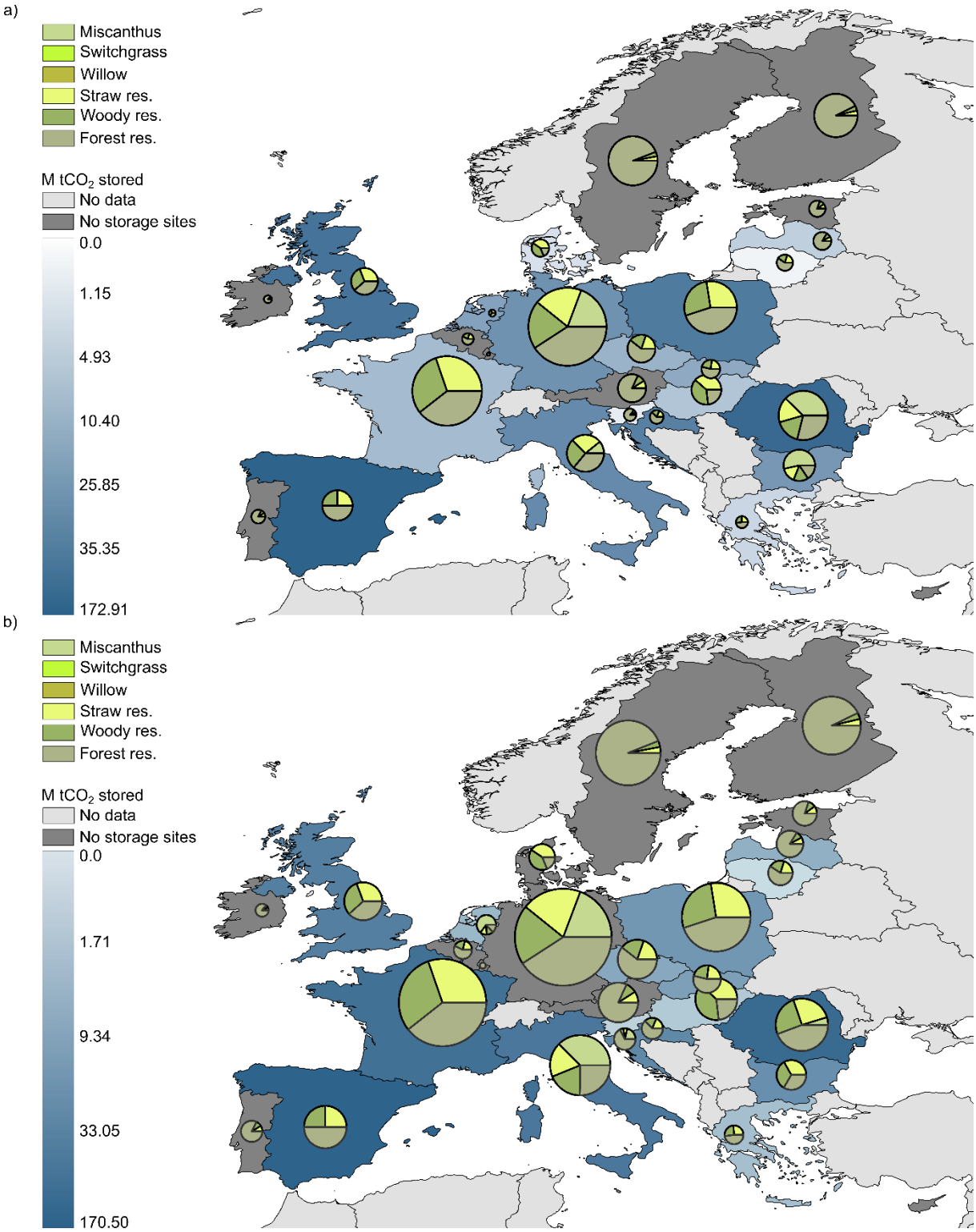

Figure 5.6: Biomass growth and CO_2 storage for the minimum cost a) and minimum human health b) scenarios. The size of the pie chart is proportional to the amount of CO_2 absorbed by each type of biomass feedstock (wet basis) *via* photosynthesis during the growth, with Cyprus being the reference point, while the countries are color-coded according to the amount of CO_2 stored.

In the following paragraphs we provide a detailed description of the minimum cost and minimum human health scenarios.

The amount of CO_2 absorbed by each type of biomass feedstock on a wet basis during photosynthesis and the amount of CO_2 stored by each country are shown in Figure 5.6 for the (a) minimum cost and (b) minimum human health scenarios (as representative of the environmental scenarios). The pie charts are scaled based on the minimum amount of CO_2 absorbed, for which Cyprus is taken as the reference point. In both cases, the strong reliance on residues to achieve the CDR is evident, with Germany and France being the countries with the greatest availability of secondary biomass[282]. However, in the minimum cost solution, *Miscanthus* is grown in Bulgaria, Germany, Italy and Romania, while in the minimum human health scenario, this is done in Germany, Italy, the Netherlands, Romania and Slovenia. The harvesting location is chosen primarily based on the yield and how much carbon the biomass can absorb, in addition to the cost of cultivation. The latter is a key parameter in the case of the minimum cost scenario, because it drives the choice of the cultivation site. In the above-mentioned scenarios, not all the available land is used in the countries mentioned, as the CDR target is already met.

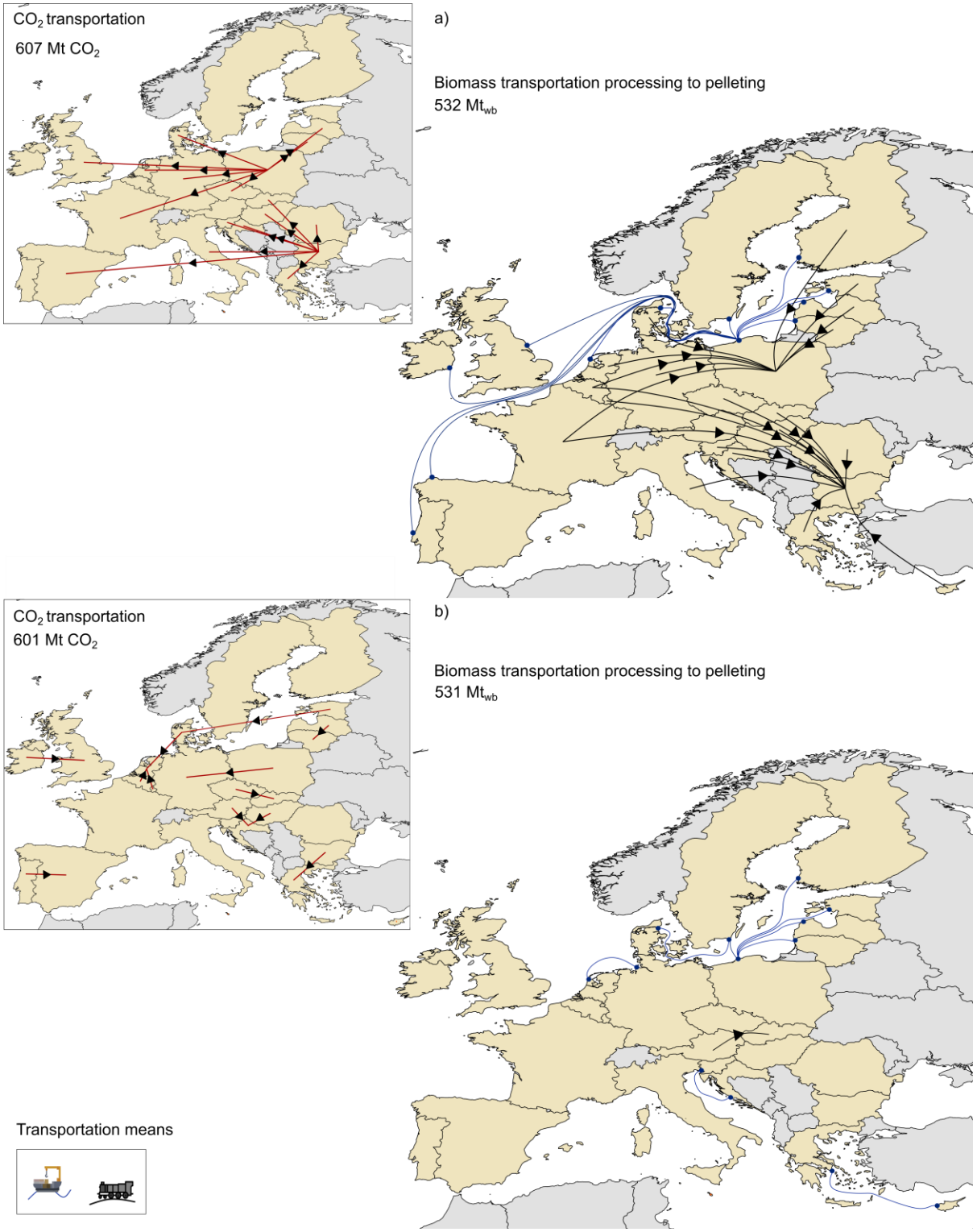

Figure 5.7: Supply chain configuration for the minimum cost (a) and minimum human health (b) scenarios. The main plots on the right refer to biomass transportation from the land to the pelleting stage, where the transportation means are indicated in black for train and blue for ship. The inserts in the top left corner represent the connections for the CO_2 transportation, where the CO_2 pipeline connections between two countries are represented by red lines.

Cost and human health LCO problems represent two opposite configurations which are displayed in Figure 5.7. On the one hand, the minimum cost solution is a centralized SC where

all the biomass feedstock is sent to Bulgaria and Poland, to take advantage of the lower processing costs. On the other hand, in the minimum human health solution, all the countries are actively involved at all SC stages, except for the storage stage, which depends on geological availability.

In the minimum cost solution, the biomass is transported by train (black line, Figure 5.7) to Bulgaria and Poland from other countries, or by ship from locations with maritime access (e.g., Spain, Denmark, Finland). Transportation of biomass *via* ship (blue lines, Figure 5.7) is favorable from both economic and environmental perspectives.

In the minimum human health scenario, transportation across borders takes place only for a few countries and mainly *via* ship or *via* pipeline due to limited storage capacity. For example, Sweden has no geological sites and features processing and combusting costs that are among the highest in the EU; thus, shipping biomass chips abroad is preferred. To minimize the cost, CO_2 is stored in coal seams and depleted hydrocarbon sites, while saline formations are preferred to reduce the environmental impact because of the lower drilling area required[283]. Due to limited geological capacity, only 20 countries can permanently lock away domestically absorbed CO_2 from the atmosphere, while a network of pipelines across the EU is built to transport the remaining CO_2 captured among the other countries.

The configuration of the SCs of minimum ecosystem quality and resource availability are designed similarly to the one of the human health scenario for the reasons explained above. In particular, ecosystem quality and human health lead to remarkably comparable configurations as well as total cost and emissions. At a regional level, only a few aspects of these two models are different. In the ecosystem quality solution, a pelleting site, not present in the human health solution, is installed in Finland to process biomass into chips. Meanwhile, Germany and Slovakia store CO_2 from Latvia and Austria, respectively. Finally, the transportation of biomass *via* ship from the land to the pelleting stage is less frequent than in the minimum human health scenario. The reason for this is that, for a given amount of biomass, there are different breakeven distances in the two cases for which using trains is more or less advantageous than ships. A more comprehensive explanation of the design of the SCs in each scenario can be found in Appendix D.

5.6. Conclusions

During this investigation of the optimal design of a BECCS supply chain to deliver a specific amount of carbon dioxide removal, we considered four different objectives: the total cost and three life cycle impacts. We have proposed a model to design supply chains based on cooperation among the EU-28 members, which would profit from regional components, but also address shortfalls at the national level, e.g., lack of geological storage.

Our results show that the target of negative CO_2 emissions can be met in the minimum cost scenario by leveraging cheaper processes in certain EU countries. In contrast, when the minimum environmental impacts are sought, every Member State contributes to each stage of the supply chain, resulting in an almost 45% increase in the total cost on average for the three endpoints.

In all scenarios, the optimal supply chain design relies mostly on residues as the primary source of biomass feedstock, complemented by dedicated energy crops grown on marginal land to avoid competition with food production. Only *Miscanthus* is chosen among the available options because of its higher yield and carbon content in the EU-28. The choice of a suitable feedstock, namely residues, ensures that the impact on land and water is minimized while satisfying the carbon removal imposed.

Transportation, pelleting and combustion processes are the main contributors to the environmental impacts endpoints in all the scenarios. A substantial improvement of these energy-demanding activities must be sought, although it is expected that these impacts will be lower in the future as the energy mix becomes decarbonized. On the other hand, biomass transportation should be avoided by combining multiple steps of the supply chain where possible.

The minimum cost supply chain provides the imposed carbon removal target at an average cost of 117 Eur_{2018}/t_{CO_2} removed, producing, in turn, 511 TWh of electricity. This solution gives rise to negative impacts on two out of three endpoints of the ReCiPe 2016 methodology, i.e., human health and ecosystem quality, while resource availability is depleted (i.e., its impact is not negative). Despite the solution already being extremely favorable for the environmental indicators, when they are optimized as single objectives an average improvement of 23% can be achieved for the three environmental endpoints, with a cost increase of less than 45%. The three resulting supply chains feature almost the same modeling choices, i.e., 1 to 3%

differences in the values achieved in the three optimizations. These similarities are explained by the extensive deployment of biomass residues as feedstock and the constraint on net electricity production. Consequently, the outcome of the analysis is exceptionally favorable for human health, species and resources at the same time, even when only one of them is minimized as the objective function. Furthermore, we found that the solutions to the minimum human health and minimum ecosystem quality cases were comparable.

In addition to the environmental benefits obtained, the BECCS supply chains provide a significant amount of reliable and carbon-negative electricity, which can help to meet the future energy demand while simultaneously improving environmental performances. Additional carbon removal *via* BECCS can also be explored in the EU if the net electricity production is not constrained in the optimization of the environmental scenarios.

We argue that the optimal large-scale deployment of the BECCS should be designed to embrace impacts beyond climate change. The solution herein proposed could be considered as a starting point by policymakers to achieve the goals set out in the Paris Agreement by explicitly expanding the scope beyond a narrow climate focus to address other dimensions and draw support from a wider set of actors.

5.A Nomenclature

Acronyms	
BECCS	bioenergy with carbon capture and storage
CCS	carbon capture and storage
CDR	carbon dioxide removal
CO2	carbon dioxide
ED	ecosystem quality endpoint of Recipe 2016
EU	European Union
EU-28	European Union of 28 countries
GHG	greenhouse gas
H	Hierarchist perspective of Recipe 2016
HH	human health endpoint of Recipe 2016
I	Individualist perspective of Recipe 2016
IAMs	Integrated assessment models
IPCC	Intergovernmental Panel on Climate Change
LCA	Life cycle assessment
LCI	life cycle inventory
LCIA	life cycle impact assessment
LCO	Life cycle optimization
LP	linear programming
LUC	land-use change
MEA	monoethanolamine
NDCs	nationally determined contributions
NETCOM	Negative Emissions Technology COoperative Model
NETPs	negative emissions technologies and practices
PB	Planetary boundaries method
PPP	purchasing power parity
RA	resource availability endpoint of Recipe 2016
SC	supply chain

Chapter 6

A tailored decomposition approach for optimization under uncertainty of carbon removal technologies in the EU power system[6]

[6] Under review in Computers and Chemical Engineering Journal as V. Negri, D. Vázquez, I. E. Grossmann and G. Guillén-Gosálbez. *A tailored decomposition approach for optimization under uncertainty of carbon removal technologies in the EU power system*

6.1 Introduction

The urgent need to counteract the adverse effects of climate change has led to a growing emphasis on reducing greenhouse gas (GHG) emissions, the rising concentration of which is primarily attributed to anthropogenic activities [270]. Among all the economic industries, the energy sector, which includes heat and electricity, contributed substantially to direct $CO_{2\text{-eq}}$ emissions in 2019, accounting for 23% of the total [5]. Given the significant mitigation potential, it is considered a key player in meeting climate targets.

The European Union (EU), responsible for roughly 10% of global emissions and one major leader in climate policies [287], in 2019 published the European Green Deal to push a political shift toward a carbon-neutral society in 2050 [268,288]. This includes efforts to decarbonize the energy sector through renewable energy deployment (amounting to 32% of the gross final energy consumption) and measures to improve energy efficiency to cut GHG emissions by 55% [289].

While these actions, already included in Integrated assessment models (IAMs), are underway, there is also the need to explore comprehensive strategies that not only prevent emissions but also actively reduce the current concentration of GHG in the atmosphere [5]. This could be accomplished via carbon dioxide (CO_2) removal (CDR) strategies or negative emissions technologies and practices (NETPs). Some of these, namely bioenergy [290] and direct air capture with carbon capture and storage (CCS) (BECCS and DACCS, respectively), are already included in the IAMs [291]. Yet, IAMs do not incorporate social or political dimensions [292] and do not have the technological or spatial resolution for detailed energy systems planning. Moreover, trade-offs appear when assessing multiple key performance indicators of these technologies, suggesting that a regionalized portfolio of NETPs integrated into the energy systems should be evaluated to exploit their complementary strengths [16]. In particular, technology readiness level and removal potential can be disproportionate to cost. Additionally, there might be a mismatch between removal potential and storage availability in some locations, requiring additional infrastructure.

Only a few studies model this coupling explicitly [293,294]. A few regional studies were carried out by Daggash et al. [36] and Prado et al. [295] in the context of the United Kingdom and by Sagues et al. [296] in the United States. Recently, a model that integrates the EU power system together with BECCS and DACCS was developed to shed light on the consequences of delaying the

deployment of CDR options [253]. Despite this work providing valuable insights into the optimal deployment pathways, the conclusions were drawn based on a deterministic model, which should be reevaluated every future time that updated data becomes available, such as energy demand and technology learning rate, as explored by Rathi and Zhang [297]. This work does not consider the handling of uncertain parameters.

Uncertainty is an inherent characteristic of energy systems, as they are influenced by a complex interplay of factors such as technological advancements, policy frameworks, economic fluctuations, and societal behaviors. Incorporating uncertainty analysis in energy system models is crucial for robust decision-making, particularly in the context of evaluating carbon removal options. Specifically for BECCS and DACCS, since they are often evaluated within long-term energy plans, the results are affected by a considerable degree of uncertainty [298], which is usually neglected, while in practice their large-scale deployment in the EU energy system is subject to numerous challenges. These challenges include technological readiness, high costs, geographical constraints such as land availability for biomass cultivation, regional factors for renewable power generation, in addition to CO_2 storage availability, scalability of the modularity of DACCS technologies, and social acceptance. Moreover, the variability and uncertainty in electricity demand pose additional complexities for the integration of these technologies into the energy system. Indeed, these CDR options are interconnected with the system because they either provide or require electricity. Thus, it is important to address the uncertain nature of the EU energy system, which has been highlighted especially in recent years, due to the COVID-19 pandemic and the Russian invasion of Ukraine.

Traditional deterministic energy system models often overlook the uncertain nature of electricity demand, assuming all the parameters to be known, and thus potentially leading to suboptimal or even infeasible decisions and unrealistic outcomes [299,300]. Hence, here we argue that including uncertainty within a suitable optimization framework is essential to comprehensively assess the impact of the power system and the potential role of BECCS and DACCS in the EU energy system.

We refer to a recent review published by Li and Grossmann [300] for a list of selected articles on stochastic programming, one of the possible modeling frameworks to perform optimization under uncertainty. It is evident from the list compiled by Li and Grossmann [300] and a recent review on uncertainty frameworks by Bevan [301] that the Process Systems Engineering (PSE)

literature on stochastic problems is quite rich, yet the literature on sustainability problems under uncertainty is scarce, despite CCS being recognized in the field as pivotal to the future transition [302] and sustainability becoming an important focus in the PSE community [42,303].

In particular, we found that there are studies assessing the standalone impact of uncertain parameters of CCS and BECCS, such as cost, carbon removal availability, and soil inputs [304–306]. However, to our knowledge, energy system models that include CDR options and exogenous uncertainty are yet to be explored. Along these lines, Grant and co-authors [307] carried out a pioneering work evaluating the policy implications of uncertain removal potential at a global scale using the TIAM-Grantham model in stochastic scenarios.

Analyzing the CDR-power nexus including uncertainty, leads to more complex problems than their deterministic counterparts. Despite recent developments in hardware and software, stochastic problems might still be intractable and require decomposition approaches to speed up the solution time to get insights from different case studies with reduced computational time. Traditional decomposition methods to solve large energy systems stochastic models include time-series aggregation [308,309], Benders and Lagrangean decomposition [310], sequential scenario decomposition [311], and shrinking and rolling horizon [312]. Tailored approaches have also been developed as a combination of these methods [313–315]. Lastly, new approaches based on neural networks or genetic algorithms have been proposed to deal with the challenging size of these models [316,317].

To close the literature gap highlighted above, the scope of this work is twofold. Here we evaluate the impact of uncertainty in electricity demand on the deployment of BECCS and DACCS in the EU energy system via multistage stochastic programming. Given the computational challenges that arise from the large size of the problem, a tailored algorithm is introduced to decompose the problem, reducing the computational time by 90%, combining decomposition techniques and heuristics. This allows us to generate insights into the optimal integration of these technologies within the EU energy system by investigating different scenarios of carbon removal by BECCS and DACCS. To the best of our knowledge, a multiregional CDR-power nexus model with rigorous modeling of uncertainty via multistage stochastic programming has never been proposed before.

The rest of the article is organized as follows. The problem statement is given next, followed by the optimization methods, including the multistage stochastic model and the decomposition

algorithm. The results section includes a comparison of the computational performance of the stochastic model without and with the decomposition algorithm for different case studies. Lastly, the conclusions and outlook for future work are presented.

6.2 Problem statement

Given are 15 state-of-the-art power technologies and the most prominent CDR-engineered options. These technologies are divided into dispatchable, which can produce heat, electricity, or both, at demand, and non-dispatchable, which require a backup capacity of dispatchable technologies to account for the time they cannot be operated. Among these, we also consider conventional fossil technologies, i.e., coal and natural gas, and their retrofit with carbon capture and storage. Among the CDR options, we include biomass-based energy, which also acts as a dispatchable energy source, and direct air capture. We consider learning cost curves and realistic diffusion rates limiting the deployment of all technologies [318]. The region of interest of this study is the EU with the United Kingdom, where its member states are considered potential locations for the installation of power technologies. These 28 countries are modeled as load nodes with specific energy demands and resource availability.

The goal is to determine the optimal planning of the EU energy system to satisfy the electricity demand and its associated uncertainty in each country, by minimizing the system's total cost subject to a given cumulative CDR target at the end of the time horizon of 30 years. The decisions to be made include the capacity and location of the power technologies and the electricity, heat and electricity required by DACCS, and CO_2 flows between the EU states. The problem statement is presented graphically in Figure 6.1.

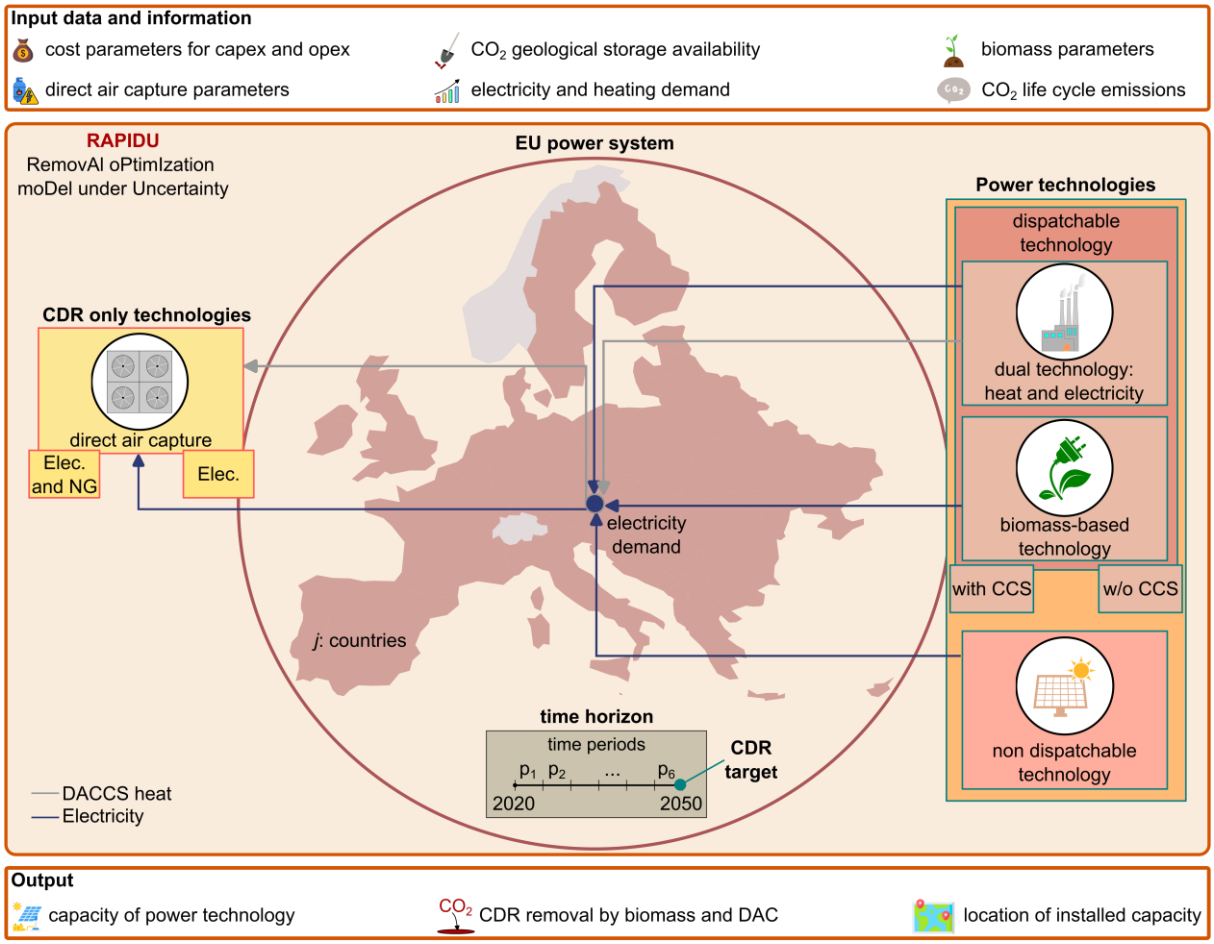

Figure 6.1: RAPIDU (RemovAl oPtImization model under Uncertainty) problem statement. We are given a set of power technologies and two already commercially available carbon dioxide removal technologies, namely bioenergy and direct air capture with CO_2 storage (BECCS and DACCS). Given is also a set of input data, including regionalized parameters for BECCS and DACCS, such as land availability and biomass CO_2 uptake, natural gas and electricity requirement, respectively. We model the 27 EU countries and the UK as load nodes with specific energy demands and resource availability. The goal is to determine the optimal deployment pathway under electricity demand uncertainty (exogenous uncertainty) that meets a given CO_2 removal (CDR) target at the end of the time horizon of 30 years, minimizing the system's total cost.

6.3. Methods

6.3.1 Deterministic model

We build on RAPID, a linear programming (LP) model model previously proposed to understand the implications of delaying the deployment of CDR options at a regional level, focusing on BECCS and DACCS within the EU power system [253]. RAPID was developed to investigate two scenarios: maximization of carbon removal and minimization of total cost subject to a carbon removal target. Perfect foresight for the input parameters was assumed in the time horizon 2020 – 2100, modeled as a set of discrete time periods. The carbon removal is computed as the difference between the positive CO_2 emissions and the CO_2 removed from

the atmosphere by BECCS and DACCS. In essence, given a set of power technologies and BECCS and DACCS that can be deployed in each country of the EU, the goal is to find the optimal capacity installed and the removal by the two NETPs, to meet the CDR target at the end of the time horizon and the energy demand in each country.

In this work, we include binary variables (b_t^s) that account for the installation of the technologies at the beginning of each time period following [319,320] making the model mixed-integer linear. We shorten the time horizon to 30 years, from 2020 to 2050, for a more realistic evaluation of the uncertainty within the EU's net-zero emissions target. Therefore, we impose a cumulative CDR target equal to zero in the year 2050, which is achieved jointly by all the countries in a cooperative strategy, and we solve for the minimum total cost of the system.

6.3.2 Uncertainty definition

Depending on how the uncertainty is revealed, it can be characterized as exogenous or endogenous [321]. The former is decision-independent and is revealed automatically at each time period, e.g., market prices. In contrast, the latter is decision-dependent; therefore, it is not associated with a particular time period, e.g., the size of an oil field, which is revealed only when the drilling starts [322]. Multiple approaches to deal with uncertainty in optimization problems have been developed, including stochastic programming [323], chance-constrained [324], and robust optimization [325], which differ in the way uncertainty is characterized and the degree of risk aversion. Stochastic programming is often considered a risk-neutral approach [326], in which the expected value of the objective function is optimized, and where the uncertainty is characterized by a given probability distribution. In contrast, in chance-constrained there is the possibility to deal with reliability and risk management. In essence, it requires solving a stochastic programming problem with some probabilistic constraints. Robust optimization is also a risk-averse approach, which tries to find an optimal solution to the "worst-case scenario" that satisfies given constraints over a defined uncertainty set.

The method of choice depends, among others, on the information available on the uncertain data, whether the emphasis is on feasibility or optimality, and if corrective actions can be taken. For more details on approaches for decision-making under uncertainty, we refer the reader to Apap and Grossmann [311] and Li and Grossmann [300].

Here, we consider exogenous uncertainty in the electricity demand by formulating a multistage stochastic mixed-integer linear programming (MSS - MILP) model [311]. We consider that at each time period the electricity demand of each country varies ± 20% from the nominal deterministic value, which is instead updated over the time periods considering a constant annual growth [253]. The choice of the demand as an uncertain parameter is justified by the fact that this parameter is dependent on multiple external factors, and hence can be highly uncertain. Some of the factors that affect demand are seasonality, economic growth and contraction, population growth and urbanization, technological innovation, e.g., increased efficiency, natural disasters, and even political and socio-cultural landscape changes.

6.3.3 Multistage stochastic model

In two-stage stochastic programming with exogenous uncertain parameters, we distinguish between first-stage and second-stage decision variables. The former are also called “here and now” variables, and are fixed at the beginning of the time period before knowing how the uncertainty will unfold. The latter, also known as recourse actions (“wait-and-see”), perform a corrective action after the uncertainty is revealed. When the models include multiple time periods within a time horizon, multistage stochastic problems are developed where decisions, realizations, and recourse actions occur sequentially as represented in Figure 6.2. Here, multiple recourse actions can be taken as uncertainties are gradually revealed.

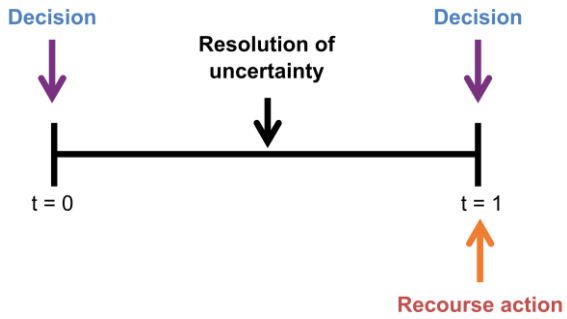

Figure 6.2: Sequence of events in stochastic programming with one exogenous uncertain parameter [311].

In what follows, we first describe the general modeling approach and then provide the stochastic formulation taken as a basis. In stochastic programming, uncertainty is assumed to be described via scenario trees obtained from discretized probability distribution functions. Let us consider three time periods and two realizations of one uncertain parameter, high and low. For these assumptions, the standard scenario tree is represented in Figure 6.3a. Hereafter, the following notation is used. A node is a possible state in a time period t. An arc is a possible

transition from a state in t to a new state in t+1. A scenario is the complete path from the root node to a leaf node. We refer to the scenario probability as the probability of reaching a leaf node from the root node.

The number of exogenous scenarios (N) is equal to the product of the number of realizations for each exogenous parameter. If we consider two realizations of the uncertain parameter at each time period, the cardinality of the scenarios set is computed as 2^t and the number of nodes is $2^{t+1} - 1$.

An alternative form of the scenario tree in Figure 6.3b proposed by Ruszczyński [327] gives each scenario a unique set of nodes. When moving from the standard to the alternative representation we create several copies of the same states that contain the same information at that point in time. Scenarios with the same information at time t are said to be indistinguishable at that time. Therefore, in indistinguishable scenarios, we must make the same decisions. This behavior is enforced through non-anticipativity constraints (NACs) represented by the red horizontal lines in Figure 6.3b.

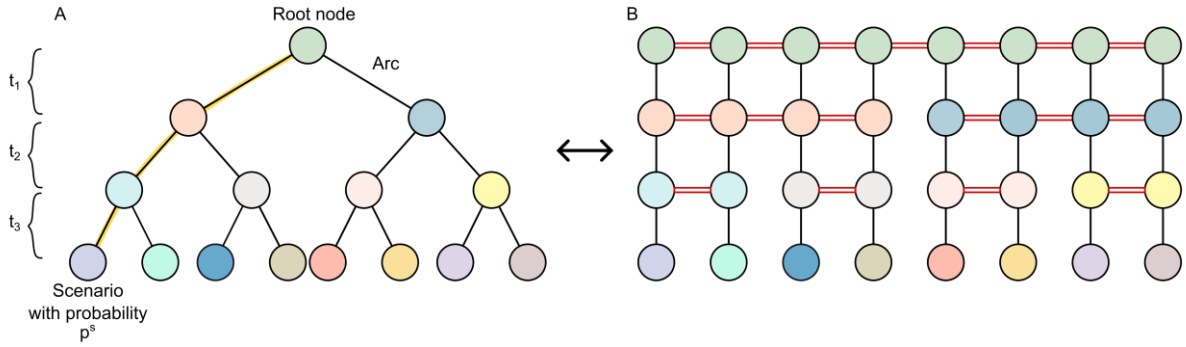

Figure 6.3: Exogenous uncertainty representation: standard (A) and alternative scenario tree (B). t represent the time periods, within t_{start} and t_{end}, each dot is a node and the black lines connecting the dots are called arc, which represent a possible transition between two states from time t to time t+1. The node at the top is the root node and the ones at the bottom are the leaf nodes. A complete path from the root node to a leaf node corresponds to a scenario, which occurs with a given probability.

We report in Eqs. (6.1) – (6.5) the compact mathematical formulation of RAPIDU (RemovAl oPtImization model under Uncertainty), hereafter referred to as MSS1. The stochastic model is represented in the deterministic-equivalent form using non-anticipativity constraints ((6.3a)-(6.4c)). MSS1 includes all the equations reported in the Supplementary information by Galán-Martín et al. [253] (see Eq. (6.2)), and therefore not repeated hereafter in their extensive form but summarized later in this section. The constraints introduced in this work are Eqs. (6.3a)-(6.4c) and the respective bounds in Eq. (6.5).

$$\min_{b,y,x} \phi = \sum_{s\in\mathcal{S}} p^s \sum_{t\in\mathcal{T}} \left({}^{y}c_t^s y_t^s + {}^{x}c_t^s x_t^s + {}^{b}c_t^s b_t^s\right) \tag{6.1}$$

$$\text{s.t. } {}^{y}A_t^s y_t^s + {}^{x}A_t^s x_t^s + {}^{b}A_t^s b_t^s \leq a_t^s \quad \forall\, t \in \mathcal{T},\ s \in \mathcal{S} \tag{6.2}$$

$$b_1^s = b_1^{s'}\ \forall\ (s,s') \in \mathcal{SP}_F \tag{6.3a}$$

$$y_1^s = y_1^{s'}\ \forall\ (s,s') \in \mathcal{SP}_F \tag{6.3b}$$

$$x_1^s = x_1^{s'}\ \forall\ (t,s,s') \in \mathcal{SP}_X \tag{6.4a}$$

$$b_{t+1}^s = b_{t+1}^{s'}\ \forall\ (t,s,s') \in \mathcal{SP}_X \tag{6.4b}$$

$$y_{t+1}^s = y_{t+1}^{s'}\ \forall\ (t,s,s') \in \mathcal{SP}_X \tag{6.4c}$$

$$b_t^s \in \{0,1\},\ \ y_t^s \in \mathcal{Y}_t^s,\ \ x_t^s \in \mathcal{X}_t^s \quad t \in \mathcal{T},\ \ s \in \mathcal{S} \tag{6.5}$$

The objective function in Eq. (6.1) is the total expected cost, computed as the weighted sum of the costs in each scenario multiplied by the probability in each scenario, p^s. The general techno-economic constraints correspond to Eq. (6.2). Eqs. (6.3a) and (6.3b) represent the first-period NACs, and Eqs. (6.4a) – (6.4c) the exogenous NACs. These constraints enforce that the same decisions are taken in all the nodes that are indistinguishable. Lastly, in Eq. (6.5) the variables' bounds and integrality restrictions are specified.

Here, we adopt the same nomenclature used in Apap and Grossmann [311] for the mathematical formulation. The multistage stochastic optimization model includes y_t^s first-stage investment decisions at the beginning of each time period, e.g., power technology capacity installed; x_t^s second-stage operation decisions that follow the investment decisions, e.g., the electricity generated from the installed capacity. These decisions are optimized over every country j ∈ J considering a set of technologies i ∈ I whose sets are omitted in the mathematical formulation for clarity (i.e., y_t^s corresponds to y_{ijt}^s). Each variable is scenario-dependent, identified by the set $\mathcal{S}$, indicated by the superscript on the right of each variable. MSS1 is presented in its most general form, where the left superscript of the A matrix indicates to which variable the parameters refer and even the cost parameters are indexed for s to allow for different values according to the scenario. E.g., ${}^{y}A_t^s$ means that the parameters included in A refer to the y_t^s

decision variable at time period t in scenario s (omitting sets i and j). We refer to Apap and Grossmann [311] for the mathematical definition of the sets $\mathcal{SP}_F$ and $\mathcal{SP}_X$.

The number of scenarios, corresponding to the cardinality of set $\mathcal{S}$, is 64 (2^t) given two realizations of the uncertainty, high and low, at each time period. The realization of the uncertainty is the same for each country, i.e., in all EU countries and the United Kingdom the electricity demand either increases or decreases, which is a sensible assumption given the strong political ties in the region and assuming that the extent to which the economy will be electrified, particularly concerning transportation but also in hard-to-abate sectors like petrochemicals production, will be similar across countries. Therefore, here we do not consider the combination of all the scenarios, which would increase the complexity of the problem substantially.

For consistency with Galán-Martín et al. [253], each time period is defined with a length of five years at first. Therefore, the chosen time horizon 2020 – 2050 is divided into six time periods $t \in \mathcal{T}$ of equal length. Then, we also assess the case of different lengths depending on the time period, with shorter time periods closer to the beginning of the time horizon and a rougher discretization towards the end of it. We report in Section 6.4 the two sets of results obtained. We adjust the input data accordingly to account for CAPEX and OPEX to match the new definition of the time periods.

A detailed description of the general techno-economic model constraints that are included in Eq. (6.2) can be found in the supplementary material of Galán-Martín et al. [253]. In essence, load-meeting and operation constraints are defined in Eqs. 1 – 31, accounting for the distinction between dispatchable and non-dispatchable technologies and ensuring that the electricity demand is fulfilled. We note that the electricity demand is met as an equality constraint in the work presented here. The modeling of the supply chain of biomass, regarding land use, availability of residues, etc., is also included. CO_2 emission constraints include Eqs. 32 – 42, and model the carbon balance regarding positive and negative emissions, as well as the trade, capture, and storage of CO_2 and its sequestration underground. Finally, cost equations include Eqs. 43 – 48, and model how the CAPEX and OPEX of the different power energy sources are obtained, as well as the cost of negative technologies.

6.3.4 Decomposition algorithm

The full space multistage stochastic programming in Eqs. (6.1) – (6.5) leads to large-scale problems that quickly become intractable. For example, for two uncertainty realizations, six periods and 28 countries, the MILP has more than 8.2 million variables and 4.2 million constraints. Hence, we propose the decomposition algorithm sketched in Figure 6.4 for its efficient solution.

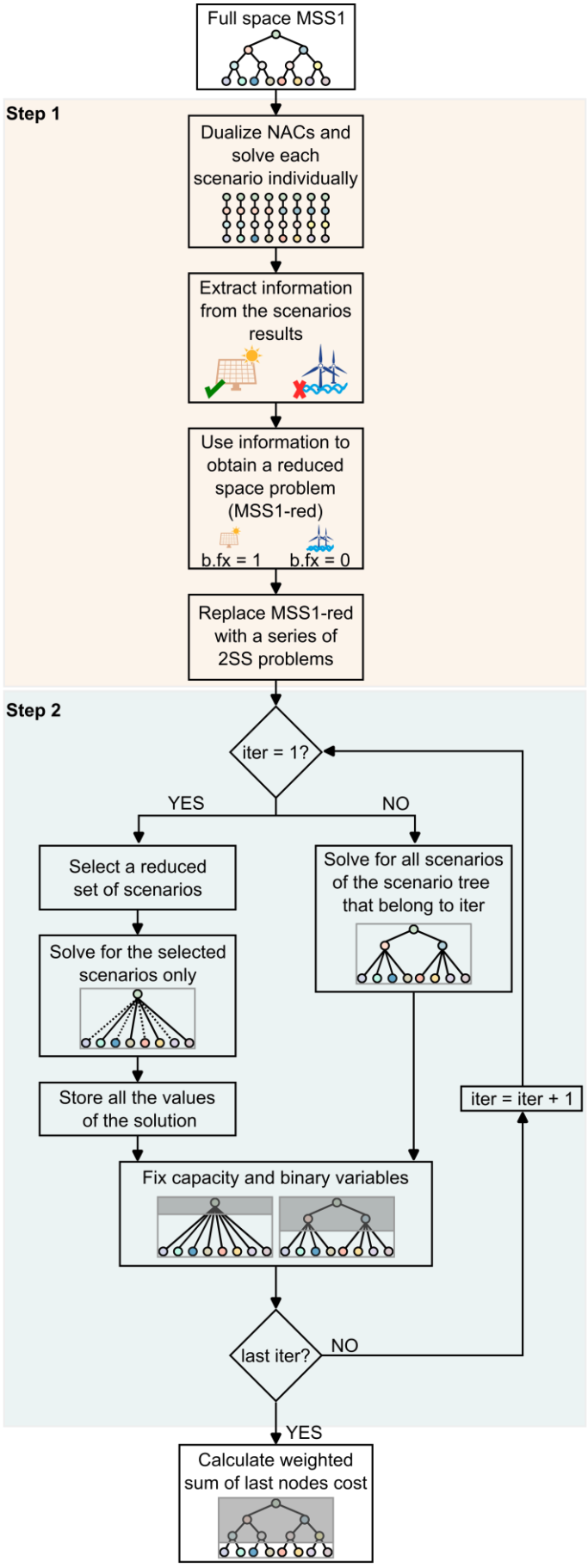

Figure 6.4: Decomposition algorithm steps. First, we decompose the original problem into single scenarios and we solve them individually. This step is performed by dualizing the NACs using zero multipliers. Afterward, we analyze the results to the optimization problems and extract information about which technologies are selected or not in the scenarios. We then use this information fixing the binary variables accordingly to obtain a reduced form of the original problem that we can solve faster. This reduced problem is further manipulated replacing it with a series of two-stage stochastic (2SS) problems solved in a rolling horizon approach.

The decomposition algorithm comprises two steps. First, we decompose the problem into single scenarios dualizing the first-period and exogenous NACs. This step can be compared to the first iteration of the Lagrangean decomposition where the NACs constraints are transferred to the objective function as penalty terms multiplied by Lagrange multipliers [311]. Yet, we do not perform any update of the dual bounds.

We note that for the problem presented in Section 2, the conventional Lagrangean decomposition algorithm proved to be inefficient, leading to high computational times to close the gap between the lower and upper bound, as described in Apap and Grossmann [311]. This can be caused by the relatively low number of scenarios, as already observed in Apap and Grossmann [311], which led to the same oscillatory behavior reported by Uribe-Rodríguez et al. [328] for the convergence.

For simplicity, let us consider only the decision variables y_t^s. Then, after relaxing the NACs, Eq. (6.1) becomes

$$\min_{y} \phi_{LR}(\lambda) = \sum_{s\in\mathcal{S}} pr^s \sum_{t\in\mathcal{T}} {}^{y}c_t^s y_t^s + \sum_{(s,s')\in\mathcal{SP}_F} {}^{F}\lambda_1^{s,s'}(y_1^s - y_1^{s'}) + \sum_{(t,s,s')\in\mathcal{SP}_X} {}^{X}\lambda_t^{s,s'}(y_{t+1}^s - y_{t+1}^{s'}) \tag{6.6}$$

We rearrange the equations of MSS1 for all the variables as in Eq. (6.6) to obtain a number of problems equal to the cardinality of $\mathcal{S}$. At this point, we set the multipliers to zero and we solve each problem individually.

Then, we can explore the solutions of the scenarios to collect information about the technology deployment. In particular, we want to know which technologies are not selected in any scenario or the technologies selected in every scenario in all countries in a given time period for capacity expansion. We note that if the binary variable that indicates the capacity expansion of a given technology is zero, it does not imply that that technology is not deployed at all. We then use the information gathered in step 1 to reduce the size of the original problem by eliminating elements from the set of technologies, i.e., setting the binary variables to zero or fixing investment decisions. However, this problem, which we call MSS1-red, might still be very large. Therefore, we decompose it further.

In the second step of our approach, we approximate the multistage stochastic problem with a series of two-stage stochastic problems (2SS) that we solve iteratively in a shrinking horizon approach, as described in Balasubramanian and Grossmann [312]. Moreover, in the first iteration, which corresponds to the first node over the entire time horizon, we solve for a subset of scenarios. The number of scenarios and the method for their selection can be chosen depending on the application. In our case studies, we use a heuristic approach dependent on the shape of the decision tree. Out of $|S|$, we select ten representative scenarios of the whole set.

An alternative approach, although computationally more expensive, is to use sample average approximation (SAA), firstly introduced by Kleywegt et al [329]. In SAA, a sample of scenarios $N < |S|$ that best represents the initial problem is selected to form a reduced set S_{red}. The probability of each scenario is adjusted to sum up to one by dividing the probability of each scenario in S_{red} by the sum of the probabilities of all scenarios in S_{red} [330]. Since the probability distribution of the uncertainty is known a priori, here we choose N scenarios such that they are representative of the full set S. This set is used to solve an approximation of MSS1.

We then store the decision variables from each scenario (y_t^s) and fix the ones at the first time period (y_1^s) according to the values of the solution obtained in the first iteration. From the second iteration onward, we solve one problem that considers all the scenarios of the corresponding 2SS problems. At each iteration, we fix the decision variables at the beginning of the time period until no more time periods are to be fixed. Notably, all the integer variables are fixed when solving the leaf nodes. Therefore, the last 64 iterations are LP problems, which can be solved efficiently. Lastly, we compute the total expected cost as a probability-weighted sum of the costs at the final nodes.

A 5% optimality gap is enforced at each iteration as termination criteria, and convergence is checked before solving the next node. The optimality gap is chosen consistently with Galán-Martín et al. [253] and set larger than zero due to the complexity of the model.

Priorities on the discrete variables are also used to speed up the algorithm further. We expect that BECCS is deployed before DACCS because of its lower cost, higher initial capacity installed and diffusion rate until no more capacity can be installed to meet the CDR target. This translates into heuristic-based constraints involving binary variables that reduce the combinatorial complexity of the problem.

RAPIDU is solved using GAMS 41.5.0 on an Intel(R) Core(TM) i7-10700 CPU @ 2.90GHz with 32.0 GB RAM using 16 parallel threads with the solver CPLEX 22.1.

6.3.5 Value of the stochastic solution for multistage stochastic models

To quantitatively assess the additional value of adding uncertainty to the optimization problem, we compute the value of the stochastic solution (VSS) [323]. Indeed, a decision-maker might argue that including recourse decisions in the model might not be worth the additional computational effort, to which the VSS provides insights into the potential value left on the table when not considering uncertainty in the decision-making process.

In the case of two-stage stochastic problems, the procedure to calculate VSS is straightforward and widely used. Firstly, the solution to the model with a mean value of the uncertain parameter is computed. This is called the expected value problem or mean value problem (EV). Once the solution to this problem is known, it is used to solve the stochastic model by fixing the first stage "here and now" variables. This is known as the expected result of using the EV solution.

For a minimization problem, the VSS is computed as the difference between EEV and RP (Eq. (6.7), where RP is the solution to the fully stochastic problem. A small VSS denotes that the deterministic model is a good approximation of the stochastic one.

$$\mathrm{VSS} = \mathrm{EEV} - \mathrm{RP} \tag{6.7}$$

In the case of multistage problems, however, computing the VSS is not as simple because each time period has "here and now" decision variables and it is not clear which variables should be fixed. Therefore, obtaining EEV would require solving a sequence of models. The issues in computing the values above and an approach to calculate the VSS for multistage stochastic problems are discussed in Escudero et al. [331].

In this work, we use an approximation of the procedure to calculate the VSS, also reported in Escudero et al. [331], where we fix only the first stage decisions in all time periods to obtain EEV. Then, the VSS is calculated as the difference between EEV and RP as in Eq. (6.7).

6.4. Computational results and discussion

6.4.1 Homogeneous discretization of the time horizon

First, we analyze the case for time periods of equal lengths. The results are discussed in this section comparing the full space model to the decomposed version.

Hereafter, we refer to the full space model, i.e., the problem which includes all equations and variables and is solved at once, as MSS1, and the version solved by applying a decomposition algorithm as MSS1-D.

6.4.1.1 Net-zero target

At the end of the time horizon, we impose a net-zero cumulative CDR target, i.e., the positive emissions are fully balanced by the CO2 removed by BECCS and DACCS.

The number of variables, equations, and solution time of MSS1 are summarized in Table.6.1. Notably, the computational time to solve MSS1 in its full form to a 5% optimality gap is considerable (around 13 hours). The total cost of the system is 10.7 trillion Euros calculated as the weighted average of each scenario objective function value, and computed according to a net present value calculation, accounting for fixed and variable costs (see [253] for more information on the cost calculation). Compared to the deterministic solution (9.9 trillion Euros) it represents an increase of 7.2%, which is not negligible. In the context of the EU, this economic burden is borne by all the Members according to some fairness principle.

Table.6.1. Model statistics of the multistage stochastic problem MSS1 for the minimization of the expected cost.

	MIP - MSS 64 scenarios
Number variables [millions]	7.9
Number binary variables [thousands]	300.7
Number equations [millions]	4.2
Resource usage (solution + generation time) [hr]	~13
Solver	CPLEX 22.1
Termination criteria: opt. gap [%]	5
Optimal objective function value [trillion Eur]	10.7

Given the large computational time, we apply our decomposition approach and solve the problem again as MSS1-D.

From step 1, which is based on the relaxation of the NACs with zero multipliers, we find that many technologies are not selected for capacity expansion in any country at any time period.

We group all these technologies in a set and force their decision binary variables to zero when solving step 2. In order to further reduce the size of the model, we identify technologies that are selected for capacity expansion in the first time period in specific countries in all time scenarios. Again, we define a set for these technologies and we impose that the decision variable in the first period is equal to one. Both sets of technologies are reported in Table 6.2.

Notably, many technologies among those available for power generation are not selected because the time horizon we assess in this work is relatively short and the target is not very ambitious compared to what it is possible to achieve [253]. The existing capacity of conventional technologies already installed in addition to the new capacity of technologies reported in Table 6.2 is sufficient to satisfy the electricity demand while satisfying all the model constraints. Thus, only biomass-based removal is employed, while DAC installed capacity is zero in all the countries.

Table 6.2. Information on technology expansion from the solution of single scenarios (step 1) for a net-zero CDR target in 2050.

Technologies not selected in any scenario for capacity expansion at any time period	**Technologies selected (country) in all the scenarios for capacity expansion at t=t_1**
•Coal	•Geothermal (Germany)
•Coal with CCS	•Natural gas (Denmark)
•Hydropower	•Forest residue with CCS (Poland)
•Hydropower reservoir	•Woody residues with CCS (Greece)
•Nuclear	•Solar PV open (Luxembourg and Malta)
•Concentrated solar power	
•Solar PV roof	
•Switchgrass	
•Wind offshore	

We make use of the information obtained in step 1 as described in Section 6.3 and proceed to step 2. We solve step 2 iterating over the number of nodes (127). At the first iteration, we use heuristics to determine the subset of scenarios used to solve MSS1-red. Indeed, MSS1-red is still very large.

We obtain a 90% reduction in the computational time while achieving the same objective function value (10.7 trillion Euros). The latter is calculated as a probability-weighted sum of the leaf nodes, as explained in Section 6.3.3. In Table 6.3, we compare the solutions between the full space model and the decomposed one in terms of computational time and optimal objective function value. The time reported in the table includes step 1 and 2 where the Lagrangean decomposition step is approximately 14 minutes. The precise resource usage of generation and solution time in seconds is reported in Table E0.5.

Table 6.3. Comparison of full space and decomposed multistage stochastic models for the minimization of the expected cost. A reduction in computational time of 90% is achieved by implementing the decomposition algorithm. * probability-weighted sum at final nodes

	MIP - MSS 64 scenarios	**Decomposed MIP - MSS**
Resource usage (generation + solution time) [hr]	~13	~1.2
Optimal objective function value [trillion Eur]	10.7	10.7*

We point out that the decomposition algorithm modifies the original structure of the problem MSS1. Despite reaching the same expected total cost while meeting the electricity demand, there are differences in the decisions taken during the time horizon. For example, in MSS1 forest residues and natural gas with CCS capacities are also chosen and expanded at the first time period (Table E0.1). Additionally, comparing the information in Table 6.2 and Table E0.1, we notice that the algorithm only selects a few countries *j* where a technology *i* is selected in all the scenarios. In other words, in the decomposed problem, it is preferred to increase the capacity installed in selected countries *j* by 100% or more, while in MSS-1 the capacity of more technologies is increased less but across different countries.

Lastly, we compare the stochastic results with the deterministic ones.
First, we fix the binary decision variables from the solution of the deterministic problem in all time periods of the stochastic problem to obtain EEV (Table 6.4). We find that the cost of EEV is 10.98 trillion Eur. Compared to the value of RP in Table 6.3, the VSS is 285 billion Eur, which is roughly 3% of the RP, on the same order of magnitude as the examples presented in Birge and Louveaux [323] and Li and Grossmann [300].

Table 6.4. Objective function value for different case studies. Given the solution of the deterministic problem, we find the EEV value to later compute the VSS.

Deterministic variables to be fixed	**Time period**	**Value of objective function [B Eur]**
Binary decisions	Up to t_5	10791.2
Binary decisions	Up to t_6	10982.6
Binary and capacity decisions	Up to t_5	Infeasible
Binary and capacity decisions	Up to t_6	Infeasible

Then, we provide a graphical summary of the two sets of solutions. Let us assume that the deterministic model is run only one time at the beginning of the time horizon, although in practice it would be run in a rolling horizon fashion. Then, the solution that we obtain can be outside the range of all the possible solutions obtained considering uncertainty.

In Figure 6.5 we show the electricity generated per country (subplot A) and per technology type (subplot B). We notice that the majority of the total electricity generated comes from a

reduced set of countries (subplot A), i.e., France, Germany, Italy, Spain, and the United Kingdom, and also affected by the greatest variability among all the countries. Additionally, the deterministic solution lies outside of the range observed for the given scenarios, i.e., it is suboptimal, in some countries such as the Netherlands, where the point lies outside of the boxplot of stochastic solutions.

Subplot B represents the same information, this time aggregated by technology. Here, it is even more evident that the solution to the deterministic problem is not one of the solutions found by the stochastic model. In particular, we highlight the case of wind onshore and solar PV open technologies. Wind onshore and nuclear follow natural gas in production volume. Among all the technologies, natural gas is the main source of electricity and also has the highest variability, while the capacity of wind offshore does not change across the scenarios.

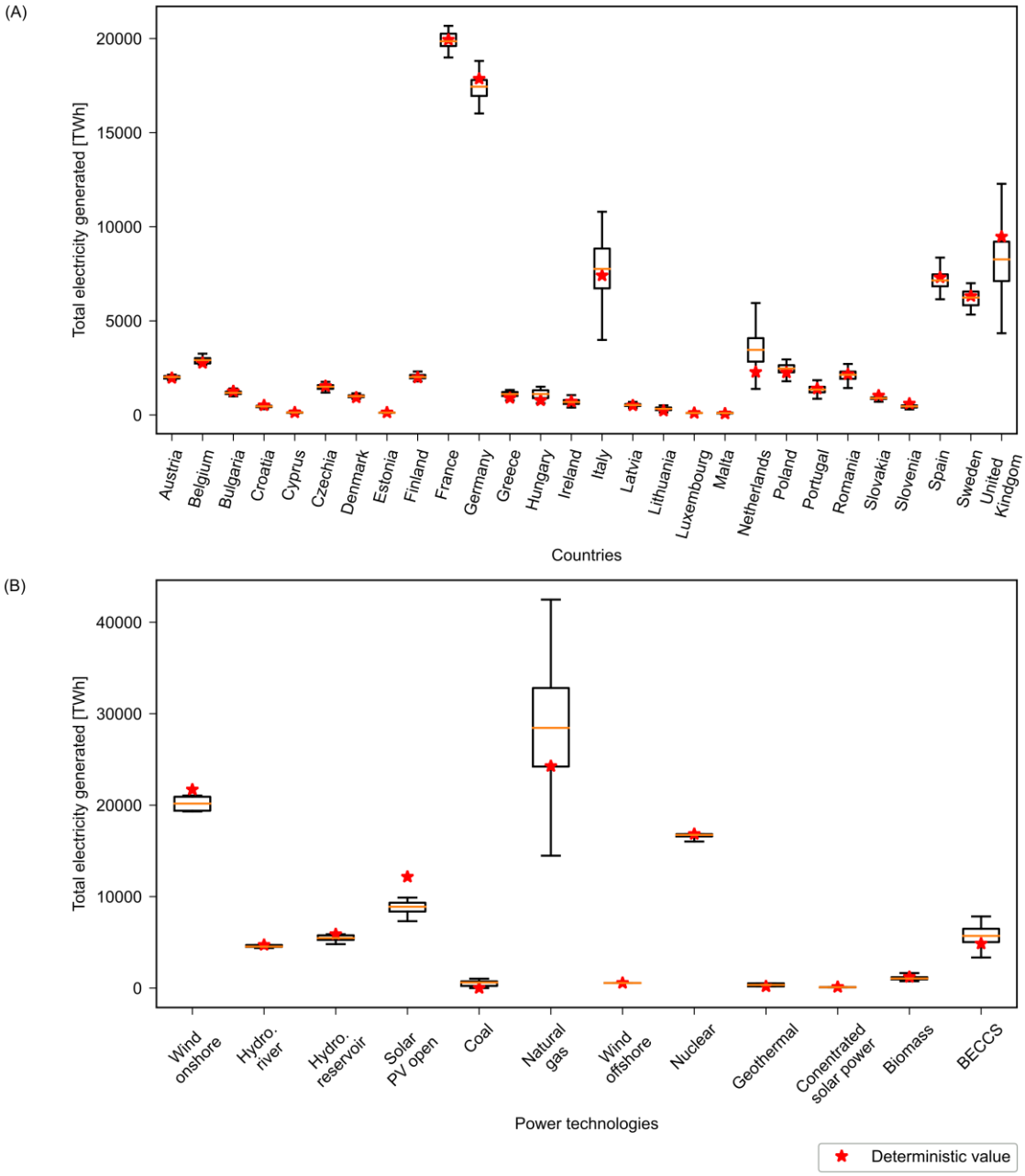

Figure 6.5: Total electricity generated aggregated by country (subplot A) and technology (subplot B). Stochastic range vs deterministic value. The box and whiskers plots are generated using the solution of all 64 scenarios of the stochastic model and they show ±25 the median value.

6.4.1.2 CDR scenarios

The decomposition algorithm presented in Section 6.3.3 allows us to more easily explore a range of case studies. We can do so by imposing a different CDR target at each iteration. In particular, our interest lies in assessing the feasibility of a carbon balance beyond the net-zero target and proving that it is possible to attain such levels by mid-century. This would imply that the electricity sector would be responsible for offsetting emissions from hard-to-abate industries, such as cement and steel. Considering that the electricity sector accounted for

approximately 30% of the total CO_2 emissions in the EU in 2021 [332], it seems reasonable for it to contribute significantly to the overall reduction in CO_2 emissions.

Our findings demonstrate that the deployment of BECCS and DACCS can potentially enable the removal of up to 9 Gt of CO_2 by 2050 by deploying BECCS and DACCS within the constraints of our model. In other words, the global carbon balance of the integrated sector, i.e., including the power technologies in addition to NETPs in the system boundaries, would result in the net removal of 9 Gt. Figure 6.6 illustrates the expected total cost of implementing solutions for the various CDR scenarios explored. A negative sign of emissions indicates that more CO_2 is removed via BECCS and DACCS than the amount emitted from all the technologies, i.e., natural gas, solar, and wind, resulting in negative emissions. We observe that the steepest increase in total cost occurs when we push the system to achieve more ambitious targets, ranging from 0 to −9 Gt of CO_2, while the cost does not decrease significantly for different positive targets, where the deployment of NETPs is minimal. Additionally, we find that DACCS, powered by electricity and heating, is only selected and deployed starting at the −9 Gt CO_2 target.

It is important to note that even in scenarios where the emissions balance is positive, bioenergy and BECCS are still deployed (Table E0.2). This is because the advantage of bioenergy is twofold: it removes CO_2 from the atmosphere while simultaneously generating electricity. Thus, it serves as a valuable technology for achieving emissions reductions. This matches previous observations made by the authors [254], where even considering the impacts of a highly detailed BECCS supply chain, negative emissions were achieved in the EU.

Our analysis reveals that achieving a target beyond 10 Gt CO_2 removal is not feasible (considering the assumptions and technologies in our analysis) within the computational time limit allowed (12 hours). This limitation is primarily driven by the rate of technology deployment rather than the availability of CO_2 storage. The high electricity demand in the most uncertain scenarios poses a significant challenge in achieving higher levels of CO_2 removal within the given timeframe.

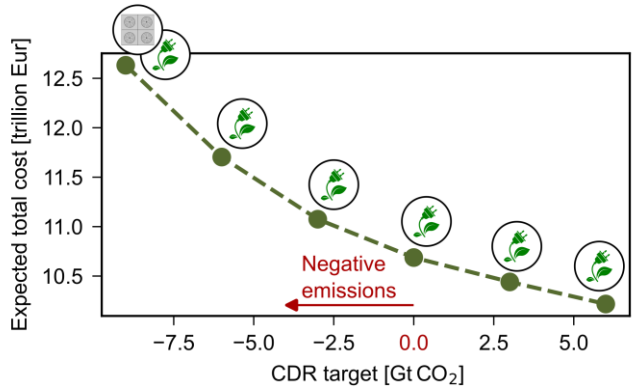

Figure 6.6: Expected total cost and technology deployed for different CDR targets. The icons of BECCS (green plant) and DACCS (gray box) indicate which CDR option is proving the required removal. Only in the case of 9 $GtCO_2$ removal, both technologies are deployed.

In Appendix A.1, we report the information relative to the technology selection in the decomposition algorithm step 1 and the computational time. We see that fewer technologies are installed as the target becomes less ambitious, and eventually the system is even allowed to reach a positive emissions balance.

6.4.2 Inhomogeneous discretization of the time horizon with net-zero target

As a last step, we are interested in the implications of discretizing the time horizon in time periods of different lengths (see Figure 6.7 A and B). This modeling decision is driven by the fact that the consequences of the years closer to the start of the horizon have greater economic and social impacts over the ones of the years further in time.

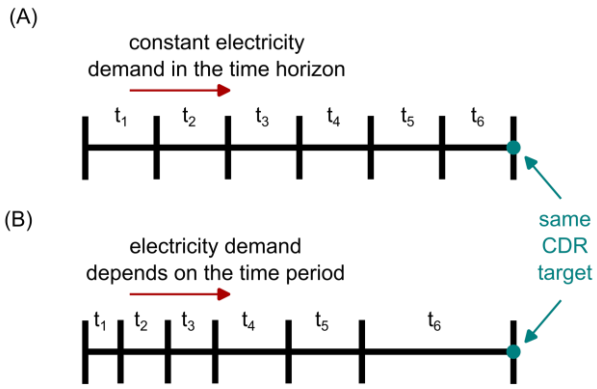

Figure 6.7: Discretization of the time periods. In the analysis presented in Section 6.4.1 (subplot A), the time horizon is divided into six time periods of equal length corresponding to five years. In this Section 6.4.2, we present the results for a non-homogenous discretization of the time horizon: six total time periods of length 2-4-4-5-5-10 years.

We report the results of the inhomogeneous time horizon discretization in Table 6.5 for the minimization of the expected total cost at a net-zero target. First, we highlight that in the full space problem we were able to reach a solution within the specified optimality gap although

infeasibilities on the original MIP problem were not resolved. On the other hand, our decomposition algorithm can reach a solution within the given tolerance without any numerical challenges highlighting the robustness of the proposed solution method. The total expected cost, calculated as the probability-weighted average of the last nodes, is 2% higher than the full space objective function, within the optimality gap. Lastly, we mention that the total expected cost in this case study is higher than the previous (10.7 trillion Eur, see Table 6.3) due to the duration of the periods being different.

The underlying assumption in the original model [253] is that the demand is maintained constant within the years of the first time period, and only updated at the start of the following period according to the following equation $d_t = d_{t-1} * \mathrm{F}$, where F is a constant factor greater than one. Therefore, it is updated more frequently when there are shorter periods. For example, since in the case of identical time periods the first time period comprises five years while here only two, the demand at the end of the time horizon is higher in the case presented in this section. We provide a clarifying example in the time horizon 2020 – 2025 with reference to Figure 6.7. In case A, it is assumed that there is no increase in the first five years, meaning that the cumulative final demand is equal to five times the one in 2020. In the inhomogeneous time period case (B), the first time period of two years follows the same assumption and therefore the cumulative demand in 2022 is two times the one in 2020, while the remaining years are updated according to the given correlation.

Table 6.5. Comparison of full space and decomposed multistage stochastic models with inhomogeneous time horizon discretization for the minimization of the expected cost to meet the net-zero target in 2050. Reduction in computational time given by the decomposition algorithm: 43%. * probability-weighted sum at final nodes. ** GAMS output: Fixed MIP status (5): *optimal with unscaled infeasibilities*

	MIP - MSS 64 scenarios	**Decomposed MIP - MSS**
Number variables [Millions]	7.9	7.9
Number binary variables [Thousands]	300.7	300.7
Number equations [Millions]	4.2	4.2
Resource usage (generation + solution time) [hr]	~3.2	~2
Solver	Cplex 22.1	Cplex 22.1
Termination criteria: Opt. gap [%]	5	5
Objective function value [Trillion Eur]	12.3**	12.5*

Next, we look into the technology deployment to meet the energy demand (Table E0.3 and Table E0.4). In this case, since the first time period is shorter, a reduced set of technologies is selected in all the scenarios, comprising wind onshore (Germany), solar PV open (Luxembourg), and forest residues with CCS (Poland). Additional capacity of solar PV open

is installed in Belgium at t_3 and t_5. The capacity of solar PV open and forest residues with CCS is expanded at the beginning of t_4 in 50% of the countries included in our model. This happens because the length of time periods t_1 and t_2 are 2 and 4 years, respectively, while in t_4 it is five years and more capacity is needed to cover the increase in electricity demand.

Overall, the net-zero target is achieved by deploying the same set of technologies shown in Figure 6.5 B.

6.5 Conclusions

In this study, we have highlighted the importance of considering uncertainty in energy system planning, particularly in relation to the implications on the total cost and technology capacity installed arising from the variability in electricity demand. The consequent complexity of the multistage stochastic programming model required the development of a tailored decomposition approach, which reduces the computational time significantly up to 90%. We observed that in the case of inhomogeneous time periods, which lead to numerical challenges to solve the full-space model, our algorithm provides a numerically robust solution within the optimality tolerance while still providing a significant speedup with respect to the monolithic model.

We found that among all the countries in the European Union, France, Germany, Italy, Spain, and the United Kingdom provide the majority of the electricity with the greatest variability across all the scenarios' solutions. The technologies with the highest capacity deployed for electricity production include natural gas, nuclear, wind onshore, solar PV and BECCS. Biomass emerged as a crucial component within the model, where its deployment was not only selected to achieve negative emission targets but also in scenarios where overshooting was allowed with capacity expansion at each time period for selected feedstocks.

Overall, effectively managing uncertainties is paramount for the successful implementation of projects, particularly in the context of climate action. Further research and attention to these uncertainties will contribute to the advancement and realization of sustainable energy systems, especially focusing on the learning curves of carbon removal options. While our analysis focused on the technical aspects, it is important to acknowledge that successful implementation of BECCS and DACCS technologies requires addressing additional considerations such as public acceptance, community engagement, policy incentives, and economic viability, which are beyond the scope of this study.

6.A Nomenclature

Abbreviations	
BECCS	bioenergy with carbon capture and storage
CCS	carbon capture and storage
CO_2	carbon dioxide
CDR	carbon dioxide removal
DACCS	direct air capture with carbon capture and storage
EU	European Union
EV	expected value problem
GHG	greenhouse gas
IAMs	Integrated assessment models
LP	linear programming model
MILP	mixed-integer linear programming model
MSS	multistage stochastic programming model
NETPs	negative emissions technologies and practices
NACs	non-anticipativity constraints
RAPIDU	RemovAl oPtImization model under Uncertainty
SAA	sample average approximation
RP	solution to the fully stochastic problem
2SS	two-stage stochastic programming model
VSS	value of the stochastic solution

Sets
I $\{i \mid i$ is a technology$\}$
J $\{j \mid j$ is a country$\}$
$\mathcal{S}$ $\{s \mid s$ is a scenario$\}$
$\mathcal{SP}_F$ $\{s \mid s$ is a scenario included in the first period NACs$\}$
$\mathcal{SP}_X$. $\{s \mid s$ is a scenario included in the exogenous period NACs$\}$
$\mathcal{S}_{red}$ $\{s \mid s$ is a scenario included in the solution of step 1$\}$
$\mathcal{T}$ {t | t is a time period}

Variables	
y_{ijt}^s	first-stage investment decisions for technology i, country j and time period t in scenario s
b_{ijt}^s	first-stage binary decisions for technology i, country j and time period t in scenario s
x_{ijt}^s	second-stage operation decisions for technology i, country j and time period t in scenario s

Parameters	
N	number of exogenous scenarios s
${}^{y}A_{ijt}^s$	parameters matrix, dependent on the variable and scenario s, for technology i, country j and time period t
p^s	probability of occurrence of scenario s

Chapter 7

Conclusions

7.1 Main findings of this dissertation

This thesis provided tools and valuable insights into carbon capture, starting from a thorough evaluation of its standalone value, and its integration within an optimal large-scale technology network in the European Union and the United Kingdom (EU, before Brexit) regional context for applications in the most contributing sectors to CO_2 emissions, namely transport, industrial heating and power generation, some of them deemed as hard-to-abate.

The ultimate objective was to inform decision-makers and contribute to the development of strategies for a sustainable transition to net negative carbon emissions by the end of this century.

In order to fulfill the goal of this thesis, several tools and frameworks were developed, which are summarized hereafter, highlighting significant accomplishments and findings of the research work presented in the previous chapters.

In Chapter 2, we presented how using straightforward models, developed with machine learning algorithms, particularly symbolic regression, can be applied to benchmark climate change mitigation technologies, such as carbon capture with storage. By applying the Bayesian machine scientist (BMS)[45] to two case studies, i.e., natural gas sweetening and flue gas cleaning, we have generated simple closed-form mathematical expressions of key variables that determine the process economic and environmental performance, i.e., net power, utilities, and solvent makeup, for a range of initial operating conditions. These equations can then be used to compare different alternatives within the models' training range. Additional analyses can be performed using these expressions, such as investigating the variables' elasticities and optimizing processes.

Here, we determined that the approach proposed is particularly suited to describe the relation between independent variables and the total power required in the system, i.e., the electricity needed to drive pumps and compressors. Additionally, in both case studies analyzed we found a strong correlation between the inlet gas composition, specifically the carbon dioxide (CO_2) concentration, and the dependent variables chosen.

Overall, the proposed approach aims to facilitate the transition toward new sustainable technologies by providing simple correlations for a more straightforward comparison with the business as usual (BAU). Furthermore, we demonstrated how the BMS can be employed to derive input-output analytical models of complex processes, whose modeling often requires

specific technical knowledge and is time-consuming. Therefore, we believe that the approach investigated is beneficial especially for experimental researchers.

Moving to applications in the transportation sector, in Chapter 3, we demonstrated how carbon capture retrofitted on-board cargo ships is an economically and environmentally viable solution to curb greenhouse gas (GHG) emissions from the freight industry in the short term. We tested this scenario on a representative ship with a conventional engine powered by heavy fuel oil, and compared it with the BAU and direct air capture (DAC).
Firstly, we assessed its feasibility based on the volume and weight of the equipment required for the CO_2 capture on-board. Based on this information, we determined that only 4% and 7% of the cargo on a volume and mass basis, respectively, are displaced to retrofit the plant for a one-week trip. The integrated system shows comparable performance to conventional post-combustion plants, with a 94% capture efficiency at 85 $\$_{2019}$/ t CO_2. Additionally, we analyzed the environmental performance of this solution within the planetary boundaries (PBs) framework. Our results show that carbon capture on-board does not transgress the full operating space, halving the pressure of the BAU on three core PBs, and outperforming DAC. We stress the importance that this solution has in the short term, while new engines powered by alternative low- or zero-carbon fuels are developed, since it can be implemented with minor modifications to the current infrastructure. Additionally, if applied to future bio-based fuels, it can even lead to a net negative emissions shipping industry.

In Chapter 4, we analyzed another potential application of carbon capture that simultaneously addresses EU climate targets and energy security. Given the recent political instabilities due to the Russian invasion of Ukraine that caused natural gas supply shortages, we investigated the production of synthetic natural gas, also known as biomethane, from biomass gasification with carbon capture and storage to be used for industrial heating. We considered two residues feedstocks, namely wheat straw and forest, and three dedicated energy crops grown on marginal land, i.e., *Miscanthus*, willow and poplar, for biomethane production at grid feed-in quality. We focus on the industrial heating sector since residential heating can be easily electrified and chemicals' production is performed directly from the syngas. Then, we compared the performance of each of the five scenarios between them and with the BAU.
We developed a detailed process simulation to determine the biomass-to-product conversion efficiency for each scenario. Based on literature data on the availability of the selected feedstocks, we concluded that 151 billion cubic meters (bcm)/year of biomethane can be

produced (i.e., theoretical potential), which is sufficient to satisfy the EU industrial heating demand. Among the EU countries, Spain, Poland, Germany and France are the largest biomethane producers, mainly based on forest residues, *Miscanthus* and poplar. In addition to being a secure energy source, biomethane is carbon negative on a cradle-to-gate basis and the theoretical potential could remove up to 0.33 Gt CO_2. We then assessed the impact of the biomethane with respect to the BAU finding that it benefits non-renewable energy resources and ozone depletion, while shifting the environmental burden to ecotoxicity freshwater and land use environmental metrics. Therefore, we developed an optimization problem to determine the optimal blend of natural gas and biomethane that limits the overall burden-shifting. Here, we found that reducing the pressure on these critical indicators is possible by deploying forest residues when little transgression is allowed, while wheat straw and forest residues and poplar for a greater transgression allowed.

In Chapter 5, we broadened the scope of the previous analyses and estimated the potential of bioenergy with carbon capture and storage (BECCS) supply chains by developing a detailed optimization model. We considered six feedstocks, e.g., three types of residues and three dedicated energy crops on marginal land, transportation links between the countries and regionalized parameters (crops carbon content, yield, land availability, costs) in the EU to meet a minimum yearly CO_2 removal target while producing electricity that can be integrated in the power system. Following a life cycle optimization approach, we conducted an economic and environmental assessment of the BECCS supply chain. The environmental indicators are finally aggregated into three metrics related to human health, ecosystem quality and resource availability according to the Recipe 2016 methodology. These are minimized in three independent scenarios, in addition to the cost minimization one.
We determined that, if residues and energy crops are deployed, the BECCS supply chain can provide benefits for human health and ecosystem quality even in the minimum total cost scenario. When the three endpoint indicators are minimized individually, an average improvement of 23% in the environmental indicators with less than 45% cost increase is achieved. Moreover, our model provides the configuration of the supply chain for the four scenarios analyzed on a regional level, i.e., regarding biomass transportation, amount of electricity produced from biomass combustion, and CO_2 storage location and type.

Lastly, in Chapter 6, we formulated a multistage stochastic programming model to address the uncertainty in the electricity demand in an integrated system that includes power generation

and carbon dioxide removal technologies, namely BECCS and DAC with CO_2 storage (DACCS), in the EU. Given the large size of the model and the consequent computational time to solve it, we developed a tailored decomposition algorithm that reduces the solution time by 90%. We then used this algorithm to investigate different case studies of carbon removal targets and gain insights into the power generation technologies and carbon removal options deployed. Our results show that neglecting uncertainties might lead to suboptimal solutions, particularly related to the total cost and technology capacity installed, i.e., a cost increase of roughly 10%, and different technology selection compared to the deterministic model are found when considering the uncertainty. Additionally, a decomposition algorithm tackling the specific structure of the problem was necessary, given the high complexity, for which conventional decomposition algorithms, e.g., Lagrangean decomposition, show poor performance. Furthermore, with our approach, we gained insights into the electricity generation technologies at a regional level in the EU (type, capacity and location) by determining which technologies are selected for capacity expansion and which ones are not necessary. Lastly, we demonstrated that BECCS plays a pivotal role in all the scenarios toward low- or net negative emissions. Indeed, even when a carbon positive emissions balance is allowed, there is electricity production from biomass and BECCS.

In conclusion, we provided simplified mathematical expressions to determine the economic and environmental performance of carbon capture and storage processes. Additionally, we demonstrated that carbon capture can serve as an interim solution for reducing direct emissions in the shipping industry and, when combined with biomass for biomethane production, for enhancing energy security for industrial heating while mitigating the effects of climate change in the EU. Furthermore, we developed a detailed optimization framework to analyze how to best deliver negative emissions while producing electricity in the EU via BECCS, which provides information on the supply chain at a regional level. Taking a step further, we have integrated DACCS and the power system in a single framework to assess the consequences of the electricity demand uncertainty on the total cost and power technology capacity installed in an integrated power system.

We expect that the combination of these tools and the insights that can be derived from their application will help decision-makers implement measures toward a more sustainable future.

7.2 Thesis limitations and future research directions

In Chapter 2, we provided analytical correlations for key economic and environmental process indicators that are valid for a range of input conditions. However, these operating conditions were run on a fixed flowsheet, i.e., the design of the equipment was optimal for the base case but not adapted to the new independent variables at each iteration. Additionally, we used the default BMS prior provided by the authors, which is based on mathematical expressions retrieved from Wikipedia, without adding specific field knowledge, i.e., from chemical and process engineering. We claim that the analytical models developed would become more accurate and simpler by tailoring the prior to include explicit chemical engineering laws. An additional improvement for future work is to develop gray box models, which combine first principles and black box approaches, and compare the performance with our correlations, at the expense of model simplicity. In Chapter 2, we presented a proof of concept; therefore, more case studies should be investigated including different and/or more independent variables, even beyond CCS processes. In particular, the approach is attractive when applied to experimental and industrial plant data. We also see the potential of this tool in many other research areas of Process Systems Engineering, such as surrogate-based optimization, and feasibility and flexibility analyses. Finally, the application of symbolic regression is not limited to process parameters, but can also embrace life cycle assessment metrics.

In Chapter 3, we proved that carbon capture on-board cargo ships could favor the transition toward a sustainable freight industry while new engines and the necessary infrastructure are developed. This solution, which we tested on a representative cargo ship, should be validated for a broader range of vessels, traveling at different speeds and considering varied routes. This extended analysis would bring insights into how technical, economic and environmental performance change. Additionally, this approach can still be implemented in the future to achieve negative emissions if combined with bio-based fuels. Indeed, in this scenario, the biomass absorbs the CO_2 from the atmosphere during the growth phase, which is then captured with a 94% efficiency after the combustion in the engine. Furthermore, our approach should be investigated for a shipping circular carbon economy, where the CO_2 is captured on-board and used to regenerate the fuel that powers the vessel's engine.

In Chapter 4, we evaluated the technical and environmental implications of biomethane production for enhancing energy security and curbing GHG emissions in the EU. In addition to the biomass availability, the logistics of the transportation of the biomass and the natural gas

imports from outside the EU to meet given transgression levels should be considered. In this case, the tools provided in this thesis should be integrated. In particular, the optimization model presented in Chapter 5 could be employed to design the optimal biomethane supply chain. Furthermore, we note that here we explored a potential future route using the gasification technology. However, as of today, the majority of the biomethane is produced by anaerobic digestion of biodegradable feedstocks followed by biogas upgrading, i.e., capturing the CO_2. These two production paths should be evaluated jointly to exploit the full potential, considering that there is competition for biomass for food, including the one for manure, and transportation fuels.

In Chapter 5, we provided an optimization model to evaluate the economic and environmental performance of a BECCS supply chain in the EU. Although the integration of more technologies would yield a more detailed framework where synergies can be exploited, we argue that the most significant coupling is the one with DACCS and the energy system, which was already investigated in this thesis and presented in Chapter 6. The reason of this claim is that other negative emissions technologies, such as afforestation and reforestation (AR), do not depend on electricity inputs, nor their characteristic parameters, such as the albedo for AR, show significant differences within the EU countries.
Additional constraints that limit the biomass transportation across countries or the design of the CO_2 pipeline network would lead to more realistic scenarios worth exploring.

In Chapter 6, we provided an optimization model of an integrated carbon removal – power technologies system in the EU and a tailored decomposition algorithm to speed up its computational time to evaluate the importance of considering uncertainty in the electricity demand, particularly in the total cost and technology deployment. As a next step, the model should also consider endogenous uncertainty parameters, such as carbon removal technologies learning curves. Given the current complexity of the model, we foresee that further decomposition will be required for the solution. Furthermore, the model should include a rigorous financial risk evaluation, which might lead to an intractable model.

In this thesis, uncertainty was not considered consistently and instead reported in each chapter on a case-by-case basis. In Chapter 2 uncertainty was not addressed, as the BMS models are stochastic. In Chapter 3 we also omit to consider uncertainty in the exhaust emissions due to lack of data. Instead, we provide one case study and estimate the equipment on-board weight and volume change for longer trips. Further work addressing different exhaust gas

compositions should be carried out in the future. In Chapter 4 we plan to include a qualitative assessment of the uncertainties that derive from the life cycle impact assessment method chosen. Based on the literature, we are aware that the impact categories of the Environmental Footprint can be characterized by low, medium or high uncertainty. A discussion of how this uncertainty affects the results reported in this thesis will be included. In Chapter 5 we assess the uncertainty of the life cycle assessment endpoint results considering the uncertainty in the life-cycle inventories provided by SimaPro. Lastly, in Chapter 6 we explicitly incorporate uncertainty in the optimization model to understand the implications on the power-carbon removal technologies nexus.

In summary, the work presented in this thesis leaves space for future methodological improvements and additional applications. From a methodological viewpoint, the models could be expanded to include different carbon capture technologies models and other sustainability metrics. Additional methods to tackle uncertainties, not only concerning the technical parameters but also the environmental assessment metrics, could be applied. In terms of application domains, the tools presented here are versatile to be implemented in the context of different problems, such as conventional chemical processes and their supply chains, and other heavy-duty transport means. Finally, the integration of the tools provided, such as surrogate models within supply chain optimization frameworks, should be explored.

7.3 List of contributions produced from this thesis: publications, conference proceedings, and oral presentations

The following contributions were produced from this dissertation:

List of journal publications and conference proceedings:

- Negri, V., Galán-Martín, Á., Pozo, C., Fajardy, M., Reiner, D. M., Mac Dowell, N., Guillén-Gosálbez, G., 2021. Life cycle optimization of BECCS supply chains in the European Union. Applied Energy 298, 117252. https://doi.org/10.1016/J.APENERGY.2021.117252
- Negri, V., Vázquez, D., Sales-Pardo, M., Guimerà, R., Guillén-Gosálbez, G., 2022. Bayesian Symbolic Learning to Build Analytical Correlations from Rigorous Process Simulations: Application to CO2 Capture Technologies. ACS Omega. https://doi.org/10.1021/acsomega.2c04736
- Negri, V., Guillén-Gosálbez, G., 2022. Implications of Optimal BECCS Supply Chains on Absolute Sustainability. Computer Aided Chemical Engineering, 49. Elsevier, pp. 619–624. https://doi.org/10.1016/B978-0-323-85159-6.50103-2
- Negri, V., A. Charalambous, M., D. Medrano-García, J., Guillén-Gosálbez, G., 2022. Navigating within the Safe Operating Space with Carbon Capture On-Board. ACS Sustainable Chemistry & Engineering 10, 17134–17142. https://doi.org/10.1021/acssuschemeng.2c04627
- Cobo, S., Negri, V., Valente, A., Reiner, D. M., Hamelin, L., Mac Dowell, N., Guillén-Gosálbez, G., 2023. Sustainable scale-up of negative emissions technologies and practices: where to focus. Environmental Research Letters 18, https://doi.org/10.1088/1748-9326/acacb3
- Negri, V., Charalambous, M. A., Medrano-García, J. D., Guillén-Gosálbez, G., 2023. Sustainable Development Goals assessment of carbon capture on-board. Computer Aided Chemical Engineering, 52. Elsevier, pp. 2927–2932. http://doi.org/10.1016/B978-0-443-15274-0.50466-2

List of oral presentations:

- Exploring the Economic and Environmental Potential of a Large-Scale Biomass Supply Chain for Carbon Dioxide Removal in the European Union. 2020 Virtual AIChE Annual Meeting. November 16 – 20, 2020
- Design and Optimization of a Sustainable BECCS Supply Chain in the European Union to Reduce the Stress on Core Planetary Boundaries. 2021 AIChE Annual Meeting, Boston (MA), USA. November 8, 2021
- Formulation of Closed-Form Mathematical Expressions Applied to Chemical Engineering Processes Using the Bayesian Machine Scientist. 2021 AIChE Annual Meeting, Boston (MA), USA. November 10, 2021
- Optimal Deployment Under Uncertainty of Negative Emissions Technologies in the European Union Power System. 2022 AIChE Annual Meeting, Phoenix (AZ), USA. November 17, 2022
- Absolute Life Cycle Optimization of the CDR-Power Nexus. FOCAPO / CPC 2023, San Antonio (TX), USA. January 10, 2023
- Sustainable Development Goals assessment of carbon capture on-board. ESCAPE 33, Athens, Greece. June 19, 2023

APPENDIX A

Supplementary information to Chapter 2

A.1 Model parameters and MCMC steps

The number of Markov chain Monte Carlo (MCMC) steps chosen to obtain the mathematical expression of each output variable, and the respective parameters are reported in Table A0.1 for the two case studies analyzed. The goodness of fit for the natural gas process variables results in an R-squared (R^2) above 99% for three out of four output variables, at low (1000-10000) MCMC steps. On the contrary, in the case of the flue gas, we require more steps (up to 50000) to achieve similar performance.

Table A0.1 MCMC steps and parameters of the dependent variables mathematical expressions for each case study analyzed.

Case study	Variable	MCMC steps	Parameters	
Natural gas	Min CU	1000	a0	4648399064
			a1	0.515205668
			a2	0.08127544
			a3	-5.251595861
			a4	22554.25141
			a5	1.203644142
	Min HU	5000	a0	2.92526E+18
			a1	3.73775E-08
			a2	351315.5
			a3	17571.65
			a4	9.752716
			a5	1752.488
			a6	-8.4617E+12
	Net power	1000	a0	6.692334
			a1	-13459
			a2	-0.85238
			a3	-0.37024
			a4	0.507276
			a5	-7115.09
			a6	20657.74
	Amount of MEA	10000	a0	14112.78686
			a1	-2935.415061
			a2	0.998725114
			a3	0.063845319
			a4	8.823491621
			a5	3.99600556
			a6	1467.217871
			a7	26.01699426

Flue gas	Min CU	50000	a0	-36.05539994
			a1	1.166973668
			a2	0.110793704
			a3	-0.439532683
			a4	3.14E-12
			a5	-0.211170691
	Min HU	20000	a0	-27.03351235
			a1	0.009314512
			a2	-10.34924972
			a3	-8979.599802
			a4	-1284.685929
			a5	0.189841719
			a6	5647.160388
			a7	854.5832804
	Net power	10000	a0	396.2374688
			a1	-86.10050791
			a2	-1.158995964
			a3	10.59161605
			a4	-1.026713473
			a5	1.990606682
			a6	17.65652763
			a7	1.494928476
	Amount of MEA	20000	a0	0.011393358
			a1	132.8078147
			a2	11.80288973
			a3	0.000671093
			a4	-2.290336089
			a5	0.602889551
			a6	-4420.333972
			a7	-117.5256979
			a8	6.326634953
			a9	1.233677766

A.2 Models assumptions and limitations

The case studies in Chapter 2 are designed based on the following assumptions:

- The natural gas feed is considered a binary mixture, similarly to other literature studies about emerging technology such as membranes [73,333,334].

- With the underlying idea of including a wider range of product purity in the natural gas case study, we also consider scenarios where further processing of the sweet gas product is required before pipeline distribution (about 50% of the results meet the specification for immediate distribution).

- The cooling and heating utilities requirements are calculated based on the composite curves for each point without determining the optimal heat exchanger network.

- Further optimization of the process design could be achieved in both case studies to decrease the amount of solvent, energy consumption, and increase the product purity. Both processes are simulated based on literature studies as a starting point. Then, sensitivity analyses are carried out on the characteristic parameter of each unit operation. For example, coolers and heaters outlet temperatures, compressor pressure, feed stage and number of trays in the absorber and stripper columns were varied in ranges of interest. The effect of the design on the product stream (sweet gas or clean gas for the first and second case study, respectively) and the CO_2 stream was monitored. We note that no optimization tool was used to define the final design of either process.

- Our designs differ from previous literature studies as we include a purge in the process. We account for pressure drop in the unit operations to represent a real system more closely. The pressure drop is fixed to 0.2 bar in the heat exchangers and 0.04 bar/stage in the columns. No pressure drop is considered in the flashes.

- The energy requirement for CO_2 injection and storage in a selected site is not considered in the models, and only the energy demand to obtain supercritical CO_2 is accounted for.

- Specifically for the flue gas treatment process, the design of the base case has not been improved further to allow for greater flexibility to explore a range of six input variables, despite the low CO_2 removal compared to the majority of literature studies. However, some literature about low CO_2 capture rate is also available [100,335]. We here aim at

exploring a wider range of input conditions while proving a lower bound for the proxies of the operating costs. Nonetheless, we report that for the same design in Fig. 3 and an overall capture rate of 90%, the reboiler duty is 3.3 MJ/kg of CO_2 captured. We obtain 6804 kW and 5280 kW from the Aspen energy analyzer as the target of cooling and heating utilities.

- The training and validation dataset depend on the ranges of the input variables chosen and are limited by the flowsheet convergence.

- To improve the goodness of fit, a higher number of MCMC steps can be explored for each output variable. At infinite MCMC steps, the error of the prediction should be zero.

Additionally, we report in Table A0.2 the upper and lower bounds of the two product streams in both case studies analyzed.

Table A0.2 Maximum and minimum flow rate values of the clean gas and CO_2 stream obtained during the sampling of the two case studies.

Case study		**Clean gas [kg/s]**	**CO_2 stream [kg/s]**	**CO_2 stream [%mol. fraction CO_2]**
Natural gas sweetening	Minimum	16.08	11.47	98.79
	Maximum	22.12	17.32	99.17
Flue gas treatment	Minimum	7.17	7.93E-3	99.57
	Maximum	8.21	1.84E-2	99.59

The sampling and training steps are carried out on an Intel Core i9-9900 machine at 3.10GHz and 32 GB RAM running Windows 10. The training of each output variable required 3 to 24 hours, depending on the number of MCMC steps. The validation is done using an Intel Core i7-10510U machine at 1.80GHz and 16 GB RAM running Windows 10.

A.3.1 Variables selection

Table 2.1 reports the selected independent and dependent variables for the two case studies analyzed. Here, we are interested in two processes that provide a CO_2-free product, natural gas or flue gas, for a wide range of inlet conditions of the untreated gas. Therefore, the independent variables are the properties of the input flow, i.e., temperature, pressure and composition. On the contrary, the dependent variables are selected based on the goal of the analysis. In our work, we want to analyze the process performance with indicators related to the economics and

environmental impacts, such as heating and cooling energy requirement. We note that different performance indicators can be chosen, e.g., CO_2 absorption efficiency or recovery, CO_2 storage conditions or alternative process design parameters. These parameters can be easily calculated when working with process simulators. However, it might be more challenging when the data are obtained from an experimental setup. In the case of experimental systems, it might not always be possible to measure the variables of interest, which can limit the choice of dependent variables substantially. The configuration of the setup might be very similar to the flowsheets presented in Figure 2.2 and 2.3, but on a smaller scale (see, for example, the pilot scale setup presented by Morgan and co-workers[120]).

A.3.2 Interpretability of the models

The most critical aspect of data-driven machine learning algorithms is the poor interpretability due to the lack of components based on chemical and physical laws in the algorithm's structure. We note that our model is trained with data based on the solution of a complex system of nonlinear equations comprising mass and energy balances and thermodynamic equations, which might be impossible to express in the form of a single simple equation based on first-principles. Noticeably, the original first-principles model is more accurate than the simplified model, but the latter comes with the great advantage of substantially simplifying the modeling[156]. As already mentioned, building mechanistic models can be time-consuming, especially when convergence issues arise. Therefore, the streamlined equations presented here can facilitate access to the modeling tools by experimental groups, with applications in a wide range of process systems engineering problems, as discussed in Section 2.5.3, and eventually in industry.

Although machine learning methods can be applied to a great variety of problems, including chemical engineering-specific problems, the trained models are valid within the range of the training set, often with very limited extrapolation capabilities. Consequently, the models presented in this work cannot be applied to a different solvent, either reactive or physical, or a different solvent composition. However different surrogate models could be conveniently introduced for all the cases. On the other hand, hybrid models are developed by integrating mass and energy balances and approximating other relationships with data-driven models. The advantage of the so-called black box models, such as those presented in our work, is having a single compact expression for each dependent variable representing the entire flowsheet. Regarding the drawbacks mentioned above, we argue that the lower accuracy shown by the

simplified model, relative to the fully mechanistic analog, would also be found in gray box (hybrid) models.

A.3.3 Application of the Bayesian machine scientist to time-dependent analyses

In our work, we show how the BMS is able to retrieve simplified equations based on synthetic data generated from simulations at steady-state. However, the BMS is also suitable to deal with time-dependent analyses, provided that time is given as an input variable. Alternatively, the BMS can be used to model differential equations instead of the time-variable quantities. In the original publication[45], the BMS is shown to accurately recover a system of coupled nonlinear differential equations.

More established machine learning methods, such as artificial neural networks (ANN), can also be applied to deal with time-dependent data. In this case, they can include internal "recycle" connections to deal with dynamic problems and time-series data[336].

A.4 Residual plots

Once the closed-form expression of a dependent variable has been obtained using the BMS, various metrics are calculated to determine the goodness of the regression. The R^2, mean relative error (MRE) and mean squared error (MSE) of the validation set are reported in the Chapter 2, while the residuals are shown in Figure A0.1 for the two case studies. The residuals are calculated as the difference between given and predicted values of the output variables in the training set.

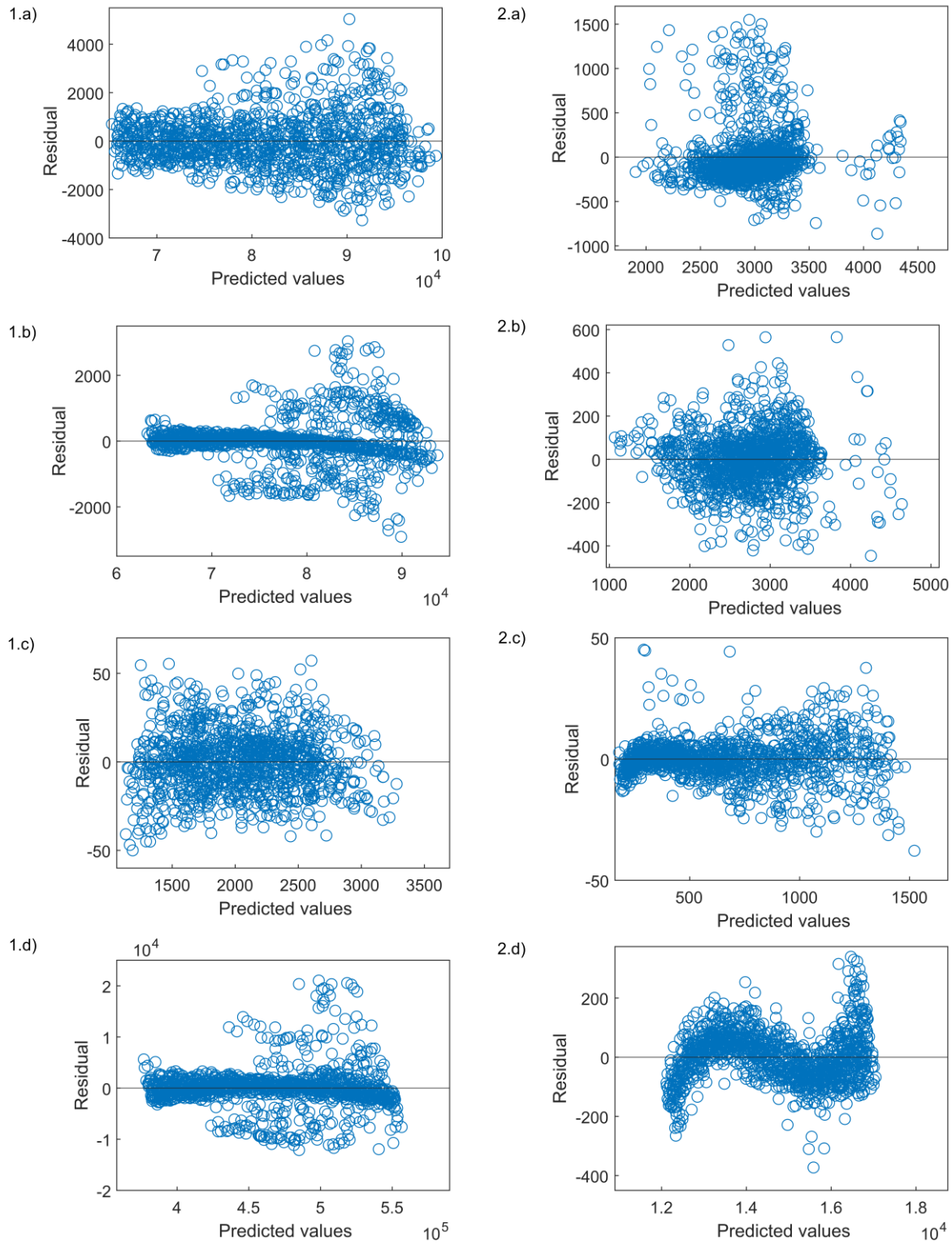

Figure A0.1: Scatter plot of the residual vs. predicted values in the training set. The plots on the left column refer to the analytical expressions of the natural gas sweetening process (1), while on the right one to the flue gas treatment (2) for the dependent variables a) cooling, b) heating utilities, c) net power required and d) amount of MEA.

A.5 Model training performance

We generated 1200 and 2500 scenarios in the natural gas and flue gas cases, respectively, out of which 1174 and 1245 converged, which were employed to determine the closed-form mathematical expressions for each output variable of the two case studies reported in Chapter 2. The scatter plot of the data around the regression line is shown in Figure A0.2 and Figure A0.3 for the natural gas and flue gas training dataset, respectively. The corresponding R^2, MRE and MSE are reported in Table A0.3 and Table A0.4.

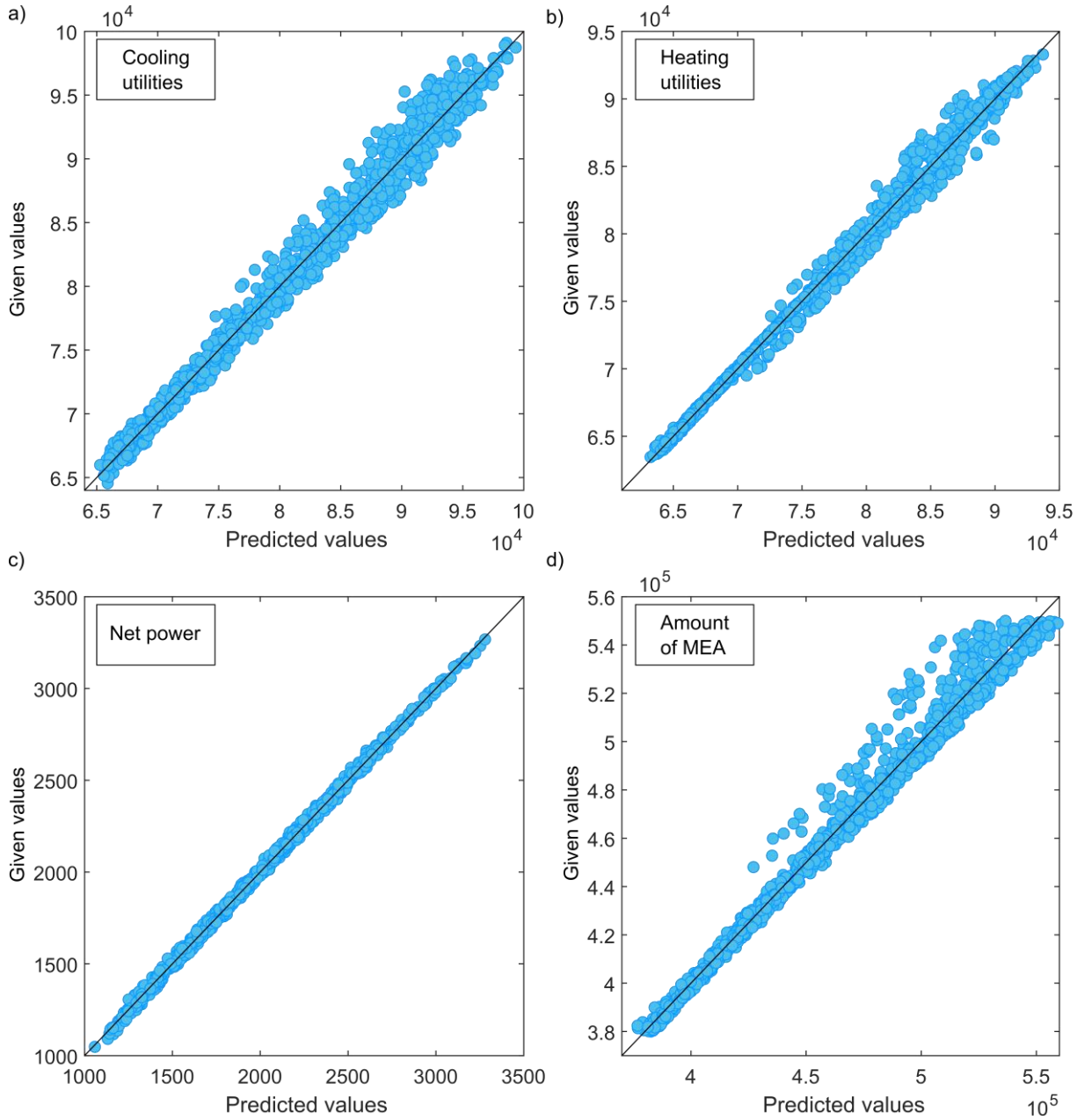

Figure A0.2: Given vs. predicted values correlation for the four output variables in the training dataset of the natural gas sweetening process. a) cooling and b) heating utilities, c) net power and d) amount of MEA. The regression line is shown in black.

Table A0.3 R^2, MRE and MSE statistics for each output variable of the natural gas sweetening process in the training dataset.

Case study	Variable	R^2	MRE	MSE
Natural gas	Min CU	0.9842	0.0102	1.27E+06
	Min HU	0.9922	0.0054	5.04E+05
	Net power	0.9986	0.0071	2.97E+02
	Amount of MEA	0.9930	0.0051	1.70E+07

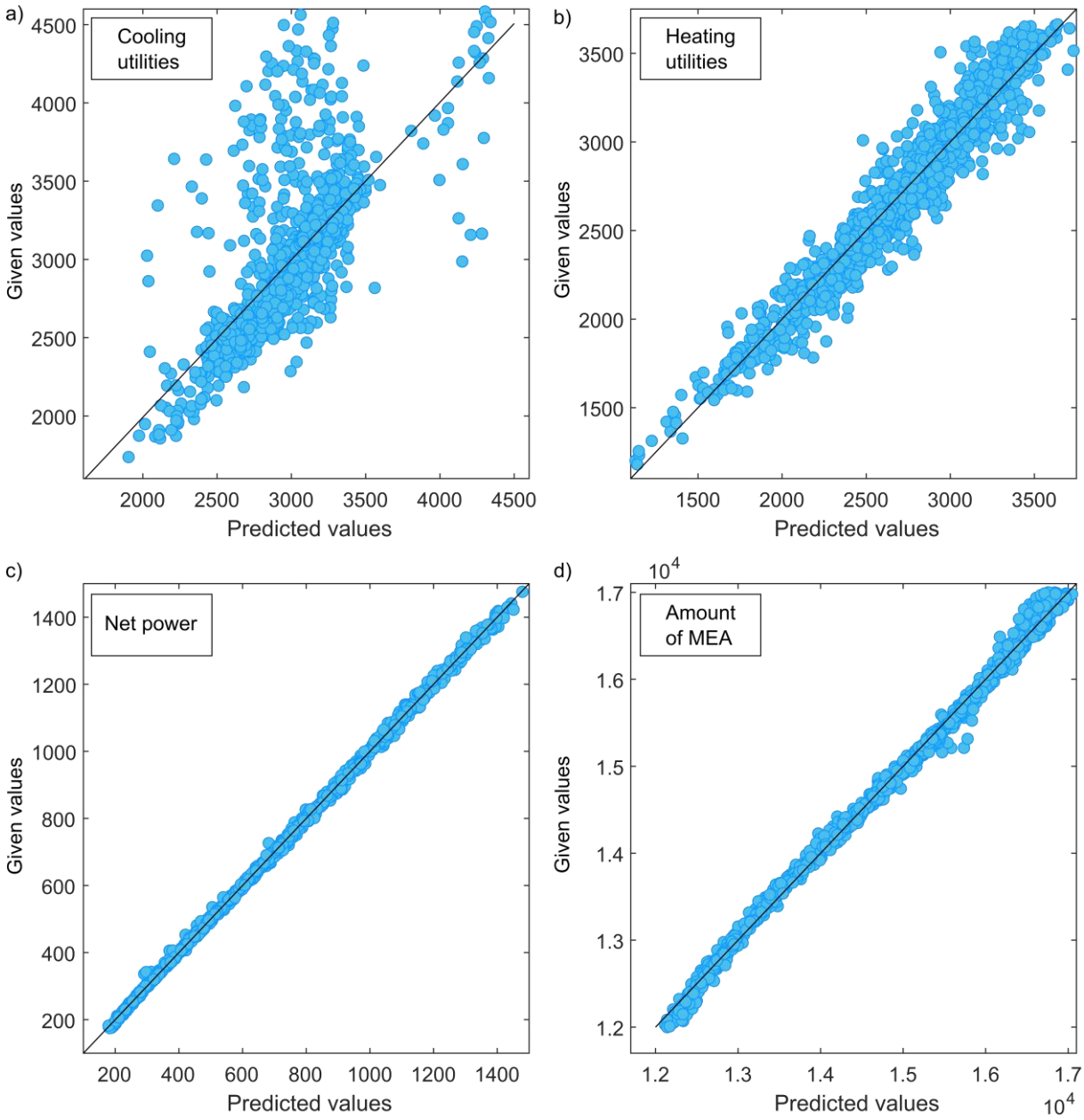

Figure A0.3: Given vs. predicted values correlation for the four output variables in the training dataset of the flue gas treatment process. a) cooling and b) heating utilities, c) net power and d) amount of MEA. The regression line is shown in black.

Table A0.4 R^2, MRE and MSE statistics for each output variable of the flue gas treatment process in the training dataset.

Case study	Variable	R^2	MRE	MSE
Flue gas	Min CU	0.4909	0.0707	1.16E+05
	Min HU	0.9434	0.0359	1.64E+04
	Net power	0.9993	0.0099	7.71E+01
	Amount of MEA	0.9962	0.0046	7.77E+03

A.6 Comparison with neural networks

Lastly, we want to compare the performance of the BMS to a standard machine learning approach. Numerical methods are well established in the process engineering community, and successful examples of input-output relationships applied to industrial processes have been presented[337–339]. However, we argue that symbolic regression offers more advantages in terms of interpretability, complexity and flexibility of the mathematical structure than neural networks, making it particularly suited to understanding complex systems[340]. ANNs, even the simplest feedforward fully connected networks, present a specific predefined structure where the number of neurons, layers, and hyperparameters must be determined beforehand. Usually, these hyperparameters are chosen through different tuning methodologies. Similarly, Gaussian processes require the selection of a kernel function, together with its hyperparameters.

In these numerical methodologies, the model has a pre-defined structure that is trained, i.e., the weights are fitted. On the contrary, the BMS does not present a singular structure, but it develops one while fitting the parameters. Additionally, the BMS can successfully identify rigorous models with as little as 100 points using less than ten parameters[45].

We use the ANN built-in function in MATLAB[341] and we activate the Bayesian regularization. The results of the ANN are given in Figure A0.4 and Figure A0.5 for the training and testing of natural gas, while Figure A0.6 and Figure A0.7 for training and testing of the flue gas, respectively. The R^2 value of the regression is reported on top of each scatter plot.

Notably, we find that a data fit with higher R^2 can be obtained using the ANN and the computational time is lower. However, the ANN is a black box model rather difficult to interpret and use, especially for the type of analyses proposed in Chapter 2 Section 2.5. We also point out that those variables that are regressed with the lowest accuracy using the BMS show the same behavior when the analysis is carried out with ANN (Figure A0.6 a)).

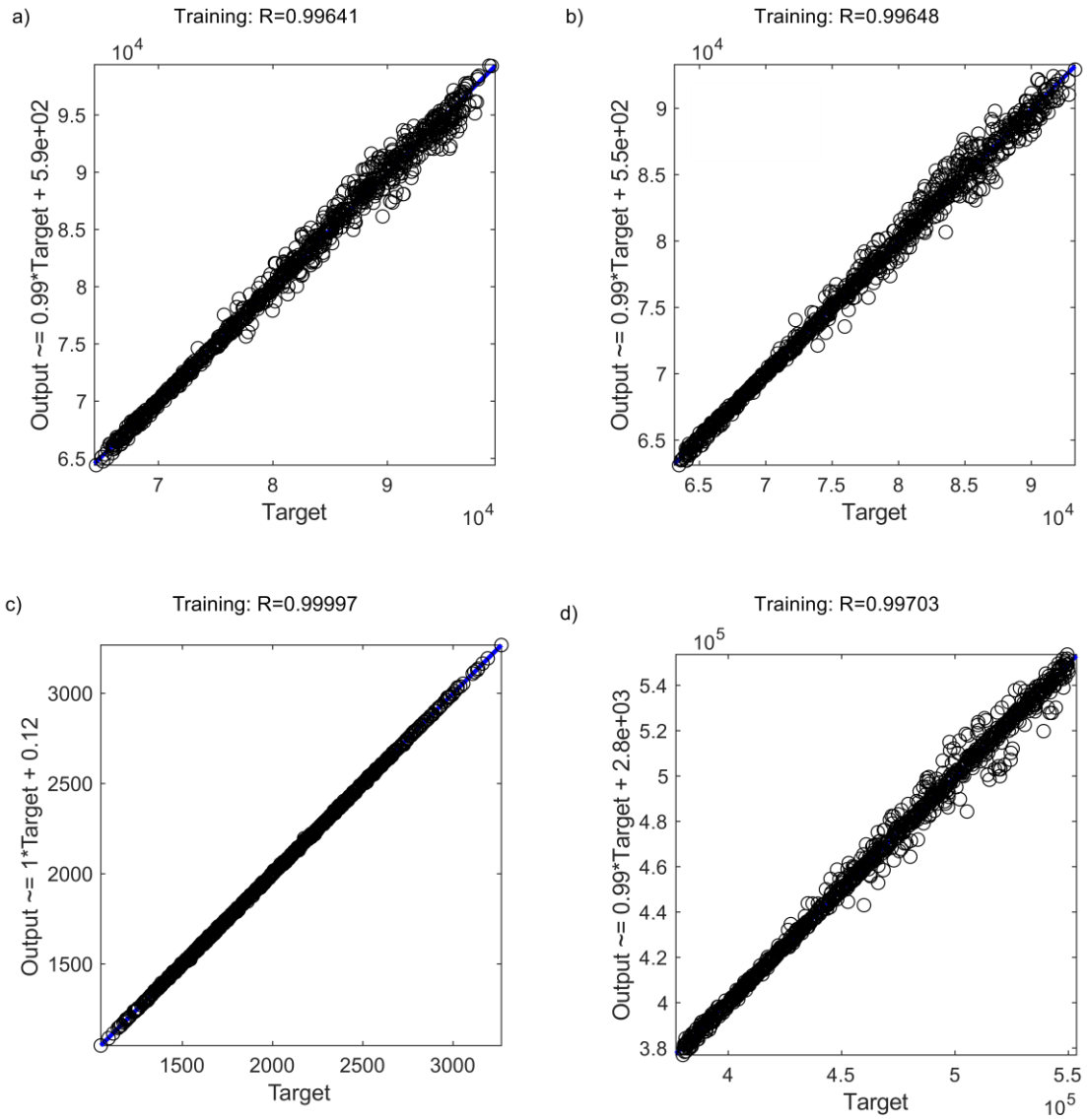

Figure A0.4: ANN results of natural gas process training dataset using the Bayesian regularization. The blue line represents the fit, the circles the data and the dashed line is the regression output = target. The four output variables in the training dataset are a) cooling and b) heating utilities, c) net power and d) amount of MEA.

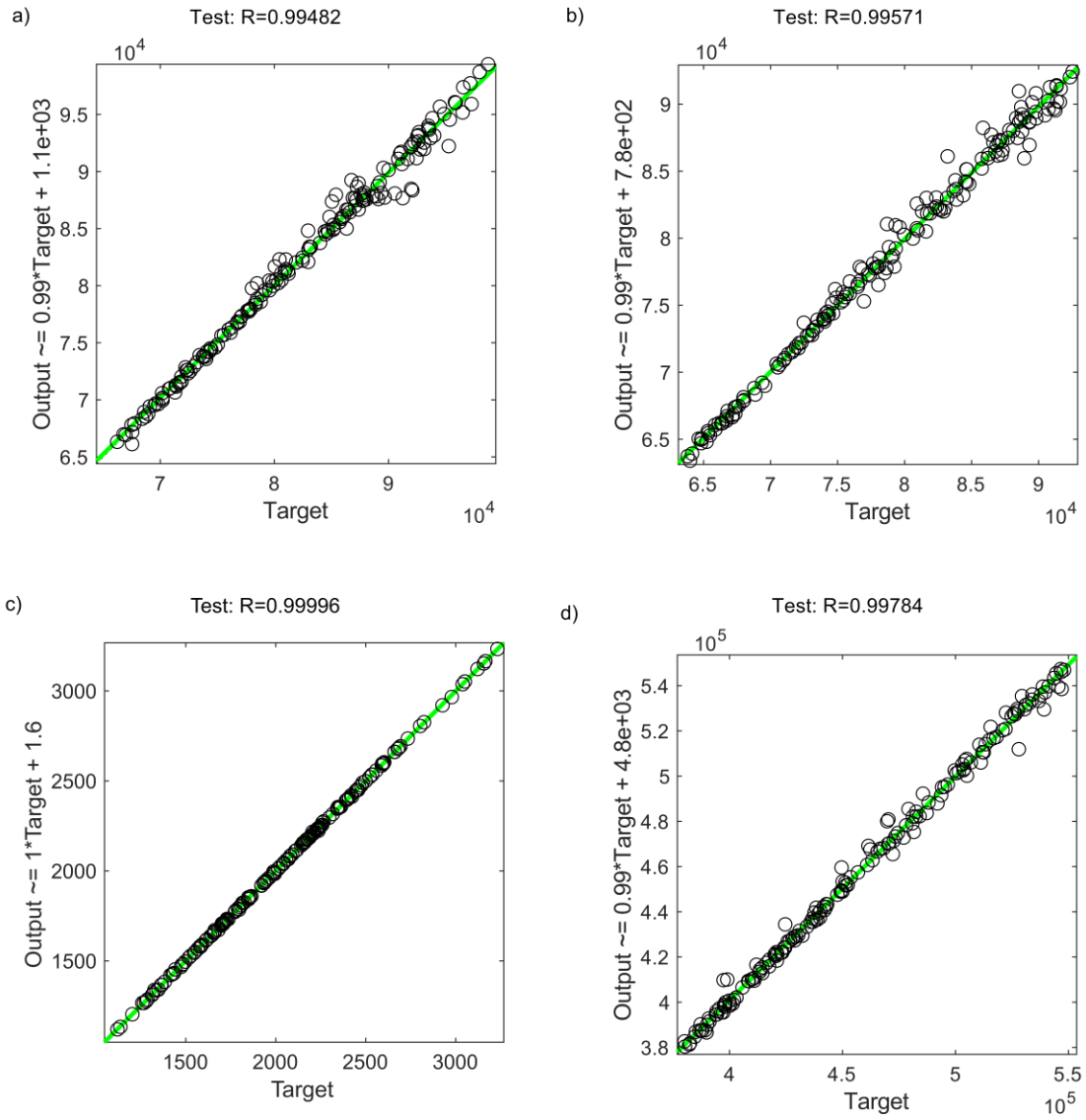

Figure A0.5: ANN results of natural gas process testing set using the Bayesian regularization. The green line represents the fit, the circles the data and the dashed line is the regression output = target. The four output variables in the testing dataset are a) cooling and b) heating utilities, c) net power and d) amount of MEA.

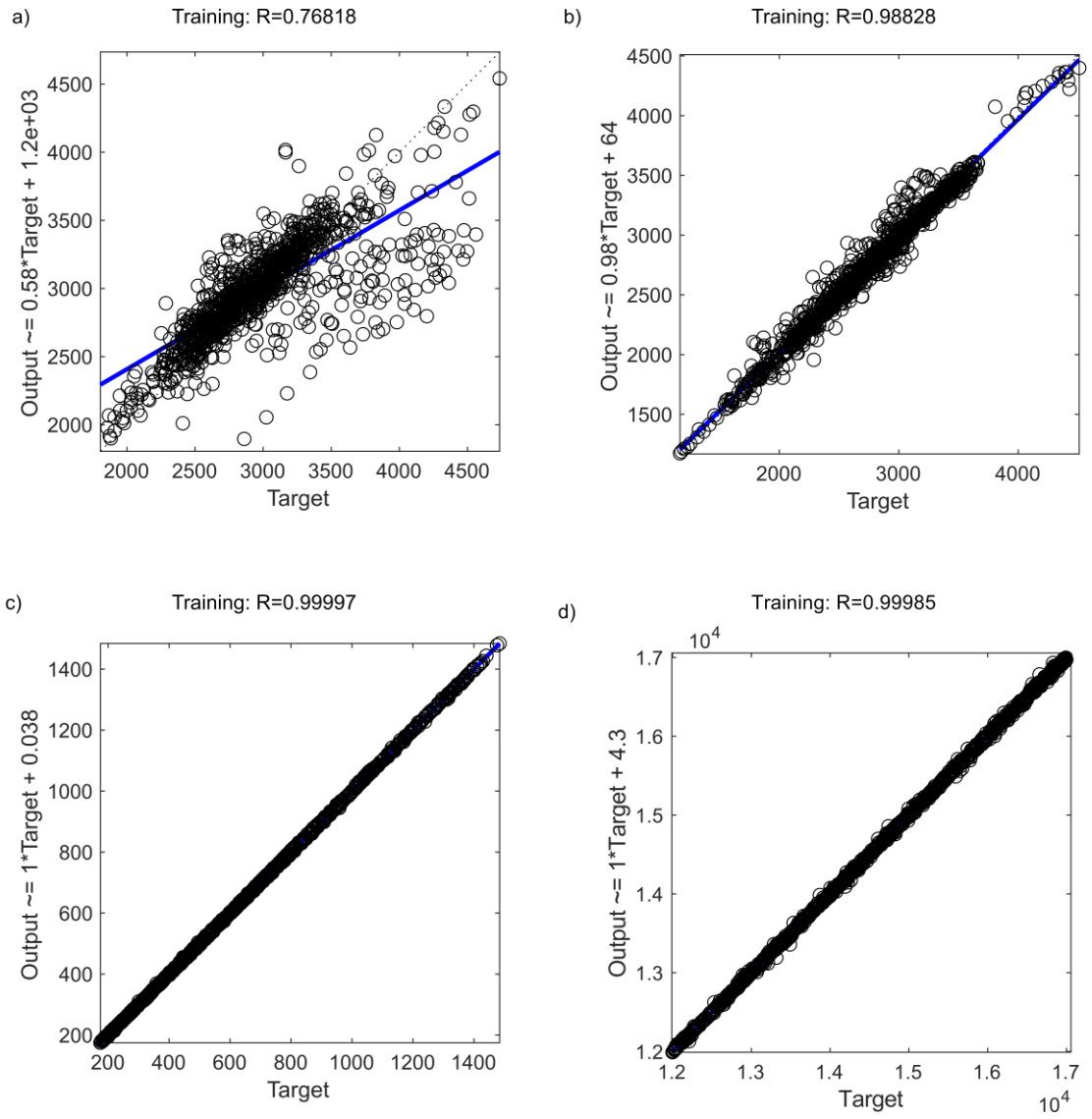

Figure A0.6: ANN results of flue gas treatment process training set using the Bayesian regularization. The blue line represents the fit, the circles the data and the dashed line is the regression output = target. The four output variables in the training dataset are a) cooling and b) heating utilities, c) net power and d) amount of MEA.

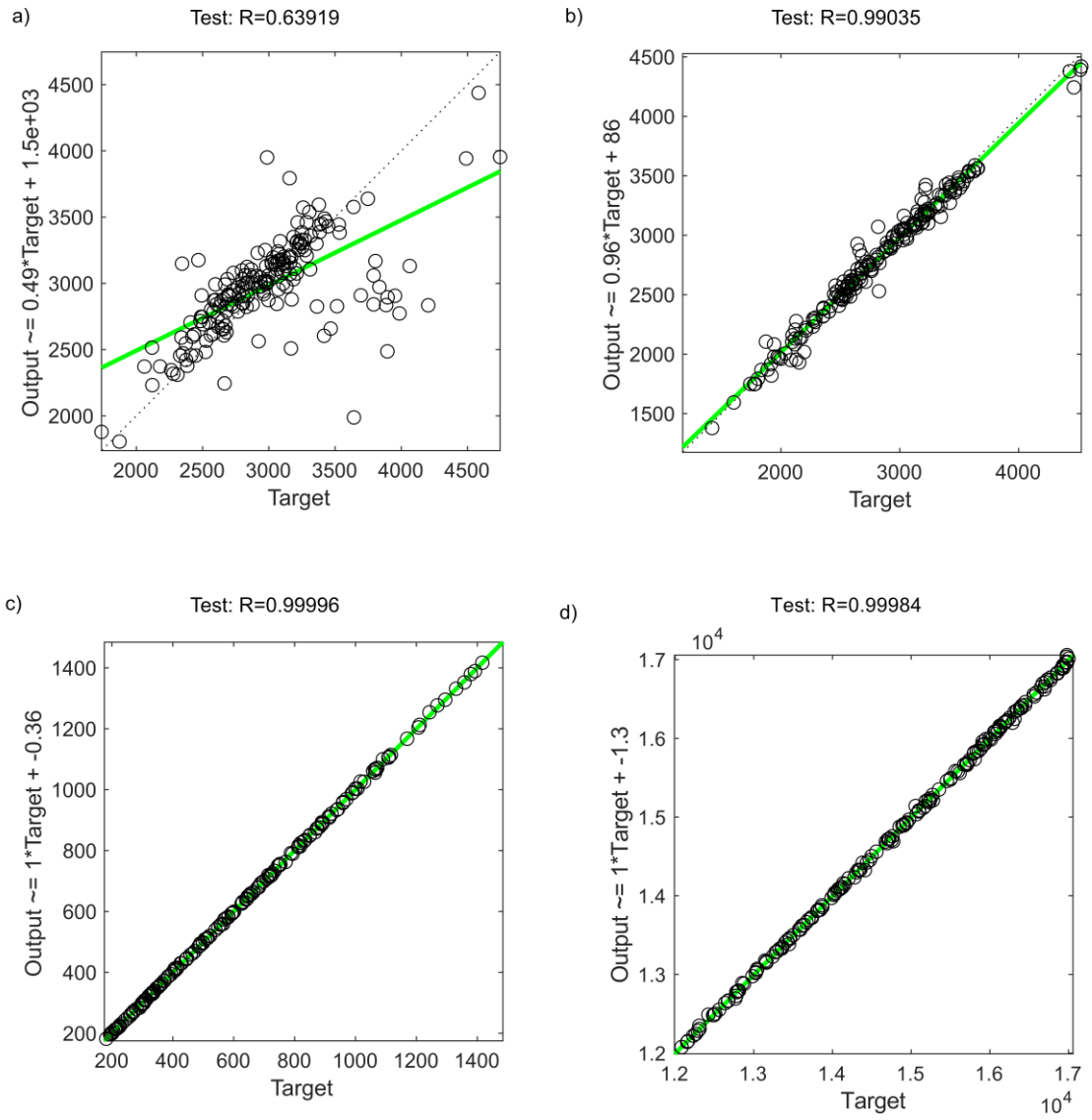

Figure A0.7: ANN results of flue gas treatment process testing set using the Bayesian regularization. The green line represents the fit, the circles the data and the dashed line is the regression output = target. The four output variables in the testing dataset are a) cooling and b) heating utilities, c) net power and d) amount of MEA.

We repeat the analysis carried out in Section 2.5.2 using ANN instead of the BMS, whose results are reported in Table A0.5. We find that the error on the extrapolation of the cooling utility ratio is 12%, while the one on the power is 3.5% compared to the result obtained within the training bounds. ANN proves once again that the new technology using Stirling coolers performs better in terms of energy consumption.

Table A0.5. Comparison of cooling and electricity requirements for the process by Song et al.[79] (*cry*) and our BAU (*BAU*) using ANN. The values are calculated as the processes' energy requirement ratio: BAU/ cryogenic normalized by the absorber top product mass flow rate.

	Case I: without heat integration			
	$MinCU^{BAU}$/ $MinCU^{cry}$		**Net $power^{BAU}$ / Net $power^{cry}$**	
	Prod. low	Prod. high	Prod. low	Prod. high
CO_2 mol. in [79] (0.5%)	2.58	2.25	1.08	0.94

APPENDIX B

Supplementary information to Chapter 3

B.1 Process simulation parameters

The exhaust gas treated in the process illustrated in Chapter 3 (Figure 1, Exhaust gas at 500.0 °C and 1.0 bar) is characterized by the composition reported in Table B0.1, which is typical of the combustion of standard heavy fuel oil (HFO).

Table B0.1. Exhaust gas composition[195,342].

Component	Mole [%]
CO_2	13.95
O_2	0.08
N_2	74.46
H_2O	10.72
SO_2	0.19
NO	0.61

After the exhaust gas is mixed with air, the resulting stream is cooled down to 400.0 °C to enter the de-nitrification reactor along with ammonia (NH_3). At this temperature, nitrogen oxides (NOx) are assumed to be nitric oxide (NO)[343]. Before the reactor, the molar ratio of NH_3 and NO is set to 1.05. NH_3 undergoes a comproportionation reaction into molecular nitrogen (N_2), where 96 % of the NO is reacted and, simultaneously, 98 % of the SO_2 is oxidized into SO_3 according to reactions (B1) and (B2).

$$2\ NH_3+3\ NO \rightarrow 2.5\ N_2+3\ H_2O \quad \text{(B1)}$$

$$SO_2+1/2\ O_2 \rightarrow SO_3 \quad \text{(B2)}$$

In the scrubber, the mixture at 150.0 °C is put into contact with water and sulfuric acid (H_2SO_4) is formed as in Eq. (B3).

$$SO_3+H_2O \rightarrow H_2SO_4 \quad \text{(B3)}$$

The process described in Figure 1 has been designed according to the following assumptions:

- 0.2 bar pressure drop in the heat exchangers.
- Centrifugal compressors are assumed for the process, except for K-102, K-103, K-104 before the CO_2 absorption section, which are blowers.
- The scrubber to neutralize H_2SO_4 is designed with 15 stages, at 1 bar and a pressure drop of 0.2 bar.

- Absorber and stripper are packed columns with Sulzer Mellapak plastic packing 250Y. The absorber has 18 stages, and operates at ambient pressure (1.0 bar) with a total pressure drop in the column of 1.0 bar, while the stripper has 35 stages, operates at 3 bar with an overall pressure drop of 1.4 bar. The total height of the columns is calculated based on the number of stages considering 0.61 m between theoretical plates.

- The CO_2 capture process is performed using a 30% wt. aqueous solution of monoethanolamine. However, other CO_2 capture technologies are commercially available. According to the latest DNV Maritime forecast to 2050 report[10], carbon capture and storage (CCS) will play a decisive role in the transition to alternative fuels because of the technical barriers that carbon-neutral fuels are facing, including high costs and large energy requirements. Notably, the report suggests that this mature technology and its infrastructure can mitigate the impact of the use of conventional fuels until the transition to cleaner options is completed. According to the DNV, the CCS technology will be operated with liquid absorbents, and in particular post-combustion using amines was already identified as TRL 9 by Bui and co-authors[6]. A detailed analysis of all possible alternatives for carbon capture is out of the scope of this work and can be found in several reviews recently summarized by Hasan et al.[302] from a process engineering perspective.

- The mass flow of natural gas (NG) required in the furnace is calculated based on the reboiler duty and adjusted accordingly in Aspen HYSYS to generate a sufficient amount of steam in the steam cycle.

  We note that we use NG to provide the heat required by the reboiler instead of the ship fuel, i.e., HFO, because we focus on assessing a short-term interim solution that would require minimal modifications in the current vessels. Using HFO would imply that additional fuel should be stored in the fuel tank to feed both the engine and the furnace. Instead, the solution proposed can be easily adapted to different types of vessels, and it can operate with other fuels that might be used in the future, such as biofuels. Additionally, once they are empty, the NG tanks are used to store the CO_2 captured until it is unloaded at the port.

- Heat integration is performed in Aspen HYSYS using Aspen Energy Analyzer, which provides the heat exchangers' size reported in Table B0.4.

- The CO_2 captured is stored in liquid form on-board, firstly into new tanks that are transported for this purpose, and secondly by refilling the tanks of liquefied NG consumed in the furnace during the trip.
- For simplicity, all units are considered in stainless steel, while the storage tanks are in carbon steel, assuming that the replacement of the tanks due to corrosion is easier than the equipment on-board.
- The dimensions of the storage tanks are taken from the commercial brochure available at the following links
    - CO_2 tanks
    - LNG cryogenic tanks
- We carry out the design of the plant on-board following the correlations in Towler and Sinnot[206], which account for process controllers, equipment erection and related civil engineering works. However, our work is a feasibility study and does not consider specific safety regulations that have to be taken into consideration based on the particular type of ship. We assume that the equipment on-board have sufficient space, building on the work by Feenstra et al.[11] who provided a technical drawing of a retrofitted plant on-board LNG and diesel vessels, considerably smaller than our reference ship.
- The design of each piece of equipment is based on data available in the literature as reported above and in the main text and further adjusted manually to meet the desired output conditions for the process, in particular, the columns' number of stages and pressure drop in the CO_2 capture section.

We report in Table B0.2 and Table B0.3 the details of the main process streams and duties in the flowsheet.

Table B0.2. Process simulation molar flow rate, temperature and pressure data of the main process streams (± 0.5 kmol/h). The name of the streams refers to Figure 3.1 in Chapter 3.

Stream	Flow rate [kmol/h]	Temperature [°C]	Pressure [bar]
NH_3	38.0	25.0	1.0
Air	100.0	25.0	1.0
Exhaust gas	5962.0	500.0	1.0
NG	256.6	25.0	1.0
Vent gas	7669.0	57.3	1.0
CO_2 to storage	1032.0	−18.0	22.0
Solvent makeup	108.0	38.0	1.2
Water makeup	1098.0	38.0	1.2

Table B0.3. Equipment duty, with reference to Figure 3.1 in Chapter 3.

Stream	Duty [MW]
Reboiler	73.5
Condenser	8.7
Furnace	52.3

A schematic of the heat exchanger network is presented in Figure B0.1, while we report in Table B0.4 the areas and the heat loads of the corresponding heat exchangers. The network does not include the steam cycle for the reboiler heat integration, NG and NH3 heat exchangers because they are integrated manually in the process simulation.

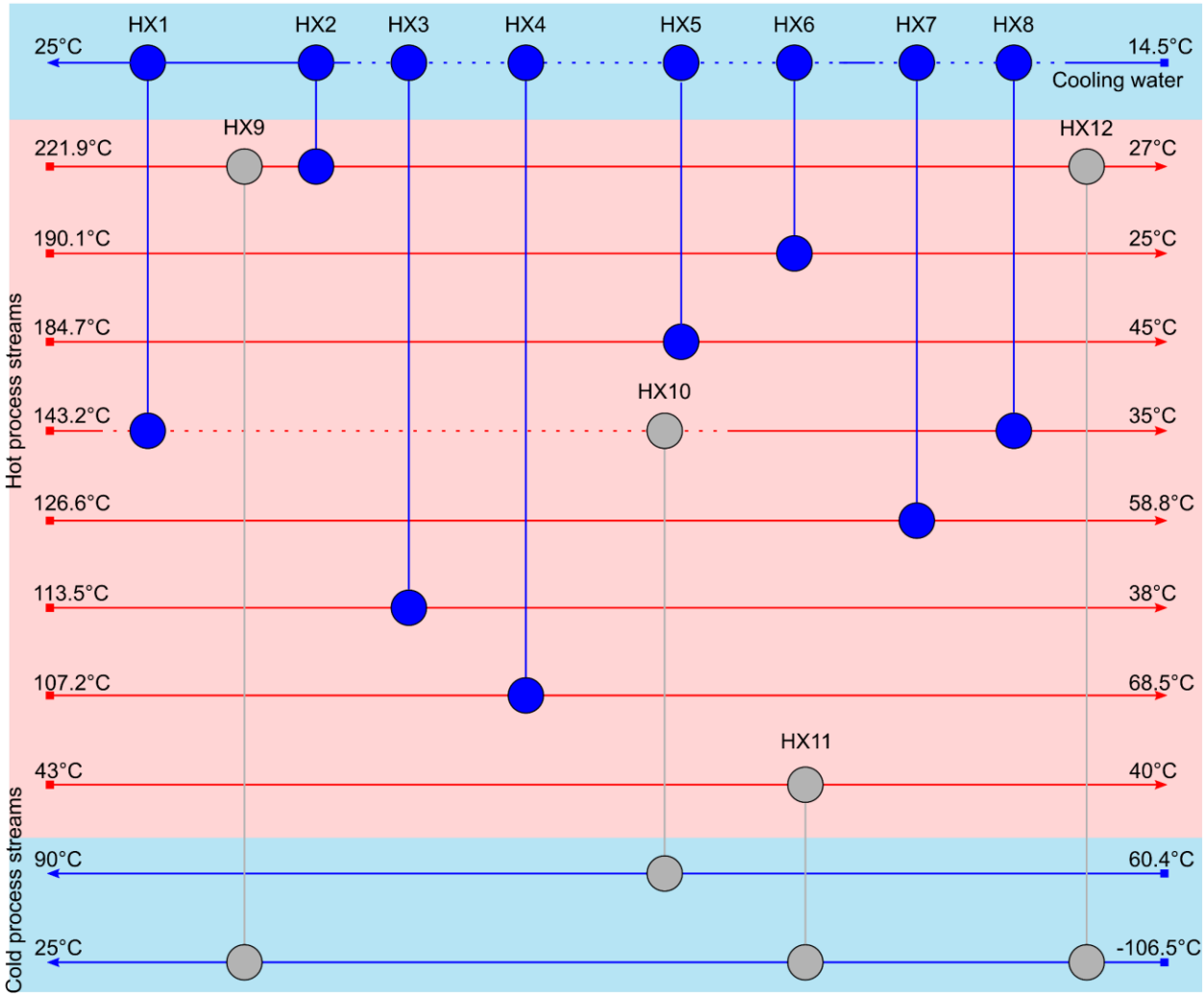

Figure B0.1: Heat exchanger network of the process in Figure 1. The streams in dotted lines are split. The network shown does not include the liquefaction section, i.e., the NG (E-111) and NH_3 (E-112) heat exchangers and the steam cycle because they are integrated manually.

Table B0.4. Heat exchanger network: areas and duties based on the nomenclature provided in Figure B0.1.

Heat exchanger ID	Area [m^2]	Load [kJ/h]	Section / connections
HX1	373.1	223901879.1	Cooling water to CO2 stream (E-109)
HX2	194.3	18565326.3	Cooling water to NH3 cooling section (E-113)
HX3	573.7	239364438.3	Cooling water to stripper bottom product (E-107)
HX4	159.1	31288186.3	Cooling water to stripper condenser
HX5	348.0	10833138.7	Cooling water to stripper top product E-108
HX6	5665.5	114877314.5	Cooling water to inlet to CO2 absorption section (E-104)
HX7	2788.6	14067378.1	Cooling water to exhaust treated stream (E-103)
HX8	810.1	204240136.7	Cooling water to CO2 stream (E-109)
HX9	50.4	416676.4	NH3 cooling section (E-113) with NG heating to furnace inlet temperature (E-110)
HX10	347.0	58697927.1	Inlet to the stripper (E-106) with CO2 stream (E-109)
HX11	234.4	700427.7	Inlet to the absorber (E-105) with NG heating to furnace inlet temperature (E-110)
HX12	7.5	43291.6	NH3 cooling section (E-113) with NG heating to furnace inlet temperature (E-110)

B.2 Assumptions in the cost calculation

The costing of the process has been performed according to the correlations in Towler and Sinnot[206], since the plant on-board is equivalent to a standard chemical plant in dimension. The reference cost functions are based on each unit's sizing factor according to Eq. (B4).

$$C_e = a + b \cdot S^n \quad \text{(B4)}$$

where C_e represents the purchasing cost of the unit (in $ USGC 2010), a represents the constant cost factor, b represents the proportional size-cost factor, n represents the cost exponent, and S represents the size factor, which is characteristic of each unit.

In the preliminary cost estimation, correction factors are used to include additional costs such as piping, instrumentation and control, and civil engineering. In our study, the latter has been included, assuming it is equivalent to naval engineering. The conversion to $\$_{2019}$ using has been performed using the CEPCI factor in Table B0.5:

Table B0.5. CEPCI value for different years.

CEPCI year	Value
2019	607.5
2015	556.8
2010	532.9
2002	395.6

We consider the following assumptions in the cost calculation:

- 30 years lifetime of the equipment, 7446 hours per year (annual utilization factor 0.85, considering the turnaround times at the port[213] and a margin for maintenance and delays) and 0.1 interest rate.
- The units that are already present on-board for desalination and exhaust gas cleaning are not considered in the cost calculation.
- A correction factor of 1.3 is considered to account for the installation of the equipment in stainless steel.
- The costing correlations of the columns packing and the furnace (non-reactive fired heater) are taken from Turton et al.[344]
- The costing of the blowers and storage tanks are based on the reference used in Danaci et al.[345], except for the monoethanolamine (MEA) tanks, which are taken from Towler and Sinnot[206].
- Mixers and valves are not included in the cost calculation.
- Electricity, cooling water and heating are supplied on-board with the equipment installed at no additional cost. Cooling water is available at an average temperature 14.5-25 °C, which has been used in the heat integration.
- In Chapter 3, we report the total cost of the capture on-board plant (85 $\$_{2019}/tCO_2$) omitting the cost of CO_2 transportation and injection underground, as it is common practice in the literature for conventional power plants with carbon capture. For completeness of the analysis, we report that the total cost of the plant including the transportation and injection would be 104 $\$_{2019}/tCO_2$ (+18%), assuming 200km of pipeline based on Budinis et al.[181] for onshore pipes of 3 $MtCO_2$/year and onshore saline aquifers sites. We also add that both solutions analyzed in this work, namely DAC and capture on-board, require transportation and storage infrastructure. Despite DAC

facilities could be placed closer to the storage sites, their installation also depends on the availability of the electricity and heating at the location. Therefore, we argue that there would be a negligible difference between the CO_2 network for capture on-board and DAC. Based on the considerations above, a detailed design and optimization of the regional CO_2 pipeline network is out of the scope of this work. Additionally, since our results are based on the global tkm and the data from the busiest ports in the world[346], which are not geographically close to each other, the economic and environmental assessments are based only on the total mass of CO_2. However, in the solution proposed we do not exclude that the CO_2 captured and unloaded at close harbors could be transported to the nearest storage site through a common network. Lastly, not only pipelines are available to transport the CO_2 to the storage site but also we argue that a pipeline network performs notably better than road transportation environmentally, and it allows building a network of connected harbors.

- The cost of MEA is taken from Nuchitprasittichai and Cremaschi[347], while NG is based on Medrano-García et al.[348].
- The final cost does not consider labor, maintenance, waste disposal and decommissioning charges.
- The cost of HX6 and HX7 is calculated extrapolating the correlation from Turton and Sinnot[206] outside of the suggested size interval.

The total capital expenditure cost of the plant is 28 million $\$_{2019}$. The breakdown of costs is given in Figure B0.2.

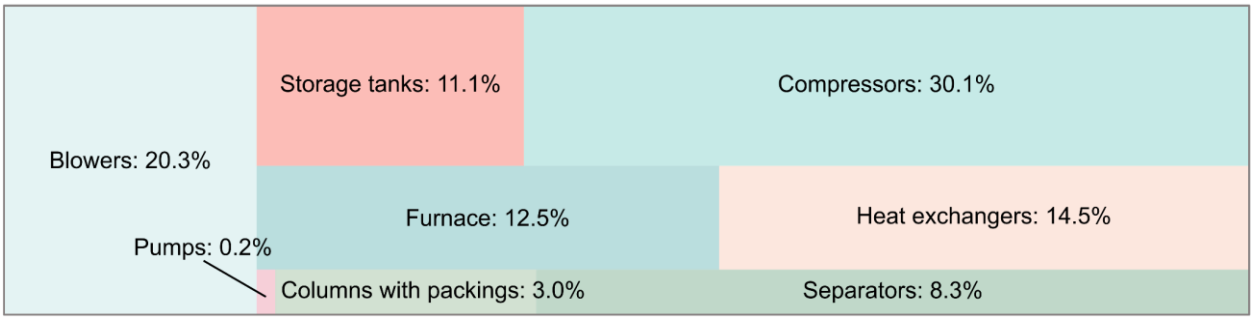

Figure B0.2: Breakdown of the total equipment capital cost. Compressors and blowers represent the highest investment, followed by heat exchangers and the NG furnace.

B.3 Technical feasibility

The installation of the units on-board comes with the displacement of the cargo to be transported, leading to an increased number of vessels to cover the annual freight demand for cargo ships (Figure B0.3). The calculations performed for the feasibility assessment are based on the volume and mass of the process equipment in Figure 1 and reported in Table B0.6. The weights and volumes listed are cumulative for the number of equipment shown. Clearly, the space on-board taken up by the NG tanks is considerable (38 % on a mass basis). However, the advantages of this additional fuel on-board are threefold, which are summarized next. It provides the heat required by the desorber reboiler, thus allowing the vessel to be energetically self-sufficient. The evaporation from the LNG to NG is used to cool down the CO_2–pure stream to storage conditions in the refrigeration cycle. Lastly, the empty tanks where the LNG is transported are used to store the liquefied CO_2 until the ship reaches the port.

We consider the weight of the ship of 8500 TEU, whose deadweight (DWT) is 115700 tonnes. The cargo accounts for 95 % of the DWT, while the rest 5 % is the fuel for the propulsion for a week trip. Therefore, the mass of the cargo displaced is compared to the DWT by subtracting the weight of the fuel. In our calculations, we assume that 1 TEU corresponds to 33.2 m^3 and 26.2 tonnes on average. We also assume that the CO_2 captured will fill the NG tanks when they are empty to reduce the total weight of the extra equipment on-board.

Table B0.6. Weight and volume of the retrofitted equipment.

Retrofitted equipment	No. of units	Weight (tn)	Size (m^3)
Absorber	1	33.6	281.4
Desorber	1	36.4	344.2
CO_2 tank	43	1419	7257.7
MEA tank	2	5.8	19.9
NG tank	16	945.3	1716.8
NH_3 refrigeration cycle	1	22.60	not available
Heat exchangers	2	21	19.4
Furnace	1	22.6	77.7
Compressors	2	8.8	28.5
Coolers	5	3.0	11.8
		2518.2	9757.2

The total mass of the cargo displaced accounts for the weight of the retrofitted plant and the additional fluids of NG, MEA, CO_2, NH_3 and the propulsion fuel. The total weight added in a week from the fluids corresponds to 4871.5 tonnes. Therefore, the total weight that needs to be displaced to keep the DWT the same (retrofitted plant + fluids) is 7389.7 tonnes, corresponding

to 7 % of the DWT. The new ships needed based on the added weight have a capacity of 8219 TEU, since the plant takes up 281 TEU.

To estimate the subsequent increase of ships caused by retrofitting the capture on-board scenario in the global fleet, we use container port traffic data from 80 of the busiest ports in 2019 (set p), extracted from The World Bank[346]. The calculations of the increase of ships are presented in Eqs. (B5) – (B8).

$$CS = \frac{\sum_p TEU_p}{8500} \tag{B5}$$

$$FS = \frac{\sum_p TEU_p}{8219} \tag{B6}$$

$$\text{New ships} = FS - CS \tag{B7}$$

$$\text{Increase of ships} = \frac{\text{New ships}}{CS} \cdot 100\% \tag{B8}$$

We sum up the TEU from all the ports (TEU_p) and then we calculate how many '8500 TEU' ships are needed to transport all the TEU (CS). Then, we repeat the same approach with the new retrofitted ships of '8219 TEU' (FS). Lastly, we calculate the number of new ships that are needed to fulfill the capture on-board scenario in the same year using Eq. (B7), and the increase of ships as in Eq. (B8).

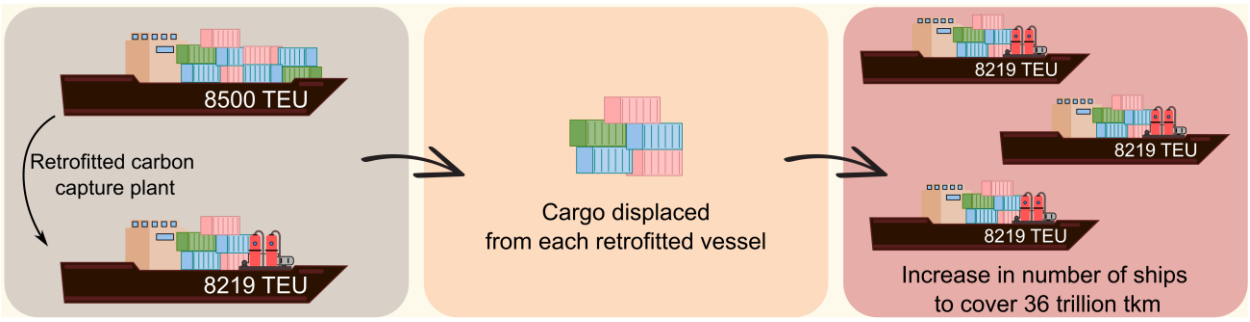

Figure B0.3: Displacement of the cargo based on the sizing of each equipment on-board with consequent increase of the total number of ships to cover the annual demand of 36 trillion tkm.

Here we assume a perfect market, where the demand for the cargo displaced by the plant on-board is completely satisfied by new ships, whose manufacturing cost has not been accounted for. However, on the contrary, it might happen that the cargo capacity is reduced with no additional ships introduced into the market. Consequently, less cargo is transported, and therefore fewer goods are available elsewhere, which would increase the prices of goods.

In the United Nations Conference on Trade and Development report published in 2010[349] the cost of gearless container vessels was $ 74 and $ 105 million for 6500 TEU and 12000TEU, respectively. Since the price does not scale linearly with the increased cargo capacity on the ship, we conservatively assume the price of a 12000 TEU ship. We calculated the additional cost the shipping industry would incur to provide carbon capture on-board. This was determined to be 299 billion $_{2010}$. When compared to the ocean economy GVA in 2010, this cost corresponds to 20 %, which is non-negligible. Nonetheless, considering that DAC is still characterized by a more limited removal potential, higher cost[350] and larger environmental impacts (Figures 3.3 and 3.4) than capture on-board, it is clear that the latter is a more appealing solution in the short-term.

B.4 Life cycle assessment inventory

For the environmental assessment, we define the life cycle inventories of the three scenarios investigated using SimaPro software v9.2.0.2 with the Ecoinvent v3.5 database. The 8500 TEU reference ship is modeled by combining data from two existing activities that match this ship size. The first activity 'Bulk carrier ocean' is from the ELCD database with a functional until (FU) of 1 tkm. This activity was necessary to calculate the fuel consumption and emissions depending on the ship size, the distance traveled and the DWT. However, the construction and maintenance of the ship, and the port facilities were not included. In our study, these are based on the activity 'Transport, freight, sea, transoceanic ship, processing', characterized by comparable fuel consumption. We report in Table B0.7 the life cycle inventory of the business as usual scenario (*BAU*).

Table B0.7. Life cycle inventory of the BAU scenario, FU = 1 tkm.

Activity	Functional Unit	Inputs
Bulk carrier ocean, (adjusted for 8500 TEU)	1 tkm	• HFO consumption • Combustion emissions (CO_2, CO, CH_4, NO_2, N_2O, PM, SO_2, NMVOC, NH_3, Arsenic, Benzene, Cadmium, Lead, Mercury, PAH, and other components)
Transport, freight sea, transoceanic ship	1 tkm	• Freight ship construction and maintenance, • Port facilities

For the *BAU + DAC* scenario, we keep the inventory of the *BAU*, and we add the inputs of the DAC process. The DAC process is scaled according to the FU of the ship activity (1 tkm). The DAC process captures 7.87 10^{-3} kg CO_2 per 1 tkm. For the definition of the DAC process, data from Keith et al.[350] were used. Table B0.8 shows the inventory of the DAC process that captures 1 kg of CO_2 from the air. Since we perform a global analysis, the electricity requirement is covered by the global electricity mix of 2019 as presented in the World Energy Outlook of 2019[351].

Table B0.8. Life cycle inventory of the DAC activity without the BAU scenario, FU = 1 kg CO_2 captured.

Product		Unit
CO_2	1	kg
Materials/fuels		
Natural gas liquids {GLO} | market for | APOS, U	0.1	kg
Tap water {GLO} | market group for | APOS, U	3.1	kg
Calcium carbonate, precipitated {RoW} | market for calcium carbonate | APOS, U	$2.2 \cdot 10^{-2}$	kg
Global electricity mix from 2019	0.2	kWh
CO_2 stored in aquifer at 200 km distance from emission source	7.9 10^{-3}	kg
Emissions to air		
Carbon dioxide, fossil	−0.7	kg

The inventory of the *capture on-board* scenario is based on the mass and energy flows taken from the process simulation. Then, all the values are scaled according to the functional unit. The inventory of the *capture on-board* is reported in Table B0.9. These inputs are added to the inventory of the *BAU*, which includes HFO consumption, freight ship construction and maintenance, port facilities, and combustion emissions. Regarding the combustion emissions, the ones not included in Table B0.9 are taken from the *BAU* inventory. In the case of the freight ship and port facilities, an increase of 3.4 % is estimated compared to the *BAU*, as stated in Chapter 3. The CO_2 transport and storage inventory is taken from the work of Wildbolz[283].

Table B0.9. Life cycle inventory of the capture on-board without the BAU scenario, FU = 1 tkm

Product		**Unit**
Bulk ocean carrier, 8500 TEU, week trip	1	tkm
Materials/fuels		
Monoethanolamine	$1.9\ 10^{-5}$	kg
Natural gas liquids {GLO} | market for | APOS, U	$7.2\ 10^{-4}$	kg
Ammonia, liquid {RoW} | market for | APOS, U	$2.0\ 10^{-5}$	kg
CO_2 stored in aquifer at 200 km distance from emission source	$7.9\ 10^{-3}$	kg
Emissions to air		
Carbon dioxide, fossil	$4.9\ 10^{-4}$	kg
Methane, fossil	$1.1 \cdot 10^{-5}$	kg
SO_2	$1.3\ 10^{-6}$	kg
Monoethanolamine	$1.9\ 10^{-5}$	kg

APPENDIX C

Supplementary information to Chapter 4

C.1 Biomass transformation processes

Due to its physical and chemical characteristic, the direct use of biomass as fuel is unappealing from a technical and logistic perspective. Biomass feedstocks have low energy densities due to high moisture content, making transportation and storage more expensive than traditional feedstocks in addition to a low thermal efficiency of energy conversion[352]. Therefore, biomass is rather converted into useful forms of energy, known as bioenergy, such as heat, electricity, liquid and gaseous fuels.

The conversion of biomass into gaseous fuels, referred to as biofuels, can be carried out via two main pathways, i.e., biochemical and thermochemical[353].

Biochemical conversion processes involve the use of microbes and/or enzymes that can be utilized with specific types of biomass, namely wet feedstocks. Consequently, the productivity depends on the biological conversion, generally slow, which requires high investment costs for large reactors. Additionally, the biochemical conversion routes produce secondary waste such as biomass sludge.

On the other hand, the thermochemical conversion can be effectively applied to any type of biomass. In this process, the reactions taking place are significantly less complex and completely chemical. Furthermore, in the thermochemical conversion route, complete utilization of the biomass is possible. Despite gasification being an efficient and high mature technology, its applications are mainly focused on hydrogen production, such as in the work by Susmoza et al.[354] and as reviewed by Tezer and co-workers [355]

In particular, here we are interested in the production of substitute natural gas from biomass for which both routes described above can be utilized. Additional process can be considered for this purpose, e.g., hydrothermal gasification or renewable methane.

C.2 Process description and modeling in Aspen Plus

The process modeled produces synthetic natural gas (biomethane), which has the same properties as conventional natural gas for grid injection (Table C0.16), from selected biomass feedstocks whose characteristics are reported in Table C0.1-Table C0.3.

C.2.1 Biomass characterization in Aspen Plus

The feedstock is characterized as non-conventional component in Aspen Plus using the HCOALGEN and DCOALIGT property models that require the ultimate and proximate analyses in order to estimate the biomass enthalpy of formation, heat capacity and density. Additionally, the moisture content is given as input.

The ultimate and proximate analysis input to the process simulator are shown in Table C0.1, Table C0.2 and Table C0.3 based on Vassilev et al.[356].

Table C0.1. Biomass feedstocks proximate analysis. Acronyms: MS = moisture, FC = fixed carbon, VM = volatile matter.

	Proxanalysis			
	MS	**FC**	**VM**	**Ash**
Wheat straw residues	30	18.1	74.8	7.1
Forest residues	30	16.9	79.9	3.2
Miscanthus	30	15.8	81.2	3
Willow	30	15.9	82.5	1.6
Poplar	30	12.3	85.6	2.1

Table C0.2. Biomass feedstocks ultimate analysis.

	Ultanalysis*						
	Ash	**Carbon**	**Hydrogen**	**Nitrogen**	**Chlorine**	**Sulfur**	**Oxygen**
Wheat straw residues	5.98	46.18	5.70	0.65	0.57	0.16	40.76
Forest residues	1.38	51.96	5.32	0.69	0.03	0.10	40.52
Miscanthus	2.63	47.87	5.84	0.39	0.13	0.15	43.00
Willow	1.38	49.13	6.02	0.59	0.01	0.06	42.81
Poplar	1.96	50.56	5.98	0.59	0.03	0.02	40.86

* redistributed to 100%

Table C0.3. Biomass feedstocks sulfate analysis.

	Sulfanalysis
	Sulfate
Wheat straw residues	0.02
Forest residues	0.02
Miscanthus	0.02
Willow	0.02
Poplar	0.02

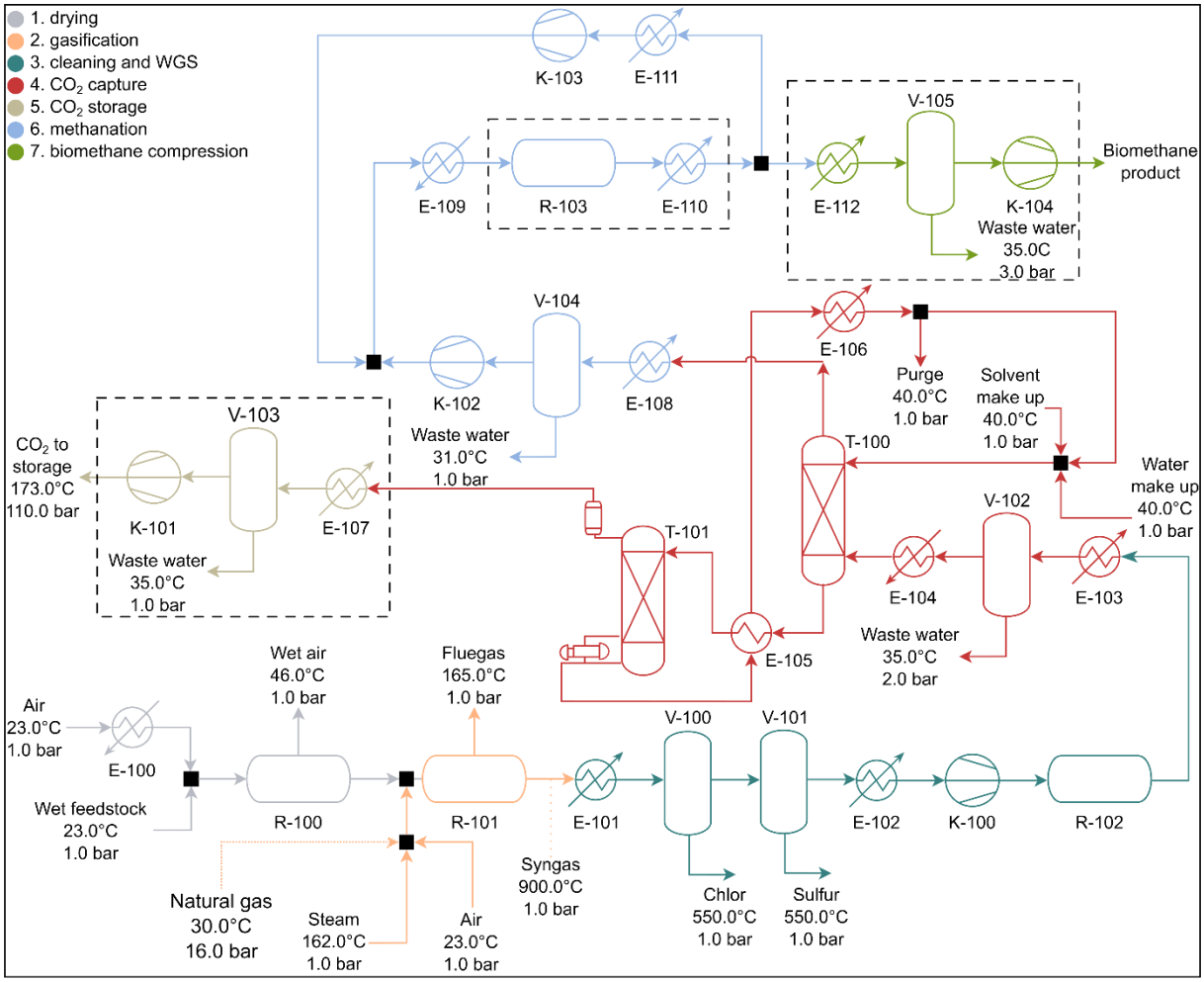

Figure C0.1: Process flow diagram of biomass conversion to biomethane. Flowsheet refers to poplar scenario, but all the scenarios are equivalent with minor modifications. The dotted box represent a sequence of repeated equipment and the dotted natural gas stream indicates that not all the feedstocks need this additional fuel input (only poplar and willow).

C.2.2 Process sections

The main structure of the process represented in Figure C0.1 is based on the GoBiGas plant[357] and available literature studies[238–246], particularly focusing on the modeling of biomass thermal gasification in Aspen Plus, and further adjusted regarding the operating conditions for the different feedstocks considered. The process comprises seven sections, which are sketched in Figure C0.1 and described in detail in Section 4.2.2. Hereafter the schematic and description refers to the poplar scenario. However, all the other scenarios feature the same design with minor modifications to the flowsheet.

The process simulation uses the Peng-Robinson equation of state with Boston-Mathias modifications for the main section, while the ELEC-NRTL and Elec-wizard packages are used for the carbon capture and storage (CCS) section.

C.2.2.1 Drying stage

The generic feedstock is assumed to arrive at the biomethane plant with a moisture content of 30%, and it needs to be dried before entering the gasifier. A calculator block was setup in the process simulator to decreases the moisture content of the non-conventional biomass stream. The moisture is converted into a conventional water stream that is later separated from the non-conventional biomass stream. In our process model, an adiabatic stoichiometric reactor, an adiabatic flash unit and a heater to preheat the drying agent are used to simulate the drier unit (Figure C0.2).

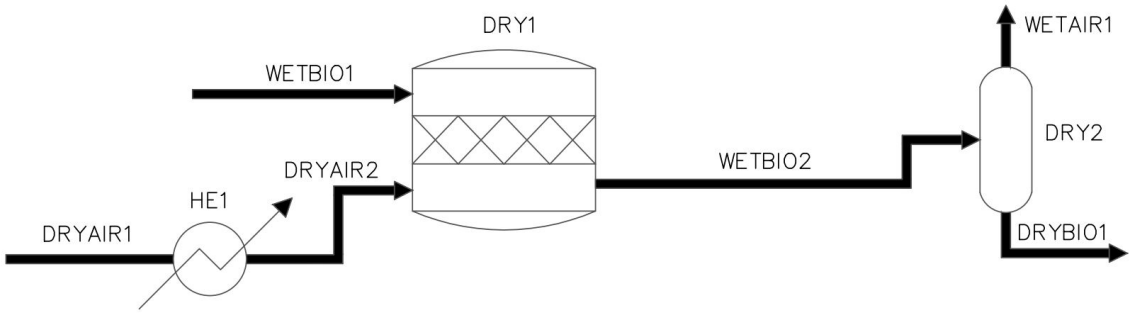

Figure C0.2: Schematic of the process modeling of the dryer in Aspen Plus[358].

Eq. (C1) was implemented in the stoichiometric reactor to represent the drying process[238,243].

$$\text{Biomass(wet)} \rightarrow 0.0555084H_2O + \text{Biomass(dry)} \quad \text{(C1)}$$

In addition to Eq. (C1), a reaction conversion was defined, which depends on the initial and target moisture content. The conversion is calculated in a calculator block as in Eq. (C2)[238].

$$X_{drying} = \frac{m_{in} - m_{out}}{100 - m_{in}} \quad \text{(C2)}$$

Where X_{drying} is the conversion, m_{in} and m_{out} are the moisture content of the biomass entering and leaving the stoichiometric reactor, respectively.

The energy demand of the drying section is determined by the duty of the heater, where air enters at 23 °C and leaves at 200 °C.

C.2.2.2 Gasification

A fast internal circulating fluidized bed gasifier (FICFB) was chosen to carry out the biomass gasification. In this technology, a nitrogen-free syngas can be produced due to the gasification and combustion reactions taking place in two separate chambers.

In an FCIFB, the dry biomass feedstock is gasified in the gasification chamber with steam entering the unit from the bottom. The amount of steam (steam to biomass ratio θ_{SB}) introduced into the gasifier is a relevant parameter discussed intensively in the literature and here defined as in Eq. (C3)[238,240].

$$\theta_{SB} = \frac{M_{bio} w_{H2O,bio} + M_{steam}}{M_{bio}(1 - w_{H2O,bio})} \quad \text{(C3)}$$

Where M_{bio} is the mass flow of the biomass, $w_{H2O,bio}$ is the water weight fraction of the biomass and M_{Steam} is the steam entering the gasification section. The water content and the end composition of the gasifier's product depend on the steam to biomass ratio, which typically ranges between 0.5 and 1.0. Here, it was adjusted by sensitivity analysis varying θ_{SB} while observing the final product composition.

Air is supplied to the combustion chamber to carry out the combustion of the char and heat up the inert bed material, typically sand, in the gasification chamber. The bed material provides the heat to carry out the endothermic gasification reactions to produce syngas.

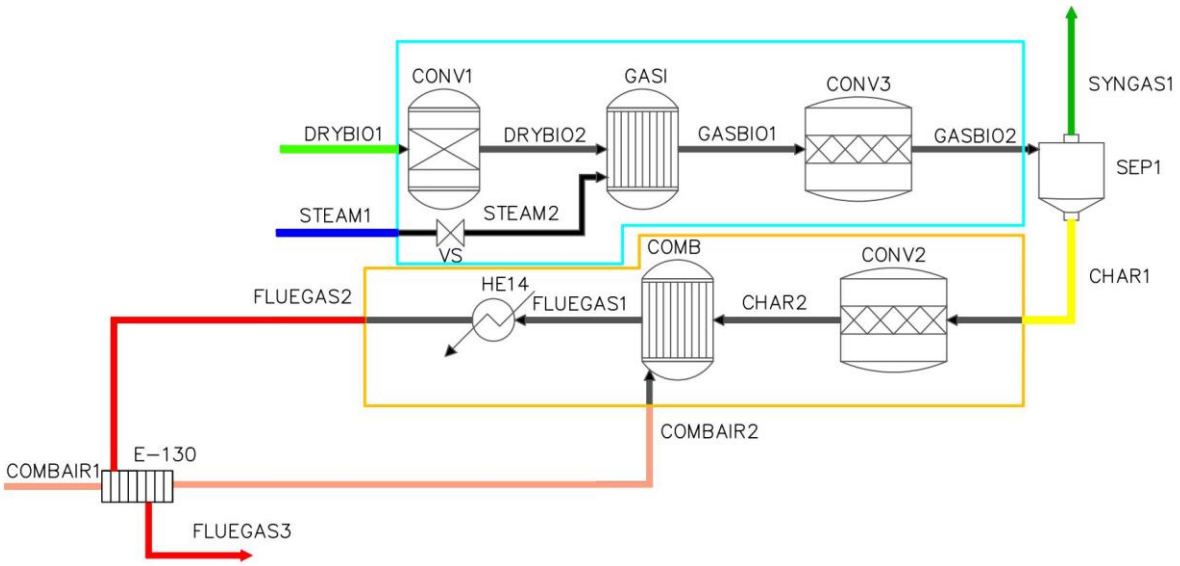

Figure C0.3: Schematic of the process modeling of the gasification in Aspen Plus[358].

The first step to model a gasification process is to convert the non-conventional elements into conventional ones using a calculator block in a yield reactor such that all the elements satisfy the atom balance, while tar and char are still modeled as non-conventional components.

The ratio of tar formation, which is not calculated by default in the process simulator, is based on the empirical correlation reported in Eq. (C4)[238].

$$M_{tar} = 0.35 M_{bio,dry} \exp[-3.04\ 10^{-3}(T - 500)] \exp\left[-4.34 \exp\left[\frac{-2.34\ 10^{4}}{R(T + 273.15)}\tau\right]\right] \quad \text{(C4)}$$

where $M_{tar}$is the mass [kg] of the tar generated from the biomass, $M_{bio,dry}$ the mass [kg] of dry biomass, T the temperature [°C] , R the gas constant and τ the residence time .

The tar is later converted into organic conventional components with molecular weight above 78 [359], whose composition depend on the feedstock and process conditions, using a stoichiometric reactor. Here we consider a composition of tar that includes only benzene, toluene and naphthalene [359].

The part of biomass that does not convert into syngas is called char, and it is based on the fixed carbon value specified in the proximate analysis. The char is used to power the gasification unit by combustion with air, after it is converted into pure carbon in a stoichiometric reactor. We use air as it is a cheaper option compared to pure oxygen from an air separation unit.

Next, the conventional elements enter a Gibbs reactor together with medium pressure steam at 162 °C, decreased to 1 bar before the reaction takes place, where the free Gibb's energy is minimized until equilibrium is reached at 900 °C and 1 bar. Char and ash are separated from the tar and syngas in a separation unit and are sent to the combustion reactor where the carbon is combusted with preheated air at 950 °C and 1 bar. The fluegas that results from the combustion is used within the process for heat integration.

In practice, the combustion reactor provides the heat for the gasifier by exchanging the heated bed material and unreacted char with the gasifier. Therefore, a heat balance is set up to calculate the heat exchange among the combustion, bed material and biomass gasification units in a calculator block. In the case of willow and poplar feedstock, a small amount of natural gas at

30 °C and 16 bar is added to the combustion to satisfy the energy balance because of the lower fixed carbon embedded in these biomass types.

The sequence of units employed in the process simulator is shown in Figure C0.3. We note that a kinetic model of the gasifier could be implemented; however, it is usually not done in the literature due to the challenges related to its correct implementation, and the approach described above instead is widely used.

A formation of inorganic contaminants such as hydrogen sulfide and hydrogen chloride also occurs inside the gasifier, which are removed in the subsequent process section.

C.2.2.3 Syngas cleaning and water gas shift

Syngas cleaning is carried out to prevent catalyst poisoning and reach the desired conditions of the final product [360]. Hydrogen sulfide and hydrogen chloride are the only inorganic impurities removed based on literature data [361], while ammonia is present in a significantly lower concentration, which is considered not critical. Among the compounds mentioned, hydrogen sulfide is the most harmful component for copper catalysts, which are often utilized in water gas shift reactors, but all contribute to corrosion and environmental issues [361].

The reforming of tar compounds can be performed in catalytic filter candles, which are here modeled in stoichiometric reactors with defined conversions based on the literature [361]. The reactions that take place convert the tars into syngas by reforming, which is then cooled down.

The modeling of hydrogen sulfide (H_2S) and hydrogen chlorine (HCl) removal was then carried out in separation units in order to avoid interference among the adsorption of different components. The cleaning of H_2S can be accomplished using a sorbent that involves a solid-gas reaction between a metal oxide and hydrogen sulfide on a zinc oxide catalyst within an operating temperature range of 450-650 °C. In our process model, the separation of H_2S and COS is performed in an ideal separator at 550 °C, which removes 99% of each component.

A promising method of removing hydrogen chloride from syngas utilizes alkali-based sorbents, e.g., sodium bicarbonate that can decrease the concentration of hydrogen chloride in syngas to concentrations below 1 ppm at approximately 550 °C. In this work, the removal of HCl is carried out in an ideal separator where 99% of HCl is removed at 550 °C.

The gas leaving the organic components cleaning section is then cooled down and compressed to 2 bar before entering the next unit at 265 °C. Indeed, in order to perform the methanation reaction, i.e., the reaction between CO and H_2 to produce methane, the molar ratio between the reactant must be 1:3 (syngas ratio). This can be achieved in a water gas shift (WGS) reactor where Eq. (C5) takes place.

$$CO + H_2O \leftrightarrow CO_2 + H_2 \quad \text{(C5)}$$

A kinetic model was implemented in an adiabatic plug flow reactor based on literature [362]. Usually, WGS reactors include a series of reactors intercooled. In our study, the desired ratio is obtained with only one reactor, whose length was adjusted using heuristics to reach an optimal syngas ratio of 3. Excess water is then flashed before recompression to compensate for pressure losses.

Table C0.4. Information on reactor design. The range of values of the reactors length is the overview of the different reactors in each scenario and across scenarios. The number of reactors refers to the number of reactors to carry out each reaction in each scenario. Acronyms: WGS = water gas shift reaction, METH = methanation reaction.

Reaction	Diameter [m]	Length range [m]	Number reactors
WGS	1.50	2.5-5.0	1
METH	2.25	3.5-9.5	6

C.2.2.4 CO_2 capture

To reduce the costs of compression, carbon dioxide is removed at atmospheric pressures before the syngas is compressed to the condition of the methanation reaction.

The CO_2 capture plant is based on the state-of-the-art post-combustion process[125], which is intensively covered in the literature and implemented at commercial scale (TRL 9^6). The syngas enters at the bottom of the absorption column and is put in countercurrent contact with a 30%wt. MEA (C_2H_7NO) aqueous solution from the top. After the carbon dioxide is absorbed by the solvent inside the column, the CO_2-free syngas is vented while the CO_2-rich solvent leaves at the bottom. Then, the CO_2-rich stream enters a second column, the stripper, where the CO_2 is separated from the solvent. The latter is sent back to the first column to be recycled. A fresh MEA make-up, calculated using a calculator block, is added to compensate for the solvent losses in the purge (1% of the total recycled stream to avoid impurities accumulation) and the rest of the streams. The CO_2 stream on the other hand, is cooled down to 35°C and separated from condensed water in an adiabatic flash unit before being compressed.

We note that CO_2 is also present in the fluegas due to char combustion. This stream, although it could be mixed with the CO_2-rich gas coming from the stripper, is not captured because it contains nitrogen, whose presence in the syngas should be avoided.

C.2.2.5 CO_2 transportation to storage site

The CO_2-rich gas leaving at the top of the stripper column is collected and pressurized in a series of compressors with a pressure ratio of 3.5. In order to reduce the temperature between two consecutive stages, the gas is cooled down after each compression to 135 °C. After each cooler water is flashed to purify the carbon dioxide stream further. This cooling, separation and pressurization sequence is repeated multiple times in order to reach a vapor pressure of 110 bar, which is a standard condition for the transportation of CO_2 in pipeline[363].

C.2.2.6 Methanation reaction

The CO_2- lean syngas leaves the capture plant at atmospheric pressure, and it enters a two-stage compression section, that raises the syngas pressure just above 16 bar. Then, the syngas is cooled down to 250 °C in a heat exchanger, the temperature at which the methanation is carried out.

$$CO + 3H_2 \leftrightarrow CH_4 + H_2O \qquad \text{(C6)}$$

Methanation, i.e., the conversion of H_2 and CO into CH_4 according to the stoichiometry in Eq. (C6), is a highly exothermic reaction ($\Delta H298K$ = -206.28 kJ mol−1), which is carried out in a series of isothermal plug flow reactors. The heat of reaction is utilized towards medium pressure steam generation, computed using Aspen Energy Analyzer. The kinetic model developed by Kopyscinksi[364] was implemented in Aspen Plus to model the methanation reaction over a commercial nickel based catalyst. The optimal reactor length at which the maximum conversion of carbon monoxide is reached was found using heuristics.

C.2.2.7 Biomethane compression

According to Eq. (C6), the products of the methanation reaction are methane and water, which has to be removed before grid feed in. After the water is partially condensed and removed using in an adiabatic flash unit, the final product is compressed to 16 bar and it is ready to be injected in the existing natural gas grid, unless further compression is needed to meet the requirement of a specific grid.

C.2.2.8 Heat integration

Heat integration is performed in Aspen Energy Analyzer, which calculates the amount of hot and cold utilities needed and the heat exchanger network. This is carried out in three steps: first, the gasification section is isolated from the rest of the flowsheet to ensure that the different units implemented as described in C.2.2.2 satisfy the heat balance. Then, the heat integration of methanation reaction is performed to calculate the amount of steam generated. Finally, the rest of the process streams is matched among themselves and the utilities to determine the number of heat exchangers needed. The heating requirement of the process is completely satisfied by exchanging heat among the streams with the additional production of low and medium pressure steam. Cooling water is used as the only cooling utility in the process.

C.2.3 Modeling assumptions

Drying

• The feedstock enters the drier at 23 °C, assuming that has been left on the land before transportation to the processing site.
• The moisture content of the feedstock is 30 wt. % before the drying section and10wt % after the drying section[365].
• Dry air preheated to 200 °C is used as a drying agent[366].

Gasification

• The biomass feedstock and bed materials are fed at uniform temperature[238].
• The temperature inside the gasifier is uniform at 900 °C and the residence time is assumed to be 14 s[367].
• The temperature inside the combustion chamber is uniform at 950 °C (based on observations in Nikoo and Mahinpey[368]).
• The steam to biomass ratio θ_{SB} in the gasifier is set to 0.5.
• The gasification is carried out at atmospheric pressure[242].
• Ash and bed materials are considered inert[238].
• The char is assumed to be pure carbon. The amount of char produced is equal to the fixed carbon in the biomass[243,359,361].
• The pressure drop in the gasification and combustion sections is 0.1 bar[369]
• Complete char combustion occurs inside the combustion chamber.

• The tar compounds formed in the gasifier are benzene (C_6H_6), naphthalene ($C_{10}H_8$) and toluene (C_7H_8)[359,361].
• No heat losses are considered within the system[243].

Syngas cleaning and cooling

• Pressure drop of 0.2 bar in heater and coolers.
• The absorption units utilized for the removal of organic impurities remove 99% of hydrogen sulfide and hydrogen chloride from the syngas, but the NaCl and ZnS formed are not considered in the environmental assessment[361].

CO_2 capture

• The solvent used for the carbon dioxide absorption is composed of 30% MEA and 70% water on a mass basis.
• Pressure drop of 0.04 bar per stage in columns.
• Isentropic efficiency of $\eta = 0.75$ in compressors.
• No pressure drop in mixers and splitters.
• RADFRAC model was used to model absorption and stripping columns.

Reactors

• Pressure drop in the water gas shift reactor was modeled using Ergun's equation embedded in Aspen Plus.
• The pressure drop in the intercooled adiabatic methanation reactor was assumed to be 1 bar.

C.3 Economic assessment

The economic assessment is based on Towler and Sinnot except for column packing material and furnace from [344]. The size of the heat exchanger determined with the Aspen Energy analyzer.

$$C_e = a + b \cdot S^n \quad \text{(C7)}$$

where Ce represents the purchasing cost of the unit (in $ USGC 2010), a represents the constant cost factor, b represents the proportional size-cost factor, n represents the cost exponent, and S represents the size factor, which is characteristic of each unit.

The cost calculations are carried out in the reference year 2022, without considering the effect of future technology learning that can reduce the total capital investment[352].

Table C0.5. Operating expenses unitary costs and references used in the process economics.

Operating expenses	Unit	Price/unit	Reference
Electricity	Eur/kWh	0.2525	[370]
Feedstocks	$\$_{2009}$/t		[254,371]
Solvent	$\$_{2011}$/kg	1.3	[347]
Process water use	$\$_{2018}$/kg	0.000177	[344]
Cooling water use	$\$_{2019}$/m3	0.033	[372]
Copper catalyst	$\$_{2019}$/kg	1.36	[373]
Nickel catalyst	$\$_{2019}$/kg	2.37	[373]
Zink sorbent	$\$_{2020}$/kg	2.6	[361]
Sodium bicarbonate	$\$_{2022}$/t	300	[374]
Waste water	$\$_{2019}$/m3	1.5	[372]
Ash treatment	$/kg	0.04	[375]
Natural gas	$\$_{2017}$/kg	0.2441	[348]

Other economic factors considered in the economic assessment are reported in Table C0.6.

Table C0.6. Additional parameters used in the cost calculations.

Parameter	Value
CEPCI 2022	830
CEPCI 2020	596
CEPCI 2019	608
CEPCI 2018	603
CEPCI 2017	568
CEPCI 2016	542
CEPCI 2011	586
CEPCI 2010	551
CEPCI 2009	522
CEPCI 2005	468
CEPCI 2000	394
USD to EUR_{2022}	0.952
Plant operating hours	8000

C.4 Biomass potential

We compute the total availability of biomass feedstocks in the EU. For the energy crops, we assume that a portion of marginal land can be employed for cultivation[253,254]. The biomass available is then calculated based on the yield of each crop. For the residues, instead, we use data on regional availability[253,254] and calculate the amount that is accessible based on sustainable removal rates for each country[252]. The biomethane potential is then calculated based on the biomass availability and the process efficiency for each feedstock.

Table C0.7. Calculated biomass potential.

	Energy crop [t_{dry}/yr]			Residues [t_{dry}/yr]	
	Miscanthus	Willow	Poplar	Wheat straw	Forest
Austria	748162	386020	537244	312568	2724349
Belgium	336311	173522	241500	254775	655149
Bulgaria	3139477	1619837	2254412	840686	809366
Cyprus	17906	9239	12858	0	0
Czechia	1250136	645017	897704	1075468	3147364
Germany	3968806	2047735	2849940	8737419	17167318
Denmark	488078	251828	350482	1304790	579274
Spain	40003048	20639870	28725593	2031278	3864628
Estonia	6629120	3420344	4760272	183072	1404421
Finland	33550	17311	24092	369998	8752247
France	5619303	2899321	4035138	8832427	10995770
United Kingdom	9033579	4660942	6486878	2079354	2496362
Greece	2826473	1458340	2029648	326057	569855
Hungary	1012664	522491	727179	2427231	1400161
Ireland	8897948	4590963	6389484	29809	353409
Italy	2941242	1517556	2112062	2830793	3684116
Lithuania	9277443	4786766	6661994	543435	1523926
Luxembourg	6979	3601	5011	0	118159
Latvia	8211547	4236809	5896589	60723	598204
Malta	0	0	0	0	0
Netherlands	539410	278312	387342	133089	161906
Poland	13858020	7150149	9951238	6164633	9644118
Portugal	7175732	3702372	5152786	114420	1021470
Romania	3791058	1956025	2722303	2326943	3870704
Croatia	982462	506908	705491	319841	1020459
Slovakia	918530	473922	659583	730442	1632622
Slovenia	197592	101949	141888	84129	951533
Sweden	2668053	1376602	1915889	502485	14630124

C.5 Life cycle assessment (LCA) methods and inventory

We carry out an attributional LCA following the four phases defined in the ISO 14040/44 standards. In the first phase, the goal and scope of the study are defined. The goal of this LCA is twofold: i) to quantify the carbon footprint of biomethane production via biomass gasification with CCS in the EU and ii) to estimate the climate mitigation potential and environmental implications of a large-scale deployment of biomethane production in the EU. For both goals, the functional unit is defined as the production of one cubic meter of biomethane at normal conditions (Ncum) via biomass gasification. The system boundaries are defined as cradle-to-gate, including biomass transportation, utilities required for the capture, and CO_2 transportation via pipeline and storage underground. The influence of considering a cradle-to-grave scope, i.e., including also emissions from biomethane combustion for heat and

power production, whose results are presented in the Supplementary information. A complete list of the activities used in the modeling of the environmental assessment is provided in Table C0.9 to Table C0.13.

The second phase in the LCA is inventory analysis, in which all the relevant inputs and outputs associated with biomethane production are compiled and quantified (i.e., emissions, energy, raw materials, etc.). A distinction can be made between foreground and background processes.

We carry out the analysis following an attributional approach and address multi-functionality by adopting a system expansion approach, i.e., we do not account for the environmental credits of steam production.

The life cycle inventory (LCI) phase is implemented in Brightway2 using the Activity Browser interface and the Ecoinvent v. 3.8 database, combining data of the foreground and background systems. The former includes the mass and energy flows from the process simulation, while the latter is modeled using average market data from the environmental database for each scenario (Supplementary Table C0.9 to Table ***C0.13***). The selection of activities, e.g., ash treatment, wastewater treatment, synthetic gas factory, is based on a sample activity for biomethane production available in Ecoinvent (*biomethane production, high pressure from synthetic gas, wood, fluidised technology*).

In the life cycle impact assessment (LCIA) phase, the elementary flows quantified in the inventory analysis phase (i.e., natural resources and emissions to air, soil, and water) are translated into potential impacts by using a set of impact assessment methods. We quantify the climate impacts by applying the IPCC 2021 method with a 100-year time horizon as well as the other 15 impact categories available in the Environmental Footprint 3.0 and updated LANCA v. 2.5 method recommended by the European Commission[376]. This method also defines links between the environmental indicators that are connected to the planetary boundaries and five Sustainable development goals.

We use a modified IPCC method that includes characterization factors (CFs) for biogenic CO_2[377]. This is needed to properly account for negative emissions technologies, particularly the CO_2 uptaken during the biomass growth and the subsequent permanent sequestration underground.

Later, we regionalize the activities of biomethane production in the EU based on the energy mix and natural gas supply, while the remaining activities are average market data for the EU. We consider average impact values for the CO_2 transportation and unlimited storage capacity at the national level.

Life cycle impact methodologies assessed:

Table C0.8. Methods and impact categories selected in this study.

Method	Impact category	Unit
IPCC 2013	climate change	GWP 100a ($kgCO_{2\text{-}eq}$)
EF v. 3.0	acidification	accumulated exceedance (ae)
	ecotoxicity: freshwater	comparative toxic unit for ecosystems (CTUe)
	energy resources: non-renewable	abiotic depletion potential (ADP): fossil fuels
	eutrophication: freshwater	fraction of nutrients reaching freshwater end compartment (P)
	eutrophication: marine	fraction of nutrients reaching marine end compartment (N)
	eutrophication: terrestrial	accumulated exceedance (AE)
	human toxicity: carcinogenic	comparative toxic unit for human (CTUh)
	human toxicity: non-carcinogenic	comparative toxic unit for human (CTUh)
	ionising radiation: human health	human exposure efficiency relative to u235
	material resources: metals/minerals	abiotic depletion potential (ADP): elements (ultimate reserves)
	ozone depletion	ozone depletion potential (ODP)
	particulate matter formation	impact on human health
	photochemical ozone formation: human health	tropospheric ozone concentration increase
	water use	user deprivation potential (deprivation-weighted water consumption)
LANCA v. 2.5	land use – erosion potential	kg soil loss

C.5.1 Cradle-to-gate analysis

The comparison with the current scenario, i.e., the business as usual (BAU), is performed using the Ecoinvent activity *market group for natural gas, high pressure EU wo CH*.

Assumptions in the environmental assessment:

- Transportation from land to processing site is assumed to be 50 km.
- Impact of catalyst negligible in the environmental assessment

The inventories of the five scenarios analyzed are reported in Table C0.9 to Table ***C0.13***. The first *market group for tap water* refers to the water required in the CCS plant, while the second entry refers to the process water used for steam generation.

Table C0.9. Life cycle inventory of biomethane production from wheat straw residues.

biomethane production, 16 bar from wheat straw residues, fluidized technology			**1 Ncum**
Technosphere flows			
	Amount	**Unit**	
carbon dioxide transport and storage, 200 km pipeline, storage 1000m	1.61084156	kilogram	
market for copper oxide	0.00001	kilogram	
market for monoethanolamine	0.082648	kilogram	
market for nickel, class 1	0.00022	kilogram	
market for sodium bicarbonate	0.00077	kilogram	
market for transport, freight, lorry 16-32 metric ton, EURO6	0.170733	ton kilometer	
market for wastewater, average	-0.00018974	cubic meter	
market for wood ash mixture, pure	-0.204197	kilogram	
market for zinc	0.00023	kilogram	
market group for electricity, medium voltage	1.51533	kilowatt hour	
market group for tap water	1.69346	kilogram	
market group for tap water	6.05302	kilogram	
synthetic gas factory construction	2.90E-09	unit	
waste biomass, wheat straw, dry	3.41466	kilogram	
Biosphere flows			
	Compartment	**Amount**	**Unit**
crbon	soil	1.94E-34	kilogram
carbon dioxide, non-fossil	air	2.264628	kilogram
carbon monoxide, non-fossil	air	3.57E-05	kilogram
nitrogen	air	19.31509	kilogram
nitrogen oxides	air	5.87E-06	kilogram
oxygen	air	4.218236	kilogram
water	air	0.001084	cubic meter
water	water	0.00351415	cubic meter
water, cooling, unspecified natural origin	natural resource - in water	0.08695899	cubic meter

Table C0.10. Life cycle inventory of biomethane production from forest residues.

biomethane production, 16 bar from forest residues, fluidized technology		**1 Ncum**
Technosphere flows		
	Amount	**Unit**
carbon dioxide transport and storage, 200 km pipeline, storage 1000m	1.775857	kilogram
market for copper oxide	0.00003	kilogram
market for monoethanolamine	0.09460595	kilogram
market for nickel, class 1	0.00066	kilogram
market for sodium bicarbonate	0.00003	kilogram
market for transport, freight, lorry 16-32 metric ton, EURO6	0.14326	ton kilometer
market for wastewater, average	-0.000196144	cubic meter
market for wood ash mixture, pure	-0.039546	kilogram
market for zinc	0.00012	kilogram
market group for electricity, medium voltage	1.51033098	kilowatt hour
market group for tap water	2.07809	kilogram
market group for tap water	4.09255	kilogram
synthetic gas factory construction	2.90E-09	unit
waste biomass, forest residues, dry	2.86513	kilogram
Biosphere flows		
	Compartment	**Amount**	**Unit**
carbon dioxide, non-fossil	air	1.7742	kilogram
carbon monoxide, non-fossil	air	3.39E-07	kilogram
nitrogen	air	16.22214	kilogram
nitrogen oxides	air	0.00040825	kilogram
oxygen	air	3.63551	kilogram
water	air	0.000909564	cubic meter
water	water	0.003247864	cubic meter
water, cooling, unspecified natural origin	natural resource - in water	0.08354768	cubic meter

Table C0.11. Life cycle inventory of biomethane production from *Miscanthus*.

biomethane production, 16 bar from miscanthus, fluidized technology			**1 Ncum**
Technosphere flows			
	Amount	Unit	
carbon dioxide transport and storage, 200 km pipeline, storage 1000m	1.71297	kilogram	
market for copper oxide	0.000023	kilogram	
market for monoethanolamine	0.093385	kilogram	
market for nickel, class 1	0.00067	kilogram	
market for sodium bicarbonate	0.000091	kilogram	
market for transport, freight, lorry 16-32 metric ton, EURO6	0.15361	ton kilometer	
market for wastewater, average	-0.00020199	cubic meter	
market for wood ash mixture, pure	-0.080705	kilogram	
market for zinc	0.00019	kilogram	
market group for electricity, medium voltage	1.529948	kilowatt hour	
market group for tap water	1.73289	kilogram	
market group for tap water	3.42066	kilogram	
miscanthus production	3.072184	kilogram	
synthetic gas factory construction	2.90E-09	unit	
Biosphere flows			
	Compartment	**Amount**	**Unit**
carbon dioxide, non-fossil	air	1.778629	kilogram
carbon monoxide, non-fossil	air	2.45E-07	kilogram
nitrogen	air	17.39844	kilogram
nitrogen oxides	air	0.000607	kilogram
oxygen	air	3.989411	kilogram
water	air	0.000975296	cubic meter
water	water	0.00323462	cubic meter
water, cooling, unspecified natural origin	natural resource - in water	0.09339	cubic meter

Table C0.12. Life cycle inventory of biomethane production from willow.

biomethane production, 16 bar from willow, fluidized technology			**1 Ncum**
Technosphere flows			
	Amount	**Unit**	
carbon dioxide transport and storage, 200 km pipeline, storage 1000m	1.65665	kilogram	
market for copper oxide	2.37E-05	kilogram	
market for monoethanolamine	0.09044	kilogram	
market for natural gas, high pressure	0.00117	cubic meter	
market for nickel, class 1	0.000726	kilogram	
market for sodium bicarbonate	6.7523E-06	kilogram	
market for transport, freight, lorry 16-32 metric ton, EURO6	0.146145	ton kilometer	
market for wastewater, average	-0.00019636	cubic meter	
market for wood ash mixture, pure	-0.04037	kilogram	
willow production, short rotation coppice	2.92291	kilogram	
market for zinc	7.36E-05	kilogram	
market group for electricity, medium voltage	1.513397552	kilowatt hour	
market group for tap water	1.65117	kilogram	
market group for tap water	3.97716	kilogram	
synthetic gas factory construction	2.90E-09	unit	
Biosphere flows			
	Compartment	**Amount**	**Unit**
ammonia	air	5.71E-16	kilogram
carbon	soil	0	kilogram
carbon dioxide, non-fossil	air	1.706115022	kilogram
carbon monoxide, non-fossil	air	2.78E-05	kilogram
hydrogen	air	5.27E-09	kilogram
methane, non-fossil	air	7.27E-30	kilogram
nitrogen	air	16.008476	kilogram
nitrogen oxides	air	4.30E-06	kilogram
oxygen	air	3.6179486	kilogram
water	air	0.00093	cubic meter
water	water	0.00305	cubic meter
water, cooling, unspecified natural origin	natural resource - in water	0.0842982	cubic meter

Table C0.13. Life cycle inventory of biomethane production from poplar.

biomethane production, 16 bar from poplar, fluidized technology			**1 Ncum**
Technosphere flows			
	Amount	**Unit**	
carbon dioxide transport and storage, 200 km pipeline, storage 1000m	1.61114	kilogram	
market for copper oxide	0.000034	kilogram	
market for monoethanolamine	0.08626405	kilogram	
market for natural gas, high pressure	0.099	cubic meter	
market for nickel, class 1	0.00065	kilogram	
market for sodium bicarbonate	0.0000172	kilogram	
market for transport, freight, lorry 16-32 metric ton, EURO6	0.12488	ton kilometer	
market for wastewater, average	-0.00018145	cubic meter	
market for wood ash mixture, pure	-0.04895	kilogram	
market for zinc	0.000021	kilogram	
market group for electricity, medium voltage	1.456843	kilowatt hour	
market group for tap water	1.75412424	kilogram	
market group for tap water	4.19827126	kilogram	
synthetic gas factory construction	2.90E-09	unit	
wood chips, poplar, dry, at plantation	2.49753	kg	
Biosphere flows			
	Compartment	**Amount**	**Unit**
ammonia	air	4.70E-13	kilogram
carbon	soil	1.40E-34	kilogram
carbon dioxide, non-fossil	air	1.39724	kilogram
carbon monoxide, non-fossil	air	2.40E-05	kilogram
hydrogen	air	4.70E-07	kilogram
methane, non-fossil	air	5.30E-26	kilogram
nitrogen	air	14.1852	kilogram
nitrogen oxides	air	4.30E-06	kilogram
oxygen	air	3.09374	kilogram
water	air	0.00102	cubic meter
water	water	0.0027224	cubic meter
water, cooling, unspecified natural origin	natural resource - in water	0.073183226	cubic meter

The following activities reported in Table C0.9 to Table C0.13 are based on the literature:

- carbon dioxide transport and storage, 200 km pipeline from [283]
- wood chips, poplar, dry, at plantation is taken from [378]
- impact of residues, e.g., emissions due to land footprint, are taken from Smith et al.[379]. The footprint of biomass residues is usually considered negligible, since they are a by-product and do not occupy land. Therefore, here we only account for the land footprint as reported above in addition to the removal.
- we do not consider the impact of the disposal of components formed from the removal of H_2S and HCl.

Table C0.14. Life cycle inventory of carbon removal by wheat straw residues.

waste biomass, wheat straw, dry			**1 kg**
Biosphere flows			
	Compartment	**Amount**	**Unit**
carbon dioxide, in air	natural resource - in air	1.693282	kilogram

Table C0.15. Life cycle inventory of carbon removal by forest residues.

waste biomass, forest residues, dry			**1 kg**
Biosphere flows			
	Compartment	**Amount**	**Unit**
carbon dioxide, in air	natural resource - in air	1.905108	kilogram

C.5.2 Cradle to-grave analysis

The reference activity of the BAU is:

BAU: *heat production, natural gas, at boiler condensing modulating <100kW EU wo CH*

The biomethane is modeled using the Ecoinvent activity *heat production, biomethane, at boiler condensing modulating <100kW*, replacing the biomethane introducing the biomethane produced using the process developed.

C.6 Optimization model

We develop the mathematical model presented in Eq. (C8) to identify the optimal portfolio of biomass resources to produce biomethane constraining the burden-shifting relative to the BAU on a set of critical non-climate change indicators. This set is determined by considering some limits proposed in the literature[55] within the EU context applying downscaling according to an egalitarian principle[218].

We do not include climate change, which we already know is not transgressed because our process is carbon negative. Instead, we compute the global warming impact of the optimal solution a posteriori based on the optimal solution.

$$
\begin{aligned}
&\max m_{bio,tot} \\
&\text{s.t.} \sum_{b,j} m_{bio\ b,j} + m_{BAU} = \text{DEMAND} \\
&\sum_{b,j} m_{bio\ b,j}\,\text{IMPACT}_{b,j,k} \le \text{TF}\, m_{BAU}\text{IMPACT}_{\text{BAU,k}}\ \forall\ \text{k} \in \text{K}' \\
&m_{bio\ b,j} \le \text{RESAVAIL}_{\text{b,j}}\ \forall\ \text{b} \in \text{RD}, \quad \text{j} \in \text{J} \\
&m_{bio\ b,j} \le \text{CROPAVAIL}_{\text{b,j}}\ \forall\ \text{b} \in \text{EC}, \quad \text{j} \in \text{J} \\
&m_{BAU} \le \text{MAXBAU} \\
&m_{bio,tot} = \sum_{b,j} m_{bio\ b,j}
\end{aligned}
\tag{C8}
$$

We constrain the amount of biomass to the availability in the European Union calculated as above, and the amount of natural gas to an arbitrary value able to satisfy the whole demand, assuming that it can be imported, e.g., from Qatar or the United States[227]. The model is implemented in GAMS and solved with CPLEX. Set $\text{b} \in \text{B}$ refers to the types of biomass, including residues (RD) and energy crops (EC), while $\text{j} \in \text{J}$ are the countries in the EU, and $\text{k} \in \text{K}$ are the EF metrics other than climate change. Variable $m_{bio,tot}$ is the amount of biomethane while m_{BAU} is the conventional fossil natural gas. The parameters included in the model are the natural demand for the industrial heat and power sector (DEMAND), the availability of the energy crops and residues (CROPAVAIL and RESAVAIL, respectively), the maximum amount of fossil natural gas imported (MAXBAU) and the impacts on the k category of the EF metrics of the BAU ($\text{IMPACT}_{\text{BAU,k}}$) and biomethane ($\text{IMPACT}_{b,j,k}$). We allow the biomethane transgression by a factor TF. K' is the subset of critical metrics that we want to constrain according to the planetary boundaries transgression.

C.7 Supplementary results

C.7.1 Techno-economic results

We study the economic performance of the biomethane routes. We first compare the product specification obtained in the five scenarios as reported in Table C0.16. Notably, the biomethane meets the grid specifications in terms of energy content and methane purity, which are results from our process simulation. The water and CO_2 concentrations are also properly monitored before the compression to the final condition, due to strict requirements for grid feed-in. While the methane content and heating value is consistent in the different scenarios, and with literature values[252], the amount of natural gas obtained in Ncum/hr is the greatest for poplar, being 37% higher than wheat straw residues, which has the lowest production rate.

Table C0.16. Biomethane product specification in the five scenarios modeled.

		Wheat straw residues	**Forest residues**	**Miscanthus**	**Willow**	**Poplar**
Density	kg/Ncum	0.735	0.723	0.710	0.716	0.714
Mass flow	kg/hr	3769	4415	4045	4285	5005
Volume flow	Ncum/hr	5125	6108	5696	5987	7007
LHV [mass]	MJ/kg	46.05	47.28	48.18	47.90	47.65
LHV [volume]	MJ/Ncum	33.87	34.17	34.21	34.28	34.03
CH_4	vol.%	0.95	0.96	0.96	0.96	0.95
*CH_4	wt.%	0.92	0.94	0.95	0.95	0.94

The process key performance indicators displayed in Table C0.17 depend on the feedstock proximate and ultimate analysis. Wheat straw is the most inefficient crop for biomethane production as it requires 3.41 kg of dry biomass to produce one cubic meter of gas at normal conditions. Additionally, it also provides the lowest CO_2 sequestration and storage efficiency. On the other hand, poplar is the energy crops that performs the best, with only 2.50 kg of dry biomass per normal cubic meter and it provides the highest CO_2 storage efficiency of approximately 70%. Indeed, poplar carbon content is the highest among the crops selected in this study, with the downside of having a low fixed carbon content, which leads to low char formation and therefore makes it necessary to add a natural gas input to provide sufficient heat for the gasification. Forest residues are a very competitive alternative to poplar, which show comparable process performance. Furthermore, forest residues have the advantage of very little impacts resulting from the cultivation stage, such as land and water usage, fertilizers and machineries, as shown later.

Table C0.17. Process performance metrics.

	Biomass to biomethane conversion efficiency	**Biogenic CO_2 sequestration efficiency**		**Process CO_2 capture efficiency**
	kg^{dry}/Ncum	$kgCO_2^{abs}$/ Ncum	$kgCO_2^{emit}$/ Ncum	CO_2 storage efficiency [%]
Wheat straw residues	3.41	5.8	2.3	60.8
Forest residues	2.87	5.5	1.8	67.5
Miscanthus	3.07	5.4	1.8	67.1
Willow	2.92	5.1	1.7	66.8
Poplar	2.50	4.6	1.4	69.7

Given the energy crisis in 2022, biomethane also appears to be an economically attractive alternative to natural gas. As a consequence of the production rate and process performance, we find that biomethane is more expensive than fossil NG (24-44% above the BAU in the reference year 2022), with forest residues being the cheapest biomass source and wheat straw the most costly (Figure C0.4). However, all the biomethane routes became economically competitive if compared to the period July-September 2022 when the NG prices peaked in the EU due to the Ukraine invasion. Therefore, biomethane would not be as volatile the business as usual market[380].

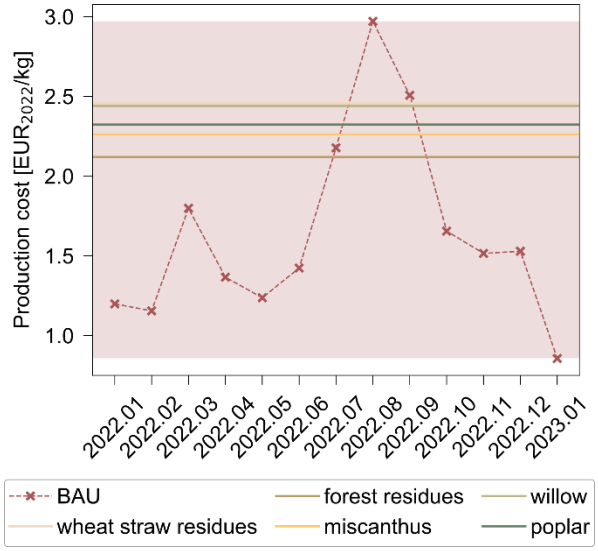

Figure C0.4: Biomethane production cost and BAU price[381] in 2022.

C.7.2 Environmental assessment results

C.7.2.1 Breakdown of cradle-to-gate impacts

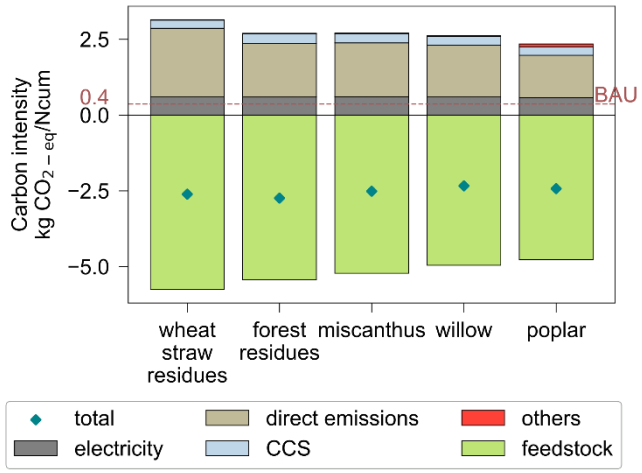

Figure C0.5: Breakdown of average EU climate change impact on a cradle-to-gate basis. Electricity is the total process electricity needed for pumps and compressors; CCS includes MEA solvent and process water make up, CO_2 transportation and storage; feedstock includes the crop cultivation and transportation (assumed 50 km) to the processing site; others includes the chemicals for the syngas cleaning, natural gas input – in the willow and poplar scenarios -, process water for steam generation, wastewater and ash treatment and reactions catalysts.

We analyze the cradle-to-gate impacts looking at the breakdown of the activities in the biomethane production. We note that the main process is similar in all the scenarios, therefore, the contribution of some inputs such as electricity production are almost constant in all the cases. The results show that in all the scenarios direct emissions are the greatest contribution to the impact on climate change, mainly due to the flue gas emissions not captured. Poplar is the only scenario where others shows a significant contribution due to the natural gas input to the gasification to compensate for the low fixed carbon of the crop.

C.7.2.2 Breakdown of cradle-to-gate Environmental Footprint impacts

Next, we analyze the breakdown of the Environmental Footprint impacts on a cradle-to-gate basis.

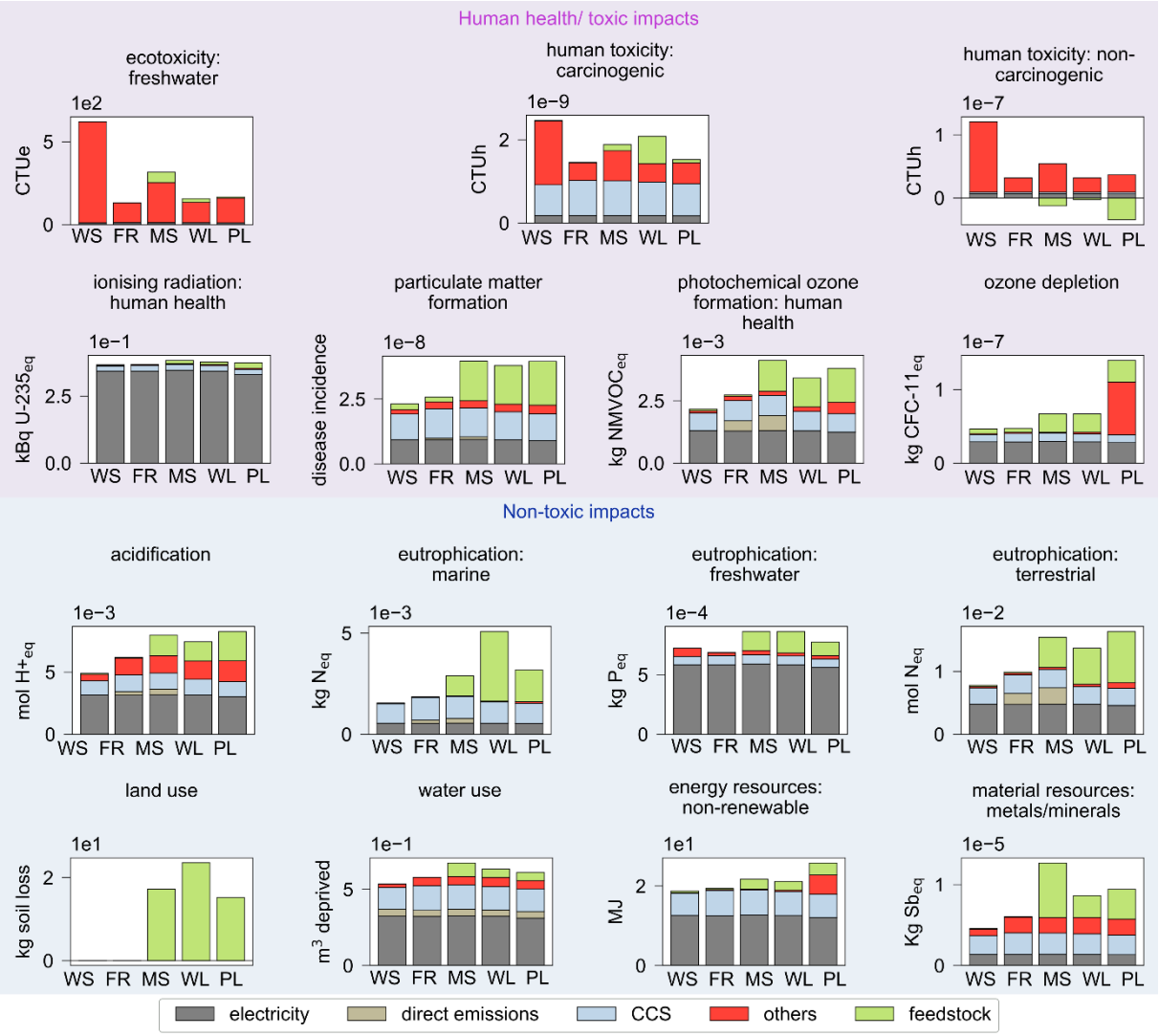

Figure C0.6: Breakdown of average EU Environmental Footprint indicators for the five scenarios on a cradle-to-gate basis. Acronyms: WS = wheat straw residues, FR = forest residues, MS = *Miscanthus*, WL = willow, PL = poplar. Electricity is the total process electricity needed for pumps and compressors; CCS includes MEA solvent and process water make up, CO_2 transportation and storage; feedstock includes the crop cultivation and transportation (assumed 50 km) to the processing site; others includes the chemicals for the syngas cleaning, natural gas input – in the willow and poplar scenarios -, process water for steam generation, wastewater and ash treatment and reactions catalysts.

We find that the ash contained in the biomass, which is sent to treatment after being collected from the gasifier (included in the macro category 'other'), is the most harmful activity on ecotoxicity freshwater and human toxicity non-carcinogenic. The impact of electricity on water use and eutrophication freshwater mainly comes from the contribution of the electricity mix of

Italy and especially France (nuclear pressure water reactor). The latter also contributes to most of the impacts on ionizing radiation due to the use of uranium. Among the land use impacts, willow shows the highest impact among the energy crops, which also affects eutrophication marine indicator.

Further analysis of the *feedstock* group is carried out in the next section (Figure C0.7).

7.2.3 Cradle-to-gate impact of energy crop cultivation

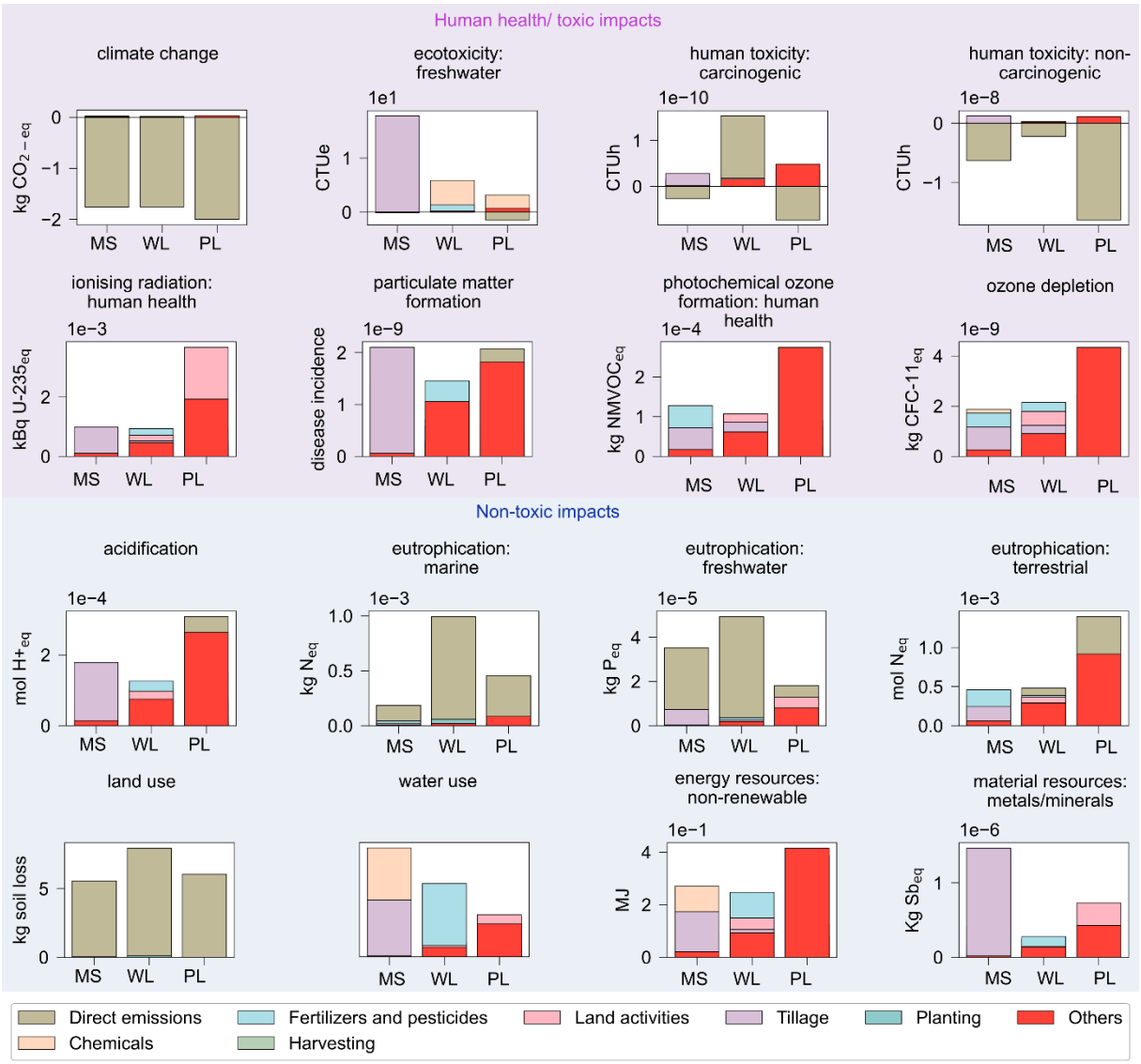

Figure C0.7: Impact of the cultivation stage on climate change and Environmental Footprint metrics. Fertilizers and pesticides include e.g., nitrogen and plant protections; land activities are hoeing, sowing, irrigation; others include e.g., tractors and other transportation on the land; and chemicals are e.g., ammonium nitrate, potassium, glyphosate. Acronyms: MS = *Miscanthus*, WL = willow, PL = poplar.

C.7.2.4 Cradle-to-grave impacts

Figure C0.8: Cradle-to-grave impacts with respect to BAU. The results are reported as: impact of biomethane over BAU for each category. The transgression reaches at most one order of magnitude more than BAU. The most critical indicators are ecotoxicity freshwater and land use, already identified in the cradle-to-gate analysis.

C.7.2.5 Prospective life cycle assessment

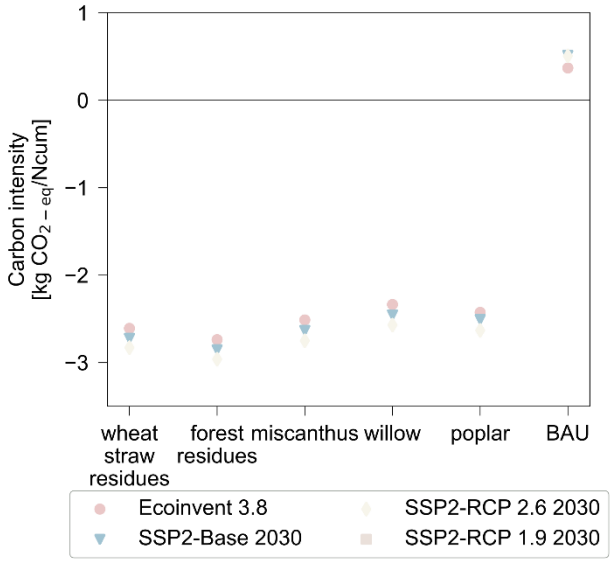

Figure C0.9: Prospective cradle-to-gate global warming potential of scenarios.

The BAU stays constant, while we can notice substantial improvement in the biomethane future scenarios despite being already carbon negative.

C.7.3 Optimization model results

Table C0.18. Environmental impact results in the optimization model.

	Blend		**wheat straw residues**		**forest residues**	
	TF10	TF100	TF10	TF100	TF10	TF100
climate change	-7.02E+09	-1.03E+11	2.86E+10	1.97E+09	-7.02E+09	-6.26E+10
acidification	2.27E+08	3.66E+08	1.69E+08	1.99E+08	2.27E+08	3.11E+08
ecotoxicity: freshwater	2.15E+12	1.16E+13	2.42E+12	7.93E+12	2.15E+12	4.47E+12
energy resources: non-renewable	4.07E+12	3.39E+12	4.32E+12	4.11E+12	4.07E+12	3.68E+12
eutrophication: freshwater	1.14E+07	3.32E+07	3.88E+06	1.02E+07	1.14E+07	2.34E+07
eutrophication: marine	5.56E+07	1.05E+08	3.71E+07	4.82E+07	5.56E+07	8.32E+07
eutrophication: terrestrial	4.52E+08	6.53E+08	3.71E+08	4.10E+08	4.52E+08	5.69E+08
human toxicity: carcinogenic	30.3608	84.5485	18.5069	39.7072	30.3608	54.7757
human toxicity: non-carcinogenic	587.501	2446.78	553.807	1622.66	587.501	1139.74
ionising radiation: human health	6.98E+09	1.81E+10	2.99E+09	6.11E+09	6.98E+09	1.33E+10
material resources: metals/minerals	9.13E+08	4.24E+10	8.46E+08	8.92E+08	1.15E+05	2.22E+05
ozone depletion	115310	297715	43361.2	85075.9	34078.8	28365.3
particulate matter formation	34078.8	24258.7	37689.6	34832	749.733	1139.79
photochemical ozone formation: human health	749.733	1444.98	493.554	664.327	1.71E+08	1.94E+08
water use	1.71E+08	2.09E+08	1.54E+08	1.60E+08	1.05E+10	2.05E+10
land use - erosion potential	1.05E+10	2.77E+10	4.06E+09	8.66E+09	9.13E+08	1.02E+09

Table C0.19. Environmental impact results in the optimization model (cont.).

	miscanthus		**willow**		**poplar**	
	TF10	TF100	TF10	TF100	TF10	TF100
climate change	3.78E+10	2.72E+10	3.82E+10	3.08E+10	3.76E+10	2.60E+10
acidification	1.60E+08	1.84E+08	1.59E+08	1.75E+08	1.61E+08	1.89E+08
ecotoxicity: freshwater	3.78E+11	1.53E+12	2.82E+11	7.02E+11	3.17E+11	1.00E+12
energy resources: non-renewable	4.39E+12	4.32E+12	4.39E+12	4.34E+12	4.39E+12	4.33E+12
eutrophication: freshwater	1.76E+06	4.88E+06	1.65E+06	3.95E+06	1.76E+06	4.92E+06
eutrophication: marine	3.39E+07	4.34E+07	3.44E+07	4.73E+07	3.43E+07	4.61E+07
eutrophication: terrestrial	3.61E+08	4.05E+08	3.59E+08	3.87E+08	3.62E+08	4.16E+08
human toxicity: carcinogenic	10.9306	17.5193	10.7693	16.1758	10.8503	16.7905
human toxicity: non-carcinogenic	147.915	296.222	138.545	215.651	129.106	132.83
ionising radiation: human health	1.92E+09	3.26E+09	1.87E+09	2.85E+09	1.94E+09	3.42E+09
material resources: metals/minerals	3.28E+04	7.94E+04	2.97E+04	5.27E+04	3.17E+04	6.97E+04
ozone depletion	38683	37581.4	38721.5	37907	38703	37759.8
particulate matter formation	442.68	573.8	437.485	529.651	444.914	592.418
photochemical ozone formation: human health	1.52E+08	1.62E+08	1.52E+08	1.57E+08	1.52E+08	1.62E+08
water use	2.54E+09	4.94E+09	2.44E+09	4.10E+09	2.55E+09	4.99E+09
land use - erosion potential	9.07E+09	7.24E+10	9.08E+09	7.32E+10	9.06E+09	7.20E+10

Table C0.20. Amount of natural gas in the optimization model.

	Max.potential	**TF10**	**TF100**	**TF10**	**TF100**
BAU	0	91	60	0	0
wheat straw residues	12	0	11	4	12
forest residues	33	15	33	15	33
miscanthus	44	0	0	0.5	4.2
willow	24	0	0	0.3	3.1
poplar	39	0	3	0.5	4.7
total	151	106	106	20	5

APPENDIX D

Supplementary information to Chapter 5

Extended nomenclature

Table D0.1: List of abbreviations of the stages considered in the supply chain by alphabetical order.

Activity	
bal	baling
balloss	losses during baling
ccs	CO_2 capture and compression unit
chip	chipping
chiploss	losses during chipping
cul	includes cultivation, luc, chipping, baling stages
culloss	includes all the losses of cul
grw	biomass growth, CO_2 uptake from the atmosphere
land	cultivation stage (includes contribution of fertilizers, pesticides, etc.)
landloss	losses occurring during the cultivation stage
lor	lorry (transportation *via*)
lp	transportation land to pelleting process
luc	land-use change
p2s	CO_2 transport *via* pipeline from combustion plant to storage
pc	transportation pelleting process to combustion
pell	pelleting
pow	combustion and electricity production
pro	pelleting process
proloss	losses during pelleting process
sh	ship (transportation *via*)
site	CO_2 storage site (coal, hydrocarbon and saline aquifer)
sto	CO_2 storage
tlp	transportation from land to pellet processing
tpc	transportation from processing to combustion
tr	train (transportation *via*)
trn	transportation LP and PC

Table D0.2: Sets used in NETCOM.

Set	
i	28 EU countries
b	six biomass types
v	three means of transportation
g	three types of geological sites
EC	set of dedicated energy crops
RD	set of residues
TR	set of transportation connections allowed
e	mid- and endpoints indicators of Recipe2016 (H)

Table D0.3: Continuous variables used in NETCOM.

Variables	
$em_{i\,b}^{grw}$	CO_2 stored in biomass b during growth in country i (NEs) [t_{CO_2}/yr]
$prod_{i\,b}^{grw}$	amount of biomass b produced in country i [t_{wb}/yr]
$land_{i\,b}$	land (marginal) surface in country i cultivated with biomass b [ha]
$em_{i\,b}^{cul}$	CO_2 emissions associated with different stages of biomass b cultivation in country i [t_{CO_2}/yr]
$em_{i\,b}^{land}$	CO_2 emissions associated with use of the land (fertilizers, pesticides, fuel, and more) [t_{CO_2}/yr]
$em_{i\,b}^{luc}$	CO_2 emissions associated with LUC for biomass b in country i [t_{CO_2}/yr]
$em_{i\,b}^{bal}$	CO_2 emissions associated with bales processing of biomass b in country i [t_{CO_2}/yr]
$em_{i\,b}^{chip}$	CO_2 emissions associated with chips processing of biomass b in country i [t_{CO_2}/yr]
$prod_{i\,b}^{land}$	amount of biomass b harvested in country i to be processed [t_{wb} /yr]
$em_{i\,b}^{landloss}$	CO_2 emissions associated with loss of biomass b in country i during land cultivation [t_{CO_2}/yr]
$avprod_{ib}^{bal}$	total amount of bales from biomass b in country i [t_{wb} /yr]
$avprod_{ib}^{chip}$	total amount of chips from biomass b in country i [t_{wb} /yr]
$prod_{i\,b}^{bal}$	amount of biomass b in country i used for bales [t_{wb} /yr]
$prod_{i\,b}^{chip}$	amount of biomass b in country i used for chips [t_{wb} /yr]
$co_{i\,b}^{cul}$	cost associated with biomass b cultivation in country i [Eur/yr]
$co_{i\,b}^{land}$	cost associated with land cultivation and farming (fertilizers, pesticides, fuel, and more) [t_{CO_2}/yr]
$co_{i\,b}^{bal}$	cost associated with baling of biomass b in country i [Eur/yr]
$co_{i\,b}^{chip}$	cost associated with chipping of biomass b in country i [Eur/yr]
$em_{i\,b}^{chiploss}$	CO_2 emissions associated with loss of biomass b in country i during chipping [t_{CO_2}/yr]
$em_{i\,b}^{balloss}$	CO_2 emissions associated with loss of biomass b in country i during baling [t_{CO_2}/yr]
$em_{i\,i'\,b}^{tlp}$	CO_2 emissions associated with transport of biomass b from land in country i to processing plant in country i' [t_{CO_2}/yr]
$tlp_{i\,i'\,b\,v}^{bal}$	amount of biomass b transported in bales from land in country i to processing plant in country i' [t_{wb} /yr]
$tlp_{i\,i'\,b\,v}^{chip}$	amount of biomass b transported in chips from land in country i to processing plant in country i' [t_{wb} /yr]
$em_{i\,i'\,b}^{tlploss}$	CO_2 emissions associated with loss of biomass b during transport from land in country i to processing plant in country i' [t_{CO_2}/yr]
$proc_{i\,b}^{bal}$	amount of biomass b available as bales in processing plant in country i [t_{wb} /yr]

$proc_{i\,b}^{chip}$	amount of biomass b available as chips in processing plant in country i [t_{wb} /yr]
$co_{i\,i'\,b}^{tlplor}$	cost associated with transport of biomass b from land in country i to processing plant in country i' *via* lorry [Eur/yr]
$co_{i\,i'\,b}^{tlptr}$	cost associated with transport of biomass b from land in country i to processing plant in country i' *via* train [Eur/yr]
$co_{i\,i'\,b}^{tlpsh}$	cost associated transport of biomass b from land in country i to processing plant in country i' *via* ship [Eur/yr]
$co_{i\,i'\,b}^{tlp}$	total cost associated with transport of biomass b from land in country i to processing plant in country i' [Eur/yr]
$pellet_{i\,b}^{pro}$	amount of pellets of biomass b produced in processing plant in country i [t_{wb} /yr]
$em_{i\,b}^{pro}$	CO_2 emissions associated with pellet processing of biomass b in country i [t_{CO_2}/yr]
$em_{i\,b}^{proloss}$	CO_2 emissions associated with loss of biomass b in country i during pellet processing [t_{CO_2}/yr]
$co_{i\,b}^{pro}$	cost associated with biomass b processing in country i [Eur/yr]
$em_{i\,i'\,b}^{tpc}$	CO_2 emissions associated with transport of biomass b from processing plant in country i to combustion power plant in country i' [t_{CO_2}/yr]
$em_{i\,i'\,b}^{tpcloss}$	CO_2 emissions associated with loss of biomass b during transport from processing plant in country i to combustion power plant in country i' [t_{CO_2}/yr]
$tpc_{i\,i'\,b\,v}^{pell}$	amount of biomass b transported in pellets from processing plant in country i to combustion plant in country i' [t_{wb} /yr]
$comb_{i\,b}^{pell}$	amount of pellets of biomass b available for combustion in country i [t_{wb}/yr]
$co_{i\,i'\,b}^{tpclor}$	cost associated with transport of biomass b from processing plant in country i to combustion power plant in country i' *via* lorry [Eur/yr]
$co_{i\,i'\,b}^{tpctr}$	cost associated with transport of biomass b from processing plant in country i to combustion power plant in country i' *via* train [Eur/yr]
$co_{i\,i'\,b}^{tpcsh}$	cost associated with transport of biomass b from processing plant in country i to combustion power plant in country i' *via* ship [Eur/yr]
$co_{i\,i'\,b}^{tpc}$	total cost associated with transport of biomass b from processing plant in country i to combustion plant in country i' [Eur/yr]
$em_{i\,b}^{pow}$	CO_2 direct emissions associated with combustion of biomass b in power plant in country i [t_{CO_2}/yr]
$CO2_{i}^{pow}$	amount of CO_2 captured at power plant in country i [t_{CO_2}/yr]
$elgen_{i\,b}^{pow}$	amount of electricity generated in country i with biomass b [MWh/yr]
$co_{i\,b}^{pow}$	cost associated with combustion of biomass b in power plant in country i [Eur/yr]
$elccs_{i}^{pow}$	Energy penalty of the ccs unit in combustion plant of country i [MWh/yr]

$elcom_i^{pow}$	amount of electricity required to compress the CO_2 in country i [MWh/yr]
$netelgen_i^{pow}$	net electricity production at the combustion plant in country i [MWh/yr]
$tCO2_{i\,i'}^{p2s}$	amount of CO_2 transported from power plant in country i to storage site in country i' [t_{CO_2}/yr]
$em_{i\,i'}^{p2s}$	CO_2 emissions associated with transport of CO_2 from power plant in country i to storage site in country i' [t_{CO_2}/yr]
$co_{i\,i'}^{p2s}$	cost associated with transport of CO_2 from power plant in country i to storage site in country i' [Eur/yr]
$CO2_i^{sto}$	amount of CO_2 stored in country i [t_{CO_2}/yr]
$CO2_{i\,g}^{site}$	amount of CO_2 stored in geological site of type g in country i [t_{CO_2}/yr]
em_i^{sto}	total CO_2 emissions associated with injection of the CO_2 in country i [t_{CO_2}/yr]
$em_{i\,g}^{site}$	CO_2 emissions associated with storing the CO_2 in geological sites of type g in country i [t_{CO_2}/yr]
co_i^{sto}	cost associated with injection of the CO_2 in country i [Eur/yr]
$co_{i\,g}^{site}$	cost associated with storing the CO_2 in geological sites of type g in country i [t_{CO_2}/yr]
em_i	total CO_2 emissions of country i [t_{CO_2}/yr]
co_i	total cost of the supply chain in country i [Eur/yr]
$gloem$	global CO_2 emissions [t_{CO_2}/yr]
$impact_{i\,b\,e}^{grw}$	impacts at mid- and endpoint level of biomass growth [unit]
$impact_{i\,b\,e}^{land}$	impacts at mid- and endpoint level of land usage [unit]
$impact_{i\,b\,e}^{luc}$	impacts at mid- and endpoint level of luc [unit]
$impact_{i\,b\,e}^{chip}$	impacts at mid- and endpoint level of chipping [unit]
$impact_{i\,b\,e}^{landloss}$	impacts at mid- and endpoint level of baling [unit]
$impact_{i\,b\,e}^{chiploss}$	impacts at mid- and endpoint level of chipping losses [unit]
$impact_{i\,b\,e}^{balloss}$	impacts at mid- and endpoint level of baling losses [unit]
$impact_{i\,i'\,b\,e}^{tlp}$	impacts at mid- and endpoint level of transportation from land to processing [unit]
$impact_{i\,i'\,b\,e}^{tlploss}$	impacts at mid- and endpoint level of transportation from land to processing losses [unit]
$impact_{i\,b\,e}^{pro}$	impacts at mid- and endpoint level of pellet processing [unit]
$impact_{i\,b\,e}^{proloss}$	impacts at mid- and endpoint level of pellet processing losses [unit]
$impact_{i\,i'\,b\,e}^{tpc}$	impacts at mid- and endpoint level of transportation from processing to combustion [unit]
$impact_{i\,i'\,b\,e}^{tpcloss}$	impacts at mid- and endpoint level of transportation from processing to combustion losses [unit]
$impact_{i\,b\,e}^{pow}$	impacts at mid- and endpoint level of combustion [unit]
$impact_{i\,i'\,e}^{p2s}$	impacts at mid- and endpoint level of CO_2 transportation *via* pipeline [unit]

$impact_{i\,g\,e}^{site}$	impacts at mid- and endpoint level of CO_2 storage [unit]
$gloco$	global cost [Eur_{2018}/yr]
hh	global environmental impact on Human Health [DALY]
ed	global environmental impact on Ecosystem Quality [species/yr]
ra	global environmental impact in Resource Availability [USD_{2013}]

Table D0.4: Parameters used in NETCOM.

Parameters	
M^{CO2}	molecular weight of CO_2
M^{C}	molecular weight of C
UCF	conversion factor from GJ to MWh
CC_{ib}	carbon content of biomass b in region i [wt% (wb)]
$YIELD_{ib}$	yield of biomass b in region i [t_{wb}/(ha yr)]
$AVLAND_i$	land (marginal) available for cultivation in region i [ha]
$AVRD_{ib}$	amount of residue b available in country i [t_{wb} /yr]
CI_{ib}^{land}	carbon intensity of use of land for biomass b in region i during cultivation phase [t_{CO_2}/(ha yr)]
CI_{ib}^{luc}	carbon intensity of land-use change for biomass b in country i [t_{CO_2}/(ha yr)]
$LOSS_b^{land}$	biomass losses of biomass b incurred during harvesting
UC_{ib}^{land}	unitary cost of cultivating land in country i for biomass b [Eur/ha]
$LOSS_b^{bal}$	biomass losses of biomass b incurred during balling
$LOSS_b^{chip}$	biomass losses of biomass b incurred during chipping
CI_{ib}^{bal}	carbon intensity of producing bales of biomass b in country i [t_{CO_2}/t_{wb})]
UC_{ib}^{bal}	unitary cost of baling biomass b in country i [Eur/t_{wb}]
CI_{ib}^{chip}	carbon intensity of producing chips of biomass b in country i [t_{CO_2}/ t_{wb})]
$CI_{ib}^{drychip}$	carbon intensity of producing chips of biomass b in country i [t_{CO_2}/ t_{db})]
UC_{ib}^{chip}	unitary cost of chipping biomass b in country i [Eur/t_{wb}]
DRY_{ib}^{chip}	conversion factor (based on moisture content) to relate chips mass in wet and dry basis [wt%]
$DIST_{v\,i\,i'}$	distance between regions i and i' covered *via* transportation mean v [km]
CI_v^{trn}	carbon intensity of transporting biomass *via* transportation mean v [t_{CO_2}/(t_{wb} km)]
$CORF_v^{bal}$	correction factor to account for capacity (carry load/max capacity) for bales in transportation mean v
$CORF_v^{chip}$	correction factor to account for capacity (carry load/max capacity) for chips in transportation mean v
$LOSS^{tlp}$	biomass losses of biomass b incurred during transportation between land and processing plant
$CFIX_{ib}^{lorbal}$	fix cost of transporting biomass b in bales from country i *via* lorry [Eur/t_{wb}]

$CVAR_{ib}^{lorbal}$	variable cost of transporting biomass b in bales from country i *via* lorry [Eur/(t_{wb} km)]
$CFIX_{ib}^{lorchip}$	fix cost of transporting biomass b in chips from country i *via* lorry [Eur/t_{wb}]
$CVAR_{ib}^{lorchip}$	variable cost of transporting biomass b in chips from country i *via* lorry [Eur/(t_{wb} km)]
$CFIX_{ib}^{tr}$	fixed cost of transporting biomass b from country i *via* train (either bales or chips) [Eur/t_{wb}]
$CVAR_{ib}^{tr}$	variable cost of transporting biomass b from country i *via* train (either bales or chips) [Eur/(t_{wb} km)]
$CFIX_{ib}^{sh}$	fixed cost of transporting biomass b from country i *via* ship (either bales or chips) [Eur/t_{wb}]
$CVar_{ib}^{sh}$	variable cost of transporting biomass b from country i *via* ship (either bales or chips) [Eur/(t_{wb} km)]
$LOSS_{b}^{ovpell}$	biomass losses incurred during pelletizing
$LOSS_{b}^{pell}$	biomass losses incurred during each stage of the pelleting process
DRY_{ib}^{pell}	conversion factor (based on moisture content) to relate pellets mass in wet and dry basis [wt%]
CI_{ib}^{pell}	carbon intensity of producing pellets of biomass b at the processing plant in region i [t_{CO_2}/ t_{db})]
CC_{b}^{pro}	carbon content of biomass b at the pelleting stage on a wet mass basis [wt_{wb}%]
CC_{b}^{pow}	carbon content of biomass b at power plant on a wet mass basis [wt_{wb}%]
CC_{b}^{drypow}	carbon content of biomass b at power plant on a dry mass basis [wt_{db}%]
UC_{ib}^{pell}	unitary cost of pelleting biomass b in country i [Eur/t_{wb}]
$CORF_{v}^{pell}$	correction factor to account for capacity (carry load/max capacity) for pellets in transportation mean v
$LOSS^{tpc}$	biomass losses incurred during transportation between processing plant and power plant
$CFIX_{ib}^{tpclor}$	fix cost of transporting biomass b in pellets from country i *via* lorry [Eur/ t_{wb}]
$CVAR_{ib}^{tpclor}$	variable cost of transporting biomass b in pellets from country i *via* lorry [Eur/(t_{wb}*km)]
$CFIX_{ib}^{tpctr}$	fix cost of transporting biomass b in pellets from country i *via* train [Eur/t_{wb}]
$CVAR_{ib}^{tpctr}$	variable cost of transporting biomass b in pellets from country i *via* train [Eur/(t_{wb} *km)]
$CFIX_{ib}^{tpcsh}$	fix cost of transporting biomass b in pellets from country i *via* ship [Eur/t_{wb}]
$CVAR_{ib}^{tpcsh}$	variable cost of transporting biomass b in pellets from country i *via* ship [Eur/(t_{wb} *km)]
R^{ccs}	capture rate of CCS system [%]

HHV_b^{pell}	HHV of pellets of biomass b [MJ/t_{wb}]
$HHV_b^{drypell}$	HHV of pellets of biomass b [MJ/t_{db}]
η^{pow}	efficiency of power plant to transform energy from biomass combustion into electricity [%]
UC_{ib}^{pow}	unitary cost of combusting biomass b at power plant in country i [Eur/MWh]
ELR^{ccs}	electricity penalty (pump) per unit of CO_2 captured [MWh/t_{CO_2}]
HER^{ccs}	electricity penalty (steam generation) per unit of CO_2 captured [MWh/t_{CO_2}]
COR^{ccs}	electricity penalty for compressing the CO_2 captured to 110 bar [MWh/t_{CO_2}]
CI^{p2s}	carbon intensity of transporting CO_2 *via* pipeline [t_{CO_2}/(t_{CO_2}*km)]
$DIST_{i\,i'}^{pipe}$	distance between regions i and i' when covered *via* pipeline [km]
$DIST_{i\,i'}^{totpipe}$	distance between regions i and i' when covered *via* pipeline including distance to storage site [km]
$DIST_{i\,i'}^{totpipen}$	distance between regions i and i' when covered *via* pipeline including distance to storage site / 250 km [km]
$CVAR_i^{P2S}$	unitary cost of transporting CO_2 *via* pipeline [Eur/(t_{CO_2} 250km)]
$LOSS^{p2s}$	CO_2 losses incurred during transportation of CO_2 between power plant and storage site
$CAP_{i\,g}^{site}$	storage capacity in geological sites of type g in region i [t_{CO_2}]
CI_g^{site}	carbon intensity of storing CO_2 in geological sites of type g [t_{CO_2}/t_{CO_2}]
$CVAR_{i\,g}^{site}$	unitary cost of storing CO_2 in geological sites of type g [Eur/t_{CO_2}]
W	weight between regions i and i' to allocate emissions responsibilities
W^{co}	weight between regions i and i' to allocate cost responsibilities
TG	CDR target [t_{CO_2}]
$ECOVEC_{ibe}^{grw}$	ecovector of impacts per functional unit at mid- and endpoint Recipe2016 biomass growth [unit]
$ECOVEC_{ibe}^{land}$	ecovector of impacts per functional unit at mid- and endpoint Recipe2016 cultivation [unit]
$ECOVEC_{ibe}^{luc}$	ecovector of impacts per functional unit at mid- and endpoint Recipe2016 luc [unit]
$ECOVEC_{ibe}^{chip}$	ecovector of impacts per functional unit at mid- and endpoint Recipe2016 chipping [unit]
$ECOVEC_{ibe}^{bal}$	ecovector of impacts per functional unit at mid- and endpoint Recipe2016 baling [unit]
$ECOVEC_{ibe}^{landloss}$	ecovector of impacts per functional unit at mid- and endpoint Recipe2016 cultivation losses [unit]
$ECOVEC_{ibe}^{chiploss}$	ecovector of impacts per functional unit at mid- and endpoint Recipe2016 chipping losses [unit]

$ECOVEC^{balloss}_{i\,b\,e}$	ecovector of impacts per functional unit at mid- and endpoint Recipe2016 baling losses [unit]
$ECOVEC^{tlp}_{i\,b\,v\,e}$	ecovector of impacts per functional unit at mid- and endpoint Recipe2016 for different transportation modes from land to pellet processing site [unit]
$ECOVEC^{tlploss}_{i\,b\,v\,e}$	ecovector of impacts per functional unit at mid- and endpoint Recipe2016 for different transportation modes losses from land to pellet processing site[unit]
$ECOVEC^{pro}_{i\,b\,e}$	ecovector of impacts per functional unit at mid- and endpoint Recipe2016 pelleting [unit]
$ECOVEC^{proloss}_{i\,b\,e}$	ecovector of impacts per functional unit at mid- and endpoint Recipe2016 pelleting losses [unit]
$ECOVEC^{tpc}_{i\,b\,v\,e}$	ecovector of impacts per functional unit at mid- and endpoint Recipe2016 for different transportation modes from pelleting to combustion site [unit]
$ECOVEC^{tpcloss}_{i\,b\,v\,e}$	ecovector of impacts per functional unit at mid- and endpoint Recipe2016 for different transportation modes losses from pelleting to combustion site [unit]
$ECOVEC^{pow}_{i\,b\,e}$	ecovector of impacts per functional unit at mid- and endpoint Recipe2016 combustion [unit]
$ECOVEC^{p2s}_{i\,b\,e}$	ecovector of impacts per functional unit at mid- and endpoint Recipe2016 CO_2 transportation *via* pipeline to storage site [unit]
$ECOVEC^{site}_{i\,b\,g\,e}$	ecovector of impacts per functional unit at mid- and endpoint Recipe2016 for different CO_2 storage sites [unit]
$NETELGEN^{mincos}$	net electricity production calculated in the minimum cost solution [MWh/yr]

D.1 Techno-economic data

Most input data to the model are sourced from published studies, referenced in the detailed model description. Other data are given in Table D0.5 to Table D0.29.

D.1.1 Cultivation stage

Table D0.5: Carbon content of wet biomass per country and type of biomass. The calculations are based on the carbon content of dry mass and the moisture content at harvest reported by Fajardy et al.[33] and the Phyllis2 database[382](*).

CC [wt% (wb)]	Miscanthus	Switchgrass	Willow	Straw cereals	Woody	Forest
AUT	0.29*	0.41	0.23	0.44	0.39	0.46
BEL	0.37	0.41	0.23	0.44	0.39	0.46
BGR	0.37	0.41	0.23	0.44	0.39	0.46
CYP	0.37	0.41	0.23	0.44	0.39	0.46
CZE	0.37	0.41	0.23	0.44	0.39	0.46
DEU	0.44*	0.41	0.23	0.44	0.39	0.46
DNK	0.37	0.41	0.23	0.44	0.39	0.46
ESP	0.37	0.41	0.23	0.44	0.39	0.46
EST	0.37	0.41	0.23	0.44	0.39	0.46
FIN	0.37	0.41	0.25*	0.44	0.39	0.48*
FRA	0.37	0.41	0.23	0.44	0.39	0.46
GBR	0.37	0.41	0.23	0.44	0.39	0.46
GRC	0.37	0.41	0.23	0.44	0.39	0.46
HUN	0.37	0.41	0.23	0.44	0.39	0.46
IRL	0.37	0.41	0.23	0.44	0.39	0.46
ITA	0.44*	0.41	0.23	0.44	0.39	0.46
LTU	0.37	0.41	0.23	0.44	0.39	0.46
LUX	0.37	0.41	0.23	0.44	0.39	0.46
LVA	0.37	0.41	0.23	0.44	0.39	0.46
MLT	0.37	0.41	0.23	0.44	0.39	0.46
NLD	0.44*	0.41	0.23	0.44	0.39	0.46
POL	0.37	0.41	0.23	0.44	0.39	0.46
PRT	0.37	0.41	0.23	0.44	0.39	0.46
ROU	0.37	0.41	0.23	0.44	0.39	0.46
HRV	0.37	0.41	0.23	0.44	0.39	0.46
SVK	0.37	0.41	0.23	0.44	0.39	0.46
SVN	0.37	0.41	0.23	0.44	0.39	0.46
SWE	0.37	0.41	0.23	0.44	0.39	0.48*

Table D0.6: Yield of different types of energy crops in each country, based on the data from IIASA (EPIC II) for *Miscanthus* and Fajardy et al.[383] for switchgrass and willow.

Yield $[t_{wb}/(ha\ yr)]$	**Miscanthus**	**Switchgrass**	**Willow**
AUT	50.89	9.09	9.17
BEL	37.27	13.64	16.04
BGR	31.00	9.09	7.08
CYP	26.23	2.27	4.79
CZE	34.71	9.09	9.38
DEU	36.03	9.09	13.75
DNK	33.33	8.07	13.13
ESP	21.97	4.55	5.63
EST	29.72	4.55	6.25
FIN	24.98	2.27	7.08
FRA	38.36	10.80	12.71
GBR	27.28	9.09	13.33
GRC	22.71	2.27	5.21
HUN	39.32	13.64	7.50
IRL	33.00	4.55	15.63
ITA	36.72	15.45	7.29
LTU	35.93	9.09	7.71
LUX	37.36	13.64	11.04
LVA	34.27	4.55	7.08
MLT	26.23	9.09	8.96
NLD	36.34	9.43	15.83
POL	35.70	9.09	7.71
PRT	31.05	9.09	2.50
ROU	39.87	9.09	5.63
HRV	23.38	9.09	9.17
SVK	38.65	9.09	7.08
SVN	48.20	9.09	9.38
SWE	29.77	1.14	10.83

Table D0.7: Available marginal land for cultivation of energy crops in each country, calculated by GIS data aggregation from Cai et al.[384] and downscaled according to Fritz et al.[385].

i	Available land [ha]
AUT	128374
BEL	57706
BGR	538689
CYP	3072
CZE	214505
DEU	680989
DNK	83747
ESP	6863941
EST	1137461
FIN	5757
FRA	964191
GBR	1550031
GRC	484982
HUN	173758
IRL	1526758
ITA	504674
LTU	1591874
LUX	1197
LVA	1408982
MLT	0
NLD	92555
POL	2377835
PRT	1231251
ROU	650490
HRV	168576
SVK	157606
SVN	33904
SWE	457799

Table D0.8: Amount of residues available in each country, from published data in the Atlas of EU biomass potentials[386] for straw cereal and woody residues, while forestry residues are sourced from IINAS[387].

AVRD [t_{wb}/yr]	**Straw cereals**	**Woody**	**Forest**
AUT	1941413	152247	16921420
BEL	957802	57093	2462967
BGR	4003269	767580	3854125
CYP	0	98326	0
CZE	4152388	31718	12151984
DEU	25473524	415508	50050490
DNK	3727973	19031	1655068
ESP	6174096	13207451	11746591
EST	817286	6344	6269738
FIN	1651779	25375	39072530
FRA	31544384	3159131	39270607
GBR	6062257	47577	7278024
GRC	1258908	2540626	2200212
HUN	9124930	0	5263762
IRL	157722	0	1869891
ITA	9190886	6556148	11961415
LTU	1651779	44405	4631995
LUX	0	0	456212
LVA	788610	22203	7768885
MLT	0	0	0
NLD	559196	41234	680275
POL	17613237	1024497	27554623
PRT	544858	1858685	4864143
ROU	9497727	995951	15798792
HRV	1142288	318939	3644498
SVK	2371564	28546	5300721
SVN	364194	63436	4119189
SWE	1709132	69780	49762326

D.1.2 Chipping and baling

Table D0.9: Dry factor to convert dry chips into wet mass, calculated from data in Fajardy et al.[33] and the Phillys2 database[382](*).

Dry^{chip} [wt%]	Miscanthus	Switchgrass	Willow	Straw cereals	Woody	Forest
AUT	0.40*	0.12	0.52	0.04	0.08	0.07
BEL	0.23	0.12	0.52	0.04	0.08	0.07
BGR	0.23	0.12	0.52	0.04	0.08	0.07
CYP	0.23	0.12	0.52	0.04	0.08	0.07
CZE	0.23	0.12	0.52	0.04	0.08	0.07
DEU	0.09*	0.12	0.52	0.04	0.08	0.07
DNK	0.23	0.12	0.52	0.04	0.08	0.07
ESP	0.23	0.12	0.52	0.04	0.08	0.07
EST	0.23	0.12	0.52	0.04	0.08	0.07
FIN	0.23	0.12	0.50*	0.04	0.08	0.06*
FRA	0.23	0.12	0.52	0.04	0.08	0.07
GBR	0.23	0.12	0.52	0.04	0.08	0.07
GRC	0.23	0.12	0.52	0.04	0.08	0.07
HUN	0.23	0.12	0.52	0.04	0.08	0.07
IRL	0.23	0.12	0.52	0.04	0.08	0.07
ITA	0.06*	0.12	0.52	0.04	0.08	0.07
LTU	0.23	0.12	0.52	0.04	0.08	0.07
LUX	0.23	0.12	0.52	0.04	0.08	0.07
LVA	0.23	0.12	0.52	0.04	0.08	0.07
MLT	0.23	0.12	0.52	0.04	0.08	0.07
NLD	0.09*	0.12	0.52	0.04	0.08	0.07
POL	0.23	0.12	0.52	0.04	0.08	0.07
PRT	0.23	0.12	0.52	0.04	0.08	0.07
ROU	0.23	0.12	0.52	0.04	0.08	0.07
HRV	0.23	0.12	0.52	0.04	0.08	0.07
SVK	0.23	0.12	0.52	0.04	0.08	0.07
SVN	0.23	0.12	0.52	0.04	0.08	0.07
SWE	0.23	0.12	0.52	0.04	0.08	0.06*

D.1.3 Transportation *via* lorry, train or ship

Table D0.10: Distances by lorry between countries i and i' [km][388,389]. Intra-country distances are assumed to be equal to 50 km[390].

	AUT	BEL	BGR	CYP	CZE	DEU	DNK	ESP	EST	FIN
AUT	50									
BEL	916	50								
BGR	1003	2116	50							
CYP	2589	3702	1578	50						
CZE	333	907	1285	2872	50					
DEU	681	765	1634	3220	349	50				
DNK	1115	920	2068	3654	783	439	50			
ESP	2399	1578	2976	4563	2242	2321	2488	50		
EST	1677	2272	2625	4212	1654	1544	1078	3822	50	
FIN	1764	2043	2712	4298	1740	1631	1136	3605	87	50
FRA	1236	312	2246	3832	1030	1055	1222	1270	2554	2341
GBR	1477	373	2486	4073	1271	1100	1255	1722	2600	2375
GRC	1716	2829	793	2123	1998	872	2779	3241	3331	3421
HUN	243	1356	768	2355	525	872	1833	2520	1858	1948
IRL	2054	950	3064	4650	1849	1678	1833	2299	3177	2952
ITA	1095	1483	1668	2748	1299	1501	1901	1953	2757	2846
LTU	1168	1763	2116	3703	1144	1035	1473	3313	604	694
LUX	946	198	1955	3542	740	769	915	1686	2259	2034
LVA	1366	1960	2313	3900	1342	1233	1671	3510	311	401
MLT	2115	2503	1668	2998	2318	2521	2920	2972	3776	3865
NLD	1148	213	2157	3743	876	654	791	1770	2154	1910
POL	683	1301	1631	3217	683	574	1012	2851	974	1063
PRT	2868	2038	3530	5116	2702	2781	2948	629	4280	4067
ROU	1054	2167	357	1665	1336	1684	2117	3327	2319	2408
HRV	376	1288	782	2369	699	1047	1475	2194	2037	2126
SVK	80	1193	962	2548	328	676	1110	2483	1662	1751
SVN	384	1193	920	2507	707	993	1393	2059	2045	2135
SWE	1759	1564	2712	4298	1427	1082	656	3126	426	479

Table D0.11: Distances by lorry between countries i and i' [km] (cont.).

	FRA	**GBR**	**GRC**	**HUN**	**IRL**	**ITA**	**LTU**	**LUX**	**LVA**	**MLT**
AUT										
BEL										
BGR										
CYP										
CZE										
DEU										
DNK										
ESP										
EST										
FIN										
FRA	50									
GBR	470	50								
GRC	2957	3210	50							
HUN	1484	1737	1476	50						
IRL	1047	583	3772	2303	50					
ITA	1420	1881	1274	1214	2462	50				
LTU	2052	2107	2824	1356	2688	2280	50			
LUX	407	573	2664	1195	1154	1300	1748	50		
LVA	2250	2304	3022	1553	2885	2477	288	1959	50	
MLT	2440	2900	1525	2233	3481	1046	3265	2323	3466	50
NLD	510	550	2865	1396	977	1650	1643	362	1844	2670
POL	1591	1645	2339	870	2226	1794	463	1300	663	2814
PRT	1735	2196	3799	3075	2777	2510	3769	2154	3970	3530
ROU	2296	2549	1153	820	3130	2024	1808	2007	2009	2030
HRV	1384	1670	1491	343	2251	890	1526	1109	1727	1910
SVK	1322	1575	1670	201	2156	1188	1151	1033	1352	2208
SVN	1242	1555	1629	463	2136	755	1534	967	1735	1775
SWE	1865	1908	3420	1951	2489	2545	791	1559	521	3564

Table D0.12: Distances by lorry between countries i and i' [km] (cont.).

	NLD	**POL**	**PRT**	**ROU**	**HRV**	**SVK**	**SVN**	**SWE**
AUT								
BEL								
BGR								
CYP								
CZE								
DEU								
DNK								
ESP								
EST								
FIN								
FRA								
GBR								
GRC								
HUN								
IRL								
ITA								
LTU								
LUX								
LVA								
MLT								
NLD	50							
POL	1192	50						
PRT	2239	3317	50					
ROU	2206	1349	3884	50				
HRV	1328	1074	2750	983	50			
SVK	1202	699	2956	1013	388	50		
SVN	1233	1082	2615	1271	140	450	50	
SWE	1435	1645	3592	2763	2114	1755	2035	50

Table D0.13: Distances by train between countries i and i' [km]. Distances between different countries are assumed to be equal to 80% of the corresponding lorry route.

	AUT	**BEL**	**BGR**	**CYP**	**CZE**	**DEU**	**DNK**	**ESP**	**EST**	**FIN**
AUT	40									
BEL	733	40								
BGR	803	1693	40							
CYP	2071	2962	1263	40						
CZE	266	726	1028	2297	40					
DEU	545	612	1307	2576	279	40				
DNK	892	736	1654	2923	627	351	40			
ESP	1919	1262	2381	3650	1793	1856	1990	40		
EST	1342	1817	2100	3369	1323	1235	863	3057	40	
FIN	1411	1635	2170	3439	1392	1305	909	2884	70	40
FRA	989	250	1796	3066	824	844	977	1016	2044	1873
GBR	1182	298	1989	3258	1017	880	1004	1377	2080	1900
GRC	1373	2263	634	1698	1598	698	2223	2593	2665	2737
HUN	194	1085	615	1884	420	698	1466	2016	1487	1558
IRL	1643	760	2451	3720	1479	1342	1466	1839	2542	2362
ITA	876	1187	1335	2198	1039	1201	1521	1562	2205	2277
LTU	935	1410	1693	2962	916	828	1179	2650	483	555
LUX	757	158	1564	2834	592	615	732	1349	1807	1628
LVA	1093	1568	1851	3120	1073	986	1336	2808	249	321
MLT	1692	2002	1335	2399	1855	2017	2336	2378	3021	3092
NLD	918	170	1726	2995	701	524	633	1416	1723	1528
POL	546	1041	1304	2574	546	459	809	2281	779	851
PRT	2294	1631	2824	4093	2162	2225	2358	503	3424	3254
ROU	843	1734	286	1332	1069	1347	1694	2662	1855	1927
HRV	301	1031	626	1895	559	837	1180	1755	1630	1701
SVK	64	954	769	2038	263	541	888	1986	1330	1401
SVN	307	955	736	2005	566	795	1114	1647	1636	1708
SWE	1407	1251	2169	3439	1142	866	525	2500	341	383

Table D0.14: Distances by train between countries i and i' [km] (cont.).

	FRA	**GBR**	**GRC**	**HUN**	**IRL**	**ITA**	**LTU**	**LUX**	**LVA**	**MLT**
AUT										
BEL										
BGR										
CYP										
CZE										
DEU										
DNK										
ESP										
EST										
FIN										
FRA	40									
GBR	376	40								
GRC	2366	2568	40							
HUN	1188	1390	1181	40						
IRL	838	467	3017	1842	40					
ITA	1136	1505	1019	971	1970	40				
LTU	1642	1685	2260	1085	2150	1824	40			
LUX	326	458	2131	956	923	1040	1398	40		
LVA	1800	1843	2417	1242	2308	1982	231	1567	40	0
MLT	1952	2320	1220	1787	2785	837	2612	1858	2772	40
NLD	408	440	2292	1117	782	1320	1315	289	1475	2136
POL	1273	1316	1871	696	1781	1435	370	1040	531	2251
PRT	1388	1757	3039	2460	2222	2008	3016	1723	3176	2824
ROU	1837	2039	923	656	2504	1619	1446	1606	1607	1624
HRV	1107	1336	1192	275	1801	712	1221	887	1381	1528
SVK	1057	1260	1336	161	1725	950	921	827	1081	1766
SVN	994	1244	1303	370	1709	604	1227	774	1388	1420
SWE	1492	1526	2736	1561	1991	2036	632	1247	417	2852

Table D0.15: Distances by train between countries i and i' [km] (cont.).

	NLD	**POL**	**PRT**	**ROU**	**HRV**	**SVK**	**SVN**	**SWE**
AUT								
BEL								
BGR								
CYP								
CZE								
DEU								
DNK								
ESP								
EST								
FIN								
FRA								
GBR								
GRC								
HUN								
IRL								
ITA								
LTU								
LUX								
LVA								
MLT								
NLD	40							
POL	953	40						
PRT	1792	2654	40					
ROU	1765	1079	3107	40				
HRV	1062	859	2200	787	40			
SVK	962	559	2365	810	310	40		
SVN	986	865	2092	1017	112	360	40	
SWE	1148	1316	2874	2210	1691	1404	1628	40

Table D0.16: Distances by ship between countries i and i' [km].

	AUT	BEL	BGR	CYP	CZE	DEU	DNK	ESP	EST	FIN
AUT										
BEL										
BGR										
CYP		6019								
CZE										
DEU		665		6393						
DNK		1420		7147		1009				
ESP		1437		5084		1811	2565			
EST		2284		8010		1872	1196	3428		
FIN		2221		7947		1809	1139	3365	296	
FRA		3934		7947		4308	5062	2998	5925	5862
GBR		861		6534		809	1172	1952	2035	1972
GRC		5556		494		5930	6684	4621	7547	7484
HUN										
IRL		1348		5662		1722	2178	1285	3041	2978
ITA		5395		2121		5769	6523	4460	7386	7323
LTU		1891		7617		1480	789	3035	585	552
LUX										
LVA		2172		7899		1761	1089	3317	539	498
MLT		4371		1695		4745	5499	3435	6362	6299
NLD		332		6062		420	1176	1480	2039	1976
POL		1796		7523		1385	698	2941	752	715
PRT		1739		4326		2113	2867	804	3730	3667
ROU										
HRV		5515		2241		5889	6643	4580	7506	7443
SVK										
SVN		5575		2300		5949	6702	4639	7565	7502
SWE		1541		7267		1130	459	2685	811	763

Table D0.17: Distances by ship between countries i and i' [km] (cont.).

	FRA	**GBR**	**GRC**	**HUN**	**IRL**	**ITA**	**LTU**	**LUX**	**LVA**	**MLT**
AUT										
BEL										
BGR										
CYP										
CZE										
DEU										
DNK										
ESP										
EST										
FIN										
FRA										
GBR	4449									
GRC	1946	6071								
HUN										
IRL	3576	1172	5199							
ITA	1733	5910	1650		5037					
LTU	5532	1643	7154		2648	6993				
LUX										
LVA	5813	1924	7436		2930	7275	437			
MLT	885	4886	1243		4013	1178	5969		6251	
NLD	3976	696	5599		1391	5437	1646		1928	4413
POL	5437	1548	7060		2554	6899	217		615	5875
PRT	2241	2254	3863		1382	3702	3337		3619	2678
ROU										
HRV	1854	6030	1771		5158	211	3337		7395	1296
SVK										
SVN	1913	6089	1830		5217	230	7173		7454	1358
SWE	5182	1293	6804		2298	6643	422		719	5619

Table D0.18: Distances by ship between countries i and i' [km] (cont.).

	NLD	POL	PRT	ROU	HRV	SVK	SVN	SWE
AUT								
BEL								
BGR								
CYP								
CZE								
DEU								
DNK								
ESP								
EST								
FIN								
FRA								
GBR								
GRC								
HUN								
IRL								
ITA								
LTU								
LUX								
LVA								
MLT								
NLD								
POL	1552							
PRT	1782	3243						
ROU								
HRV	5558	7019	3823					
SVK								
SVN	5617	7078	3882		204			
SWE	1296	333	2987		6764		6823	

Table D0.19: Correction factors used to calculate the amount of lorries, trains or ships based on the biomass transported as chips, bales or pellets.It relates the density of the biomass to the volume and carry load of the transportation mean.

	Lorry	Train	Ship
$CORF_v^{chip}$	1.25	1	1
$CORF_v^{bal}$	2.16	1	1
$CORF_v^{pell}$	1.70	1	1

D.1.4 Combustion and carbon capture

Table D0.20: Parameters for the modeling of the combustion plant and capture unit retrieved from Volkart et al.[363], the efficiency is sourced from Fajardy[33], while the HHV from Fajardy[33] and Pozo[14]. CC and HHV depend on the type of biomass, while the remaining parameters are valid for any feedstock.

Parameter	**Value**					
	Miscanthus	Switchgrass	Willow	Straw cereals	Woody	Forest
CC_b^{pow} [wt% (db)]	0.48	0.47	0.48	0.41	0.40	0.48
HHV_b^{pell} [MJ/ kg_{db}]	18.40	18.40	19.10	17.75	18.24	20.59
R_{ccs}	0.90					
HER^{ccs} [MWh/ t_{CO_2}]	0.97					
ELR^{ccs} [MWh/ t_{CO_2}]	0.02					
COR^{ccs} [MWh/ t_{CO_2}]	0.15					
η^{pow}	0.39					

Table D0.21: Losses considered at each activity during the modeling. * are sourced from Fajardy et al.[33], while the other values are based on assumptions.

Activity	**Losses EC**	**Losses RD**
Harvesting	0.03	0
Chipping/Baling	0.05	0.05
Transportation*	0.05	0.05
Pelleting* [per stage]	0.02	0.02
CO_2 transportation	0	0

D.2 LCA background and inventories

LCA is a methodology used to assess a product or a process throughout its life. In accordance with the requirements and guidelines of the ISO standards 14040[391] and 14044[392], LCA is performed in four steps.

Goal and scope definition. This step involves the determination of the study: intended application and target audience, selection of the functional unit, system boundaries, impact categories, objective of the analysis and assumptions.

Life cycle inventory (*LCI*). This step includes the data collection for the foreground and background system and the quantification of the relevant input and outputs of the product system.

*Life cycle impact assessmen*t (*LCIA).* The results of the LCI are transformed into potential environmental impacts on the impact categories selected, using the so-called characterization factors retrieved from SimaPro.

Interpretation. This step is carried out based on the assumptions and limitations of the study, according to the goal and scope outlined in the first step.

The endpoint characterization, which is the focus of this environmental analysis, corresponds to three areas of protection: human health, natural environment and resource scarcity [51]. The endpoint of the first category is expressed in DALY (disability adjusted life years) as it shows the number of years lost or that a person is disabled by a disease or an accident. Natural environment is expressed by the endpoint ecosystem quality, which represents the species loss over time and, therefore, it has a unit of [species year]. Lastly resource availability, in dollars [USD], quantifies the extra cost that will be needed for the extraction of mineral and fossil resources in the future, after depleting the most accessible sources[51].

All the activities modeled in SimaPro are based on the APOS, U methodology because it allows to track back the flows of every activity.

Table D0.22: Activities modeled at each stage of the supply chain. The majority of them is sourced from Ecoinvent; for those the name and the allocation type are reported. Land usage, CO_2 transportation and storage have been modeled based on literature data.

Activity	Source	Notes
Land miscanthus, switchgrass and willow	FEAT database[393]	
LUC	Ecoinvent - Land use change, perennial crop {RoW} | APOS	
Chipping	Ecoinvent - Wood chipping, industrial residual wood, stationary electric chipper {RER} | APOS	
Baling	Ecoinvent - Baling {CH} | APOS	
Pelleting	Ecoinvent - Wood pellet production {RER} | APOS	Biomass input set to zero
Transportation lorry	Ecoinvent - Market for transport, freight, lorry 16-32 metric ton, EURO6 {RER} | APOS	
Transportation train	Ecoinvent - Market for transport, freight train {Europe without Switzerland} | APOS	
Transportation ship	Ecoinvent - Market for transport, freight, sea, transoceanic ship {GLO} | APOS	
CO_2 transportation	Modeled from Wildbolz[283]	
CO_2 storage	Modeled from Wildbolz[283]	

The impact of dedicated crop at the cultivation stage has been modeled based on the available data reported in the agricultural database FEAT[393].

Table D0.23: Farm inputs from FEAT database[393] to model the impact of the cultivation of dedicated crops. The corresponding entries in Ecoinvent are reported. At this stage only the CO_2 emissions are modeled, while the amount of water necessary for the cultivation is not considered. The yield and crop moisture reported in the table is an average among all the countries.

Farm inputs FEAT				**Ecoinvent activity and allocation**
Crop field area (ha)	1	1	1	
Crops	Miscanthus	Switchgrass	Willow	
Yield [t_{wb}/(ha yr)] average EU-28	33.58	8.18	11.81	
Crop moisture at harvest (%)	0.23	0.12	0.52	
N rate [kg/(ha yr)]	92.80	80.72	80.17	Nitrogen fertilizer, as N {GLO}| market for | APOS
P_2O_5 rate [kg/(ha yr)]	53.20	64.58	15.25	Phosphate fertilizer, as P2O5 {GLO}| market for | APOS
K_2O rate [kg/(ha yr)]	121.80	64.58	40.25	Potassium fertilizer, as K2O {GLO}| market for | APOS
Lime [kg/(ha yr)]	643	643	643	Soil pH raising agent, as CaCO3 {GLO}| lime to generic market for soil pH raising agent | APOS
Seed/cuttings rate [kg/(ha yr)]	50	0.77	608	Grass seed, organic, for sowing {GLO}| market for | APOS
Herbicide rate [kg/(ha yr)]	0.72	0.42	0.43	Glyphosate {GLO}| market for | APOS
Diesel fuel [L/(ha yr)]	99.92	72.54	43.97	Diesel, burned in agricultural machinery {GLO}| diesel, burned in agricultural machinery | APOS
Transportation of inputs [MJ/(ha yr)]	0.64	0.64	0.64	Transport, freight train {RoW}| diesel | APOS

The inventory for CO_2 transportation and storage is reported in Table D0.24 to Table D0.29, adapted from Wildbolz[283], to match the available entries of Ecoinvent.

Table D0.24: Pipeline, supercritical CO_2 inventory used from Ecoinvent activities.

Pipeline, supercritical CO_2	**1 km**	
Resources		
Occupation, construction site	3330	m2a
Transformation, from forest, unspecified	2000	m2
Transformation, to heterogeneous, agricultural	2000	m2
Water, unspecified natural origin/m3	187	m3
Materials/fuels		
Diesel, burned in building machine {GLO}| processing | APOS, U	3310000	MJ
Steel, low-alloyed {GLO}| market for | APOS, U	270000	kg
Sand {GLO}| market for | APOS, U	4400000	kg
Drawing of pipe, steel {RER}| processing | APOS, U	270000	kg
Stone wool, packed {CH}| stone wool production, packed | APOS, U	5119	kg
Transport, helicopter {GLO}| market for | APOS, U	26	hr
Transport, helicopter, LTO cycle {GLO}| market for | APOS, U	10.4	p
Transport, freight, lorry 16-32 metric ton, euro6 {RER}| market for transport, freight, lorry 16-32 metric ton, EURO6 | APOS, U	315000	tkm
Transport, freight train {RER}| market group for transport, freight train | APOS, U	55100	tkm
Waste to treatment		
Inert waste, for final disposal {CH}| treatment of inert waste, inert material landfill | APOS, U	4400000	kg
Scrap steel {CH}| treatment of, inert material landfill | APOS, U	135000	kg
Waste mineral wool, for final disposal {CH}| treatment of waste mineral wool, inert material landfill | APOS, U	5120	kg

Table D0.25: Transport, pipeline, supercritical CO_2, with recompression inventory used from Ecoinvent activities.

Transport, pipeline, supercritical CO_2, w/o recompression	**1 tkm**	
Materials/fuels		
Pipeline, supercritical CO_2	6.34E-09	km
Emissions to air		
Carbon dioxide, fossil	0.00026	kg

Table D0.26: Well double, aquifer inventory used from Ecoinvent activities.

Well double, aquifer	**1 p**	
Resources		
Occupation, industrial area	900	m2a
Occupation, industrial area, vegetation	8100	m2a
Transformation, from grassland/pasture/meadow	600	m2
Transformation, to industrial area	60	m2
Transformation, to industrial area, vegetation	540	m2
Materials/fuels		
Deep well, drilled, for geothermal power {CH}| deep well drilling, for deep geothermal power | APOS, U	3600	m
Cement, unspecified {CH}| market for cement, unspecified | APOS, U	126000	kg
Gravel, crushed {CH}| production | APOS, U	1320000	kg
Transport, freight, lorry 16-32 metric ton, euro6 {RER}| market for transport, freight, lorry 16-32 metric ton, EURO6 | APOS, U	28900	tkm
Transport, freight train {RER}| market group for transport, freight train | APOS, U	12600	tkm

Table D0.27: Well double, depleted gas field inventory used from Ecoinvent activities.

Well double, depleted gas field	**1 p**	
Resources		
Occupation, industrial area	900	m2a
Occupation, industrial area, vegetation	8100	m2a
Transformation, from unknown	600	m2
Transformation, to industrial area	60	m2
Transformation, to industrial area, vegetation	540	m2
Materials/fuels		
Deep well, drilled, for geothermal power {CH}| deep well drilling, for deep geothermal power | APOS, U	11300	m
Cement, unspecified {CH}| market for cement, unspecified | APOS, U	126000	kg
Gravel, crushed {CH}| production | APOS, U	1320000	kg
Transport, freight, lorry 16-32 metric ton, euro6 {RER}| market for transport, freight, lorry 16-32 metric ton, EURO6 | APOS, U	28900	tkm
Transport, freight train {RER}| market group for transport, freight train | APOS, U	12600	tkm

Table D0.28: Storage, CO_2, aquifer, 200 km pipeline inventory used from Ecoinvent activities.

Storage, CO_2, aquifer, 200 km pipeline	**1 kg**	
Materials/fuels		
Well double, aquifer	2.54E-11	p
Transport, pipeline, supercritical CO_2, w/o recompression	0.2	tkm

Table D0.29: Storage, CO_2, depleted gas field, 200 km pipeline inventory used from Ecoinvent activities.

Storage, CO_2, depleted gas field, 200 km pipeline	**1 kg**	
Materials/fuels		
Well double, depleted gas field	2.54E-11	p
Transport, pipeline, supercritical CO_2, w/o recompression	0.2	tkm

D.3 Additional results

D.3.1 Regional implications

While the general solution to the four scenarios is reported in the main text, a detailed description of the supply chains is given in this section.

In the minimum cost scenario, the biomass feedstock is grown and harvested in Bulgaria, Germany, Italy - where not all the available land is used - and Romania, while all the other countries rely solely on the reserve of residues. In Spain, France and Portugal, however, woody residues are not fully used up. The model chooses Bulgaria and Romania because of the lowest cost for cultivation, while *Miscanthus* can be found in Germany and Italy, where the carbon content of *Miscanthus* is the highest. Biomass is processed into chips before it is transported by train to the pelleting sites in Bulgaria and Poland, while Romania processes the biomass within the country. Ship transportation is also used to transport the chips to Poland from all countries with access to the sea. The pellets are then transported *via* train solely to the combustion plants within Bulgaria and Poland. Simultaneously, Romania has its own supply chain within the regional borders. These three countries offer competitive prices on the market for pelleting and combustion stages. The CO_2 captured at the plant in Bulgaria and Poland is transported *via* pipeline to 18 countries of the EU, filling all the coal and hydrocarbon storage sites; while Romania relies on regional storage. Note that nine countries do not offer any type of geological site.

The topology of the minimum human health scenario's optimal configuration shows that *Miscanthus* is grown in Germany, Italy, the Netherlands, Romania - where not all the available land is used - and in Slovenia. In the rest of the EU Members, residues are collected. Then, the

biomass is transformed into chips on the land where it is harvested. In Slovenia, *Miscanthus* has the second-highest yield among all the countries, while in the Netherlands, Germany and Italy, one of the highest carbon content of *Miscanthus* is found. Cyprus, Finland, Sweden and Lithuania send all the biomass harvested abroad to Greece and Poland. Transportation of chips *via* ship from the land to the pelleting site is employed. The pellets are then transported by train to the combustion plants within the same countries to minimize transportation emissions. The carbon dioxide captured at each plant is sent *via* pipeline to the storage, prioritizing saline sites in both scenarios, i.e., minimum human health and minimum ecosystem quality.

The solution to the minimum ecosystem quality is largely similar to the one of human health. Biomass is harvested in the same countries (Germany, Italy, the Netherlands, Romania and Slovenia) and processed into chips. As opposed to the previous solution, a pelleting site is installed in Finland; Germany and Slovakia store a greater amount of CO_2, while Denmark reduces its contribution. As already mentioned in Chapter 5, the reason for these differences relies on different breakeven distances for a given amount of biomass, leading to choices for which train transportation is more or less advantageous than ship.

Lastly, resource availability has been minimized. Austria, France, where only part of the available land is used, Romania and Slovenia are the countries where *Miscanthus* is harvested. Once again, Austria and France are chosen because of the high yield of *Miscanthus*. In the same countries where the biomass is cultivated, the chipping, pelleting and combustion processes are carried out and transportation by train connects the different plants within and across the countries. Sweden and Lithuania constitute an exception because chips are sent *via* ship to Poland. The carbon dioxide captured at the combustion plant is mainly injected into saline aquifers.

In all the scenarios described above, Malta does not contribute to the global target because it can offer neither land for cultivation nor residues. As opposed to the base case (minimization of the total cost), in the environmental solutions, a small supply chain is found in every country where all the stages are carried out within the national borders. This configuration allows reducing the emissions and, ultimately, the impact of transportation on the environment. In particular, the most striking difference between the cost and the environmental scenarios is the reduced number of links from the cultivation to the pelleting. On the other hand, a network of pipelines will be required to store the CO_2, especially in the case of minimum environmental indicators, where CO_2 is exchanged among all the countries.

D.3.2 Midpoints of optimal solutions

In the LCA practice, the impacts are first aggregated into several different categories of midpoints that add up to obtain human health, ecosystem quality and resource availability. For each endpoint, numerous stressors are included in the Recipe 2016 method and they are shown in Figure D0.1 for human health a), ecosystem quality b) and resource availability c) for the four different scenarios.

In the case of human health, the main contributors are global warming, which is negative for the carbon dioxide absorbed from the atmosphere, and fine particulate matter formation on the positive side. Human carcinogenic and non-carcinogenic toxicity are highly impacting activities too. The activity contributing the most to these two midpoints is the pelleting stage because of the high heat consumption and particulates' formation during the process.

Global warming is once again the principal negative stressor of ecosystem quality, while land use constitutes the biggest positive impact. Ozone formation and terrestrial acidification are relevant positive contributions as well. In the case of ecosystem quality, carbon dioxide and land are the main components.

Lastly, in resource availability, only two sub-categories are present: mineral and fossil resource scarcity. In all the analyses performed, fossil resources' impact exceeds the one of mineral by two orders of magnitude, with land use, pelleting and CO_2 transportation being the most significant contributors.

In all the problems analyzed, the biomass feedstock is residues and, therefore, land does not play a major role given the model's assumptions. Hence, a negative endpoint of ecosystem quality is assured by the negative carbon dioxide.

It has been mentioned in the description of the Ecoinvent entries that the data collected from the FEAT database does not include the water necessary for the crops' growth. This translates into underestimating the impact of water consumption, which has implications on human health and ecosystem quality. However, since the biomass feedstock is almost entirely relying on residues, with the assumption of zero environmental impact, the neglected entry of water usage should not be significant. The opposite would be valid for energy crop-based BECCS and, therefore, trade-offs between the two indicators would be significant.

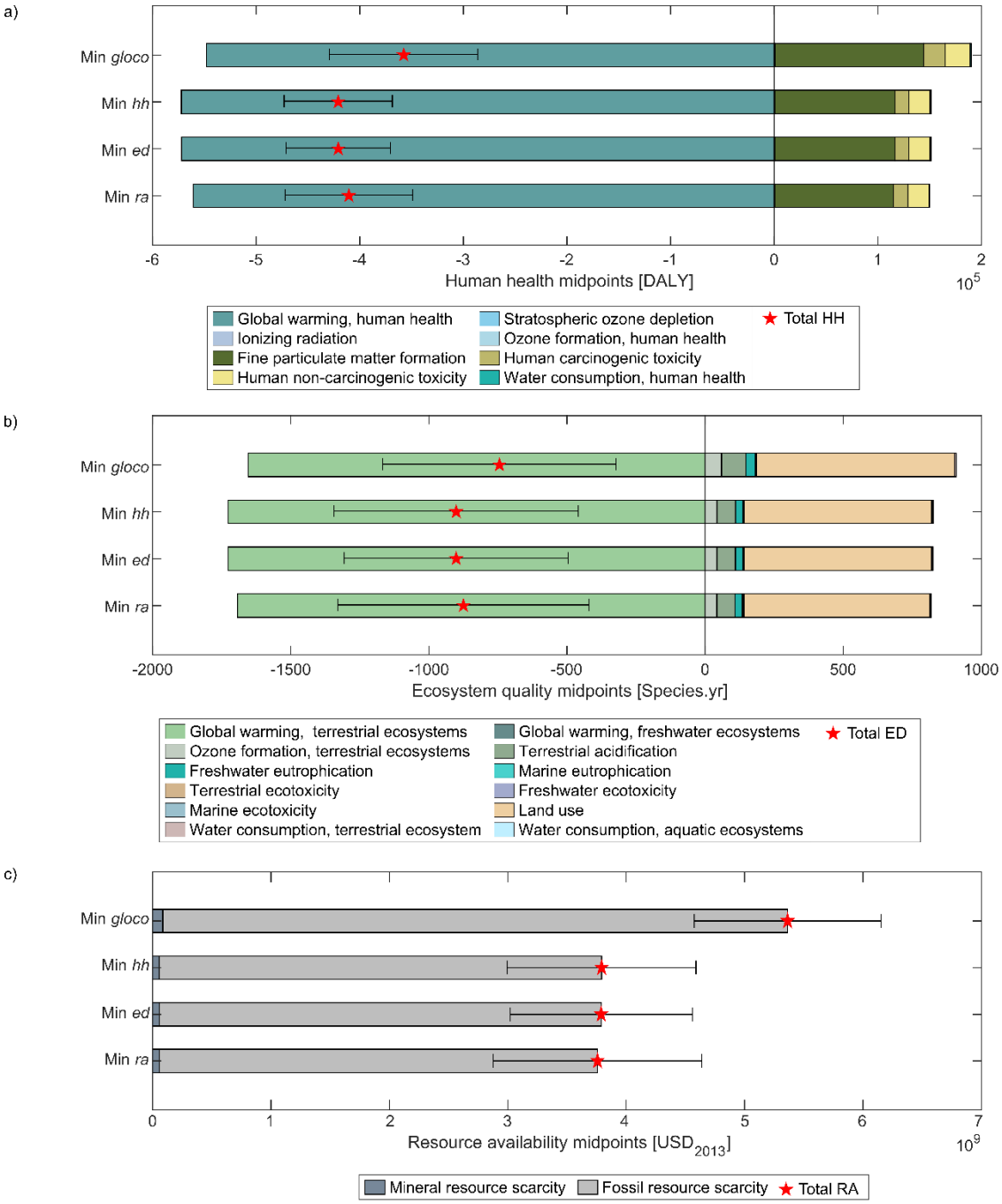

Figure D0.1: Midpoints of human health a), ecosystem quality b) and resource availability c) for the scenarios analyzed. The error bars represent the uncertainty of the data calculated as the standard deviation of 1000 scenarios generated in SimaPro using Monte Carlo sampling. The limits of the error bars denote the worst and best-case scenario of the total impact.

D.3.3 Residues usage

The negative emission target is satisfied almost entirely by using residues (straw cereals, woody and forest), as a consequence of one of the model prevailing assumptions that only energy crops affect the costs and the environmental performances of the supply chain. The amount of residues that each country can utilize is given as input to NETCOM. Figure D0.2 shows the percentage of usage of each different residue with respect to the total residues feedstock in the minimum cost solution a), human health b), ecosystem quality c) and resource availability c). Only in the minimum cost solution, part of the available woody residues is not used in Spain, France, Great Britain and Portugal. In all the other optimizations, the 100% of residues employed corresponds to the total residues availability. Malta does not have any residues available, as reported in Table D0.8.

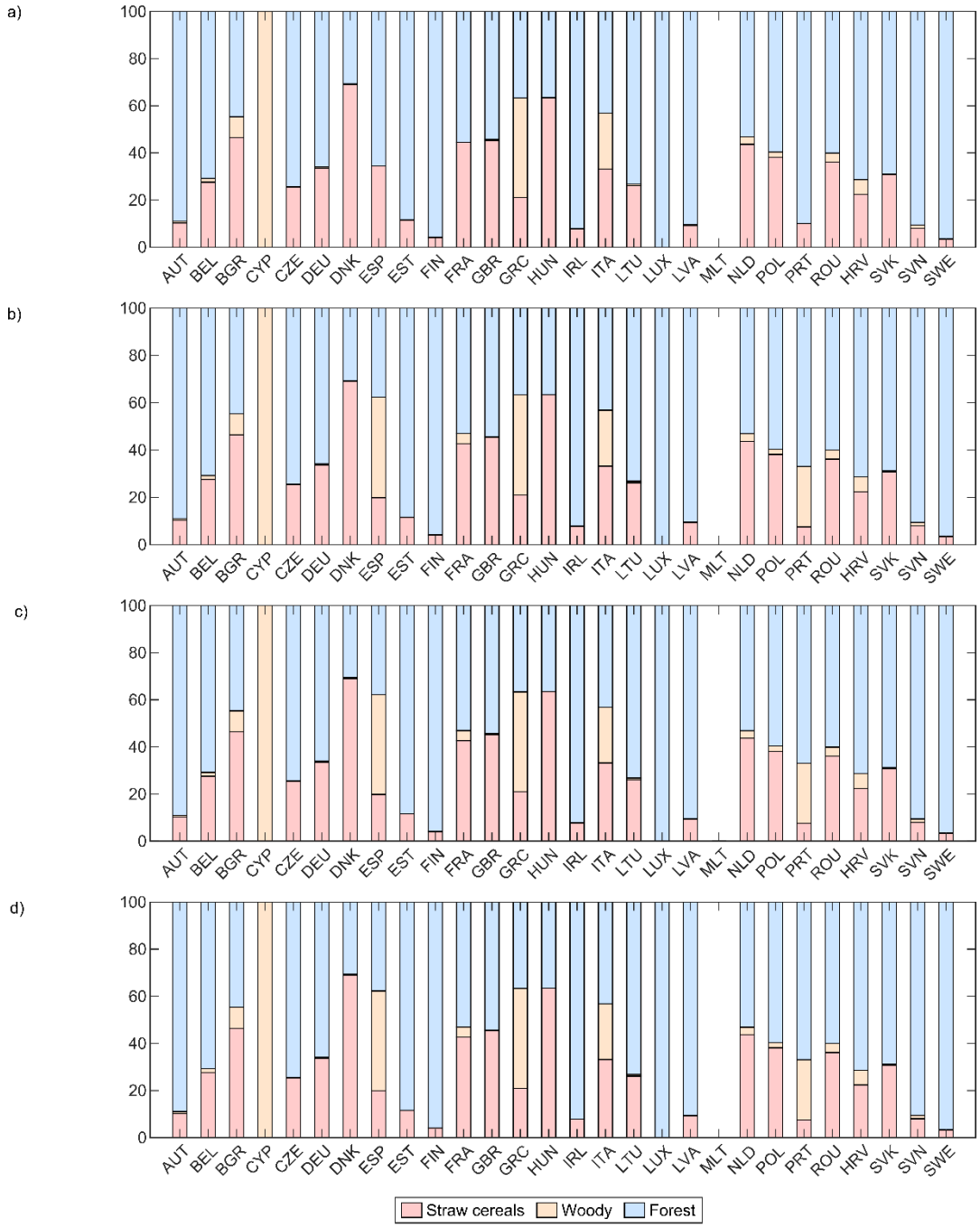

Figure D0.2: Use of residues in each country for the minimum cost case a), human health b), ecosystem quality c) and resource availability d). The figure shows the percentage of each category of residues that is used as biomass feedstock with respect to the total of residues utilized. In b), c) and d), it corresponds to the total available.

D.4 Assumptions and limitations of NETCOM

Two different sets of biomass feedstock are available, i.e., dedicated bioenergy crops (*Miscanthus*, switchgrass and willow) that grow on marginal land and agricultural residues (straw cereals and woody and forest residues). Given the high uncertainty in the definition of marginal land, here we consider marginal lands as those unsuitable for agriculture because of the low productivity[33].

The selection of the biomass types is primarily driven by the goal to avoid competition with agricultural land and water, which would increase the food prices, to prove BECCS sustainability. Therefore, we considered non-edible biomass, commonly defined as second generation, e.g., Miscanthus, switchgrass, willow and poplar grown on marginal land or residues (agricultural and forestry). These biomass types are different from first-generation biomass (i.e., those competing for land and water, such as starch and sugar) and third-generation (e.g., algae), not yet competitive, and frequently deployed for bioenergy applications[33,394–396]. The variety of NETCOM feedstock is then based on the availability in the geographical area considered (EU-28) and the ease of data collection. Since the energy crop cultivation is modeled based on regional inputs, e.g., land availability, moisture content and yield[383,386,387,397], it is of paramount importance to choose a feedstock which is common to all the countries considered and a viable option for bioenergy production *via* combustion at the same time.

Two different biomass processing methods are available, i.e., chipping or baling, carried out in the same biomass harvest location. We assume that processing and pelleting, as well as pelleting and combustion facilities, are connected *via* three possible transport means, namely lorry, train or ship.

The distance between the countries has been calculated based on the travel routes between the national capitals to rely on realistic figures, although farms are unlikely located close to high population density sites. Four types of operations have been modeled in the pelleting activity: pre-treatment, drying, comminution and mixing. We consider a direct combustion-steam turbine system at the combustion stage. Biomass is the feedstock for the boiler, which produces steam to operate a steam turbine and a generator for the electricity. A post-combustion carbon capture technology with an aqueous solution 30 wt.% of monoethanolamine (MEA) retrofitting plant is included in this study, with a capture rate of 90%[398].

Combustion is the most common option for bioenergy production[19], which implies negligible or no modification of the current furnace or burner technologies[399,400]. The ability to retrofit current power plants for electricity production using biomass makes the combustion technology highly advantageous and very promising for a transition toward cleaner electricity production. Additionally, the combustion technology has a high technology readiness level (TRL) and it is implemented at Mt scale. As a consequence, the CO_2 which is produced in the flue gas is captured using a MEA liquid solution[401] in a post-combustion capture unit. The latter can also be retrofitted, contributing to reducing the emissions.

We consider a set of onshore storage sites (i.e., depleted hydrocarbon fields, coal seams, and saline formations) available in each country, where the CO_2 transported *via* pipeline from the combustion plant can be injected. Based on the literature source for the EU-28 countries[402], specific storage sites have been considered and quantified. As previous works show, the type of geological site is highly dependent on the specific country and even within the EU some members lack storage capacity for the types considered[403].

We use regionalized (for each country of EU-28) input data for crops and for the cost calculation, while the biomass carbon intensity factors and the environmental impacts indicators used in the modeling of the emissions are assumed to be equal for each country. However, we express each of them with the country *i* and the biomass type *b* subscripts to indicate that regional factors can and should be investigated, as climate and regional energy-mixes could greatly influence the impacts. The ecovectors used in the mathematical model include the impacts at mid- and endpoints per unit of flow of each stage of the SC.

The modeling of the cultivation stage is based on the FEAT database[393] and it accounts for emissions mainly related to fertilizers and transportation, as reported in Table D0.23. However, specifically for the assessment of BECCS, the water consumption of the crop should be considered because it can lead to substantial trade-offs in the environmental indicators. In this case, the impact of water consumption is estimated to be negligible, because the model relies almost entirely on residues feedstock, which are collected on the land.

Following common practice in the literature[404], the contribution of the infrastructure of the combustion plant is here omitted, as it is negligible particularly for biomass-based plants. The accounting of these indirect emissions can be relevant when the supply chain is not centralized, e.g., in the human health scenario, and the number of plants installed increases substantially.

On the other hand, losses occurring throughout the supply chain are meticulously considered. The impact of land-use change have been overestimated for the crop and the transformation selected (from marginal land), because of the specific entry chosen from the Ecoinvent database[280].

Since NETCOM costs are calculated for the reference year 2018, the United Kingdom is included as part of the European Union in our analysis.

D.5 Numerical implementation in GAMS

Each optimization problem has been solved in GAMS using CPLEX for linear programming. Options for scalability, such as *scaind,* and tolerance parameters have been implemented to improve the numerical solution of the environmental endpoints.

In the case of ecosystem quality, the midpoints contribute to the total with a substantial difference. Indeed, they are several orders of magnitude lower than the other variables, and the solver faces numerical difficulties due to the wide range of the parameters. The minimum of this environmental objective function has been achieved by setting an additional constraint to solve starting from the value obtained in the minimum human health case as the upper bound. The two solutions are comparable in terms of total cost and emission, despite the above-mentioned differences in the supply chains.

Table D0.30 reports the CPU time for each optimization problem. In the case of minimum ecosystem quality the CPU is almost two times the one obtained for the calculation of the other objective functions. The CPU of the environmental impacts solutions refers to the minimization of the endpoint and not to the overall processing time: it excludes the computational time to find the minimum cost solution for a fixed minimum impact.

Table D0.30: CPU time calculated in the optimization problems.

Objective function	CPU
$gloco$	2.83
hh	2.45
ed	4.47
ra	2.47

D.5.1. Mass and energy balances

D.5.1.1 Biomass growth and cultivation stage

The model accounts for the amount of feedstock obtained from each country *i* for each of the six biomass types *b* considered ($prod_{ib}^{grw}$). In the case of energy crops (biomass types in set *EC*), this is determined from the marginal land used ($land_{ib}$) and a yield parameter (YIELD_{ib}) providing the metric tons of biomass that can be grown per hectare and year (Eq. (D1)). The yield is based on the data from IIASA (EPIC II) for *Miscanthus* and Fajardy et al.[383] for switchgrass and willow and corresponds to the annual average among the growing period. As an example, willow is a three-year rotation coppice; consequently, its annual yield is obtained by dividing the total yield by three years. On the other hand, the supply of biomass residues (biomass types contained in set *RD*) is constrained by the maximum amount available in a given country (AVRD_{ib}) (Eq. (D2)), which refers to data provided in the Atlas of EU biomass potentials[386] for straw cereal and woody residues, while forestry residues are sourced from IINAS[387].

$$prod_{ib}^{grw} = land_{ib}\text{YIELD}_{\text{ib}} \quad \forall i, b \in EC \tag{D1}$$

$$prod_{ib}^{grw} \leq \text{AVRD}_{\text{ib}} \quad \forall i, b \in RD \tag{D2}$$

The land surface ($land_{ib}$) utilized for energy crops cultivation in each country is restricted to the maximum marginal land available in that country, as dictated by parameter AVLAND_{i} (Eq. (D3)). The available marginal land is calculated by aggregating GIS data from Cai et al.[397] at the country level and downscaling the final number according to Fritz et al.[385], which provides a conservative data source for land availability consistent for each country in the EU.

$$\sum_{b \in EC} land_{ib} \leq \text{AVLAND}_{\text{i}} \; \forall i \tag{D3}$$

The amount of biomass lost is considered in the mass balances throughout the entire model as a loss factor (as a percentage), which multiplies the flow of biomass at every stage where losses occur. Accounting of losses is relevant because the biomass is assumed to decay and release the carbon back into the atmosphere.

The amount of biomass feedstock available for processing ($prod_{ib}^{land}$) takes into consideration that part of the biomass grown, which is lost during harvesting due to inadequate farming

practices, late harvesting or poor storage conditions. This is reflected in the parameter $\mathrm{LOSS}_{\mathrm{b}}^{\mathrm{land}}$ (expressed as a percentage), affecting the energy crops input as described in Eq. (D4). We assume that at this stage the loss factor for biomass of type EC is 3%. In contrast, no losses are assumed for residues, for which the amount of biomass to be processed ($prod_{ib}^{land}$) equals the amount of residues gathered ($prod_{ib}^{grw}$) in Eq. (D5).

$$prod_{ib}^{land} = prod_{ib}^{grw}\left(1 - \mathrm{LOSS}_{\mathrm{b}}^{\mathrm{land}}\right) \quad \forall i, b \in EC \tag{D4}$$

$$prod_{ib}^{land} = prod_{ib}^{grw} \quad \forall i, b \in RD \tag{D5}$$

D.5.1.2 Processing into bales or chips

After the biomass is harvested (both of type *EC* and *RD*), the feedstock has to be prepared for transportation in one of the two available forms: bales ($prod_{ib}^{bal}$) or chips ($prod_{ib}^{chip}$). This process takes place in the same country where the biomass is harvested and is of fundamental importance to increase the bulk density of the biomass, thus minimizing transportation costs [405]. The total amount of biomass available after harvesting and the production of bales ($avprod_{ib}^{bal}$) and chips ($avprod_{ib}^{chip}$) are linked in Eq. (D6). See Eq. (D71) for the formulation of Eqs. (D6) to (D8) as they are implemented in GAMS.

$$prod_{ib}^{land} = avprod_{ib}^{bal} + avprod_{ib}^{chip} \quad \forall i, b \tag{D6}$$

The total production of bales $prod_{ib}^{bal}$ and chips $prod_{ib}^{chip}$ is calculated using Eqs. (D7) and (D8), respectively, discounting from the amount of biomass available in the form of bales ($avprod_{ib}^{bal}$) or chips ($avprod_{ib}^{chip}$) the losses of the baling and chipping processes by considering suitable loss factors related to each processing mode ($\mathrm{LOSS}_{\mathrm{b}}^{\mathrm{bal}}$ and $\mathrm{LOSS}_{\mathrm{b}}^{\mathrm{chip}}$). The latter are related to machine operation, e.g., to the baler or mower, and biomass management during baling and chipping and are assumed to be both equal to 5%.

$$avprod_{ib}^{bal} = \frac{prod_{ib}^{bal}}{\left(1 - \mathrm{LOSS}_{\mathrm{b}}^{\mathrm{bal}}\right)} \quad \forall i, b \tag{D7}$$

$$avprod_{ib}^{chip} = \frac{prod_{ib}^{chip}}{\left(1 - \mathrm{LOSS}_{\mathrm{b}}^{\mathrm{chip}}\right)} \quad \forall i, b \tag{D8}$$

D.5.1.3 Transport from farmland to the processing site

All the biomass *b* prepared in each country *i* as bales or chips ($prod_{ib}^{bal}$ or $prod_{ib}^{chip}$) is transported to country *i' via* transportation mean *v* ($tlp_{ii'bv}^{bal}$ or $tlp_{ii'bv}^{chip}$, respectively), as shown in Eqs. (D9) and (D10). The transportation modes *v* considered are lorry, train and ship.

$$prod_{ib}^{bal} = \sum_{v}\sum_{i'} tlp_{ii'bv}^{bal} \quad \forall i, b \tag{D9}$$

$$prod_{ib}^{chip} = \sum_{v}\sum_{i'} tlp_{ii'bv}^{chip} \quad \forall i, b \tag{D10}$$

Eqs. (D11) and (D12) remove infeasible transport flows of bales ($tlp_{ii'bv}^{bal}$) and chips ($tlp_{ii'bv}^{chip}$): e.g., transportation *via* ship between two countries with no access to the sea. $TR_{i,i',v}$ is the set of connections allowed between country *i* and *i'* for each means of transportation *v*.

$$tlp_{ii'bv}^{bal} = 0 \quad \forall i, i', b, v \notin TR_{i,i'} \tag{D11}$$

$$tlp_{ii'bv}^{chip} = 0 \quad \forall i, i', b, v \notin TR_{i,i'} \tag{D12}$$

D.5.1.4 Pelleting stage

Biomass in the form of bales or chips is usually converted into pellets, due to the resulting higher energy density, which leads to lower transportation costs and related emissions[406].

The amount of biomass bales or chips available for processing at the pelleting stage in country *i* ($proc_{ib}^{bal}$ and $proc_{ib}^{chip}$) includes for domestic as well as imported bales or chips ($tlp_{i'ibv}^{bal}$ and $tlp_{i'ibv}^{chip}$, respectively), after discounting the biomass losses incurred during the transportation to the pelleting plant ($\mathrm{LOSS}^{\mathrm{tlp}}$) (Eqs. (D13) and (D14)). These losses stand at 5%, according to Fajardy et al.[33].

$$proc_{ib}^{bal} = \sum_{v}\sum_{i'} tlp_{i'ibv}^{bal}\left(1 - \mathrm{LOSS}^{\mathrm{tlp}}\right) \quad \forall i, b \tag{D13}$$

$$proc_{ib}^{chip} = \sum_{v}\sum_{i'} tlp_{i'ibv}^{chip}\left(1 - \mathrm{LOSS}^{\mathrm{tlp}}\right) \quad \forall i, b \tag{D14}$$

The pelleting process takes place in four steps: pre-treatment, drying, comminution and mixing, ensuring a uniform feedstock regarding size, heating value and moisture content. Hence, the total amount of biomass pellets produced ($pellet_{ib}^{pro}$) is calculated as reported in Eq. (D15), i.e., by considering the biomass input of bales and chips and the potential losses occurring during the pelleting. Fajardy et al.[33] provided biomass losses for each pelleting stage equal to 2%; these are lumped here into a single parameter $\mathrm{LOSS}_{\mathrm{b}}^{\mathrm{ovpell}}$ covering the overall process, equal to 7.8%. The equations modeled in GAMS to account for the losses occurring during the four pelleting stages are reported in Eqs. (D72) and (D73).

$$pellet_{ib}^{pro} = \left(proc_{ib}^{bal} + proc_{ib}^{chip}\right)\left(1 - \mathrm{LOSS}_{\mathrm{b}}^{\mathrm{ovpell}}\right) \quad \forall i, b \tag{D15}$$

D.5.1.5 Transport from pelleting to the combustion plant

The total amount of pellets produced ($pellet_{ib}^{pro}$) is transported from the pelleting stage to the power plant using the same transportation options described above, namely lorry, train and ship. Eq. (D16) ensures that all the pellets of biomass *b* produced in a certain country *i* will be transported to a power plant in a country *i'* (where *i* equal to *i'* is also possible) using one of the possible transportation means *v* ($tpc_{ii'bv}^{pell}$). Note that all the pellets must be transported using one of the allowable transportation routes: Eq. (D17) prevents the transportation of pellets using unsuitable means *v* for the connection between countries *i* and *i'*, as included in set $TR_{i,i'}$.

$$pellet_{ib}^{pro} = \sum_{v}\sum_{i'} tpc_{ii'bv}^{pell} \quad \forall i, b \tag{D16}$$

$$tpc_{ii'bv}^{pell} = 0 \quad \forall i, i', b, v \notin TR_{i,i'} \tag{D17}$$

Therefore, the amount of pellets of biomass type *b* available for combustion at the power plant in country *i* ($comb_{ib}^{pell}$) is given by the amount of biomass pellets arriving from any country *i'* ($tpc_{i'ibv}^{pell}$), after discounting the biomass losses occurring during transportation ($\mathrm{LOSS}^{\mathrm{tpc}}$) (Eq. (D18)). The latter are assumed to be 5%, as reported in Fajardy et al.[33].

$$comb_{ib}^{pell} = \sum_{v}\sum_{i\prime} tpc_{i'ibv}^{pell}\ (1 - \mathrm{LOSS}^{\mathrm{tpc}}) \quad \forall i, b \tag{D18}$$

D.5.1.6 Power generation

All the pellets that are transported to the power plant are combusted in a direct combustion-steam turbine system to produce electricity. A retrofitting post-combustion MEA plant is implemented for the capture of the CO_2. It is well known that the amount of carbon captured and stored plays an important role. A wide range of capture percentages can be explored: values between 90% and 98% are commonly employed in similar studies in the literature. Here, a conservative capture rate of 90% is employed[398] (R^{ccs}), leading to a net 10% of direct CO_2 emissions.

The amount of CO_2 captured by the amine post-combustion plant in country i ($CO2_i^{pow}$) is calculated in Eq. (D19) from the amount of pellets combusted ($comb_{ib}^{pell}$), the specific capture rate employed ($\mathrm{R}^{\mathrm{ccs}}$) and the carbon content of the biomass ($\mathrm{CC}_{\mathrm{b}}^{\mathrm{pow}}$), which is expressed as the percentage of carbon in wet biomass, according to literature values. A factor ($\mathrm{DRY}_{\mathrm{ib}}^{\mathrm{pell}}$) is used to convert the carbon content based on dry mass ($\mathrm{CC}_{\mathrm{b}}^{\mathrm{drypow}}$) to a wet basis and thereby maintain the consistency with the amount of biomass, always expressed in a wet basis in the model. The drying of the biomass is indeed performed in the previous step during the pelleting. The conversion of the carbon content from dry mass to wet mass is reported in Eq. (D75). Finally, the amount of CO_2 resulting from the oxidation of the carbon contained in the biomass can be obtained through the ratio of molecular weights ($\mathrm{M}^{\mathrm{CO2}}/\mathrm{M}^{\mathrm{C}}$).

$$CO2_i^{pow} = \sum_{b} comb_{ib}^{pell}\,\mathrm{CC}_{\mathrm{b}}^{\mathrm{pow}}\,\frac{\mathrm{M}^{\mathrm{CO2}}}{\mathrm{M}^{\mathrm{C}}}\,\mathrm{R}^{\mathrm{ccs}} \quad \forall i \tag{D19}$$

Note that a BECCS technology is not only employed for CO_2 capture but also delivers electricity. The electricity produced at the power plant ($elgen_{ib}^{pow}$) is calculated from the amount of biomass combusted ($comb_{ib}^{pell}$) and the heating value of the biomass HHV_b^{pell} as reported in Eq. (D20). HHV values for *Miscanthus*, switchgrass and willow pellets are provided by Fajardy et al. as the average of previously published data[33], while we use Pozo et al.[14] for residues [GJ/t]. The base efficiency (η^{pow}) is based on a supercritical coal-fired power plant studied in Fajardy et al.[33].

$$elgen_{ib}^{pow} = comb_{ib}^{pell} \mathrm{HHV}_{b}^{pell} \eta^{pow} \quad \forall i, b \tag{D20}$$

The CCS system requires heat to regenerate the MEA solvent ($\mathrm{HER}^{\mathrm{ccs}}$) and electricity for the CO_2 capture ($\mathrm{ELR}^{\mathrm{ccs}}$), both expressed as MWh/tCO_2, as shown in Eq. (D21). This equation provides the extra electricity needed by the post combustion plant, given the CO_2 captured and the energy penalties. The parameters $\mathrm{HER}^{\mathrm{ccs}}$ and $\mathrm{ELR}^{\mathrm{ccs}}$ are sourced from Volkart et al.[407] and reported in Table D0.20. The summation of the two energy penalties of the CCS system is embodied in the variable $elccs_i^{pow}$, which needs to be discounted from the electricity output of the plant.

$$elccs_i^{pow} = CO2_i^{pow} \left(\mathrm{HER}^{\mathrm{ccs}} \eta^{pow} + \mathrm{ELR}^{\mathrm{ccs}}\right) \quad \forall i \tag{D21}$$

The CO_2 captured must be compressed before being sent for injection, which imposes an additional energy penalty ($elcom_i^{pow}$) on the power station proportional to $\mathrm{COR}^{\mathrm{ccs}}$ (electricity requirement for CO_2 compression), expressed as MWh/tCO_2. Eq. (D22) relates the electricity needed for the compression to the CO_2 captured by the amine plant and the factor $\mathrm{COR}^{\mathrm{ccs}}$.

$$elcom_i^{pow} = CO2_i^{pow} \mathrm{COR}^{\mathrm{ccs}} \quad \forall i \tag{D22}$$

Therefore, the balance for the net electricity production $netelgen_i^{pow}$ at the combustion plant is calculated in Eq. (D23), which states that the total amount of electricity is given by the difference between the electricity generated by direct biomass combustion ($elgen_{ib}^{pow}$) and the energy penalties ($elccs_i^{pow}$ and $elcom_i^{pow}$ for the regeneration of the solvent and the CO_2 capture and the CO_2 compression, respectively).

$$netelgen_i^{pow} = \sum_b \left(elgen_{ib}^{pow}\right) - elccs_i^{pow} - elcom_i^{pow} \; \forall i \tag{D23}$$

D.5.1.7 CO_2 transportation and storage

All the CO_2 captured at the power plant in each country *i* ($CO2_i^{pow}$) must be sent to storage sites in the same or any other country *i'* ($tCO2_{ii'}^{p2s}$) (Eq. (D24)).

$$CO2_i^{pow} = \sum_{i'} tCO2_{ii'}^{p2s} \quad \forall i \tag{D24}$$

The final amount of CO_2 available for storage in each country *i* ($CO2_i^{sto}$) is given by the amount sent to that country ($tCO2_{ii'}^{p2s}$) *via* pipeline (Eq. (D25)). In this case, losses are considered negligible as it is reported in Table D0.21.

$$CO2_i^{sto} = \sum_{i'} tCO2_{i'i}^{p2s} \quad \forall i \tag{D25}$$

Finally, all the CO_2 actually available is sequestered in the different storage sites *g* of the country ($CO2_{ig}^{site}$) (Eq. (D26)). Three different types of storage sites *g* are considered: coal and hydrocarbon depleted fields and saline aquifers, each with given national capacity (CAP_{ig}^{site}) as imposed *via* Eq. (D27). Capacities of the different types of storage sites are retrieved from Vangkilde-Pedersen et al.[402]; here we only consider the equivalent capacity of one year.

$$CO2_i^{sto} = \sum_{g} CO2_{ig}^{site} \quad \forall i \tag{D26}$$

$$CO2_{ig}^{site} \leq \mathrm{CAP_{ig}^{site}} \quad \forall i, g \tag{D27}$$

D.5.2 Life cycle CO_2 emissions

D.5.2.1 Biomass growth and cultivation stage

The net emissions during biomass farming result from balancing the negative and positive contributions. The former is related to the CO_2 uptake from the atmosphere occurring during the plant growth *via* the photosynthesis process. Eq. (D28) represents the CO_2 absorbed by each biomass type *b* in each country *i* (em_{ib}^{grw}), which is calculated from the carbon content of the biomass (expressed as percentage of carbon in wet biomass $\mathrm{CC_{ib}}$) and the amount of biomass cultivated ($prod_{ib}^{grw}$). The carbon content of each crop $\mathrm{CC_{ib}}$ is an input data retrieved from Fajardy et al.[33] and Phyllis2[382], the online database for biomass and waste (see Table D0.5). The ratio of molecular weights of CO_2 and carbon ($\mathrm{M}^{CO2}/\mathrm{M}^{C}$) allows us to translate the amount of carbon in the plant to the equivalent amount of CO_2 absorbed from the atmosphere.

$$em_{ib}^{grw} = -prod_{ib}^{grw} \mathrm{CC_{ib}} \frac{\mathrm{M^{CO2}}}{\mathrm{M}^{C}} \quad \forall i, b \tag{D28}$$

In turn, the positive emissions associated with the cultivation stage (em_{ib}^{cul}) result from several contributions, as illustrated in Eq. (D29). These contributions are: emissions from the use of the land (em_{ib}^{land}), direct land-use change (LUC) emissions (em_{ib}^{luc}) and the emissions occurring due to biomass losses ($em_{ib}^{landloss}$). Note that we consider that indirect land-use change (ILUC) is zero for marginal land; thus, only LUC is considered.

$$em_{ib}^{cul} = em_{ib}^{land} + em_{ib}^{luc} + em_{ib}^{landloss} \quad \forall i, b \tag{D29}$$

Variable em_{ib}^{land} provides the CO_2 emitted during the cultivation stage. It is computed from the specific energy and selected farm inputs (e.g., herbicides, pesticides, farm inputs, and others) for each crop of type *EC*. The farm inputs are sourced from the FEAT database[393] and reported in Table D0.23 for each specific crop and country. All these contributions are finally aggregated into the carbon intensity factor $\mathrm{CI}_{\mathrm{ib}}^{\mathrm{land}}$, expressing the amount of CO_2 emissions released per hectare of land used. This factor, modelled in SimaPro[279] using Ecoinvent activities based on the FEAT inputs, is used in Eq. (D30) to relate CO_2 emissions to the amount of land used for the cultivation of energy crops (biomass types in set *EC*). The inventories used in Ecoinvent to model this stage based on FEAT database are reported in Table D0.23.

$$em_{ib}^{land} = land_{ib}\mathrm{CI}_{\mathrm{ib}}^{\mathrm{land}} \quad \forall i, b \in EC \tag{D30}$$

In the case of residues (i.e., biomass of type b contained in set *RD*), we assume that no environmental impact is assigned to them, as all the emissions incurred during cultivation are allocated to the main crop (Eq. (D31)).

$$em_{ib}^{land} = 0 \quad \forall i, b \in RD \tag{D31}$$

Biomass losses which occur at the different stages of the SC are also considered and they are calculated as a percentage ($\mathrm{LOSS}_{\mathrm{b}}$) of each input flow. Emissions from losses derive from the decay of the biomass and the oxidation of the carbon back to CO_2 in the atmosphere. The calculation of the CO_2 emissions defines the performance of the SC with respect to the global CDR target imposed. Only energy crops (biomass of the set *EC*) contribute to emissions due to biomass losses during harvesting ($em_{ib}^{landloss}$). These are calculated in Eq. (D32), where the amount of biomass produced ($prod_{ib}^{grw}$) and the loss factor ($\mathrm{LOSS}_{\mathrm{b}}^{\mathrm{land}}$) provide the amount of biomass lost. Then, the carbon content of the biomass ($\mathrm{CC}_{\mathrm{ib}}$) and the ratio of the molecular

weights of CO_2 and carbon (M^{CO2}/M^{C}) relate this quantity to the amount of CO_2 that is released into the atmosphere during the biomass decay. Losses deriving from the harvesting of residues are allocated no direct emissions (Eq. (D33)).

$$em_{ib}^{landloss} = prod_{ib}^{grw} \mathrm{LOSS}_{\mathrm{b}}^{\mathrm{land}} \mathrm{CC}_{\mathrm{ib}} \frac{\mathrm{M}^{\mathrm{CO2}}}{\mathrm{M}^{\mathrm{C}}} \quad \forall i, b \in EC \tag{D32}$$

$$em_{ib}^{landloss} = 0 \quad \forall i, b \in RD \tag{D33}$$

In addition to the emissions produced by the land use, we also consider LUC ones. In general, LUC refers to the conversion of a land type (e.g., grassland, forest) to a crop land[33]. A detailed definition is given by Fargione et al.[408]. For marginal land transformations, LUC emissions are calculated as in Eqs. (D34) and (D35) for energy crops and residues, respectively. For the case of energy crops, the emissions due to LUC (em_{ib}^{luc}) are calculated from the amount of land used for the cultivation ($land_{ib}$) and the carbon intensity of the LUC activity ($\mathrm{CI}_{\mathrm{ib}}^{\mathrm{luc}}$), expressed in tCO_2 per hectare of land used. At this stage, LUC emissions associated with residues (em_{ib}^{luc}) are considered to be zero owing to the allocation previously mentioned.

$$em_{ib}^{luc} = land_{ib} \mathrm{CI}_{\mathrm{ib}}^{\mathrm{luc}} \quad \forall i, b \in EC \tag{D34}$$

$$em_{ib}^{luc} = 0 \quad \forall i, b \in RD \tag{D35}$$

We use the carbon intensity factor for LUC ($\mathrm{CI}_{\mathrm{ib}}^{\mathrm{luc}}$) based on a land-use change activity in Ecoinvent in SimaPro[279], which accounts for different land use transformations and considers and average of the impacts (not only marginal land, but also cropland, forest and grassland); hence, this choice leads to an overestimation of the impact of crop growth on marginal land.

D.5.2.2 Processing into bales or chips

The emissions associated with the baling (em_{ib}^{bal}) and chipping (em_{ib}^{chip}) processes and the respective losses ($em_{ib}^{balloss}$ and $em_{ib}^{chiploss}$) are reported in Eqs. (D36) and (D37). The associated carbon intensities for both processes ($\mathrm{CI}_{\mathrm{ib}}^{\mathrm{bal}}$ and $\mathrm{CI}_{\mathrm{ib}}^{\mathrm{chip}}$), sourced from SimaPro[279], express the amount of CO_2 emitted per metric ton of bales and chips. Then, Eqs. (D36) and (D37) are used to calculate the emissions deriving from baling and chipping (em_{ib}^{bal} and em_{ib}^{chip}) based on the amount of bales and chips produced ($prod_{ib}^{bal}$ and $prod_{ib}^{chip}$) and the respective carbon intensity of the activities. Note that the product of the chipping process is

expressed in SimaPro as dry amount of chips. Here we report the carbon intensity already expressed per wet amount of biomass.

$$em_{ib}^{bal} = prod_{ib}^{bal}\mathrm{CI}_{\mathrm{ib}}^{\mathrm{bal}} + em_{ib}^{balloss} \quad \forall i, b \tag{D36}$$

$$em_{ib}^{chip} = prod_{ib}^{chip}\mathrm{CI}_{\mathrm{ib}}^{\mathrm{chip}} + em_{ib}^{chiploss} \quad \forall i, b \tag{D37}$$

The direct emissions due to the decay of biomass losses occurring during baling ($em_{ib}^{balloss}$) and chipping ($em_{ib}^{chiploss}$) are calculated according to Eqs. (D38) and (D39), respectively. In essence, biomass losses are first obtained from the amount of bales or chips produced ($prod_{ib}^{bal}$ and $prod_{ib}^{chip}$, respectively), and the corresponding loss factors ($\mathrm{LOSS}_{\mathrm{b}}^{\mathrm{bal}}$ and $\mathrm{LOSS}_{\mathrm{b}}^{\mathrm{chip}}$); then, this is converted into the corresponding amount of CO_2 that would be released according to the carbon content of the particular biomass type *b* ($\mathrm{CC}_{\mathrm{ib}}$) and the ratio of molecular weights of CO_2 and carbon ($\mathrm{M}^{\mathrm{CO2}}/\mathrm{M}^{\mathrm{C}}$).

$$em_{ib}^{balloss} = prod_{ib}^{bal}\mathrm{LOSS}_{\mathrm{b}}^{\mathrm{bal}}\mathrm{CC}_{\mathrm{ib}}\frac{\mathrm{M}^{\mathrm{CO2}}}{\mathrm{M}^{\mathrm{C}}} \quad \forall i, b \tag{D38}$$

$$em_{ib}^{chiploss} = prod_{ib}^{chip}\mathrm{LOSS}_{\mathrm{b}}^{\mathrm{chip}}\mathrm{CC}_{\mathrm{ib}}\frac{\mathrm{M}^{\mathrm{CO2}}}{\mathrm{M}^{\mathrm{C}}} \quad \forall i, b \tag{D39}$$

D.5.2.3 Transport from farmland to the processing site

In Eq. (D40), the emissions associated with the transportation of biomass of type *b* from the farmland of country *i* to the pelleting plant in country *i'* ($em_{ii'b}^{tlp}$) are based on the distance between the countries *i* and *i'* ($\mathrm{DIST}_{\mathrm{vii'}}$) and the carbon intensity factor ($\mathrm{CI}_{\mathrm{v}}^{\mathrm{trn}}$), indicating the amount of CO_2 emitted during the transportation of one metric ton of biomass in one km using the transportation mean *v*. The latter was sourced from Ecoinvent in SimaPro for lorry, train and ship, as reported in Table D0.22. Correction factors have been added in Eq. (D40) where required to account for the transportation capacity of lorries for bales and chips ($\mathrm{CORF}_{\mathrm{v}}^{\mathrm{bal}}$ and $\mathrm{CORF}_{\mathrm{v}}^{\mathrm{chip}}$, respectively). The correction factors relate the capacity of the transportation mean (maximum carry load/volume of the transport) to the density of the biomass. For lorry-based transport we assume a volume of 70m^3 and a maximum carry load of 22.7 t[371], from which the capacity can be calculated (324kg/m^3). Depending on the density of the biomass (bales or

chips), the correction factor is applied to account for emissions deriving from not fully loaded lorries. It is set to 1 for the other transportation means other than lorries, as reported In Table D0.19. The emissions due to the transportation losses are included in Eq. (D40).

Distances between different countries ($\mathrm{DIST_{vii'}}, i \neq i'$) have been obtained using online tools[388,389,409] for lorry and ship. We add intra-country distances in the case of lorries, assumed to be 50 km[390]. The distance covered by train is assumed to be 80% of the distance calculated for lorries, assuming a lower tortuosity for railroads compared to roads. The values used as input data to the model can be found in Table D0.10 - Table D0.19.

$$em_{ii'b}^{tlp} = \sum_{v} \mathrm{DIST_{vii'}} \mathrm{CI_{v}^{trn}} \left(\mathrm{CORF_{v}^{bal}} tlp_{ii'bv}^{bal} + \mathrm{CORF_{v}^{chip}} tlp_{ii'bv}^{chip} \right) + em_{ii'b}^{tlploss} \quad \forall i, i', b \tag{D40}$$

In order to calculate the emissions associated with the decay of biomass losses during transportation ($em_{ii'b}^{tlploss}$), biomass losses, as given by the product between the amount of bales and chips produced and the loss factor ($\mathrm{LOSS^{tlp}}$), are multiplied by the carbon content of the biomass and the ratio of the molecular weights ($\mathrm{M^{CO2}/M^{C}}$) (Eq. (D41)). Note that we keep track of differences in indigenous biomass since the same carbon content as in the harvesting location i ($\mathrm{CC_{ib}}$) is assumed, regardless of the transportation form (bales or chips) or mean (lorry, train or ship).

$$em_{ii'b}^{tlploss} = \sum_{v} \left(tlp_{ii'bv}^{bal} + tlp_{ii'bv}^{chip} \right) \mathrm{LOSS^{tlp}} \mathrm{CC_{ib}} \frac{\mathrm{M^{CO2}}}{\mathrm{M^{C}}} \quad \forall i, i', b \tag{D41}$$

D.5.2.4 Pelleting stage

The process of converting the biomass feedstock into pellets generates positive emissions (em_{ib}^{pro}) that are calculated according to Eq. (D42). These emissions are related to the amount of pellets produced ($pellet_{ib}^{pro}$, expressed in metric ton of wet biomass) and the carbon intensity of the pelleting activity (in tCO_2 per metric ton of dry pellets). Here we report the carbon intensity ($\mathrm{CI_{ib}^{pell}}$) already converted to a wet basis of biomass with a moisture factor ($\mathrm{DRY_{ib}^{pell}}$) to convert the amount of biomass from a wet-basis to a dry basis. The carbon intensity is retrieved from Ecoinvent in SimaPro and accounts for all the energy and material inputs needed at this stage.

$$em_{ib}^{pro} = pellet_{ib}^{pro}\mathrm{CI}_{\mathrm{ib}}^{\mathrm{pell}} + em_{ib}^{proloss} \quad \forall i, b \tag{D42}$$

Eq. (D42) also includes the emissions associated with the decay of biomass losses produced at the pelleting stage ($em_{ib}^{proloss}$), which are calculated in Eq. (D43). These emissions depend on the amount of biomass produced as pellets from the bales and chips that were transported to the plant ($proc_{ib}^{bal}$ and $proc_{ib}^{chip}$). We assume that the pelleting stage can be divided in four different processes and, therefore, we calculate the losses accordingly to the loss parameter ($\mathrm{LOSS}_{\mathrm{b}}^{\mathrm{ovpell}}$). At this stage we assume that pellets were homogenized during the process: the carbon content of each type of biomass *b* ($\mathrm{CC}_{\mathrm{b}}^{\mathrm{pro}}$) no longer depends on the country of origin and is here expressed on wet biomass basis. The ratio of molecular weights of CO_2 and carbon ($\mathrm{M}^{\mathrm{CO2}}/\mathrm{M}^{\mathrm{C}}$) relates the amount of carbon with the associated CO_2 emissions released during the decay.

$$em_{ib}^{proloss} = \left(proc_{ib}^{bal} + proc_{ib}^{chip}\right)\mathrm{LOSS}_{\mathrm{b}}^{\mathrm{ovpell}}\mathrm{CC}_{\mathrm{b}}^{\mathrm{pro}}\frac{\mathrm{M}^{\mathrm{CO2}}}{\mathrm{M}^{\mathrm{C}}} \quad \forall i, b \tag{D43}$$

D.5.2.5 Transport from pelleting to the combustion plant

Next, the pellets produced are transported from the pelleting site to the power plant *via* the possible transportation options, namely lorry, train and ship. Eq. (D44) shows that the emissions associated with the transport depend on the amount of pellets transported ($tpc_{ii'bv}^{pell}$), the distance between the origin and destination countries *i* and *i'* ($\mathrm{DIST}_{\mathrm{vii'}}$), the carbon intensity factor of the transport mean *v* ($\mathrm{CI}_{\mathrm{v}}^{\mathrm{trn}}$) and the correction factor for pellets ($\mathrm{CORF}_{\mathrm{v}}^{\mathrm{pell}}$). The carbon intensity factor is retrieved from SimaPro for the different transport options and it provides the amount of CO_2 emitted per metric ton of biomass transported during one km. The correction factor relates the capacity of the transportation mode (maximum carry load/volume) to the density of the pellets. It is assumed to be equal to 1 for trains and ships, while it is calculated based on a $70m^3$ volume and maximum carry load of 22.7 t for lorries.

The emission associated to the decay of biomass losses occurring during transportation ($em_{ii'b}^{tpcloss}$) are calculated in Eq. (D45) from the amount of biomass losses. These are obtained from the product between the amount of pellets transported ($tpc_{ii'bv}^{pell}$) and the loss factor ($\mathrm{LOSS}^{\mathrm{tpc}}$). Then, the carbon content of the type of biomass *b* (already converted to wet basis $\mathrm{CC}_{\mathrm{b}}^{\mathrm{pro}}$), independent from the country of origin of the feedstock, provides the amount of

biogenic carbon in the biomass. Finally, the ratio of CO_2 and C molecular weights (M^{CO2}/M^{C}) transforms this quantity into the CO_2 emissions associated with the oxidation taking place during the natural decay of the biomass.

$$em_{ii'b}^{tpc} = \sum_{v} \mathrm{DIST}_{\mathrm{vii'}} \mathrm{CI}_{\mathrm{v}}^{\mathrm{trn}} \mathrm{CORF}_{\mathrm{v}}^{\mathrm{pell}} tpc_{ii'bv}^{pell} + em_{ii'b}^{tpcloss} \quad \forall i, i', b \tag{D44}$$

$$em_{ii'b}^{tpcloss} = \sum_{v} tpc_{ii'bv}^{pell} \mathrm{LOSS}^{\mathrm{tpc}} \mathrm{CC}_{\mathrm{b}}^{\mathrm{pro}} \frac{M^{CO2}}{M^{C}} \quad \forall i, i', b \tag{D45}$$

D.5.2.6 Power generation

In the next step we consider direct emissions from combustion of the biomass (em_{ib}^{pow}), which are only part of the total emissions resulting from the combustion since a portion of it is avoided thanks to the post-combustion MEA plant. Eq. (D46) is used to calculate the direct emissions to air at the power plant. The emissions depend on the amount of biomass pellets combusted at the power plant of country *i* ($comb_{ib}^{pell}$), the capture rate of the post-combustion MEA plant (R^{ccs}, here assumed to be 90%), and the carbon content (CC_{b}^{pow}, expressed as the percentage of carbon in wet biomass *b*). Finally, the amount of CO_2 released is directly obtained from the amount of carbon by using the molecular weights (M^{CO2}/M^{C}). At this stage the carbon intensity of the plant infrastructure (construction, maintenance, dismantling and waste management), is not taken into consideration.

$$em_{ib}^{pow} = (1 - R^{ccs}) comb_{ib}^{pell} CC_{b}^{pow} \frac{M^{CO2}}{M^{C}} \quad \forall i, b \tag{D46}$$

D.5.2.7 CO_2 transportation and storage

Once the CO_2 is captured and compressed to the desired pressure of 110 bar, it is transported *via* pipeline for injection ($tCO2_{i'i}^{p2s}$). Eq. (D47) relates the amount of CO_2 transported to the distance transported *via* pipeline between country *i* and *i* ' ($DIST_{ii'}^{pipe}$) and the carbon intensity of the pipeline transport (CI^{p2s}), which considers indirect emissions from materials and energy inputs sourced from Wildbolz[283]. We assume that the pipeline distance is equal to the railroad distance between the same countries plus 150 km to account for the transportation from the capitals to the storage site (many times located offshore), already included in $DIST_{ii'}^{totpipe}$. In contrast, intra-country distances are considered zero. The carbon intensity of the CO_2

transportation is modeled in SimaPro, from the inventory of Wildbolz[283], given in tCO_2 per km.

$$em_{ii'}^{p2s} = \mathrm{DIST}_{\mathrm{ii'}}^{\mathrm{totpipe}} tCO2_{i'i}^{p2s} \mathrm{CI}^{\mathrm{p2s}} \quad \forall i, i' \tag{D47}$$

The total emissions associated with the injection of CO_2 (em_i^{site}) are calculated as the summation of the site-specific emission in Eq. (D48). Emissions related to the CO_2 injection are calculated for each specific site type g in each country i (em_{ig}^{site}), and are given by the product between the amount of CO_2 stored in the site ($CO2_{ig}^{site}$) and the carbon intensity of the injection process ($\mathrm{CI}_{\mathrm{g}}^{\mathrm{site}}$, expressed as tCO_2 released per tCO_2 injected) (Eq. (D49)). To obtain such carbon intensity, the CO_2 injection process is modeled in SimaPro with activities from Ecoinvent according to the inventories of Wildbolz[283], which consider the energy and material inputs for this activity for the different storage site types considered. Injection of CO_2 in one of the storage sites g considered can be a source of emissions due to the land usage at the injection site and the drilling activity, in addition to material inputs such as cement and gravel and transportation[283].

$$em_i^{sto} = \sum_g em_{ig}^{site} \quad \forall i \tag{D48}$$

$$em_{ig}^{site} = CO2_{ig}^{site} \mathrm{CI}_{\mathrm{g}}^{\mathrm{site}} \quad \forall i, g \tag{D49}$$

D.5.2.8 Global emissions

Finally, total emissions for each country i (em_i) are calculated as the summation of the country contributions to the different stages in the SC, as reported in Eq. (D50). Note that, in the transportation term we include the parameter W to allocate the CO_2 emissions. The solutions reported in section 5.5 have been obtained for a value of W equal to 0.5, meaning that the burden is equally shared.

$$em_i = \sum_b \left(em_{ib}^{grw} + em_{ib}^{cul} + em_{ib}^{bal} + em_{ib}^{chip}\right) + \sum_b \sum_{i\prime} \left(em_{ii\prime b}^{tlp} \mathrm{W} \quad + em_{i\prime ib}^{tlp}(1 - \mathrm{W} \quad)\right) + \sum_b em_{ib}^{pro} + \sum_b \sum_{i\prime} \left(em_{ii\prime b}^{tpc} \mathrm{W} \quad + em_{i\prime ib}^{tpc}(1 - \mathrm{W} \quad)\right) + \sum_b em_{ib}^{pow} + \sum_{i\prime} \left(em_{ii\prime}^{p2s} \mathrm{W} \quad + em_{i\prime i}^{p2s}(1 - \mathrm{W} \quad)\right) + em_{ig}^{sto} \quad \forall i \tag{D50}$$

Once the emissions deriving from the activities of the SC in each country have been computed, they can be summed to obtain the net global emissions of the whole EU-28.

Global emissions ($gloem$) equal the sum of the direct and indirect emissions of each country *i* (em_i) (Eq. (D51)), while Eq. (D52) enforces that net global emissions must be less or equal to the CDR target TG. The global emission target is based on the target removal in Peters and Geden[13]. The target proposed has been annualized linearly dividing the net CDR to 2100 by 80 years (from 2018 to 2100) to compute the amount of CO_2 to be removed in one year.

$$gloem = \sum_i em_i \tag{D51}$$

$$gloem \leq \mathrm{TG} \tag{D52}$$

D.5.3. Life cycle costs

The cost of each activity is calculated using unitary cost data for each activity (e.g., cultivation of 1 ha of land), mainly sourced from literature studies. The costs are then regionalized using the Purchasing Power Parity (PPP)[410].

D.5.3.1 Cultivation stage

The cost of the cultivation stage is the cost of harvesting (co_{ib}^{land}), given by the amount of land used in each country *i* for the production of energy crops *b* (i.e., biomass types included in set *EC*) ($land_{ib}$) and the unitary cost of cultivation ($\mathrm{UC}_{\mathrm{ib}}^{\mathrm{land}}$). The latter, based on de Wit and Faaij[411], considers fertilizers, labor costs and capital costs (including establishment and planting, harvesting, field transportation and storage and more). Note that the unitary cost of harvesting is region- and biomass type-specific.

$$co_{ib}^{land} = land_{ib}\mathrm{UC}_{\mathrm{ib}}^{\mathrm{land}} \quad \forall i, b \in EC \tag{D53}$$

Residues do not contribute to the total cost of the harvesting, as in the case of emissions, owing to the assumption that the cost is allocated to the original product. Thus, Eq. (D54) sets those costs to zero for each country *i* and biomass types in *RD*.

$$co_{ib}^{land} = 0 \quad \forall i, b \in RD \tag{D54}$$

D.5.3.2 Processing into bales or chips

The cost of producing bales (co_{ib}^{bal}) or chips (co_{ib}^{chip}) is calculated from the amount of biomass produced as bales ($prod_{i,b}^{bal}$) or chips ($prod_{ib}^{chip}$) and the unitary cost per metric ton of chips ($\mathrm{UC}_{\mathrm{ib}}^{\mathrm{bal}}$) or bales ($\mathrm{UC}_{\mathrm{ib}}^{\mathrm{chip}}$) (see Eqs. (D55) and (D56), respectively). These unitary costs were investigated by Sultana et al.[371] and include collection and wrapping for bales from *Miscanthus*, switchgrass and straw cereals, while bundling for willow, woody and forestry residues. For chips made out of *Miscanthus*, switchgrass and straw cereals we consider the costs of tube-grinding, while we select the chipping activity for willow, woody and forestry residues.

$$co_{ib}^{bal} = prod_{i,b}^{bal}\mathrm{UC}_{\mathrm{ib}}^{\mathrm{bal}} \ \forall i, b \tag{D55}$$

$$co_{ib}^{chip} = prod_{ib}^{chip}\mathrm{UC}_{\mathrm{ib}}^{\mathrm{chip}} \ \forall i, b \tag{D56}$$

D.5.3.3 Transport from farmland to the processing site

Once transformed into bales or chips, the biomass is transported to the pelleting site. The costs of this transportation stage ($co_{ii'b}^{tlp}$), as shown in Eq. (D57), includes the costs incurred by the three different means of transportation *v*, namely lorry ($co_{ii'b}^{tlplor}$), train ($co_{ii'b}^{tlptr}$) and ship ($co_{ii'b}^{tlpsh}$). The reason for explicitly maintaining separate terms for the different means is that each of them is characterized by transportation-specific variable and fix contributions, as described in the following equations.

$$co_{ii'b}^{tlp} = co_{ii'b}^{tlplor} + co_{ii'b}^{tlptr} + co_{ii'b}^{tlpsh} \ \forall i, i', b \tag{D57}$$

In the case of lorries, Eq. (D58) describes the relation between the cost of the transportation, the amount transported in the form of bales ($tlp_{ii'bv}^{bal}$) or chips ($tlp_{ii'bv}^{chip}$) and the distance

between the origin and destination countries ($\mathrm{DIST_{vii'}}$). The total cost is based on fix ($\mathrm{CFIX_{ib}}$) and variable ($\mathrm{CVAR_{ib}}$) contributions, both depending on the use of bales or chips, as published in Sultana et al.[371] and Searcy et al.[412]. In addition, the variable contributions depend on the distance travelled.

$$co_{ii'b}^{tlplor} = \sum_{v} \Big[\big(\mathrm{CFIX_{ib}^{lorbal}} + \mathrm{CVAR_{ib}^{lorbal}} \mathrm{DIST_{vii'}}\big) tlp_{ii'bv}^{bal} + \Big(\mathrm{CFIX_{ib}^{lorchip}} + \mathrm{CVAR_{ib}^{lorchip}} \mathrm{DIST_{vii'}}\Big) tlp_{ii'bv}^{chip} \Big] \quad \forall i, i', b, v = lorry \tag{D58}$$

Eq. (D59) shows the calculation for the cost of transportation *via* train ($co_{ii'b}^{tlptr}$), where no difference in fixed and variables costs is assumed for chips and bales. The cost calculation for ships, $co_{ii'b}^{tlpsh}$ is reported in Eq. (D60).

$$co_{ii'b}^{tlptr} = \sum_{v} \Big[\big(\mathrm{CFIX_{ib}^{tr}} + \mathrm{CVAR_{ib}^{tr}} \mathrm{DIST_{vii'}}\big) \big(tlp_{ii'bv}^{bal} + tlp_{ii'bv}^{chip}\big) \Big] \quad \forall i, i', b, v = train \tag{D59}$$

$$co_{ii'b}^{tlpsh} = \sum_{v} \Big[\big(\mathrm{CFIX_{ib}^{sh}} + \mathrm{CVar_{ib}^{sh}} \mathrm{DIST_{vii'}}\big) \big(tlp_{ii'bv}^{bal} + tlp_{ii'bv}^{chip}\big) \Big] \quad \forall i, i', b, v = ship \tag{D60}$$

D.5.3.4 Pelleting stage

At the next stage, the biomass is processed into pellets. The cost of the pelleting process in Eq. (D61) depends on the amount of pellets produced ($pellet_{ib}^{pro}$) and the unitary cost per metric ton of pellets ($\mathrm{UC_{ib}^{pell}}$), sourced from Samson and Duxbury[413]. The costs include raw materials, energy, labor and bagging costs, as they represent the main contributions to the total cost.

$$co_{ib}^{pro} = pellet_{ib}^{pro} \mathrm{UC_{ib}^{pell}} \quad \forall i, b \tag{D61}$$

D.5.3.5 Transport from pelleting to the combustion plant

From the pelleting site the biomass reaches the power plant *via* one of the transportation modes introduced, along an allowed route. The cost of pellets transportation ($co_{ii'b}^{tpc}$) is calculated

according to Eq. (D62) as the summation of the costs related to the three different means of transportation *v*, namely lorry ($co_{ii'b}^{tlplor}$), train ($co_{ii'b}^{tlptr}$) and ship ($co_{ii'b}^{tlpsh}$), in order to keep the contributions of fixed and variable costs separate for each category of transport.

$$co_{ii'b}^{tpc} = co_{ii'b}^{tpclor} + co_{ii'b}^{tpctr} + co_{ii'b}^{tpcsh} \quad \forall i, i', b \tag{D62}$$

Sultana et al.[371] and Searcy et al.[412] studied the cost of the transportation *via* lorry ($co_{ii'b}^{tpclor}$), finding that it could be estimated from fixed ($\mathrm{CFIX}_{\mathrm{ib}}^{\mathrm{tpclor}}$) and variable ($\mathrm{CVAR}_{\mathrm{ib}}^{\mathrm{tpclor}}$) costs, the latter depending on the distance between the two countries ($\mathrm{DIST}_{\mathrm{vii'}}$), and both costs proportional to the amount of pellets produced ($tpc_{ii'bv}^{pell}$) (see Eq. (D63)).

$$co_{ii'b}^{tpclor} = \sum_v \left[\left(\mathrm{CFIX}_{\mathrm{ib}}^{\mathrm{tpclor}} + \mathrm{CVAR}_{\mathrm{ib}}^{\mathrm{tpclor}} \mathrm{DIST}_{\mathrm{vii'}}\right) tpc_{ii'bv}^{pell}\right] \quad \forall i, i', b, v = lorry \tag{D63}$$

The costs for the transportation of pellets *via* train ($co_{ii'b}^{tpctr}$) or ship ($co_{ii'b}^{tpcsh}$), $tpc_{ii'bv}^{pell}$ are calculated in Eqs. (D64) and (D65). These equations are analogue to Eqs. (D59) and (D60).

$$co_{ii'b}^{tpctr} = \sum_v \left[\left(\mathrm{CFIX}_{\mathrm{ib}}^{\mathrm{tpctr}} + \mathrm{CVAR}_{\mathrm{ib}}^{\mathrm{tpctr}} \mathrm{DIST}_{\mathrm{vii'}}\right) tpc_{ii'bv}^{pell}\right] \quad \forall i, i', b, v = train \tag{D64}$$

$$co_{ii'b}^{tpcsh} = \sum_v \left[\left(\mathrm{CFIX}_{\mathrm{ib}}^{\mathrm{tpcsh}} + \mathrm{CVAR}_{\mathrm{ib}}^{\mathrm{tpcsh}} \mathrm{DIST}_{\mathrm{vii'}}\right) tpc_{ii'bv}^{pell}\right] \quad \forall i, i', b, \in v = ship \tag{D65}$$

D.5.3.6 Power generation

The pellets transported to the power plant are used in a direct-combustion system. Here, we consider only the costs of electricity production, while the costs of the power plant and CCS system infrastructure is neglected. The cost of electricity production (co_{ib}^{pow}) is given in Eq. (D66) by the amount of electricity obtained from the generator ($elgen_{ib}^{pow}$) and the unitary cost per MWh ($\mathrm{UC}_{\mathrm{ib}}^{\mathrm{pow}}$), all depending on the biomass type used as feedstock owing to their characteristic HHV. The cost per MWh is derived from own calculations based on a bioenergy plant that includes fixed and variable costs.

$$co_{ib}^{pow} = elgen_{ib}^{pow} \mathrm{UC}_{\mathrm{ib}}^{\mathrm{pow}} \quad \forall i, b \tag{D66}$$

D.5.3.7 CO_2 transportation and storage

After the biomass is burned, the CO_2 released during the process is captured and compressed to 110 bar before being sent *via* pipeline to the storage sites for injection.

The costs of CO_2 transported *via* pipeline ($co_{ii'}^{p2s}$) are based on a low estimate of a capacity of 10 $\mathrm{M}t_{CO_2}$/year ($\mathrm{CVAR}_{\mathrm{i}}^{\mathrm{P2S}}$), considering the reference prices reported in Budinis et al.[181] (see Eq. (D67)). The distance between the countries *i* and *i'* is assumed to be equal to the same distance covered by train, except for additional intra-country routes, equal to 150 km, already included in the parameter $\mathrm{DIST}_{\mathrm{ii'}}^{\mathrm{totpipe}}$ altogether with the distance factor of 250 km reported by Budinis et al.[181].

$$co_{ii'}^{p2s} = \mathrm{CVAR}_{\mathrm{i}}^{\mathrm{P2S}} \mathrm{DIST}_{\mathrm{ii'}}^{\mathrm{totpipe}} tCO2_{ii'}^{p2s} \quad \forall i, i' \tag{D67}$$

The CO_2 reaches one of the possible storage sites *g via* pipeline and it is injected there for permanent storage. Eq. (D68) shows that the total costs of storage in each country *i* co_i^{sto} are calculated from the summation of the costs of the different storage sites co_{ig}^{site}. The cost of each storage site depends on the amount of CO_2 stored $CO2_{ig}^{site}$ and a variable cost factor $\mathrm{CVAR}_{\mathrm{ig}}^{\mathrm{site}}$ reported in Budinis et al.[181], according to Eq. (D69).

$$co_i^{sto} = \sum_g co_{ig}^{site} \quad \forall i \tag{D68}$$

$$co_{ig}^{site} = \mathrm{CVAR}_{\mathrm{ig}}^{\mathrm{site}} CO2_{ig}^{site} \quad \forall i, g \tag{D69}$$

D.5.3.8 Global costs

Finally, the total cost for each country (co_i) includes the cost incurred in all the stages of the SC, reported in Eq. (D70).

$$co_i = \sum_b (co_{ib}^{land} + co_{ib}^{bal} + co_{ib}^{chip}) + \sum_b \sum_{i'} \left(co_{ii'b}^{tlp} \mathrm{W^{co}} + co_{i'ib}^{tlp}(1 - \mathrm{W^{co}})\right) + \sum_b co_{ib}^{pro} + \sum_b \sum_{i'} \left(co_{ii'b}^{tpc} \mathrm{W^{co}} + co_{i'ib}^{tpc}(1 - \mathrm{W^{co}})\right) + \sum_b co_{ib}^{pow} + \sum_{i'} \left(co_{ii'}^{p2s} \mathrm{W^{co}} + co_{i'i}^{p2s}(1 - \mathrm{W^{co}})\right) + co_{ig}^{sto} \quad \forall i \tag{D70}$$

The omega parameter $\mathrm{W^{co}}$ is used to share the cost burden between the countries involved in the transportation route, in the same way as for the emissions. The same value of 0.5 has been used for the calculations.

D.6 Reformulation of the mathematical model

D.6.1 Mass and energy balances

Processing into bales or chips

After the biomass has been harvested (Eqs. (D1) – (D5)), it is transformed into bales and chips on the same land where it is cultivated. The variables $avprod_{ib}^{bal}$ and $avprod_{ib}^{chip}$ define the amount of bales and chips, respectively, that can be obtained. In Eq. (D71), which refers to the system of equations precisely as in the GAMS code, the two variables defined in Eq. (D7) and D8 are not been included.

$$prod_{ib}^{land} = \frac{prod_{ib}^{bal}}{\left(1 - \mathrm{LOSS_b^{bal}}\right)} + \frac{prod_{ib}^{chip}}{\left(1 - \mathrm{LOSS_b^{chip}}\right)} \quad \forall i, b \tag{D71}$$

Pelleting stage

Once the biomass has been converted into bales or chips and transported to the pelleting stage, it is transformed into pellets. This process is assumed to take place in four individual steps, each of them being a potential source of emissions due to biomass losses. In order to simplify the losses parameter (see Eq. (D15)) the transformations reported in Eqs. (D72) and (D73) have been applied. The equations reported here related the single step loss factor $\mathrm{LOSS_b^{pell}}$ to the overall loss factor of the pelleting stage ($\mathrm{LOSS_b^{ovpell}}$).

$$pellet_{ib}^{pro} = \left(proc_{ib}^{bal} + proc_{ib}^{chip}\right)\left(1 - \mathrm{LOSS}_{\mathrm{b}}^{\mathrm{pell}}\right)^{4} \forall i, b \quad \text{(D72)}$$

$$1 - \mathrm{LOSS}_{\mathrm{b}}^{\mathrm{ovpell}} = \left(1 - \mathrm{LOSS}_{\mathrm{b}}^{\mathrm{pell}}\right)^{4} \forall i, b \quad \text{(D73)}$$

The amount of biomass, either cultivated or processed, is always defined on a wet basis. However, the pelleting activity selected from the ones available in Ecoinvent (implemented in SimaPro) refers to a product of 1 t of pellets on a dry basis. In Eq. (D74), we transform the carbon content of the pellets ($\mathrm{CC}_{\mathrm{b}}^{\mathrm{drypow}}$) on a dry basis to the one used in Eq. (D43) on a wet basis ($\mathrm{CC}_{\mathrm{b}}^{\mathrm{pro}}$), through the dry factor ($\mathrm{DRY}_{\mathrm{ib}}^{\mathrm{pell}}$) which expresses the moisture content in the pellets.

$$\mathrm{CC}_{\mathrm{b}}^{\mathrm{pro}} = \mathrm{DRY}_{\mathrm{ib}}^{\mathrm{pell}} \mathrm{CC}_{\mathrm{b}}^{\mathrm{drypow}} \ \forall i, b \quad \text{(D74)}$$

Power generation

The biomass combusted at the power plant, which is used for electricity production, generates emissions of CO_2 during the process. The amount of CO_2 is calculated from the amount of biomass combusted ($comb_{ib}^{pell}$) and the carbon content ($\mathrm{CC}_{\mathrm{b}}^{\mathrm{drypow}}$). The latter is expressed on a dry basis while the biomass is always accounted for on a wet basis. In Eq. (D75) we use a dry factor ($\mathrm{DRY}_{\mathrm{ib}}^{\mathrm{pell}}$) based on moisture content of the biomass to related the quantities in a consistent way. The value assumed for $\mathrm{DRY}_{\mathrm{ib}}^{\mathrm{pell}}$ is based on the target moisture content for ideal combustion conditions described by Fajardy et al.[33].

$$CO2_{i}^{pow} = \sum_{b} \mathrm{R}_{\mathrm{CCS}} comb_{ib}^{pell} \mathrm{DRY}_{\mathrm{ib}}^{\mathrm{pell}} \mathrm{CC}_{\mathrm{b}}^{\mathrm{drypow}} \frac{\mathrm{M}_{\mathrm{CO2}}}{\mathrm{M}_{\mathrm{C}}} \quad \forall i \quad \text{(D75)}$$

The electricity generated from the combustion ($comb_{ib}^{pell}$) is calculated using the high heating value of the biomass ($\mathrm{HHV}_{b}^{drypell}$), expressed on a dry basis (Eq. (D20)). The amount combusted ($comb_{ib}^{pell}$, on a wet basis) and the HHV on a dry basis, are linked by the dry factor ($\mathrm{DRY}_{\mathrm{ib}}^{\mathrm{pell}}$), based on moisture content, in Eq. (D76).

$$elgen_{ib}^{pow} = comb_{ib}^{pell} \mathrm{DRY}_{\mathrm{ib}}^{\mathrm{pell}} \mathrm{HHV}_{b}^{drypell} \eta^{pow} \mathrm{UCF} \quad \forall i, b \quad \text{(D76)}$$

CO_2 transportation and storage

The final amount of CO_2 available for storage in each country *i* ($CO2_i^{sto}$) will be slightly lower than the amount sent to that country ($tCO2_{ii'}^{p2s}$) owing to the losses produced in the pipeline transportation ($\mathrm{LOSS}^{\mathrm{p2s}}$) (Eq. (D77)). Here the losses are considered negligible, as it is reported in Table D0.21. Therefore, in Eq. (D25) we neglect the loss factor, while it is reported in Eq. (D77) as in GAMS. We define the loss factor to be able to consider the losses in other scenarios.

$$CO2_i^{sto} = \sum_{i'} tCO2_{i'i}^{p2s}(1 - \mathrm{LOSS}^{\mathrm{p2s}}) \quad \forall i \tag{D77}$$

D.6.2 Life cycle CO_2 emissions

Processing into bales or chips

The emissions associated with the chipping process are calculated from the carbon intensity $\mathrm{CI}_{\mathrm{ib}}^{\mathrm{drychip}}$ sourced from SimaPro[279] expresses the amount of CO_2 emitted per metric ton of dry chips. The activity used from Ecoinvent of expresses the product of the chipping process on a dry basis. In Eq. (D78) we report the calculations used to convert $\mathrm{CI}_{\mathrm{ib}}^{\mathrm{drychip}}$ to a wet basis, as it is expressed in Eq. (D37), using a dry factor based on the moisture content of the biomass ($\mathrm{DRY}_{\mathrm{ib}}^{\mathrm{chip}}$). The value of this parameter, retrieved from Fajardy et al.[33] and the Phyllis database[382] for the different biomass types *b* and countries *i*, can be found in Table D0.9.

$$\mathrm{CI}_{\mathrm{ib}}^{\mathrm{chip}} = \mathrm{DRY}_{\mathrm{ib}}^{\mathrm{chip}} \mathrm{CI}_{\mathrm{ib}}^{\mathrm{drychip}} \quad \forall i, b \tag{D78}$$

The emissions related to biomass losses during the chipping and baling processes are calculated based on the amount of biomass produced as bales and chips, respectively, and a loss parameter that stands for the percentage of biomass lost. The original formulation of Eqs. (D38) and (D39) using the new variables $avprod_{ib}^{bal}$ and $avprod_{ib}^{chip}$ is reported in Eqs. (D79) and (D80).

$$em_{ib}^{balloss} = \frac{prod_{ib}^{bal}}{\left(1 - \mathrm{LOSS}_{\mathrm{b}}^{\mathrm{bal}}\right)} \mathrm{LOSS}_{\mathrm{b}}^{\mathrm{bal}} \mathrm{CC}_{\mathrm{ib}} \frac{\mathrm{M}_{\mathrm{CO_2}}}{\mathrm{M}_{\mathrm{C}}} \quad \forall i, b \tag{D79}$$

$$em_{ib}^{chiploss} = \frac{prod_{ib}^{chip}}{\left(1 - \mathrm{LOSS_b^{chip}}\right)} \mathrm{LOSS_b^{chip}} \mathrm{CC_{ib}} \frac{\mathrm{M_{CO_2}}}{\mathrm{M_C}} \quad \forall i, b \tag{D80}$$

Pelleting stage

Similarly to the chipping process, the pelleting activity chosen from those available in SimaPro calculates the carbon intensity per metric ton of dry pellet. To be consistent with the mass balance of biomass on a wet basis, a dry factor ($\mathrm{DRY_{ib}^{pell}}$) has been employed to relate web and dry quantities, based on the moisture content. Eq. (D81) reports the extensive formulation of Eq. (D42).

$$em_{ib}^{pro} = pellet_{ib}^{pro} \mathrm{DRY_{ib}^{pell}} \mathrm{CI_{ib}^{drypell}} + em_{ib}^{proloss} \quad \forall i, b \tag{D81}$$

The pelleting occurs in four different steps, each of them being a potential source of biomass loss. This is expressed by the parameter $\mathrm{LOSS_b^{pell}}$ that indicates the percentage of losses. In Eq. (D82) the losses are explicitly calculated for the four steps, while we report in Eq. (D43) the compact form.

$$em_{ib}^{proloss} = \left(proc_{ib}^{bal} + proc_{ib}^{chip}\right) \left[1 - \left(1 - \mathrm{LOSS_b^{pell}}\right)^4\right] \mathrm{DRY_{ib}^{pell}} \mathrm{CC_b^{pow}} \frac{\mathrm{M_{CO_2}}}{\mathrm{M_C}} \quad \forall i, b \tag{D82}$$

CO_2 transportation and storage

During the combustion of the biomass, 10% of the CO_2 produced is released to the atmosphere. However, the 90% which is captured is compressed and transported to be permanently stored underground. We assume an additional distance of 150km to the distance from the capture plant in country i and i' ($\mathrm{DIST_{ii'}^{pipe}}$) to transport the CO_2 by pipeline (see Eq. (D83)). In Eq. (D84) we group all the terms related to the distance in the parameter $\mathrm{DIST_{ii'}^{totpipe}}$ used in Eq. (D47).

$$em_{ii'}^{p2s} = \mathrm{CI^{p2s}}\left(\mathrm{DIST_{ii'}^{pipe}} + 150\right) tCO2_{i'i}^{p2s} \quad \forall i, i' \tag{D83}$$

$$\mathrm{DIST}_{\mathrm{ii'}}^{\mathrm{totpipe}} = \mathrm{DIST}_{\mathrm{ii'}}^{\mathrm{pipe}} + 150 \quad \forall i, i' \tag{D84}$$

D.6.3 Life cycle costs

CO_2 transportation

The costs of CO_2 transportation are based on a low estimate from Budinis et al.[181], given for 250km. The distance covered by the pipeline and the additional distance from the storage site, already included in $\mathrm{DIST}_{\mathrm{ii'}}^{\mathrm{totpipe}}$, are here normalized on 250km. The parameter $\mathrm{DIST}_{\mathrm{ii'}}^{\mathrm{totpipen}}$ used in Eq. (D67) includes all the contribution that are reported in Eq.(D85).

$$co_{ii'}^{p2s} = \mathrm{CVAR}_{\mathrm{i}}^{\mathrm{P2S}} \frac{\mathrm{DIST}_{\mathrm{ii'}}^{\mathrm{pipeii}} + 150}{250} tCO2_{ii'}^{p2s} \quad \forall i, i' \tag{D85}$$

APPENDIX E

Supplementary information to Chapter 6

We report in this appendix additional results and analyses related to the studies presented in Chapter 6. In Section E.1 the insights obtained from the decomposition algorithm are given, while in Section E.2 we discuss the risk-averse model. In Section E.3 we report the results to the uncertainty variability sensitivity analysis.

E.1 Additional results

The following tables include detailed information referring to time period t_1 on the solution obtained from the multistage stochastic model in its full-space form (Table E0.1) and the decomposed one for different CDR targets (Table E0.2). Table E0.3 includes the technologies not selected at any time period and Table E0.4 the technologies selected for capacity expansion at t_1 for the case study with inhomogeneous time periods.

Table E0.1. Technology expansion and respective location at t_1 in the solution of MSS-1.

Technology	Country
Forest residues	Estonia, Finland
Forest residues with CCS	Bulgaria, Croatia, Germany, Hungary, Luxembourg, Poland, Sweden
Geothermal	Germany, Portugal
Natural gas	Denmark, Germany, Luxembourg, Poland
Natural gas with CCS	Denmark
Solar PV open	Hungary, Luxembourg, Malta, Poland, Slovakia

Table E0.2. Technology information obtained from the decomposition algorithm step 1, and computational time of step 1.

CDR target [$GtCO_2$]	Computational time [min]	Technologies not selected in any scenario for capacity expansion at any time period	Technologies selected in all the scenarios in (country) for capacity expansion at t1
−9	21	•Coal •Hydropower •Nuclear •Solar PV roof •Switchgrass •Switchgrass with CCS	•Forest residues with CCS (Poland) •Solar PV open (Luxembourg)
−6	16	•Wind offshore •Hydropower •Hydropower reservoir •Solar PV roof •Coal •Nuclear •Switchgrass	•Solar PV open(Luxembourg, Malta) •Natural gas (Luxembourg) •Forest residues with CCS (Poland)
−3	15	•Wind offshore •Hydropower	•Geothermal (Germany) •Natural gas (Denmark, Luxembourg)

		•Hydropower reservoir •Solar PV roof •Concentrated solar power •Coal •Nuclear •Coal with CCS •Switchgrass	•Solar PV open(Luxembourg, Malta) •Forest residues with CCS (Poland)
+3	14	•Wind offshore •Hydropower •Hydropower reservoir •Solar PV roof •Concentrated solar power •Coal •Nuclear •Coal with CCS •Natural gas with CCS •Miscanthus •Switchgrass •Miscanthus with CCS •Switchgrass with CCS	•Geothermal (Germany) •Natural gas (Denmark) •Woody residues with CCS (Greece) •Solar PV open(Luxembourg) •Forest residues with CCS (Poland)
+6	14	•Wind offshore •Hydropower •Hydropower reservoir •Solar PV roof •Concentrated solar power •Coal •Nuclear •Coal with CCS •Natural gas with CCS •Miscanthus •Switchgrass •Miscanthus with CCS •Switchgrass with CCS	•Geothermal (Germany) •Woody residues with CCS (Greece) •Solar PV open(Luxembourg) •Forest residues with CCS (Poland)

Table E0.3. Technologies not selected for capacity expansion in any county, any scenario and any time period for the minimization of the total cost with inhomogeneous time periods under a net-zero target.

Technologies not selected
Wind offshore
Hydropower
Hydropower reservoir
Solar PV roof
Concentrated solar power
Coal
Nuclear
Coal with CCS
Natural gas with CCS
Miscanthus
Switchgrass
Willow
Straw residues
Woody residues
Forest residues
Miscanthus with CCS
Switchgrass with CCS

Table E0.4. Technology selection at time period t_1 in step 1 using a time horizon with inhomogeneous time periods. No expansion occurs at t_6.

Time period	Technology expanded	Country
t_1	Wind onshore	Germany
	Solar	Luxembourg
	Forest residues with CCS	Poland
t_2		
t_3	Solar PV open	Belgium
t_4	Solar PV open	Austria, Bulgaria, Spain, Estonia, Finland, Hungary, Italy, Lithuania, Luxembourg, Poland, Portugal, Slovakia
	Forest residues with CCS	Denmark, Sweden
t_5	Solar PV open	Belgium
t_6		

Lastly, we report in Table E0.5 the precise resource usage time in seconds with reference to Table.6.1, Table 6.3 and Table 6.5.

Table E0.5 Resource usage of model generation and solution time in seconds for the case studies investigated, i.e., with homogeneous and inhomogeneous time periods. The resource usage reported does not include model presolve time and .gdx unloading.

Case study/ resource usage time [s]	Full-space	Decomposed
Homogeneous time horizon discretization	46597	4444
Inhomogeneous time horizon discretization	11490	7815

E.2 Risk management

Among the possible frameworks to include uncertainty in optimization problems, stochastic programming is a risk-neutral approach, because it optimizes the expectation of the objective function by neglecting that some of the scenarios might incur high costs [414].

Risk management is most widely explored in two-stage stochastic problems [414–416], although applications to multistage have also been explored [326]. The reason for richer literature in two-stage stochastic models with risk metrics is that including a term that represents the risk in the model leads to a considerable increase in the model complexity. Different metrics to manage risk have been defined in the literature: downside risk, value at risk, and conditional value at risk.

Following Oliveira et al. [414], we calculate the expected shortage risk (ES). The latter has the advantage of adding only one constraint and one continuous variable in the model. Nonetheless, given the complexity of our problem, we decide to explore the risk-averse case by replacing our model with a two-stage stochastic model where we include the formulation of ES. The mathematical formulation is given in Eq. (E1) and (E2), which adopts the same nomenclature as Oliveira et al. [414].

$$\min_{x,y,\delta}\left(cx + \sum_{u} P^u q y^u + \text{PEN}\sum_{u} P^u \delta^u\right) \tag{E1}$$

$$\begin{gathered} s.t.\, Ax + b \leq 0 \\ Tx + Wy^u \leq h^u \quad \forall\, u \in U \\ y^u \in Y \\ cx + qy^u - \omega \leq \delta^u \\ \delta^u \geq 0 \quad \forall\, u \in U \end{gathered} \tag{E2}$$

ES is calculated as in Eq. (E3).

$$ES(\omega,\, x) = \frac{1}{\sum_{u|\delta^u \geq 0} P^u} \sum_{u} P^u \delta^u \tag{E3}$$

We observe that a small trade-off of cost vs. risk can be observed because the model is highly constrained. Indeed, the demand for electricity has to be met as an equality constraint. In the case of adding a slack variable, increasing the demand uncertainty, e.g., ±50% instead of 20%, and a longer time horizon would allow us to observe more significant trade-offs. However, this would lead to a computationally intractable model with the evaluated solution method.

E.3 Variability of electricity demand uncertainty: a sensitivity analysis

Given the high uncertainty in the electricity demand, we perform a sensitivity analysis on the variability of the parameter. Our base scenario considers that the electricity demand varies ±20% from the nominal value for each country in each time period. We remind that the nominal value at each time period is calculated assuming a constant growth until the end of the time horizon, resulting in an annual increment of 0.7% [253].

In Table E0.6, we report the results of the total expected cost and decision variable selection for ±3%, 7.5%, 10% and 15% obtained with MSS1. We also include the total electricity generated by country compared to the deterministic solution, similar to the analysis presented in Figure 6.5 A.

Table E0.6 Total expected cost and technology information for different uncertainty variability values and fixed net-zero target at the end of the time horizon with homogeneous time periods.

Uncertainty variability [%]	**CDR target [$GtCO_2$]**	**Total expected cost [trillion Eur]**	**Technologies not selected in any scenario for capacity expansion at any time period**	**Technologies selected in all the scenarios in (country) for capacity expansion at t_1**
3	0	10.1	•Coal •Coal with CCS •Concentrated solar power •Hydropower •Hydropower reservoir •Miscanthus •Miscanthus with CCS •Natural gas with CCS •Nuclear •Solar PV roof •Switchgrass •Switchgrass with CCS •Wind offshore	•Forest (Estonia, Finland, Luxembourg) •Forest residues with CCS (Bulgaria, Croatia, Czechia, Greece, Hungary, Poland, Slovakia, Sweden) •Geothermal (Germany, Portugal) •Natural gas (Denmark, Luxembourg, Poland) •Woody residues with CCS (Bulgaria, Greece, United Kingdom) •Solar PV open (Estonia, Hungary, Luxembourg, Malta, Poland)
7.5	0	10.2	•Coal	•Forest (Estonia, Finland)

			•Coal with CCS •Concentrated solar power •Hydropower •Hydropower reservoir •Miscanthus •Natural gas with CCS •Nuclear •Solar PV roof •Switchgrass •Wind offshore	•Forest residues with CCS (Bulgaria, Croatia, Czechia, Greece, Hungary, Luxembourg, Poland, Sweden) •Geothermal (Germany, Portugal) •Natural gas (Denmark, Luxembourg, Poland) •Woody residues with CCS (Greece, United Kingdom) •Solar PV open (Estonia, Hungary, Luxembourg, Malta, Poland)
10	0	10.3	•Coal •Coal with CCS •Concentrated solar power •Hydropower •Hydropower reservoir •Miscanthus •Natural gas with CCS •Nuclear •Solar PV roof •Switchgrass •Wind offshore	•Forest (Estonia, Finland) •Forest residues with CCS (Bulgaria, Croatia, Czechia, Greece, Hungary, Luxembourg, Poland, Sweden) •Geothermal (Germany, Portugal) •Natural gas (Denmark, Luxembourg, Poland) •Woody residues with CCS (Greece, United Kingdom) •Solar PV open (Estonia, Hungary, Luxembourg, Malta, Poland, Slovakia)
15	0	10.5	•Coal with CCS •Concentrated solar power •Hydropower •Hydropower reservoir •Miscanthus •Natural gas with CCS •Nuclear •Solar PV roof •Switchgrass •Wind offshore	•Forest (Estonia, Finland) •Forest residues with CCS (Bulgaria, Croatia, Czechia, Germany, Greece, Hungary, Luxembourg, Poland, Sweden) •Geothermal (Germany, Portugal) •Natural gas (Denmark, Luxembourg, Poland) •Woody residues with CCS (Greece, United Kingdom) •Solar PV open (Estonia, Hungary, Luxembourg, Malta, Poland, Slovakia)

The results of the sensitivity analysis in Table E0.6 show that the technology selection varies slightly among the different scenarios. We can observe this behavior because, as we already

mentioned, the time horizon is relatively short, and the model is highly constrained, primarily related to the equality constraint on the electricity demand, in addition to the not-too-ambitious carbon removal target. Overall, these factors do not allow for larger differences in the technology selection.

Mainly, the increased variability of electricity demand uncertainty from 3% to 20% is reflected in the capacity installed. As was predictable, the total expected cost is rising as the variability of the energy demand uncertainty increases because the decision variables, i.e., installed capacity at t_1, need to be able to satisfy the electricity generation of all the scenarios.

Furthermore, we analyze the results of total electricity generated by country compared to the deterministic solution. This example demonstrates that regardless of the value of the uncertainty, the stochastic model provides more information than the deterministic one and might prevent practical suboptimal or unrealistic solutions. We show in Figure E0.1 the results with uncertainty ±3% and ±7.5% and in Figure E0.2 ±10% and ±15%. We note that, despite differences in the decision variables given by the range of variability of the uncertain parameter (Table E0.6), the stochastic model provides a broad range of values represented by the box and whiskers plots within which the deterministic solution is not always included. The higher the variability of the uncertain parameter, the more spread the box and whiskers plots are and the further from the median value of stochastic solutions the deterministic is.

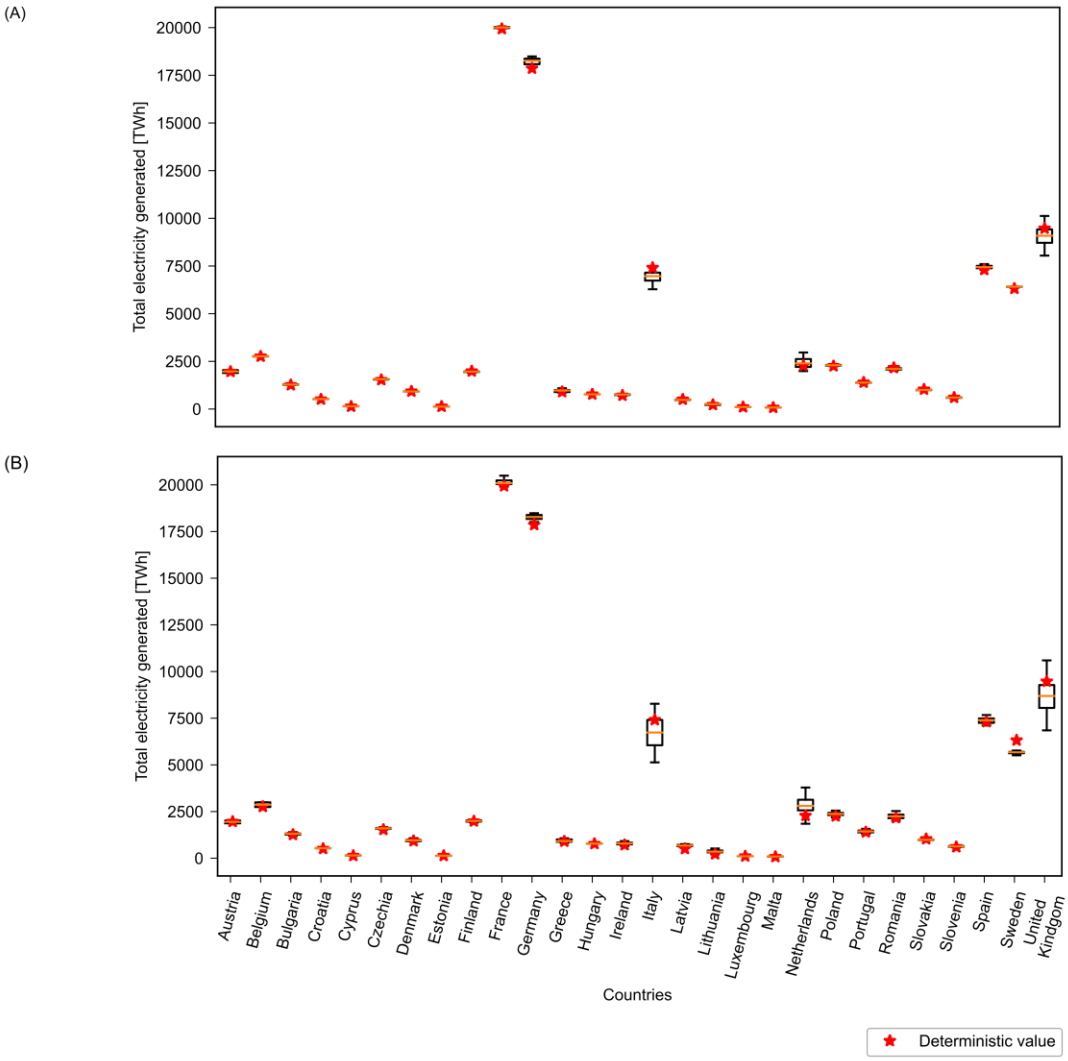

Figure E0.1: Total electricity generated aggregated by country for demand uncertainty ±3% (subplot A) and ±7.5% (subplot B). Stochastic range vs. deterministic value. The box and whiskers plots are generated using the solution of all 64 scenarios of the stochastic model and they show ±25 the median value.

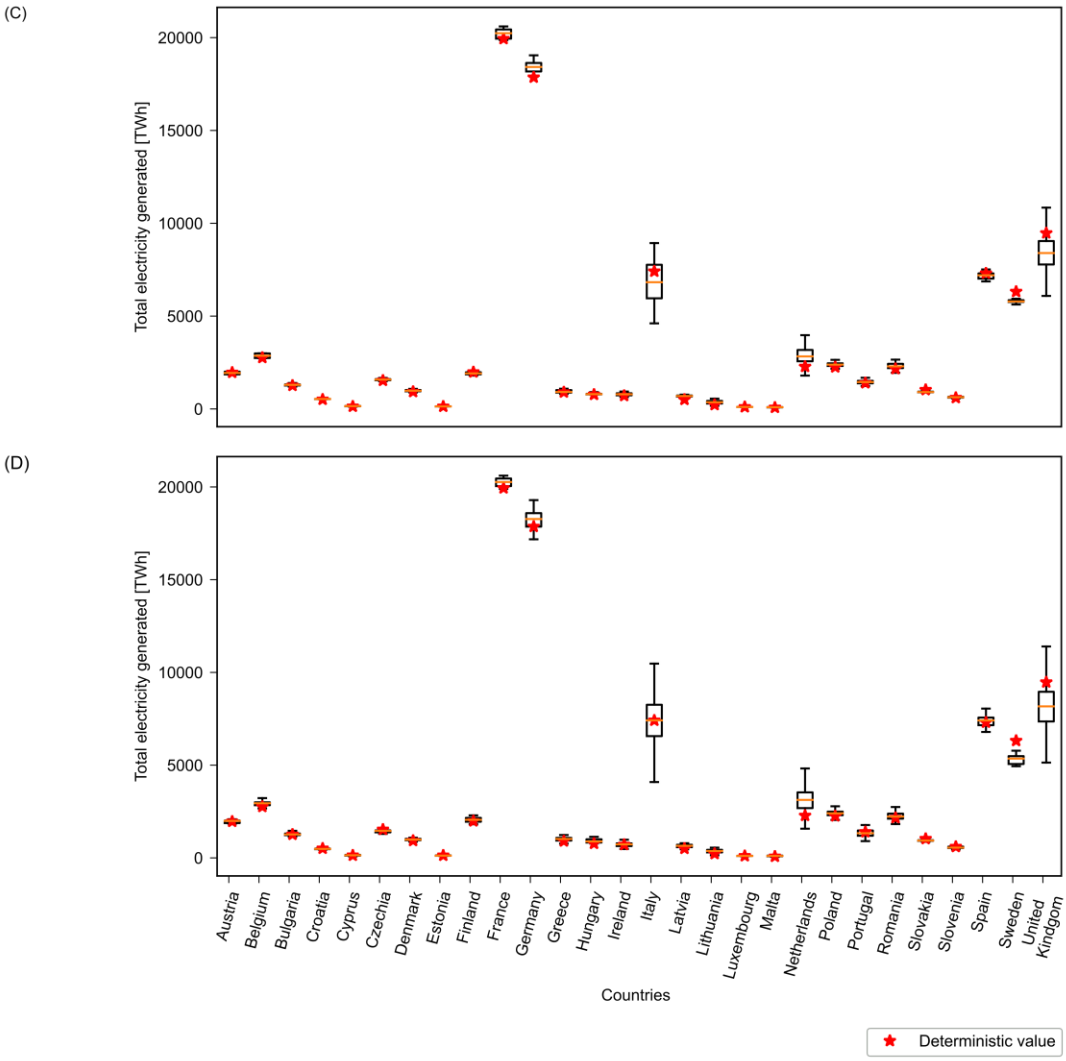

Figure E0.2: Total electricity generated aggregated by country for demand uncertainty ±10% (subplot C) and ±15% (subplot D). Stochastic range vs. deterministic value. The box and whiskers plots are generated using the solution of all 64 scenarios of the stochastic model and they show ±25 the median value.

Bibliography

(1) *The Paris Agreement | UNFCCC*. https://unfccc.int/process-and-meetings/the-paris-agreement/the-paris-agreement.

(2) Wang, F.; Harindintwali, J. D.; Yuan, Z.; Wang, M.; Wang, F.; Li, S.; Yin, Z.; Huang, L.; Fu, Y.; Li, L.; Chang, S. X.; Zhang, L.; Rinklebe, J.; Yuan, Z.; Zhu, Q.; Xiang, L.; Tsang, D. C. W.; Xu, L.; Jiang, X.; Liu, J.; Wei, N.; Kästner, M.; Zou, Y.; Ok, Y. S.; Shen, J.; Peng, D.; Zhang, W.; Barceló, D.; Zhou, Y.; Bai, Z.; Li, B.; Zhang, B.; Wei, K.; Cao, H.; Tan, Z.; Zhao, L.; He, X.; Zheng, J.; Bolan, N.; Liu, X.; Huang, C.; Dietmann, S.; Luo, M.; Sun, N.; Gong, J.; Gong, Y.; Brahushi, F.; Zhang, T.; Xiao, C.; Li, X.; Chen, W.; Jiao, N.; Lehmann, J.; Zhu, Y.-G.; Jin, H.; Schäffer, A.; Tiedje, J. M.; Chen, J. M. Technologies and Perspectives for Achieving Carbon Neutrality. *The Innovation* **2021**, *2* (4), 100180. https://doi.org/10.1016/j.xinn.2021.100180.

(3) Jackson, R. B.; Friedlingstein, P.; Quéré, C. L.; Abernethy, S.; Andrew, R. M.; Canadell, J. G.; Ciais, P.; Davis, S. J.; Deng, Z.; Liu, Z.; Korsbakken, J. I.; Peters, G. P. Global Fossil Carbon Emissions Rebound near Pre-COVID-19 Levels. *Environ. Res. Lett.* **2022**, *17* (3), 031001. https://doi.org/10.1088/1748-9326/ac55b6.

(4) (Eds.) Masson-Delmotte V.; Zhai, P.; Pörtner, H.-O.; Roberts, D.; Skea, J.; Shukla, P. R.; Pirani, A.; Moufouma-Okia, W.; Péan, C.; Pidcock, R.; Connors, S.; Matthews, J. B. R.; Chen, Y.; Zhou, X.; Gomis, M. I.; Lonnoy, E.; Maycock, T.; Tignor, M.; Waterfield, T. *IPCC, 2018: Global Warming of 1.5°C. An IPCC Special Report on the Impacts of Global Warming of 1.5°C above Pre-Industrial Levels and Related Global Greenhouse Gas Emission Pathways, in the Context of Strengthening the Global Response to the Threat of Cli*; IPCC, 2018.

(5) IPCC. *Climate Change 2022. Mitigation of Climate Change. Working Group III Contribution to the Sixth Assessment Report of the Intergovernmental Panel on Climate Change.*; IPCC, 2022.

(6) Bui, M.; Adjiman, C. S.; Bardow, A.; Anthony, E. J.; Boston, A.; Brown, S.; Fennell, P. S.; Fuss, S.; Galindo, A.; Hackett, L. A.; Hallett, J. P.; Herzog, H. J.; Jackson, G.; Kemper, J.; Krevor, S.; Maitland, G. C.; Matuszewski, M.; Metcalfe, I. S.; Petit, C.; Puxty, G.; Reimer, J.; Reiner, D. M.; Rubin, E. S.; Scott, S. A.; Shah, N.; Smit, B.; Trusler, J. P. M.; Webley, P.; Wilcox, J.; Mac Dowell, N. Carbon Capture and Storage (CCS): The Way Forward. *Energy and Environmental Science* **2018**, *11*, 1062–1176. https://doi.org/10.1039/c7ee02342a.

(7) Peters, L.; Hussain, A.; Follmann, M.; Melin, T.; Hägg, M. B. CO_2 Removal from Natural Gas by Employing Amine Absorption and Membrane Technology-A Technical and Economical Analysis. *Chemical Engineering Journal* **2011**, *172* (2–3), 952–960. https://doi.org/10.1016/j.cej.2011.07.007.

(8) Quang, D. V.; Milani, D.; Abu Zahra, M. A Review of Potential Routes to Zero and Negative Emission Technologies via the Integration of Renewable Energies with CO2 Capture Processes. *International Journal of Greenhouse Gas Control* **2023**, *124*, 103862. https://doi.org/10.1016/j.ijggc.2023.103862.

(9) Sharma, S.; Maréchal, F. Carbon Dioxide Capture From Internal Combustion Engine Exhaust Using Temperature Swing Adsorption. *Frontiers in Energy Research* **2019**, *0*, 143. https://doi.org/10.3389/FENRG.2019.00143.

(10) DNV. *Maritime Forecast to 2050*; DNV, 2022. https://eto.dnv.com/2021/maritime-forecast-2050 (accessed 2022-09-14).

(11) Feenstra, M.; Monteiro, J.; van den Akker, J. T.; Abu-Zahra, M. R. M.; Gilling, E.; Goetheer, E. Ship-Based Carbon Capture Onboard of Diesel or LNG-Fuelled Ships. *International Journal of Greenhouse Gas Control* **2019**, *85*, 1–10. https://doi.org/10.1016/J.IJGGC.2019.03.008.

(12) McLaren, D. A Comparative Global Assessment of Potential Negative Emissions Technologies. *Process Safety and Environmental Protection* **2012**, *90* (6), 489–500. https://doi.org/10.1016/j.psep.2012.10.005.

(13) Peters, G. P.; Geden, O. Catalysing a Political Shift from Low to Negative Carbon. *Nature Climate Change* **2017**, *7* (9), 619–621. https://doi.org/10.1038/nclimate3369.

(14) Pozo, C.; Galán-Martín, A.; Reiner, D.; MacDowell, N.; Guillén-Gosálbez, G. Equity in Allocating Carbon Dioxide Removal Quotas. *Nature Climate Change 2020* **2020**, 1–7. https://doi.org/10.1038/s41558-020-0802-4.

(15) Anderson, K.; Peters, G. The Trouble with Negative Emissions. *Science* **2016**, *354* (6309), 182–183. https://doi.org/10.1126/science.aah4567.

(16) Cobo, S.; Negri, V.; Valente, A.; Reiner, D. M.; Hamelin, L.; Mac Dowell, N.; Guillén-Gosálbez, G. Sustainable Scale-up of Negative Emissions Technologies and Practices: Where to Focus. *Environ. Res. Lett.* **2023**, *18* (2), 023001. https://doi.org/10.1088/1748-9326/acacb3.

(17) Fuss, S.; Jones, C. D.; Kraxner, F.; Peters, G. P.; Smith, P.; Tavoni, M.; Van Vuuren, D. P.; Canadell, J. G.; Jackson, R. B.; Milne, J.; Moreira, J. R.; Nakicenovic, N.; Sharifi, A.; Yamagata, Y. Research Priorities for Negative Emissions. *Environmental Research Letters* **2016**, *11* (11), 115007. https://doi.org/10.1088/1748-9326/11/11/115007.

(18) Köberle, A. C. The Value of BECCS in IAMs: A Review. *Current Sustainable/Renewable Energy Reports* **2019**, *6* (4), 107–115. https://doi.org/10.1007/s40518-019-00142-3.

(19) Fajardy, M.; Köberle, A.; Dowell, N. M. A. C.; Fantuzzi, A. *BECCS Deployment: A Reality Check*; Imperial College London Grantham Institute, 2019.

(20) Galik, C. S. A Continuing Need to Revisit BECCS and Its Potential. *Nature Climate Change* **2020**, *10* (1), 2–3. https://doi.org/10.1038/s41558-019-0650-2.

(21) Selosse, S.; Ricci, O. Achieving Negative Emissions with BECCS (Bioenergy with Carbon Capture and Storage) in the Power Sector: New Insights from the TIAM-FR (TIMES Integrated Assessment Model France) Model. *Energy* **2014**, *76*, 967–975. https://doi.org/10.1016/j.energy.2014.09.014.

(22) Van Vuuren, D. P.; Deetman, S.; Van Vliet, J.; Van Den Berg, M.; Van Ruijven, B. J.; Koelbl, B. The Role of Negative CO 2 Emissions for Reaching 2 °C-Insights from Integrated Assessment Modelling. *Climatic Change* **2013**, 15–27. https://doi.org/10.1007/s10584-012-0680-5.

(23) Babacan, O.; De Causmaecker, S.; Gambhir, A.; Fajardy, M.; Rutherford, A. W.; Fantuzzi, A.; Nelson, J. Assessing the Feasibility of Carbon Dioxide Mitigation Options in Terms of Energy Usage. *Nature Energy* **2020**, *5* (9), 720–728. https://doi.org/10.1038/s41560-020-0646-1.

(24) Fyson, C. L.; Baur, S.; Gidden, M.; Schleussner, C. F. Fair-Share Carbon Dioxide Removal Increases Major Emitter Responsibility. *Nature Climate Change* **2020**, *10* (9), 836–841. https://doi.org/10.1038/s41558-020-0857-2.

(25) Geden, O.; Peters, G. P.; Scott, V. Targeting Carbon Dioxide Removal in the European Union. *Climate Policy* **2019**, *19* (4), 487–494. https://doi.org/10.1080/14693062.2018.1536600.

(26) Scott, V.; Geden, O. The Challenge of Carbon Dioxide Removal for EU Policy-Making. *Nature Energy* **2018**, *3* (5), 350–352. https://doi.org/10.1038/s41560-018-0124-1.

(27) Oberthür, S.; Groen, L. The European Union and the Paris Agreement: Leader, Mediator, or Bystander? *Wiley Interdisciplinary Reviews: Climate Change* **2017**, *8* (1), e445. https://doi.org/10.1002/wcc.445.
(28) Honegger, M.; Reiner, D. The Political Economy of Negative Emissions Technologies: Consequences for International Policy Design. *Climate Policy* **2018**, *18* (3), 306–321. https://doi.org/10.1080/14693062.2017.1413322.
(29) Bednar, J.; Obersteiner, M.; Wagner, F. On the Financial Viability of Negative Emissions. *Nature Communications* **2019**, *10* (1), 1–4. https://doi.org/10.1038/s41467-019-09782-x.
(30) Fajardy, M.; Morris, J.; Gurgel, A.; Herzog, H.; Dowell, N. M.; Paltsev, S.; Mac Dowell, N. *The Economics of Bioenergy with Carbon Capture and Storage (BECCS) Deployment in a 1.5°C or 2°C World*; MIT Joint Program on the Science and Policy of Global, 2020. http://globalchange.mit.edu/ (accessed 2020-11-27).
(31) Muratori, M.; Calvin, K.; Wise, M.; Kyle, P.; Edmonds, J. Global Economic Consequences of Deploying Bioenergy with Carbon Capture and Storage (BECCS). *Environmental Research Letters* **2016**, *11* (9), 095004. https://doi.org/10.1088/1748-9326/11/9/095004.
(32) Emenike, O.; Michailos, S.; Finney, K. N.; Hughes, K. J.; Ingham, D.; Pourkashanian, M. Initial Techno-Economic Screening of BECCS Technologies in Power Generation for a Range of Biomass Feedstock. *Sustainable Energy Technologies and Assessments* **2020**, *40*, 100743. https://doi.org/10.1016/j.seta.2020.100743.
(33) Fajardy, M.; Mac Dowell, N. Can BECCS Deliver Sustainable and Resource Efficient Negative Emissions? *Energy and Environmental Science* **2017**, *10* (6), 1389–1426. https://doi.org/10.1039/c7ee00465f.
(34) Algunaibet, I. M.; Guillén-Gosálbez, G. Life Cycle Burden-Shifting in Energy Systems Designed to Minimize Greenhouse Gas Emissions: Novel Analytical Method and Application to the United States. *Journal of Cleaner Production* **2019**, *229*, 886–901. https://doi.org/10.1016/j.jclepro.2019.04.276.
(35) Heck, V.; Gerten, D.; Lucht, W.; Popp, A. Biomass-Based Negative Emissions Difficult to Reconcile with Planetary Boundaries. *Nature Climate Change* **2018**, *8* (2), 151–155. https://doi.org/10.1038/s41558-017-0064-y.
(36) Daggash, H. A.; Heuberger, C. F.; Mac Dowell, N. The Role and Value of Negative Emissions Technologies in Decarbonising the UK Energy System. *International Journal of Greenhouse Gas Control* **2019**, *81*, 181–198. https://doi.org/10.1016/j.ijggc.2018.12.019.
(37) Stamford, L.; Azapagic, A. Life Cycle Sustainability Assessment of UK Electricity Scenarios to 2070. *Energy for Sustainable Development* **2014**, *23*, 194–211. https://doi.org/10.1016/j.esd.2014.09.008.
(38) Fajardy, M.; Mac Dowell, N. The Energy Return on Investment of BECCS: Is BECCS a Threat to Energy Security? *Energy and Environmental Science* **2018**, *11* (6), 1581–1594. https://doi.org/10.1039/c7ee03610h.
(39) Fajardy, M.; Mac Dowell, N. Recognizing the Value of Collaboration in Delivering Carbon Dioxide Removal. *One Earth* **2020**, *3* (2), 214–225. https://doi.org/10.1016/j.oneear.2020.07.014.
(40) Mannhardt, J.; Gabrielli, P.; Sansavini, G. Collaborative and Selfish Mitigation Strategies to Tackle Energy Scarcity: The Case of the European Gas Crisis. *iScience* **2023**, *26* (5), 106750. https://doi.org/10.1016/j.isci.2023.106750.
(41) IEA. *Outlook for Biogas and Biomethane*; 2020.
(42) Pistikopoulos, E. N.; Barbosa-Povoa, A.; Lee, J. H.; Misener, R.; Mitsos, A.; Reklaitis, G. V.; Venkatasubramanian, V.; You, F.; Gani, R. Process Systems Engineering – The

Generation Next? *Computers & Chemical Engineering* **2021**, *147*, 107252. https://doi.org/10.1016/j.compchemeng.2021.107252.

(43) *AspenTech | Asset Optimization Software - Asset Performance Management, Process Engineering for Chemicals, Energy and Engineering & Construction*. AspenTech. https://www.aspentech.com/en/ (accessed 2023-07-17).

(44) *Welcome to Python.org*. Python.org. https://www.python.org/ (accessed 2023-07-18).

(45) Guimerà, R.; Reichardt, I.; Aguilar-Mogas, A.; Massucci, F. A.; Miranda, M.; Pallarès, J.; Sales-Pardo, M. A Bayesian Machine Scientist to Aid in the Solution of Challenging Scientific Problems. *Science Advances* **2020**, *6*. https://doi.org/10.1126/sciadv.aav6971.

(46) *GAMS - Cutting Edge Modeling*. https://www.gams.com/.

(47) Hellweg, S.; Canals, L. M. I. Emerging Approaches, Challenges and Opportunities in Life Cycle Assessment. *Science* **2014**, *344* (6188), 1109–1113. https://doi.org/10.1126/science.1248361.

(48) PRé. SimaPro Database Manual Methods Library Title: SimaPro Database Manual Methods Library Written by: PRé, Various Authors. **2019**, 75.

(49) Mutel, C. Brightway: An Open Source Framework for Life Cycle Assessment. *Journal of Open Source Software* **2017**, *2* (12), 236. https://doi.org/10.21105/joss.00236.

(50) Wernet, G.; Bauer, C.; Steubing, B.; Reinhard, J.; Moreno-Ruiz, E.; Weidema, B. The Ecoinvent Database Version 3 (Part I): Overview and Methodology. *International Journal of Life Cycle Assessment* **2016**, *21* (9), 1218–1230. https://doi.org/10.1007/s11367-016-1087-8.

(51) Huijbregts, M.; Steinmann, Z. J. N.; Elshout, P. M. F. M.; Stam, G.; Verones, F.; Vieira, M. D. M.; Zijp, M.; van Zelm, R. *ReCiPe 2016*; 2016; p 194. https://doi.org/10.1007/s11367-016-1246-y.

(52) European Commission. *Environmental Footprint methods*. https://green-business.ec.europa.eu/environmental-footprint-methods_en (accessed 2023-07-17).

(53) Rockström, J.; Steffen, W.; Noone, K.; Persson, Å.; Chapin, F. S.; Lambin, E.; Lenton, T. M.; Scheffer, M.; Folke, C.; Schellnhuber, H. J.; Nykvist, B.; de Wit, C. A.; Hughes, T.; van der Leeuw, S.; Rodhe, H.; Sörlin, S.; Snyder, P. K.; Costanza, R.; Svedin, U.; Falkenmark, M.; Karlberg, L.; Corell, R. W.; Fabry, V. J.; Hansen, J.; Walker, B.; Liverman, D.; Richardson, K.; Crutzen, P.; Foley, J. Planetary Boundaries: Exploring the Safe Operating Space for Humanity. *Ecology and Society* **2009**, *14* (2). https://doi.org/10.5751/ES-03180-140232.

(54) Steffen, W.; Richardson, K.; Rockström, J.; Cornell, S. E.; Fetzer, I.; Bennett, E. M.; Biggs, R.; Carpenter, S. R.; De Vries, W.; De Wit, C. A.; Folke, C.; Gerten, D.; Heinke, J.; Mace, G. M.; Persson, L. M.; Ramanathan, V.; Reyers, B.; Sörlin, S. Planetary Boundaries: Guiding Human Development on a Changing Planet. *Science* **2015**, *347* (6223). https://doi.org/10.1126/science.1259855.

(55) Sala, S.; Crenna, E.; Secchi, M.; Sanyé-Mengual, E. Environmental Sustainability of European Production and Consumption Assessed against Planetary Boundaries. *Journal of Environmental Management* **2020**, *269*, 110686. https://doi.org/10.1016/j.jenvman.2020.110686.

(56) United Nations. *Sustainable Development Goals*. https://sdgs.un.org/ (accessed 2023-07-17).

(57) De Laurentiis, V.; Secchi, M.; Bos, U.; Horn, R.; Laurent, A.; Sala, S. Soil Quality Index: Exploring Options for a Comprehensive Assessment of Land Use Impacts in LCA. *Journal of Cleaner Production* **2019**, *215*, 63–74. https://doi.org/10.1016/j.jclepro.2018.12.238.

(58) Cooper, R. G. Managing Technology Development Projects. *Research-Technology Management* **2006**, *49* (6), 23–31. https://doi.org/10.1080/08956308.2006.11657405.

(59) Mulvihill, M. J.; Beach, E. S.; Zimmerman, J. B.; Anastas, P. T. Green Chemistry and Green Engineering: A Framework for Sustainable Technology Development. *Annual Review ofEnvironment and Resources* **2011**. https://doi.org/10.1146/annurev-environ-032009-095500.

(60) Haszeldine, R. S.; Flude, S.; Johnson, G.; Scott, V. Negative Emissions Technologies and Carbon Capture and Storage to Achieve the Paris Agreement Commitments. *Philosophical Transactions of the Royal Society A* **2018**, *376* (2119). https://doi.org/10.1098/rsta.2016.0447.

(61) Bruhn, T.; Naims, H.; Olfe-Kräutlein, B. Separating the Debate on CO_2 Utilisation from Carbon Capture and Storage. *Environmental Science and Policy* **2016**, *60*, 38–43. https://doi.org/10.1016/j.envsci.2016.03.001.

(62) Oreggioni, G. D.; Brandani, S.; Luberti, M.; Baykan, Y.; Friedrich, D.; Ahn, H. CO_2 Capture from Syngas by an Adsorption Process at a Biomass Gasification CHP Plant: Its Comparison with Amine-Based CO2 Capture. *International Journal of Greenhouse Gas Control* **2015**, *35*, 71–81. https://doi.org/10.1016/j.ijggc.2015.01.008.

(63) Muhammad, A.; GadelHak, Y. Simulation Based Improvement Techniques for Acid Gases Sweetening by Chemical Absorption: A Review. *International Journal of Greenhouse Gas Control* **2015**, *37*, 481–491. https://doi.org/10.1016/j.ijggc.2015.03.014.

(64) Deutz, S.; Bardow, A. Life-Cycle Assessment of an Industrial Direct Air Capture Process Based on Temperature–Vacuum Swing Adsorption. *Nature Energy* **2021**, 1–11. https://doi.org/10.1038/s41560-020-00771-9.

(65) Page, B.; Turan, G.; Zapantis, A. *Global Status of CCS 2020*; Global CCS Institute, 2020.

(66) Kidnay, A. J.; Parrish, W. R. *Fundamentals of Natural Gas Processing*; CRC Press, Taylor & Francis Group, 2006. https://doi.org/10.1201/9781420014044.

(67) Adib, H.; Sharifi, F.; Mehranbod, N.; Kazerooni, N. M.; Koolivand, M. Support Vector Machine Based Modeling of an Industrial Natural Gas Sweetening Plant. *Journal of Natural Gas Science and Engineering* **2013**, *14*, 121–131. https://doi.org/10.1016/j.jngse.2013.06.004.

(68) Vega, F.; Baena-Moreno, F. M.; Gallego Fernández, L. M.; Portillo, E.; Navarrete, B.; Zhang, Z. Current Status of CO_2 Chemical Absorption Research Applied to CCS: Towards Full Deployment at Industrial Scale. *Applied Energy* **2020**, *260*, 114313. https://doi.org/10.1016/j.apenergy.2019.114313.

(69) Raksajati, A.; Ho, M. T.; Wiley, D. E. Comparison of Solvent Development Options for Capture of CO_2 from Flue Gases. *Industrial & Engineering Chemistry Research* **2018**, *57* (19), 6746–6758. https://doi.org/10.1021/ACS.IECR.8B00283.

(70) Asif, M.; Suleman, M.; Haq, I.; Jamal, S. A. Post-Combustion CO_2 Capture with Chemical Absorption and Hybrid System: Current Status and Challenges. *Greenhouse Gases: Science and Technology* **2018**, *8* (6), 998–1031. https://doi.org/10.1002/ghg.1823.

(71) Lund, H.; Mathiesen, B. V. The Role of Carbon Capture and Storage in a Future Sustainable Energy System. *Energy* **2012**, *44* (1), 469–476. https://doi.org/10.1016/j.energy.2012.06.002.

(72) Qian, Q.; Asinger, P. A.; Lee, M. J.; Han, G.; Mizrahi Rodriguez, K.; Lin, S.; Benedetti, F. M.; Wu, A. X.; Chi, W. S.; Smith, Z. P. MOF-Based Membranes for Gas Separations. *Chemical Reviews* **2020**, acs.chemrev.0c00119. https://doi.org/10.1021/acs.chemrev.0c00119.

(73) Hoorfar, M.; Alcheikhhamdon, Y.; Chen, B. A Novel Tool for the Modeling, Simulation and Costing of Membrane Based Gas Separation Processes Using Aspen HYSYS:

Optimization of the CO_2/CH_4 Separation Process. *Computers and Chemical Engineering* **2018**, *117*, 11–24. https://doi.org/10.1016/j.compchemeng.2018.05.013.

(74) Ahmad, F.; Lau, K. K.; Shariff, A. M.; Murshid, G. Process Simulation and Optimal Design of Membrane Separation System for CO 2 Capture from Natural Gas. *Computers and Chemical Engineering* **2012**, *36* (1), 119–128. https://doi.org/10.1016/j.compchemeng.2011.08.002.

(75) Hasan, M. M. F.; Baliban, R. C.; Elia, J. A.; Floudas, C. A. Modeling, Simulation, and Optimization of Postcombustion CO_2 Capture for Variable Feed Concentration and Flow Rate. 1. Chemical Absorption and Membrane Processes. *Industrial and Engineering Chemistry Research* **2012**, *51* (48), 15642–15664. https://doi.org/10.1021/ie301571d.

(76) Gabrielli, P.; Gazzani, M.; Mazzotti, M. On the Optimal Design of Membrane-Based Gas Separation Processes. *Journal of Membrane Science* **2017**, *526*, 118–130. https://doi.org/10.1016/j.memsci.2016.11.022.

(77) Belaissaoui, B.; Le Moullec, Y.; Willson, D.; Favre, E. Hybrid Membrane Cryogenic Process for Post-Combustion CO 2 Capture. *Journal of Membrane Science* **2012**, *415–416*, 424–434. https://doi.org/10.1016/j.memsci.2012.05.029.

(78) Song, C.; Liu, Q.; Ji, N.; Deng, S.; Zhao, J.; Li, Y.; Song, Y.; Li, H. Alternative Pathways for Efficient CO_2 Capture by Hybrid Processes—A Review. *Renewable and Sustainable Energy Reviews* **2018**, *82*, 215–231. https://doi.org/10.1016/j.rser.2017.09.040.

(79) Song, C.; Liu, Q.; Ji, N.; Deng, S.; Zhao, J.; Kitamura, Y. Advanced Cryogenic CO_2 Capture Process Based on Stirling Coolers by Heat Integration. *Applied Thermal Engineering* **2017**, *114*, 887–895. https://doi.org/10.1016/j.applthermaleng.2016.12.049.

(80) Xie, N.; Chen, B.; Tan, C.; Liu, Z. Energy Consumption and Exergy Analysis of MEA-Based and Hydrate-Based CO_2 Separation. *Industrial and Engineering Chemistry Research* **2017**, *56* (51), 15094–15101. https://doi.org/10.1021/ACS.IECR.7B03729.

(81) Thompson, M. L.; Kramer, M. A. Modeling Chemical Processes Using Prior Knowledge and Neural Networks. *AIChE Journal* **1994**, *40* (8), 1328–1340. https://doi.org/10.1002/aic.690400806.

(82) Lee, J. H.; Shin, J.; Realff, M. J. Machine Learning: Overview of the Recent Progresses and Implications for the Process Systems Engineering Field. *Computers and Chemical Engineering* **2018**, *114*, 111–121. https://doi.org/10.1016/j.compchemeng.2017.10.008.

(83) Bradford, E.; Imsland, L.; Zhang, D.; del Rio Chanona, E. A. Stochastic Data-Driven Model Predictive Control Using Gaussian Processes. *Computers and Chemical Engineering* **2020**, *139*, 106844. https://doi.org/10.1016/j.compchemeng.2020.106844.

(84) Shrivastava, R.; Mahalingam, H.; Dutta, N. N. Application and Evaluation of Random Forest Classifier Technique for Fault Detection in Bioreactor Operation. *Chemical Engineering Communications* **2017**, *204* (5), 591–598. https://doi.org/10.1080/00986445.2017.1292259.

(85) Saxén, B.; Saxén, H. A Neural-Network Based Model of Bioreaction Kinetics. *Canadian Journal of Chemical Engineering* **1996**, *74* (1), 124–131. https://doi.org/10.1002/cjce.5450740116.

(86) Patnaik, P. R. Hybrid Neural Simulation of a Fed-Batch Bioreactor for a Nonideal Recombinant Fermentation. *Bioprocess and Biosystems Engineering* **2001**, *24* (3), 151–161. https://doi.org/10.1007/s004490100246.

(87) Tholudur, A.; Ramirez, W. F. Optimization of Fed-Batch Bipreactors Using Neural Network Parameter Function Models. *Biotechnology Progress* **1996**, *12* (3), 302–309. https://doi.org/10.1021/bp960012h.

(88) von Stosch, M.; Oliveira, R.; Peres, J.; Feyo de Azevedo, S. Hybrid Semi-Parametric Modeling in Process Systems Engineering: Past, Present and Future. *Computers and*

Chemical Engineering **2014**, *60*, 86–101. https://doi.org/10.1016/j.compchemeng.2013.08.008.

(89) Cozad, A.; Sahinidis, N. V. A Global MINLP Approach to Symbolic Regression. *Mathematical Programming* **2018**, *170* (1), 97–119. https://doi.org/10.1007/s10107-018-1289-x.

(90) Sahinidis, N. V. BARON: A General Purpose Global Optimization Software Package. *Journal of Global Optimization* **1996**, *8* (2), 201–205. https://doi.org/10.1007/BF00138693.

(91) Cozad, A.; Sahinidis, N. V.; Miller, D. C. Learning Surrogate Models for Simulation-Based Optimization. *AIChE Journal* **2014**, *60* (6), 2211–2227. https://doi.org/10.1002/aic.14418.

(92) Cozad, A.; Sahinidis, N. V.; Miller, D. C. A Combined First-Principles and Data-Driven Approach to Model Building. *Computers and Chemical Engineering* **2015**, *73*, 116–127. https://doi.org/10.1016/j.compchemeng.2014.11.010.

(93) Wilson, Z. T.; Sahinidis, N. V. The ALAMO Approach to Machine Learning. *Computers and Chemical Engineering* **2017**, *106*, 785–795. https://doi.org/10.1016/j.compchemeng.2017.02.010.

(94) Grossmann, I. Review of Nonlinear Mixed-Integer and Disjunctive Programming Techniques. *Optimization and Engineering* **2002**, *3* (3), 227–252. https://doi.org/10.1023/A:1021039126272.

(95) Rao, A. B.; Rubin, E. S. Identifying Cost-Effective CO_2 Control Levels for Amine-Based CO_2 Capture Systems. *Industrial and Engineering Chemistry Research* **2006**, *45*, 2421–2429. https://doi.org/10.1021/ie050603p.

(96) Zhou, Q.; Chan, C. W.; Tontiwachiwuthikul, P. Regression Analysis Study on the Carbon Dioxide Capture Process. *Industrial and Engineering Chemistry Research* **2008**, *47* (14), 4937–4943. https://doi.org/10.1021/IE701747F.

(97) Zhou, Q.; Wu, Y.; Chan, C. W.; Tontiwachwuthikul, P. Modeling of the Carbon Dioxide Capture Process System Using Machine Intelligence Approaches. *Engineering Applications of Artificial Intelligence* **2011**, *24* (4), 673–685. https://doi.org/10.1016/J.ENGAPPAI.2011.01.003.

(98) Liang, Z. (Henry); Rongwong, W.; Liu, H.; Fu, K.; Gao, H.; Cao, F.; Zhang, R.; Sema, T.; Henni, A.; Sumon, K.; Nath, D.; Gelowitz, D.; Srisang, W.; Saiwan, C.; Benamor, A.; Al-Marri, M.; Shi, H.; Supap, T.; Chan, C.; Zhou, Q.; Abu-Zahra, M.; Wilson, M.; Olson, W.; Idem, R.; Tontiwachwuthikul, P. (PT). Recent Progress and New Developments in Post-Combustion Carbon-Capture Technology with Amine Based Solvents. *International Journal of Greenhouse Gas Control* **2015**, *40*, 26–54. https://doi.org/10.1016/J.IJGGC.2015.06.017.

(99) Li, Z.; Sharma, M.; Khalilpour, R.; Abbas, A. Optimal Operation of Solvent-Based Post-Combustion Carbon Capture Processes with Reduced Models. In *Energy Procedia*; Elsevier, 2013; Vol. 37, pp 1500–1508. https://doi.org/10.1016/J.EGYPRO.2013.06.025.

(100) Danaci, D.; Bui, M.; Petit, C.; Mac Dowell, N. En Route to Zero Emissions for Power and Industry with Amine-Based Post-Combustion Capture. *Environmental Science and Technology* **2021**. https://doi.org/10.1021/acs.est.0c07261.

(101) Pascual-González, J.; Pozo, C.; Guillén-Gosálbez, G.; Jiménez-Esteller, L. Combined Use of MILP and Multi-Linear Regression to Simplify LCA Studies. *Computers and Chemical Engineering* **2015**, *82*, 34–43. https://doi.org/10.1016/j.compchemeng.2015.06.002.

(102) Miró, A.; Pozo, C.; Guillén-Gosálbez, G.; Egea, J. A.; Jiménez, L. Deterministic Global Optimization Algorithm Based on Outer Approximation for the Parameter Estimation of

Nonlinear Dynamic Biological Systems. *BMC Bioinformatics* **2012**, *13* (1), 1–12. https://doi.org/10.1186/1471-2105-13-90.

(103) Gkioulekas, I.; Papageorgiou, L. G. Tree Regression Models Using Statistical Testing and Mixed Integer Programming. *Computers and Industrial Engineering* **2021**, *153*, 107059. https://doi.org/10.1016/j.cie.2020.107059.

(104) Ferreira, J.; Torres, A. I.; Pedemonte, M. Towards a Multi-Output Kaizen Programming Algorithm. In *2021 IEEE Latin American Conference on Computational Intelligence*; Institute of Electrical and Electronics Engineers Inc., 2021. https://doi.org/10.1109/LA-CCI48322.2021.9769841.

(105) Neumann, P.; Cao, L.; Russo, D.; Vassiliadis, V. S.; Lapkin, A. A. A New Formulation for Symbolic Regression to Identify Physico-Chemical Laws from Experimental Data. *Chemical Engineering Journal* **2020**, *387*, 123412. https://doi.org/10.1016/j.cej.2019.123412.

(106) Ouyang, R.; Curtarolo, S.; Ahmetcik, E.; Scheffler, M.; Ghiringhelli, L. M. SISSO: A Compressed-Sensing Method for Identifying the Best Low-Dimensional Descriptor in an Immensity of Offered Candidates. *Physical review materials* **2018**, *2*, 83802. https://doi.org/10.1103/PhysRevMaterials.2.083802.

(107) Ansari, M.; Gandhi, H. A.; Foster, D. G.; White, A. D. Iterative Symbolic Regression for Learning Transport Equations. *AIChE Journal* **2022**, *68*. https://doi.org/10.1002/AIC.17695.

(108) Sun, W.; Braatz, R. D. ALVEN: Algebraic Learning via Elastic Net for Static and Dynamic Nonlinear Model Identification. *Computers & Chemical Engineering* **2020**, *143*, 107103. https://doi.org/10.1016/J.COMPCHEMENG.2020.107103.

(109) Sun, W.; Braatz, R. D. Smart Process Analytics for Predictive Modeling. *Computers & Chemical Engineering* **2021**, *144*, 107134. https://doi.org/10.1016/J.COMPCHEMENG.2020.107134.

(110) Dobbelaere, M. R.; Plehiers, P. P.; Van de Vijver, R.; Stevens, C. V.; Van Geem, K. M. Machine Learning in Chemical Engineering: Strengths, Weaknesses, Opportunities, and Threats. *Engineering* **2021**, *7* (9), 1201–1211. https://doi.org/10.1016/J.ENG.2021.03.019.

(111) Schweidtmann, A. M.; Esche, E.; Fischer, A.; Kloft, M.; Repke, J.-U.; Sager, S.; Mitsos, A. Machine Learning in Chemical Engineering: A Perspective. *Chemie Ingenieur Technik* **2021**, *93* (12), 2029–2039. https://doi.org/10.1002/cite.202100083.

(112) Otte, C. *Safe and Interpretable Machine Learning: A Methodological Review*; Springer, Berlin, Heidelberg, 2013; Vol. 445. https://doi.org/10.1007/978-3-642-32378-2_8/COVER.

(113) Vázquez, D.; Guimerà, R.; Sales-Pardo, M.; Guillén-Gosálbez, G. Automatic Modeling of Socioeconomic Drivers of Energy Consumption and Pollution Using Bayesian Symbolic Regression. *Sustainable Production and Consumption* **2022**, *30*, 596–607. https://doi.org/10.1016/J.SPC.2021.12.025.

(114) Liu, H.; Zhang, Z. Probing the Carbon Emissions in 30 Regions of China Based on Symbolic Regression and Tapio Decoupling. *Environmental Science and Pollution Research* **2022**, *29*, 2650–2663. https://doi.org/10.1007/S11356-021-15648-X/FIGURES/10.

(115) Li, W.; Yang, G.; Li, X. Modeling the Evolutionary Nexus between Carbon Dioxide Emissions and Economic Growth. *Journal of Cleaner Production* **2019**, *215*, 1191–1202. https://doi.org/10.1016/J.JCLEPRO.2019.01.100.

(116) Subraveti, S. G.; Li, Z.; Prasad, V.; Rajendran, A. Machine Learning-Based Multiobjective Optimization of Pressure Swing Adsorption. *Industrial & Engineering*

Chemistry Research **2019**, *58* (44), 20412–20422. https://doi.org/10.1021/ACS.IECR.9B04173.

(117) Liu, H.; Chan, C.; Tontiwachwuthikul, P.; Idem, R. Analysis of CO_2 Equilibrium Solubility of Seven Tertiary Amine Solvents Using Thermodynamic and ANN Models. *Fuel* **2019**, *249*, 61–72. https://doi.org/10.1016/J.FUEL.2019.02.088.

(118) Venkatraman, V.; Alsberg, B. K. Predicting CO_2 Capture of Ionic Liquids Using Machine Learning. *Journal of CO_2 Utilization* **2017**, *21*, 162–168. https://doi.org/10.1016/J.JCOU.2017.06.012.

(119) Mesbah, M.; Shahsavari, S.; Soroush, E.; Rahaei, N.; Rezakazemi, M. Accurate Prediction of Miscibility of CO2 and Supercritical CO2 in Ionic Liquids Using Machine Learning. *Journal of CO_2 Utilization* **2018**, *25*, 99–107. https://doi.org/10.1016/J.JCOU.2018.03.004.

(120) Morgan, J. C.; Chinen, A. S.; Anderson-Cook, C.; Tong, C.; Carroll, J.; Saha, C.; Omell, B.; Bhattacharyya, D.; Matuszewski, M.; Bhat, K. S.; Miller, D. C. Development of a Framework for Sequential Bayesian Design of Experiments: Application to a Pilot-Scale Solvent-Based CO_2 Capture Process. *Applied Energy* **2020**, *262*, 114533. https://doi.org/10.1016/J.APENERGY.2020.114533.

(121) Kim, Y.; Jang, H.; Kim, J.; Lee, J. Prediction of Storage Efficiency on CO_2 Sequestration in Deep Saline Aquifers Using Artificial Neural Network. *Applied Energy* **2017**, *185*, 916–928. https://doi.org/10.1016/J.APENERGY.2016.10.012.

(122) Helei, L.; Tantikhajorngosol, P.; Chan, C.; Tontiwachwuthikul, P. Technology Development and Applications of Artificial Intelligence for Post-Combustion Carbon Dioxide Capture: Critical Literature Review and Perspectives. *International Journal of Greenhouse Gas Control* **2021**, *108*, 103307. https://doi.org/10.1016/J.IJGGC.2021.103307.

(123) Shalaby, A.; Elkamel, A.; Douglas, P. L.; Zhu, Q.; Zheng, Q. P. A Machine Learning Approach for Modeling and Optimization of a CO_2 Post-Combustion Capture Unit. *Energy* **2021**, *215*, 119113. https://doi.org/10.1016/J.ENERGY.2020.119113.

(124) Sipöcz, N.; Tobiesen, F. A.; Assadi, M. The Use of Artificial Neural Network Models for CO_2 Capture Plants. *Applied Energy* **2011**, *88* (7), 2368–2376. https://doi.org/10.1016/J.APENERGY.2011.01.013.

(125) Wilberforce, T.; Baroutaji, A.; Soudan, B.; Al-Alami, A. H.; Olabi, A. G. Outlook of Carbon Capture Technology and Challenges. *Science of the Total Environment* **2019**, *657*, 56–72. https://doi.org/10.1016/j.scitotenv.2018.11.424.

(126) Song, C.; Liu, Q.; Ji, N.; Deng, S.; Zhao, J.; Kitamura, Y. Natural Gas Purification by Heat Pump Assisted MEA Absorption Process. *Applied Energy* **2017**, *204*, 353–361. https://doi.org/10.1016/j.apenergy.2017.07.052.

(127) Schach, M.-O.; Schneider, R.; Schramm, H.; Repke, J.-U. Techno-Economic Analysis of Postcombustion Processes for the Capture of Carbon Dioxide from Power Plant Flue Gas. *Industrial and Engineering Chemistry Research* **2010**, *49* (5), 2363–2370. https://doi.org/10.1021/IE900514T.

(128) Tay, W. H.; Lau, K. K.; Lai, L. S.; Shariff, A. M.; Wang, T. Current Development and Challenges in the Intensified Absorption Technology for Natural Gas Purification at Offshore Condition. *Journal of Natural Gas Science and Engineering* **2019**, *71*, 102977. https://doi.org/10.1016/j.jngse.2019.102977.

(129) Adams II, T. A.; Salkuyeh, Y. K.; Nease, J. Processes and Simulations for Solvent-Based CO_2 Capture and Syngas Cleanup. In *Reactor and Process Design in Sustainable Energy Technology*; Elsevier Inc., 2014; pp 163–231. https://doi.org/10.1016/B978-0-444-59566-9.00006-5.

(130) Adams, D. *Flue Gas Treatment for CO_2 Capture*; IEA Clean Coal Centre, 2010; pp 1–61.
(131) Li, K.; Leigh, W.; Feron, P.; Yu, H.; Tade, M. Systematic Study of Aqueous Monoethanolamine (MEA)-Based CO_2 Capture Process: Techno-Economic Assessment of the MEA Process and Its Improvements. *Applied Energy* **2016**, *165*, 648–659. https://doi.org/10.1016/j.apenergy.2015.12.109.
(132) Wattanaphan, P.; Sema, T.; Idem, R.; Liang, Z.; Tontiwachwuthikul, P. Effects of Flue Gas Composition on Carbon Steel (1020) Corrosion in MEA-Based CO_2 Capture Process. *International Journal of Greenhouse Gas Control* **2013**, *19*, 340–349. https://doi.org/10.1016/j.ijggc.2013.08.021.
(133) Petrakopoulou, F. Comparative Evaluation of Power Plants with CO 2 Capture: Thermodynamic, Economic and Environmental Performance, Technischen Universität Berlin, 2011.
(134) Wu, X.; Wang, M.; Liao, P.; Shen, J.; Li, Y. Solvent-Based Post-Combustion CO_2 Capture for Power Plants: A Critical Review and Perspective on Dynamic Modelling, System Identification, Process Control and Flexible Operation. *Applied Energy* **2020**, *257*, 113941. https://doi.org/10.1016/J.APENERGY.2019.113941.
(135) Scholes, C. A.; Stevens, G. W.; Kentish, S. E. Membrane Gas Separation Applications in Natural Gas Processing. *Fuel* **2012**, *96*, 15–28. https://doi.org/10.1016/j.fuel.2011.12.074.
(136) Baker, R. W.; Lokhandwala, K. Natural Gas Processing with Membranes: An Overview. *Industrial and Engineering Chemistry Research* **2008**, *47* (7), 2109–2121. https://doi.org/10.1021/ie071083w.
(137) Agbonghae, E. O.; Hughes, K. J.; Ingham, D. B.; Ma, L.; Pourkashanian, M. Optimal Process Design of Commercial-Scale Amine-Based CO_2 Capture Plants. *Industrial and Engineering Chemistry Research* **2014**, *53* (38), 14815–14829. https://doi.org/10.1021/IE5023767.
(138) Žegklitz, J.; Pošík, P. Benchmarking State-of-the-Art Symbolic Regression Algorithms. *Genetic Programming and Evolvable Machines* **2021**, *22* (1), 5–33. https://doi.org/10.1007/S10710-020-09387-0/FIGURES/9.
(139) Franceschini, G.; Macchietto, S. Model-Based Design of Experiments for Parameter Precision: State of the Art. *Chemical Engineering Science* **2008**, *63* (19), 4846–4872. https://doi.org/10.1016/J.CES.2007.11.034.
(140) Amine Scrubbing with Aspen HYSYS V8 . 0, 2012.
(141) Savage, T. R.; Almeida-Trasvina, F.; del-Rio Chanona, E. A.; Smith, R.; Zhang, D. An Integrated Dimensionality Reduction and Surrogate Optimization Approach for Plant-Wide Chemical Process Operation. *AIChE Journal* **2021**, *67* (11), 1–14. https://doi.org/10.1002/AIC.17358.
(142) van de Berg, D.; Savage, T.; Petsagkourakis, P.; Zhang, D.; Shah, N.; del Rio-Chanona, E. A. Data-Driven Optimization for Process Systems Engineering Applications. *Chemical Engineering Science* **2022**, *248*, 117135. https://doi.org/10.1016/J.CES.2021.117135.
(143) Bongartz, D.; Najman, J.; Sass, S.; Mitsos, A. *MAiNGO – McCormick-Based Algorithm for Mixed-Integer Nonlinear Global Optimization*; Process Systems Engineering (AVT.SVT), RWTH Aachen University, 2018. http://permalink.avt.rwth-aachen.de/?id=729717 (accessed 2022-05-25).
(144) Schweidtmann, A. M.; Mitsos, · Alexander. Deterministic Global Optimization with Artificial Neural Networks Embedded. *Journal of Optimization Theory and Applications* **2019**, *180*, 925–948. https://doi.org/10.1007/s10957-018-1396-0.

(145) Santos, L. F.; Costa, C. B. B.; Caballero, J. A.; Ravagnani, M. A. S. S. Framework for Embedding Black-Box Simulation into Mathematical Programming via Kriging Surrogate Model Applied to Natural Gas Liquefaction Process Optimization. *Applied Energy* **2022**, *310*, 118537. https://doi.org/10.1016/J.APENERGY.2022.118537.

(146) Ye, W.; You, F. A Computationally Efficient Simulation-Based Optimization Method with Region-Wise Surrogate Modeling for Stochastic Inventory Management of Supply Chains with General Network Structures. *Computers & Chemical Engineering* **2016**, *87*, 164–179. https://doi.org/10.1016/J.COMPCHEMENG.2016.01.015.

(147) Zhimian Hao; H. Barecka, M.; A. Lapkin, A. Accelerating Net Zero from the Perspective of Optimizing a Carbon Capture and Utilization System. *Energy & Environmental Science* **2022**, *15* (5), 2139–2153. https://doi.org/10.1039/D1EE03923G.

(148) Kim, S. H.; Boukouvala, F. Surrogate-Based Optimization for Mixed-Integer Nonlinear Problems. *Computers & Chemical Engineering* **2020**, *140*, 106847. https://doi.org/10.1016/J.COMPCHEMENG.2020.106847.

(149) Boukouvala, F.; Ierapetritou, M. G. Surrogate-Based Optimization of Expensive Flowsheet Modeling for Continuous Pharmaceutical Manufacturing. *Journal of Pharmaceutical Innovation* **2013**, *8* (2), 131–145. https://doi.org/10.1007/S12247-013-9154-1/FIGURES/5.

(150) Vollmer, N. I.; Al, R.; Gernaey, K. V.; Sin, G. Synergistic Optimization Framework for the Process Synthesis and Design of Biorefineries. *Frontiers of Chemical Science and Engineering* **2021**, *16* (2), 251–273. https://doi.org/10.1007/S11705-021-2071-9.

(151) Halemane, K. P.; Grossmann, I. E. Optimal Process Design under Uncertainty. *AIChE Journal* **1983**, *29* (3), 425–433. https://doi.org/10.1002/AIC.690290312.

(152) Grossmann, I. E.; Floudas, C. A. Active Constraint Strategy for Flexibility Analysis in Chemical Processes. *Computers & Chemical Engineering* **1987**, *11* (6), 675–693. https://doi.org/10.1016/0098-1354(87)87011-4.

(153) Rogers, A.; Ierapetritou, M. Feasibility and Flexibility Analysis of Black-Box Processes Part 1: Surrogate-Based Feasibility Analysis. *Chemical Engineering Science* **2015**, *137*, 986–1004. https://doi.org/10.1016/J.CES.2015.06.014.

(154) Dias, L. S.; Ierapetritou, M. G. Integration of Planning, Scheduling and Control Problems Using Data-Driven Feasibility Analysis and Surrogate Models. *Computers & Chemical Engineering* **2020**, *134*, 106714. https://doi.org/10.1016/J.COMPCHEMENG.2019.106714.

(155) Badejo, O.; Ierapetritou, M. Integrating Tactical Planning, Operational Planning and Scheduling Using Data-Driven Feasibility Analysis. *Computers & Chemical Engineering* **2022**, *161*, 107759. https://doi.org/10.1016/J.COMPCHEMENG.2022.107759.

(156) Ding, C.; Ierapetritou, M. A Novel Framework of Surrogate-Based Feasibility Analysis for Establishing Design Space of Twin-Column Continuous Chromatography. *International Journal of Pharmaceutics* **2021**, *609*, 121161. https://doi.org/10.1016/J.IJPHARM.2021.121161.

(157) Zhang, D.; Del Rio-Chanona, E. A.; Petsagkourakis, P.; Wagner, J. Hybrid Physics-Based and Data-Driven Modeling for Bioprocess Online Simulation and Optimization. *Biotechnology and Bioengineering* **2019**, *116* (11), 2919–2930. https://doi.org/10.1002/BIT.27120.

(158) Boukouvala, F.; Floudas, C. A. ARGONAUT: AlgoRithms for Global Optimization of coNstrAined Grey-Box compUTational Problems. *Optimization Letters* **2017**, *11* (5), 895–913. https://doi.org/10.1007/S11590-016-1028-2/FIGURES/4.

(159) Tsay, C. Sobolev Trained Neural Network Surrogate Models for Optimization. *Computers & Chemical Engineering* **2021**, *153*, 107419. https://doi.org/10.1016/J.COMPCHEMENG.2021.107419.
(160) IEA. *Tracking Transport 2021*; IEA: Paris, 2021. https://www.iea.org/reports/tracking-transport-2021 (accessed 2022-06-03).
(161) Le Quéré, C.; Peters, G. P.; Friedlingstein, P.; Andrew, R. M.; Canadell, J. G.; Davis, S. J.; Jackson, R. B.; Jones, M. W. Fossil CO_2 Emissions in the Post-COVID-19 Era. *Nature Climate Change* **2021**, *11* (3), 197–199. https://doi.org/10.1038/s41558-021-01001-0.
(162) Reilly, J. M.; Chen, Y. H. H.; Jacoby, H. D. The COVID-19 Effect on the Paris Agreement. *Nature Humanities and Social Sciences Communications* **2021**, *8*, 1–4. https://doi.org/10.1057/s41599-020-00698-2.
(163) Istrate, I.; Iribarren, D.; Dufour, J.; Ortiz Cebolla, R.; Arrigoni, A.; Moretto, P.; Dolci, F. *Quantifying Emissions in the European Maritime Sector*; Joint Research Centre (JRC), European Commission, 2022. https://doi.org/10.2760/496363.
(164) IMO. *Fourth IMO GHG Study 2020*; International Maritime Organization: London, 2021.
(165) Rogelj, J.; Den Elzen, M.; Höhne, N.; Fransen, T.; Fekete, H.; Winkler, H.; Schaeffer, R.; Sha, F.; Riahi, K.; Meinshausen, M. Paris Agreement Climate Proposals Need a Boost to Keep Warming Well below 2 °C. *Nature* **2016**, *534*, 631–639. https://doi.org/10.1038/nature18307.
(166) Held, M.; Stolz, B.; Hoffmann, J.; Georges, G.; Bolla, M.; Boulouchos, K. Scrapping Probabilities and Committed CO_2 Emissions of the International Ship Fleet. In *The 7th International Symposium on Ship Operations, Management & Economics*; OnePetro: Virtual Event, 2021. https://doi.org/10.5957/SOME-2021-006.
(167) Brynolf, S.; Fridell, E.; Andersson, K. Environmental Assessment of Marine Fuels: Liquefied Natural Gas, Liquefied Biogas, Methanol and Bio-Methanol. *Journal of Cleaner Production* **2014**, *74*, 86–95. https://doi.org/10.1016/J.JCLEPRO.2014.03.052.
(168) IMO. *2014 Guidelines on the Method of Calculation of the Attained Energy Efficiency Design Index (EEDI) for New Ships*; International Maritime Organization, 2014.
(169) IMO. *2018 Guidelines on the Method of Calculation of the Attained Energy Efficiency Design Index (EEDI) for New Ships*; International Maritime Organization, 2018.
(170) IMO. *Initial IMO Strategy on Reduction of GHG Emissions from Ships*. https://www.imo.org/en/MediaCentre/HotTopics/Pages/Reducing-greenhouse-gas-emissions-from-ships.aspx (accessed 2022-06-09).
(171) European Commission. *Study on Methods and Considerations for the Determination of Greenhouse Gas Emission Reduction Targets for International Shipping*; UMAS, CE Delft, European Commission, Lloyd's Register, Öko-Institut e.V., 2019. https://doi.org/10.2834/651129.
(172) IMO. *Resolution MEPC.304(72)*; 2018.
(173) Kim, K.; Roh, G.; Kim, W.; Chun, K. A Preliminary Study on an Alternative Ship Propulsion System Fueled by Ammonia: Environmental and Economic Assessments. *Journal of Marine Science and Engineering* **2020**, *8* (3), 183. https://doi.org/10.3390/JMSE8030183.
(174) Horvath, S.; Fasihi, M.; Breyer, C. Techno-Economic Analysis of a Decarbonized Shipping Sector: Technology Suggestions for a Fleet in 2030 and 2040. *Energy Conversion and Management* **2018**, *164*, 230–241. https://doi.org/10.1016/J.ENCONMAN.2018.02.098.
(175) Korberg, A. D.; Brynolf, S.; Grahn, M.; Skov, I. R. Techno-Economic Assessment of Advanced Fuels and Propulsion Systems in Future Fossil-Free Ships. *Renewable and*

Sustainable Energy Reviews **2021**, *142*, 110861. https://doi.org/10.1016/J.RSER.2021.110861.

(176) Stolz, B.; Held, M.; Georges, G.; Boulouchos, K. Techno-Economic Analysis of Renewable Fuels for Ships Carrying Bulk Cargo in Europe. *Nature Energy* **2022**, *7*, 203–212. https://doi.org/10.1038/s41560-021-00957-9.

(177) Svanberg, M.; Ellis, J.; Lundgren, J.; Landälv, I. Renewable Methanol as a Fuel for the Shipping Industry. *Renewable and Sustainable Energy Reviews* **2018**, *94*, 1217–1228. https://doi.org/10.1016/J.RSER.2018.06.058.

(178) Van Hoecke, L.; Laffineur, L.; Campe, R.; Perreault, P.; Verbruggen, S. W.; Lenaerts, S. Challenges in the Use of Hydrogen for Maritime Applications. *Energy & Environmental Science* **2021**, *14* (2), 815–843. https://doi.org/10.1039/D0EE01545H.

(179) Foretich, A.; Zaimes, G. G.; Hawkins, T. R.; Newes, E. Challenges and Opportunities for Alternative Fuels in the Maritime Sector. *Maritime Transport Research* **2021**, *2*, 100033. https://doi.org/10.1016/J.MARTRA.2021.100033.

(180) Keith, D. W.; Holmes, G.; St. Angelo, D.; Heidel, K. A Process for Capturing CO2 from the Atmosphere. *Joule* **2018**, *2*, 1573–1594. https://doi.org/10.1016/j.joule.2018.05.006.

(181) Budinis, S.; Krevor, S.; Dowell, N. M.; Brandon, N.; Hawkes, A. An Assessment of CCS Costs, Barriers and Potential. *Energy Strategy Reviews* **2018**, *22* (August), 61–81. https://doi.org/10.1016/j.esr.2018.08.003.

(182) Brandl, P.; Bui, M.; Hallett, J. P.; Mac Dowell, N. Beyond 90% Capture: Possible, but at What Cost? *International Journal of Greenhouse Gas Control* **2021**, *105*, 103239. https://doi.org/10.1016/J.IJGGC.2020.103239.

(183) Awoyomi, A.; Patchigolla, K.; Anthony, E. J. CO_2/SO_2 Emission Reduction in CO_2 Shipping Infrastructure. *International Journal of Greenhouse Gas Control* **2019**, *88*, 57–70. https://doi.org/10.1016/J.IJGGC.2019.05.011.

(184) Awoyomi, A.; Patchigolla, K.; Anthony, E. J. Process and Economic Evaluation of an Onboard Capture System for LNG-Fueled CO_2 Carriers. *Industrial & Engineering Chemistry Research* **2020**, *59* (15), 6951–6960. https://doi.org/10.1021/ACS.IECR.9B04659.

(185) Luo, X.; Wang, M. Study of Solvent-Based Carbon Capture for Cargo Ships through Process Modelling and Simulation. *Applied Energy* **2017**, *195*, 402–413. https://doi.org/10.1016/J.APENERGY.2017.03.027.

(186) Zhou, P.; Wang, H. Carbon Capture and Storage—Solidification and Storage of Carbon Dioxide Captured on Ships. *Ocean Engineering* **2014**, *91*, 172–180. https://doi.org/10.1016/J.OCEANENG.2014.09.006.

(187) Al Baroudi, H.; Awoyomi, A.; Patchigolla, K.; Jonnalagadda, K.; Anthony, E. J. A Review of Large-Scale CO_2 Shipping and Marine Emissions Management for Carbon Capture, Utilisation and Storage. *Applied Energy* **2021**, *287*, 116510. https://doi.org/10.1016/J.APENERGY.2021.116510.

(188) Wang, H.; Zhou, P.; Wang, Z. Reviews on Current Carbon Emission Reduction Technologies and Projects and Their Feasibilities on Ships. *Journal of Marine Science and Application* **2017**, *16* (2), 129–136. https://doi.org/10.1007/S11804-017-1413-Y.

(189) Rockström, J.; Steffen, W.; Noone, K.; Persson, Å.; Chapin, F. S.; Lambin, E. F.; Lenton, T. M.; Scheffer, M.; Folke, C.; Schellnhuber, H. J.; Nykvist, B.; de Wit, C. A.; Hughes, T.; van der Leeuw, S.; Rodhe, H.; Sörlin, S.; Snyder, P. K.; Costanza, R.; Svedin, U.; Falkenmark, M.; Karlberg, L.; Corell, R. W.; Fabry, V. J.; Hansen, J.; Walker, B.; Liverman, D.; Richardson, K.; Crutzen, P.; Foley, J. A. A Safe Operating Space for Humanity. *Nature* **2009**, *461* (7263), 472–475. https://doi.org/10.1038/461472a.

(190) Wang, P.; Ryberg, M.; Yang, Y.; Feng, K.; Kara, S.; Hauschild, M.; Chen, W.-Q. Efficiency Stagnation in Global Steel Production Urges Joint Supply- and Demand-Side

Mitigation Efforts. *Nature Communications* **2021**, *12* (1), 1–11. https://doi.org/10.1038/s41467-021-22245-6.

(191) Valente, A.; Tulus, V.; Galán-Martín, Á.; Huijbregts, M. A. J.; Guillén-Gosálbez, G. The Role of Hydrogen in Heavy Transport to Operate within Planetary Boundaries. *Sustainable Energy & Fuels* **2021**. https://doi.org/10.1039/D1SE00790D.

(192) IEA. *Energy Technology Perspectives 2020*; International Energy Agency: Paris, 2020. www.iea.org/t&c/.

(193) Wärtsilä. *Encyclopedia of Marine and Energy Technology*. https://www.wartsila.com/encyclopedia (accessed 2022-06-10).

(194) Rodrigue, J.-P. *The Geography of Transport Systems*; 5, Ed.; Routledge, 2020. https://doi.org/10.4324/9780429346323.

(195) Global Combustion Systems. *Oil Fuel Properties*. http://www.globalcombustion.com/oil-fuel-properties/ (accessed 2022-06-09).

(196) *GUDRUN MAERSK, Container Ship - Details and current position - IMO 9302877 - VesselFinder*. https://www.vesselfinder.com/vessels/GUDRUN-MAERSK-IMO-9302877-MMSI-220379000 (accessed 2022-07-15).

(197) Guo, M.; Fu, Z.; Ma, D.; Ji, N.; Song, C.; Liu, Q. A Short Review of Treatment Methods of Marine Diesel Engine Exhaust Gases. *Procedia Engineering* **2015**, *121*, 938–943. https://doi.org/10.1016/J.PROENG.2015.09.059.

(198) Cau, G.; Tola, V.; Bassano, C. Performance Evaluation of High-Sulphur Coal-Fired USC Plant Integrated with SNOX and CO_2 Capture Sections. *Applied Thermal Engineering* **2015**, *74*, 136–145. https://doi.org/10.1016/J.APPLTHERMALENG.2014.03.027.

(199) Wang, M.; Lawal, A.; Stephenson, P.; Sidders, J.; Ramshaw, C. Post-Combustion CO_2 Capture with Chemical Absorption: A State-of-the-Art Review. *Chemical Engineering Research and Design* **2011**, *89* (9), 1609–1624. https://doi.org/10.1016/j.cherd.2010.11.005.

(200) Kazemifar, F. A Review of Technologies for Carbon Capture, Sequestration, and Utilization: Cost, Capacity, and Technology Readiness. *Greenhouse Gases: Science and Technology* **2021**. https://doi.org/10.1002/GHG.2131.

(201) Reyes-Lúa, A.; Arellano, Y.; Røe, I. T.; Rycroft, L.; Wildenborg, T.; Jordal, K. *CO_2 Ship Transport: Benefits for Early Movers and Aspects to Consider*; EU CCUS PROJECTS NETWORK (No ENER/C2/2017-65/SI2.793333), 2021; p 33.

(202) Pearson, A. Refrigeration with Ammonia. *International Journal of Refrigeration* **2008**, *31*, 545–551. https://doi.org/10.1016/J.IJREFRIG.2007.11.011.

(203) Luyben, W. L. Estimating Refrigeration Costs at Cryogenic Temperatures. *Computers & Chemical Engineering* **2017**, *103*, 144–150. https://doi.org/10.1016/J.COMPCHEMENG.2017.03.013.

(204) Linde GmbH. *Carbon Dioxide Safety advice*. www.linde-gas.com (accessed 2022-07-12).

(205) *TEU in Shipping*. https://www.marineinsight.com/maritime-law/teu-in-shipping-everything-you-wanted-to-know/ (accessed 2022-07-07).

(206) Towler, G.; Sinnott, R. K. *Chemical Engineering Design*; Elsevier Ltd, 2013. https://doi.org/10.1016/C2009-0-61216-2.

(207) *Wärtsilä - Enabling sustainable societies through innovation in technology and services*. https://www.wartsila.com/ (accessed 2022-06-13).

(208) ISO 14044. *Environmental Management - Life Cycle Assessment - Requirement and Guidelines*; Geneva, 2006.

(209) ISO 14040. *Enviromental Management - Life Cycle Assessment - Principles and Framework*; Geneva, 2006.

(210) Ryberg, M. W.; Owsianiak, M.; Richardson, K.; Hauschild, M. Z. Development of a Life-Cycle Impact Assessment Methodology Linked to the Planetary Boundaries Framework. *Ecological Indicators* **2018**, *88*, 250–262. https://doi.org/10.1016/j.ecolind.2017.12.065.
(211) Galán-Martín, Á.; Tulus, V.; Díaz, I.; Pozo, C.; Pérez-Ramírez, J.; Guillén-Gosálbez, G. Sustainability Footprints of a Renewable Carbon Transition for the Petrochemical Sector within Planetary Boundaries. *One Earth* **2021**, *4*, 565–583. https://doi.org/10.1016/J.ONEEAR.2021.04.001.
(212) Kearns;, D.; Liu;, H.; Consoli, C. *Technology Readiness and Costs of CCS*; Global CCS Institute, 2021.
(213) *Review of Maritime Transport 2019*; 2019; pp 57–80. https://doi.org/10.18356/990c6959-en.
(214) *Direct Air Capture Summit 2021*. https://www.youtube.com/watch?v=ZoMz7dmfitY&t=1039s (accessed 2022-07-26).
(215) Fuss, S.; Lamb, W. F.; Callaghan, M. W.; Hilaire, J.; Creutzig, F.; Amann, T.; Beringer, T.; De Oliveira Garcia, W.; Hartmann, J.; Khanna, T.; Luderer, G.; Nemet, G. F.; Rogelj, J.; Smith, P.; Vicente, J. V.; Wilcox, J.; Del Mar Zamora Dominguez, M.; Minx, J. C. Negative Emissions - Part 2: Costs, Potentials and Side Effects. *Environmental Research Letters* **2018**, *13* (6). https://doi.org/10.1088/1748-9326/aabf9f.
(216) Turan, G.; Zapantis, A. *Global Status of CCS 2021*; Global CCS Institute, 2021.
(217) Loria, P.; Bright, M. B. H. Lessons Captured from 50 Years of CCS Projects. *The Electricity Journal* **2021**, *34*, 106998. https://doi.org/10.1016/J.TEJ.2021.106998.
(218) Ryberg, M. W.; Andersen, M. M.; Owsianiak, M.; Hauschild, M. Z. Downscaling the Planetary Boundaries in Absolute Environmental Sustainability Assessments – A Review. *Journal of Cleaner Production* **2020**, *276*. https://doi.org/10.1016/j.jclepro.2020.123287.
(219) Häyhä, T.; Lucas, P. L.; van Vuuren, D. P.; Cornell, S. E.; Hoff, H. From Planetary Boundaries to National Fair Shares of the Global Safe Operating Space — How Can the Scales Be Bridged? *Global Environmental Change* **2016**, *40*, 60–72. https://doi.org/10.1016/j.gloenvcha.2016.06.008.
(220) OECD. *The Ocean Economy in 2030*; OECD Publishing Paris, Ed.; 2016.
(221) Bilgili, L. Comparative Assessment of Alternative Marine Fuels in Life Cycle Perspective. *Renewable and Sustainable Energy Reviews* **2021**, *144*, 110985. https://doi.org/10.1016/J.RSER.2021.110985.
(222) Watanabe, M. D. B.; Cherubini, F.; Cavalett, O. Climate Change Mitigation of Drop-in Biofuels for Deep-Sea Shipping under a Prospective Life-Cycle Assessment. *Journal of Cleaner Production* **2022**, *364*, 132662. https://doi.org/10.1016/J.JCLEPRO.2022.132662.
(223) Mukherjee, A.; Bruijnincx, P.; Junginger, M. A Perspective on Biofuels Use and CCS for GHG Mitigation in the Marine Sector. *iScience* **2020**, *23*, 101758. https://doi.org/10.1016/J.ISCI.2020.101758.
(224) Deniz, C.; Zincir, B. Environmental and Economical Assessment of Alternative Marine Fuels. *Journal of Cleaner Production* **2016**, *113*, 438–449. https://doi.org/10.1016/J.JCLEPRO.2015.11.089.
(225) Ampah, J. D.; Yusuf, A. A.; Afrane, S.; Jin, C.; Liu, H. Reviewing Two Decades of Cleaner Alternative Marine Fuels: Towards IMO's Decarbonization of the Maritime Transport Sector. *Journal of Cleaner Production* **2021**, *320*, 128871. https://doi.org/10.1016/J.JCLEPRO.2021.128871.
(226) IMO. *Third IMO GHG Study 2014*; 2015. www.imo.org (accessed 2022-07-17).

(227) European Council. *Where does the EU's gas come from?* https://www.consilium.europa.eu/en/infographics/eu-gas-supply/ (accessed 2023-05-02).
(228) Pastore, L. M.; Lo Basso, G.; de Santoli, L. Towards a Dramatic Reduction in the European Natural Gas Consumption: Italy as a Case Study. *Journal of Cleaner Production* **2022**, *369*, 133377. https://doi.org/10.1016/j.jclepro.2022.133377.
(229) European Commission. *REPowerEU: affordable, secure and sustainable energy for Europe*. https://commission.europa.eu/strategy-and-policy/priorities-2019-2024/european-green-deal/repowereu-affordable-secure-and-sustainable-energy-europe_en (accessed 2023-05-02).
(230) Pedersen, T. T.; Gøtske, E. K.; Dvorak, A.; Andresen, G. B.; Victoria, M. Long-Term Implications of Reduced Gas Imports on the Decarbonization of the European Energy System. *Joule* **2022**, *6* (7), 1566–1580. https://doi.org/10.1016/j.joule.2022.06.023.
(231) Kemfert, C.; Präger, F.; Braunger, I.; Hoffart, F. M.; Brauers, H. The Expansion of Natural Gas Infrastructure Puts Energy Transitions at Risk. *Nat Energy* **2022**, *7* (7), 582–587. https://doi.org/10.1038/s41560-022-01060-3.
(232) Rosa, L.; Sanchez, D. L.; Mazzotti, M. Assessment of Carbon Dioxide Removal Potential *via* BECCS in a Carbon-Neutral Europe. *Energy Environ. Sci.* **2021**, *14* (5), 3086–3097. https://doi.org/10.1039/D1EE00642H.
(233) Scarlat, N.; Dallemand, J.-F.; Fahl, F. Biogas: Developments and Perspectives in Europe. *Renewable Energy* **2018**, *129*, 457–472. https://doi.org/10.1016/j.renene.2018.03.006.
(234) Alberici, S.; Moultak, M.; Peters, J. *The Future Role of Biomethane*; Guidehouse, 2021.
(235) Alberici, S.; Grimme, W.; Toop, G. *Biomethane Production Potentials in the EU - Feasibility of REPowerEU 2030 Targets, Production Potentials in the Member States and Outlook to 2050 - A Gas for Climate Report*; 2022. https://www.europeanbiogas.eu/wp-content/uploads/2022/07/GfC_national-biomethane-potentials_070722.pdf (accessed 2022-07-25).
(236) Hamelin, L.; Møller, H. B.; Jørgensen, U. Harnessing the Full Potential of Biomethane towards Tomorrow's Bioeconomy: A National Case Study Coupling Sustainable Agricultural Intensification, Emerging Biogas Technologies and Energy System Analysis. *Renewable and Sustainable Energy Reviews* **2021**, *138*, 110506. https://doi.org/10.1016/j.rser.2020.110506.
(237) Liu, B.; Rajagopal, D. Life-Cycle Energy and Climate Benefits of Energy Recovery from Wastes and Biomass Residues in the United States. *Nat Energy* **2019**, *4* (8), 700–708. https://doi.org/10.1038/s41560-019-0430-2.
(238) He, J.; Göransson, K.; Söderlind, U.; Zhang, W. Simulation of Biomass Gasification in a Dual Fluidized Bed Gasifier. *Biomass Conv. Bioref.* **2012**, *2* (1), 1–10. https://doi.org/10.1007/s13399-011-0030-2.
(239) Miccio, F.; Ruoppolo, G.; Kalisz, S.; Andersen, L.; Morgan, T. J.; Baxter, D. Combined Gasification of Coal and Biomass in Internal Circulating Fluidized Bed. *Fuel Processing Technology* **2012**, *95*, 45–54. https://doi.org/10.1016/j.fuproc.2011.11.008.
(240) Doherty, W.; Reynolds, A.; Kennedy, D. Aspen Plus Simulation of Biomass Gasification in a Steam Blown Dual Fluidised Bed. In *Materials and processes for energy: communicating current research and technological developments*; A. Méndez-Vilas (Ed.), 2013.
(241) Rauch, R.; Hrbek, J.; Hofbauer, H. Biomass Gasification for Synthesis Gas Production and Applications of the Syngas. *Wiley Interdisciplinary Reviews: Energy and Environment* **2014**, *3* (4), 343–362. https://doi.org/10.1002/wene.97.

(242) Pala, L. P. R.; Wang, Q.; Kolb, G.; Hessel, V. Steam Gasification of Biomass with Subsequent Syngas Adjustment Using Shift Reaction for Syngas Production: An Aspen Plus Model. *Renewable Energy* **2017**, *101*, 484–492. https://doi.org/10.1016/j.renene.2016.08.069.
(243) Aghaalikhani, A.; Schmid, J. C.; Borello, D.; Fuchs, J.; Benedikt, F.; Hofbauer, H.; Rispoli, F.; Henriksen, U. B.; Sárossy, Z.; Cedola, L. Detailed Modelling of Biomass Steam Gasification in a Dual Fluidized Bed Gasifier with Temperature Variation. *Renewable Energy* **2019**, *143*, 703–718. https://doi.org/10.1016/j.renene.2019.05.022.
(244) Ren, J.; Liu, Y. L.; Zhao, X. Y.; Cao, J. P. Methanation of Syngas from Biomass Gasification: An Overview. *International Journal of Hydrogen Energy* **2020**, *45* (7), 4223–4243. https://doi.org/10.1016/j.ijhydene.2019.12.023.
(245) Mutlu, Ö. Ç.; Zeng, T. Challenges and Opportunities of Modeling Biomass Gasification in Aspen Plus: A Review. *Chemical Engineering and Technology* **2020**, *43* (9), 1674–1689. https://doi.org/10.1002/ceat.202000068.
(246) Pilar González-Vázquez, M.; Rubiera, F.; Pevida, C.; Pio, D. T.; Tarelho, L. A. C. Thermodynamic Analysis of Biomass Gasification Using Aspen Plus: Comparison of Stoichiometric and Non-Stoichiometric Models. *Energies* **2021**, *14* (1), 189. https://doi.org/10.3390/en14010189.
(247) Skorek-Osikowska, A.; Martín-Gamboa, M.; Dufour, J. Thermodynamic, Economic and Environmental Assessment of Renewable Natural Gas Production Systems. *Energy Conversion and Management: X* **2020**, *7*, 100046.
(248) Bargiacchi, E.; Candelaresi, D.; Valente, A.; Frigo, S.; Spazzafumo, G. Life Cycle Assessment of Substitute Natural Gas Production from Biomass and Electrolytic Hydrogen. *International Journal of Hydrogen Energy* **2021**. https://doi.org/10.1016/j.ijhydene.2021.01.033.
(249) Frigo, S.; Spazzafumo, G. Comparison of Different System Layouts to Generate a Substitute of Natural Gas from Biomass and Electrolytic Hydrogen. *International Journal of Hydrogen Energy* **2020**, *45* (49), 26166–26178. https://doi.org/10.1016/j.ijhydene.2020.03.205.
(250) Yao, D.; Xu, Z.; Qi, H.; Zhu, Z.; Gao, J.; Wang, Y.; Cui, P. Carbon Footprint and Water Footprint Analysis of Generating Synthetic Natural Gas from Biomass. *Renewable Energy* **2022**, *186*, 780–789. https://doi.org/10.1016/j.renene.2022.01.014.
(251) Lodato, C.; Hamelin, L.; Tonini, D.; Astrup, T. F. Towards Sustainable Methane Supply from Local Bioresources: Anaerobic Digestion, Gasification, and Gas Upgrading. *Applied Energy* **2022**, *323*, 119568. https://doi.org/10.1016/j.apenergy.2022.119568.
(252) Alberici, S.; Grimme, W.; Toop, G. *Biomethane Production Potentials in the EU*; Guidehouse, 2022. https://gasforclimate2050.eu/ (accessed 2022-09-19).
(253) Galán-Martín, Á.; Vázquez, D.; Cobo, S.; Dowell, N. M.; Caballero, J. A.; Guillén-Gosálbez, G. Delaying Carbon Dioxide Removal in the European Union Puts Climate Targets at Risk. *Nature Communications* **2021**, *12*, 6490. https://doi.org/10.1038/s41467-021-26680-3.
(254) Negri, V.; Galán-Martín, Á.; Pozo, C.; Fajardy, M.; Reiner, D. M.; Mac Dowell, N.; Guillén-Gosálbez, G. Life Cycle Optimization of BECCS Supply Chains in the European Union. *Applied Energy* **2021**, *298*, 117252. https://doi.org/10.1016/J.APENERGY.2021.117252.
(255) Zampori, L.; Pant, R. *Suggestions for Updating the Product Environmental Footprint (PEF) Method*; European Commission, 2019. https://eplca.jrc.ec.europa.eu/permalink/PEF_method.pdf (accessed 2023-09-07).
(256) Fuss, S.; Canadell, J. G.; Peters, G. P.; Tavoni, M.; Andrew, R. M.; Ciais, P.; Jackson, R. B.; Jones, C. D.; Kraxner, F.; Nakicenovic, N.; Le Quéré, C.; Raupach, M. R.; Sharifi,

A.; Smith, P.; Yamagata, Y. Betting on Negative Emissions. *Nature Climate Change* **2014**, *4*, 850–853. https://doi.org/10.1038/nclimate2392.

(257) Jones, C. D.; Ciais, P.; Davis, S. J.; Friedlingstein, P.; Gasser, T.; Peters, G. P.; Rogelj, J.; van Vuuren, D. . P.; Canadell, J. . G.; Cowie, A.; Jackson, R. B.; Jonas, M.; Kriegler, E.; Littleton, E.; Lowe, J. . A. .; Milne, J.; Shrestha, G.; Smith, P.; Torvanger, A.; Wiltshire, A. Simulating the Earth System Response to Negative Emissions. *Environmental Research Letters* **2016**, *11*. https://doi.org/10.1088/1748-9326/11/9/095012.

(258) Lomax, G.; Lenton, T. M.; Adeosun, A.; Workman, M. Investing in Negative Emissions. *Nature Climate Change* **2015**, *5* (6), 498–500. https://doi.org/10.1038/nclimate2627.

(259) Calvo-Serrano, R.; Guo, M.; Pozo, C.; Galán-Martín, Á.; Guillén-Gosálbez, G. Biomass Conversion into Fuels, Chemicals, or Electricity? A Network-Based Life Cycle Optimization Approach Applied to the European Union. *ACS Sustainable Chemistry and Engineering* **2019**, *7* (12), 10570–10582. https://doi.org/10.1021/acssuschemeng.9b01115.

(260) Kalinci, Y.; Hepbasli, A.; Dincer, I. Biomass-Based Hydrogen Production: A Review and Analysis. *International Journal of Hydrogen Energy* **2009**, *34* (21), 8799–8817. https://doi.org/10.1016/j.ijhydene.2009.08.078.

(261) Mendiara, T.; García-Labiano, F.; Abad, A.; Gayán, P.; de Diego, L. F.; Izquierdo, M. T.; Adánez, J. Negative CO_2 Emissions through the Use of Biofuels in Chemical Looping Technology: A Review. *Applied Energy* **2018**, *232*, 657–684. https://doi.org/10.1016/j.apenergy.2018.09.201.

(262) Bhave, A.; Taylor, R. H. S.; Fennell, P.; Livingston, W. R.; Shah, N.; Dowell, N. Mac; Dennis, J.; Kraft, M.; Pourkashanian, M.; Insa, M.; Jones, J.; Burdett, N.; Bauen, A.; Beal, C.; Smallbone, A.; Akroyd, J. Screening and Techno-Economic Assessment of Biomass-Based Power Generation with CCS Technologies to Meet 2050 CO2 Targets. *Applied Energy* **2017**, *190*, 481–489. https://doi.org/10.1016/j.apenergy.2016.12.120.

(263) Tanzer, S. E.; Ramírez, A. When Are Negative Emissions Negative Emissions? *Energy and Environmental Science* **2019**, *12* (4), 1210–1218. https://doi.org/10.1039/c8ee03338b.

(264) Canadell, J. G.; Schulze, E. D. Global Potential of Biospheric Carbon Management for Climate Mitigation. *Nature Communications* **2014**, *5* (1), 1–12. https://doi.org/10.1038/ncomms6282.

(265) McGlashan, N.; Shah, N.; Caldecott, B.; Workman, M. High-Level Techno-Economic Assessment of Negative Emissions Technologies. *Process Safety and Environmental Protection* **2012**, *90* (6), 501–510. https://doi.org/10.1016/j.psep.2012.10.004.

(266) Searchinger, T.; Heimlich, R. *Avoiding Bioenergy Competition for Food Crops and Land*; World resources institute, 2015. http://www.worldresourcesreport.org.

(267) Fridahl, M.; Lehtveer, M. Bioenergy with Carbon Capture and Storage (BECCS): Global Potential, Investment Preferences, and Deployment Barriers. *Energy Research and Social Science* **2018**, *42*, 155–165. https://doi.org/10.1016/j.erss.2018.03.019.

(268) European Commission. *The European Green Deal*; European Commission, 2019. https://eur-lex.europa.eu/legal-content/EN/TXT/PDF/?uri=CELEX:52019DC0640.

(269) *Circular Economy Action Plan*.

(270) Daggash, H. A.; Mac Dowell, N. Higher Carbon Prices on Emissions Alone Will Not Deliver the Paris Agreement. *Joule* **2019**, *3* (9), 2120–2133. https://doi.org/10.1016/j.joule.2019.08.008.

(271) Ricci, O. Providing Adequate Economic Incentives for Bioenergies with CO 2 Capture and Geological Storage. *Energy Policy* **2012**, *44*, 362–373. https://doi.org/10.1016/j.enpol.2012.01.066.

(272) Bellamy, R. Incentivize Negative Emissions Responsibly. *Nature Energy* **2018**, *3* (7), 532–534. https://doi.org/10.1038/s41560-018-0156-6.
(273) *Nationally Determined Contributions (NDCs) | UNFCCC*. https://unfccc.int/process-and-meetings/the-paris-agreement/the-paris-agreement/nationally-determined-contributions-ndcs.
(274) Sanchez, D. L.; Callaway, D. S. Optimal Scale of Carbon-Negative Energy Facilities. *Applied Energy* **2016**, *170*, 437–444. https://doi.org/10.1016/j.apenergy.2016.02.134.
(275) Dowell, N. M.; Fajardy, M. Inefficient Power Generation as an Optimal Route to Negative Emissions via BECCS? *Environmental Research Letters* **2017**, *12*. https://doi.org/10.1088/1748-9326/aa67a5.
(276) Daggash, H. A.; Mac Dowell, N. The Implications of Delivering the UK's Paris Agreement Commitments on the Power Sector. *International Journal of Greenhouse Gas Control* **2019**, *85*, 174–181. https://doi.org/10.1016/j.ijggc.2019.04.007.
(277) Ghaderi, H.; Pishvaee, M. S.; Moini, A. Biomass Supply Chain Network Design: An Optimization-Oriented Review and Analysis. *Industrial Crops and Products* **2016**, *94*, 972–1000. https://doi.org/10.1016/j.indcrop.2016.09.027.
(278) Patrizio, P.; Leduc, S.; Kraxner, F.; Fuss, S.; Kindermann, G.; Mesfun, S.; Spokas, K.; Mendoza, A.; Mac Dowell, N.; Wetterlund, E.; Lundgren, J.; Dotzauer, E.; Yowargana, P.; Obersteiner, M. Reducing US Coal Emissions Can Boost Employment. *Joule* **2018**, *2* (12), 2633–2648. https://doi.org/10.1016/j.joule.2018.10.004.
(279) *SimaPro | The world's leading LCA software*. https://simapro.com/.
(280) *ecoinvent*. https://www.ecoinvent.org/.
(281) Hauschild, M. Z.; Huijbregts, M. A. J. Introducing Life Cycle Impact Assessment; Springer, Dordrecht, 2015; pp 1–16. https://doi.org/10.1007/978-94-017-9744-3_1.
(282) Wiesenthal, T.; Mourelatou, A.; Petersen, J. E.; Taylor, P. How Much Bioenergy Can Europe Produce without Harming the Environment? *Eea* **2006**, *No. 7* (7).
(283) Wildbolz, C. Life Cycle Assessment of Selected Technologies for CO_2 Transport and Sequestration, Swiss Federal Institute of Technology Zurich, 2007.
(284) *Electricity and heat statistics*. https://ec.europa.eu/eurostat/statistics-explained/index.php/Electricity_and_heat_statistics#Consumption_of_electricity_and_derived_heat (accessed 2020-10-21).
(285) Shen, W.; Chen, X.; Qiu, J.; Hayward, J. A.; Sayeef, S.; Osman, P.; Meng, K.; Dong, Z. Y. A Comprehensive Review of Variable Renewable Energy Levelized Cost of Electricity. *Renewable and Sustainable Energy Reviews* **2020**, *133*, 110301. https://doi.org/10.1016/j.rser.2020.110301.
(286) Popp, A.; Rose, S. K.; Calvin, K.; Van Vuuren, D. P.; Dietrich, J. P.; Wise, M.; Stehfest, E.; Humpenöder, F.; Kyle, P.; Van Vliet, J.; Bauer, N.; Lotze-Campen, H.; Klein, D.; Kriegler, E. Land-Use Transition for Bioenergy and Climate Stabilization: Model Comparison of Drivers, Impacts and Interactions with Other Land Use Based Mitigation Options. *Climatic Change* **2014**, *123* (3–4), 495–509. https://doi.org/10.1007/s10584-013-0926-x.
(287) Meckling, J.; Sterner, T.; Wagner, G. Policy Sequencing toward Decarbonization. *Nat Energy* **2017**, *2* (12), 918–922. https://doi.org/10.1038/s41560-017-0025-8.
(288) Schenuit, F.; Colvin, R.; Fridahl, M.; McMullin, B.; Reisinger, A.; Sanchez, D. L.; Smith, S. M.; Torvanger, A.; Wreford, A.; Geden, O. Carbon Dioxide Removal Policy in the Making: Assessing Developments in 9 OECD Cases. *Frontiers in Climate* **2021**, *3*.
(289) Victoria, M.; Zhu, K.; Brown, T.; Andresen, G. B.; Greiner, M. Early Decarbonisation of the European Energy System Pays Off. *Nat Commun* **2020**, *11* (1), 6223. https://doi.org/10.1038/s41467-020-20015-4.

(290) Solano Rodriguez, B.; Drummond, P.; Ekins, P. Decarbonizing the EU Energy System by 2050: An Important Role for BECCS. *Climate Policy* **2017**, *17* (sup1), S93–S110. https://doi.org/10.1080/14693062.2016.1242058.
(291) Realmonte, G.; Drouet, L.; Gambhir, A.; Glynn, J.; Hawkes, A.; Köberle, A. C.; Tavoni, M. An Inter-Model Assessment of the Role of Direct Air Capture in Deep Mitigation Pathways. *Nat Commun* **2019**, *10* (1), 3277. https://doi.org/10.1038/s41467-019-10842-5.
(292) Doukas, H.; Nikas, A.; González-Eguino, M.; Arto, I.; Anger-Kraavi, A. From Integrated to Integrative: Delivering on the Paris Agreement. *Sustainability* **2018**, *10* (7), 2299. https://doi.org/10.3390/su10072299.
(293) Bistline, J. E. T.; Blanford, G. J. Impact of Carbon Dioxide Removal Technologies on Deep Decarbonization of the Electric Power Sector. *Nature Communications 2021 12:1* **2021**, *12* (1), 1–12. https://doi.org/10.1038/s41467-021-23554-6.
(294) Creutzig, F.; Breyer, C.; Hilaire, J.; Minx, J.; Peters, G. P.; Socolow, R. The Mutual Dependence of Negative Emission Technologies and Energy Systems. *Energy and Environmental Science* **2019**, *12* (6), 1805–1817. https://doi.org/10.1039/c8ee03682a.
(295) Prado, A.; Chiquier, S.; Fajardy, M.; Mac Dowell, N. Assessing the Impact of Carbon Dioxide Removal on the Power System. *iScience* **2023**, *26* (4), 106303. https://doi.org/10.1016/j.isci.2023.106303.
(296) Sagues, W. J.; Park, S.; Jameel, H.; Sanchez, D. L. Enhanced Carbon Dioxide Removal from Coupled Direct Air Capture-Bioenergy Systems. *Sustainable Energy and Fuels* **2019**, *3* (11), 3135–3146. https://doi.org/10.1039/c9se00384c.
(297) Rathi, T.; Zhang, Q. Capacity Planning with Uncertain Endogenous Technology Learning. *Computers & Chemical Engineering* **2022**, *164*, 107868. https://doi.org/10.1016/J.COMPCHEMENG.2022.107868.
(298) Fajardy, M.; Patrizio, P.; Daggash, H. A.; Mac Dowell, N. Negative Emissions: Priorities for Research and Policy Design. *Frontiers in Climate* **2019**, *1* (6), 6. https://doi.org/10.3389/fclim.2019.00006.
(299) Chen, Z.; Avraamidou, S.; Liu, P.; Li, Z.; Ni, W.; Pistikopoulos, E. N. Optimal Design of Integrated Urban Energy Systems under Uncertainty and Sustainability Requirements. *Computers & Chemical Engineering* **2021**, *155*, 107502. https://doi.org/10.1016/j.compchemeng.2021.107502.
(300) Li, C.; Grossmann, I. E. A Review of Stochastic Programming Methods for Optimization of Process Systems Under Uncertainty. *Frontiers in Chemical Engineering* **2021**, *0*, 34. https://doi.org/10.3389/FCENG.2020.622241.
(301) Bevan, L. D. The Ambiguities of Uncertainty: A Review of Uncertainty Frameworks Relevant to the Assessment of Environmental Change. *Futures* **2022**, *137*, 102919. https://doi.org/10.1016/j.futures.2022.102919.
(302) Hasan, M. M. F.; Zantye, M. S.; Kazi, M. K. Challenges and Opportunities in Carbon Capture, Utilization and Storage: A Process Systems Engineering Perspective. *Computers & Chemical Engineering* **2022**, *166*, 107925. https://doi.org/10.1016/j.compchemeng.2022.107925.
(303) Weidner, T.; Galán-Martín, Á.; Ryberg, M. W.; Guillén-Gosálbez, G. Energy Systems Modeling and Optimization for Absolute Environmental Sustainability: Current Landscape and Opportunities. *Computers & Chemical Engineering* **2022**, *164*, 107883. https://doi.org/10.1016/J.COMPCHEMENG.2022.107883.
(304) Chen, X.; Wu, X. The Roles of Carbon Capture, Utilization and Storage in the Transition to a Low-Carbon Energy System Using a Stochastic Optimal Scheduling Approach. *Journal of Cleaner Production* **2022**, *366*, 132860. https://doi.org/10.1016/j.jclepro.2022.132860.

(305) Giannousakis, A.; Hilaire, J.; Nemet, G. F.; Luderer, G.; Pietzcker, R. C.; Rodrigues, R.; Baumstark, L.; Kriegler, E. How Uncertainty in Technology Costs and Carbon Dioxide Removal Availability Affect Climate Mitigation Pathways. *Energy* **2021**, *216*, 119253. https://doi.org/10.1016/j.energy.2020.119253.

(306) Shepherd, A.; Martin, M.; Hastings, A. Uncertainty of Modelled Bioenergy with Carbon Capture and Storage Due to Variability of Input Data. *GCB Bioenergy* **2021**, *13* (4), 691–707. https://doi.org/10.1111/gcbb.12803.

(307) Grant, N.; Hawkes, A.; Mittal, S.; Gambhir, A. The Policy Implications of an Uncertain Carbon Dioxide Removal Potential. *Joule* **2021**, *5* (10), 2593–2605. https://doi.org/10.1016/J.JOULE.2021.09.004.

(308) Bahl, B.; Lützow, J.; Shu, D.; Hollermann, D. E.; Lampe, M.; Hennen, M.; Bardow, A. Rigorous Synthesis of Energy Systems by Decomposition via Time-Series Aggregation. *Computers & Chemical Engineering* **2018**, *112*, 70–81. https://doi.org/10.1016/j.compchemeng.2018.01.023.

(309) Teichgraeber, H.; Küpper, L. E.; Brandt, A. R. Designing Reliable Future Energy Systems by Iteratively Including Extreme Periods in Time-Series Aggregation. *Applied Energy* **2021**, *304*, 117696. https://doi.org/10.1016/j.apenergy.2021.117696.

(310) Ioannou, I.; Grossmann, I.; Guillén-Gosálbez, G. Life Cycle Optimization of Power Generation and Transmission Expansion Planning. In *Foundations of Computer-Aided Process Operations*; 2023.

(311) Apap, R. M.; Grossmann, I. E. Models and Computational Strategies for Multistage Stochastic Programming under Endogenous and Exogenous Uncertainties. *Computers & Chemical Engineering* **2017**, *103*, 233–274. https://doi.org/10.1016/J.COMPCHEMENG.2016.11.011.

(312) Balasubramanian, J.; Grossmann, I. E. Approximation to Multistage Stochastic Optimization in Multiperiod Batch Plant Scheduling under Demand Uncertainty. *Industrial & Engineering Chemistry Research* **2004**, *43*, 3695–3713. https://doi.org/10.1021/IE030308.

(313) Fusco, A.; Gioffrè, D.; Francesco Castelli, A.; Bovo, C.; Martelli, E. A Multi-Stage Stochastic Programming Model for the Unit Commitment of Conventional and Virtual Power Plants Bidding in the Day-Ahead and Ancillary Services Markets. *Applied Energy* **2023**, *336*, 120739. https://doi.org/10.1016/j.apenergy.2023.120739.

(314) Lee, J.; Bae, S.; Kim, W. C.; Lee, Y. Value Function Gradient Learning for Large-Scale Multistage Stochastic Programming Problems. *European Journal of Operational Research* **2023**, *308* (1), 321–335. https://doi.org/10.1016/j.ejor.2022.10.011.

(315) Meersman, T.; Maenhout, B.; Van Herck, K. A Nested Benders Decomposition-Based Algorithm to Solve the Three-Stage Stochastic Optimisation Problem Modeling Population-Based Breast Cancer Screening. *European Journal of Operational Research* **2023**, *310* (3), 1273–1293. https://doi.org/10.1016/j.ejor.2023.04.027.

(316) Amusat, O. O.; Shearing, P. R.; Fraga, E. S. On the Design of Complex Energy Systems: Accounting for Renewables Variability in Systems Sizing. *Computers & Chemical Engineering* **2017**, *103*, 103–115. https://doi.org/10.1016/j.compchemeng.2017.03.010.

(317) Kämper, A.; Delorme, R.; Leenders, L.; Bardow, A. Boosting Operational Optimization of Multi-Energy Systems by Artificial Neural Nets. *Computers & Chemical Engineering* **2023**, *173*, 108208. https://doi.org/10.1016/j.compchemeng.2023.108208.

(318) Iyer, G.; Hultman, N.; Eom, J.; McJeon, H.; Patel, P.; Clarke, L. Diffusion of Low-Carbon Technologies and the Feasibility of Long-Term Climate Targets. *Technological Forecasting and Social Change* **2015**, *90*, 103–118. https://doi.org/10.1016/j.techfore.2013.08.025.

(319) Guillén-Gosálbez, G.; Mele, F. D.; Grossmann, I. E. A Bi-Criterion Optimization Approach for the Design and Planning of Hydrogen Supply Chains for Vehicle Use. *AIChE Journal* **2010**, *56* (3), 650–667. https://doi.org/10.1002/AIC.12024.
(320) Sahinidis, N. V.; Grossmann, I. E.; Fornari, R. E.; Chathrathi, M. Optimization Model for Long Range Planning in the Chemical Industry. *Computers & Chemical Engineering* **1989**, *13* (9), 1049–1063. https://doi.org/10.1016/0098-1354(89)87046-2.
(321) Gupta, V.; Grossmann, I. E. Solution Strategies for Multistage Stochastic Programming with Endogenous Uncertainties. *Computers & Chemical Engineering* **2011**, *35* (11), 2235–2247. https://doi.org/10.1016/J.COMPCHEMENG.2010.11.013.
(322) Grossmann, I. E.; Apap, R. M.; Calfa, B. A.; García-Herreros, P.; Zhang, Q. Recent Advances in Mathematical Programming Techniques for the Optimization of Process Systems under Uncertainty. *Computers & Chemical Engineering* **2016**, *91*, 3–14. https://doi.org/10.1016/j.compchemeng.2016.03.002.
(323) Birge, J. R.; Louveaux, F. *Introduction to Stochastic Programming*; Springer Science & Business Media, 2011.
(324) Li, P.; Arellano-Garcia, H.; Wozny, G. Chance Constrained Programming Approach to Process Optimization under Uncertainty. *Computers and Chemical Engineering* **2008**, *32* (1–2), 25–45. https://doi.org/10.1016/j.compchemeng.2007.05.009.
(325) Lappas, N. H.; Gounaris, C. E. Multi-Stage Adjustable Robust Optimization for Process Scheduling under Uncertainty. *AIChE Journal* **2016**, *62* (5), 1646–1667. https://doi.org/10.1002/aic.15183.
(326) Shapiro, A. Tutorial on Risk Neutral, Distributionally Robust and Risk Averse Multistage Stochastic Programming. *European Journal of Operational Research* **2021**, *288* (1), 1–13. https://doi.org/10.1016/j.ejor.2020.03.065.
(327) Ruszczyński, A. Decomposition Methods in Stochastic Programming. *Mathematical Programming* **1997**, *79* (1), 333–353. https://doi.org/10.1007/BF02614323.
(328) Uribe-Rodríguez, A.; Castro, P. M.; Guillén-Gosálbez, G.; Chachuat, B. Assessment of Lagrangean Decomposition for Short-Term Planning of Integrated Refinery-Petrochemical Operations. *Computers & Chemical Engineering* **2023**, *174*, 108229. https://doi.org/10.1016/j.compchemeng.2023.108229.
(329) Kleywegt, A. J.; Shapiro, A.; Homem-de-Mello, T. The Sample Average Approximation Method for Stochastic Discrete Optimization. *SIAM J. Optim.* **2002**, *12* (2), 479–502. https://doi.org/10.1137/S1052623499363220.
(330) Ehrenstein, M.; Wang, C. H.; Guillén-Gosálbez, G. Strategic Planning of Supply Chains Considering Extreme Events: Novel Heuristic and Application to the Petrochemical Industry. *Computers & Chemical Engineering* **2019**, *125*, 306–323. https://doi.org/10.1016/J.COMPCHEMENG.2019.03.020.
(331) Escudero, L. F.; Garín, A.; Merino, M.; Pérez, G. The Value of the Stochastic Solution in Multistage Problems. *TOP* **2007**, *15* (1), 48–64. https://doi.org/10.1007/s11750-007-0005-4.
(332) Statista. *EU-27: energy sector GHG emission shares*. Statista. https://www.statista.com/statistics/1000061/ghg-emissions-sources-energy-sector-european-union-eu/ (accessed 2023-07-05).
(333) Safari, M.; Ghanizadeh, A.; Montazer-Rahmati, M. M. Optimization of Membrane-Based CO_2-Removal from Natural Gas Using Simple Models Considering Both Pressure and Temperature Effects. *International Journal of Greenhouse Gas Control* **2009**, *3*, 3–10. https://doi.org/10.1016/j.ijggc.2008.05.001.
(334) Qi, R.; Henson, M. A. Optimization-Based Design of Spiral-Wound Membrane Systems for CO_2-CH_4 Separations. *Separation and Purification Technology* **1998**, *13* (3), 209–225. https://doi.org/10.1016/S1383-5866(98)00044-6.

(335) Zhang, Y.; Chen, C.-C. Modeling CO_2 Absorption and Desorption by Aqueous Monoethanolamine Solution with Aspen Rate-Based Model. In *Energy Procedia*; Elsevier, 2013; Vol. 37, pp 1584–1596. https://doi.org/10.1016/J.EGYPRO.2013.06.034.
(336) Trinh, C.; Meimaroglou, D.; Hoppe, S. Machine Learning in Chemical Product Engineering: The State of the Art and a Guide for Newcomers. *Processes* **2021**, *9* (8), 1456. https://doi.org/10.3390/PR9081456.
(337) Feng, L.; Zhao, C.; Sun, Y. Dual Attention-Based Encoder-Decoder: A Customized Sequence-to-Sequence Learning for Soft Sensor Development. *IEEE Transactions on Neural Networks and Learning Systems* **2021**, *32* (8), 3306–3317. https://doi.org/10.1109/TNNLS.2020.3015929.
(338) Chai, Z.; Zhao, C.; Huang, B. Variational Progressive-Transfer Network for Soft Sensing of Multirate Industrial Processes. *IEEE Transactions on Cybernetics* **2021**. https://doi.org/10.1109/TCYB.2021.3090996.
(339) Qin, Y.; Zhao, C.; Huang, B. A New Soft-Sensor Algorithm with Concurrent Consideration of Slowness and Quality Interpretation for Dynamic Chemical Process. *Chemical Engineering Science* **2019**, *199*, 28–39. https://doi.org/10.1016/J.CES.2019.01.011.
(340) Bongard, J.; Lipson, H. Automated Reverse Engineering of Nonlinear Dynamical Systems. *Proceedings of the National Academy of Sciences of the United States of America* **2007**, *104* (24), 9943–9948. https://doi.org/10.1073/PNAS.0609476104/SUPPL_FILE/09476FIG4.PDF.
(341) *MATLAB - MathWorks*. https://ch.mathworks.com/products/matlab.html.
(342) Wärtsilä Encyclopedia of Marine and Energy Technology. *Exhaust gas emissions from ships*. https://www.wartsila.com/encyclopedia/term/exhaust-gas-emissions-from-ships (accessed 2022-06-09).
(343) *Emissions from Continuous Combustion Systems*; Cornelius, W.; Agnew, W. G., Ed.; Springer, 1972. https://doi.org/10.1007/978-1-4684-1998-6/COVER.
(344) Turton, R.; Shaeiwitz, J. A.; Bhattacharyya, D.; Whiting, W. B. *Analysis, Synthesis, and Design of Chemical Processes*; Pearson College Div, 2013.
(345) Danaci, D.; Bui, M.; Dowell, N. M.; Petit, C. Exploring the Limits of Adsorption-Based CO_2 Capture Using MOFs with PVSA – from Molecular Design to Process Economics. *Molecular Systems Design & Engineering* **2020**, *5* (1), 212–231. https://doi.org/10.1039/C9ME00102F.
(346) The World Bank. *Container port traffic (TEU: 20 foot equivalent units) | Data*. https://data.worldbank.org/indicator/IS.SHP.GOOD.TU (accessed 2022-08-03).
(347) Nuchitprasittichai, A.; Cremaschi, S. Optimization of CO_2 Capture Process with Aqueous Amines Using Response Surface Methodology. *Computers and Chemical Engineering* **2011**, *35* (8), 1521–1531. https://doi.org/10.1016/j.compchemeng.2011.03.016.
(348) Medrano-García, J. D.; Ruiz-Femenia, R.; Caballero, J. A. Multi-Objective Optimization of Combined Synthesis Gas Reforming Technologies. *Journal of CO_2 Utilization* **2017**, *22*, 355–373. https://doi.org/10.1016/J.JCOU.2017.09.019.
(349) United Nations Conference on Trade and Development. *Review of Maritime Transport 2010*. United Nations Conference on Trade and Development.
(350) Keith, D. W.; Holmes, G.; St. Angelo, D.; Heidel, K. A Process for Capturing CO_2 from the Atmosphere. *Joule* **2018**, *2* (8), 1573–1594. https://doi.org/10.1016/j.joule.2018.05.006.
(351) IEA. *World Energy Outlook 2019*; Paris, 2019. https://www.iea.org/reports/world-energy-outlook-2019 (accessed 2022-08-02).

(352) Aranda, G.; Drift, B.; Smit, R. *The Economy of Large Scale Biomass to Substitute Natural Gas (bioSNG) Plants*; ECN, 2014. https://www.researchgate.net/profile/Bram-Drift/publication/269687694_The_Economy_of_Large_Scale_Biomass_to_Substitute_Natural_Gas_bioSNG_plants/links/5491615a0cf222ada858685d/The-Economy-of-Large-Scale-Biomass-to-Substitute-Natural-Gas-bioSNG-plants.pdf.

(353) Lodato, C.; Hamelin, L.; Tonini, D.; Astrup, T. F. Towards Sustainable Methane Supply from Local Bioresources: Anaerobic Digestion, Gasification, and Gas Upgrading. *Applied Energy* **2022**, *323*, 119568. https://doi.org/10.1016/J.APENERGY.2022.119568.

(354) Susmozas, A.; Iribarren, D.; Dufour, J. Life-Cycle Performance of Indirect Biomass Gasification as a Green Alternative to Steam Methane Reforming for Hydrogen Production. *International Journal of Hydrogen Energy* **2013**, *38* (24), 9961–9972. https://doi.org/10.1016/j.ijhydene.2013.06.012.

(355) Tezer, Ö.; Karabağ, N.; Öngen, A.; Çolpan, C. Ö.; Ayol, A. Biomass Gasification for Sustainable Energy Production: A Review. *International Journal of Hydrogen Energy* **2022**, *47* (34), 15419–15433. https://doi.org/10.1016/j.ijhydene.2022.02.158.

(356) Vassilev, S. V.; Baxter, D.; Andersen, L. K.; Vassileva, C. G. An Overview of the Chemical Composition of Biomass. *Fuel* **2010**, *89* (5), 913–933. https://doi.org/10.1016/j.fuel.2009.10.022.

(357) Thunman, H.; Seeman, M. Chapter 17 - The GoBiGas Plant. In *Substitute Natural Gas from Waste*; Academic Press, 2019. https://doi.org/10.1016/B978-0-12-815554-7.00017-9.

(358) Klukowski, S. H. *Biomass to SNG Process Modeling and Assessment*; Master's thesis; ETH Zurich: Zurich, 2021.

(359) Basu, P. Chapter 6 - Tar Production and Destruction. In *Biomass Gasification, Pyrolysis and Torrefaction (Second Edition)*; Basu, P., Ed.; Academic Press: Boston, 2013; pp 177–198. https://doi.org/10.1016/B978-0-12-396488-5.00006-X.

(360) Rönsch, S.; Kaltschmitt, M. Bio-SNG Production - Concepts and Their Assessment. *Biomass Conversion and Biorefinery* **2012**, *2* (4), 285–296. https://doi.org/10.1007/s13399-012-0048-0.

(361) Marcantonio, V.; Bocci, E.; Ouweltjes, J. P.; Del Zotto, L.; Monarca, D. Evaluation of Sorbents for High Temperature Removal of Tars, Hydrogen Sulphide, Hydrogen Chloride and Ammonia from Biomass-Derived Syngas by Using Aspen Plus. *International Journal of Hydrogen Energy* **2020**, *45* (11), 6651–6662. https://doi.org/10.1016/j.ijhydene.2019.12.142.

(362) Robinson, P. J.; Luyben, W. L. Integrated Gasification Combined Cycle Dynamic Model: H2S Absorption/Stripping, Water-Gas Shift Reactors, and CO_2 Absorption/Stripping. *Industrial and Engineering Chemistry Research* **2010**, *49* (10), 4766–4781. https://doi.org/10.1021/ie901549s.

(363) Volkart, K.; Bauer, C.; Boulet, C. Life Cycle Assessment of Carbon Capture and Storage in Power Generation and Industry in Europe. *International Journal of Greenhouse Gas Control* **2013**, *16*, 91–106. https://doi.org/10.1016/j.ijggc.2013.03.003.

(364) Kopyscinski, J.; Schildhauer, T. J.; Biollaz, S. M. A. Methanation in a Fluidized Bed Reactor with High Initial CO Partial Pressure: Part II— Modeling and Sensitivity Study. *Chemical Engineering Science* **2011**, *66* (8), 1612–1621. https://doi.org/10.1016/j.ces.2010.12.029.

(365) Kirchmeyr, F. *Categorization of European Gasification Technologies*; DiBiCoo: Vienna, 2021. www.dibicoo.org. (accessed 2022-09-19).

(366) Haque, N.; Somerville, M. Techno-Economic and Environmental Evaluation of Biomass Dryer. *Procedia Engineering* **2013**, *56*, 650–655. https://doi.org/10.1016/j.proeng.2013.03.173.
(367) Andreux, R.; Petit, G.; Hemati, M.; Simonin, O. Hydrodynamic and Solid Residence Time Distribution in a Circulating Fluidized Bed: Experimental and 3D Computational Study. *Chemical Engineering and Processing: Process Intensification* **2008**, *47* (3), 463–473. https://doi.org/10.1016/j.cep.2007.01.023.
(368) Nikoo, M. B.; Mahinpey, N. Simulation of Biomass Gasification in Fluidized Bed Reactor Using ASPEN PLUS. *Biomass and Bioenergy* **2008**, *32* (12), 1245–1254. https://doi.org/10.1016/j.biombioe.2008.02.020.
(369) Gröbl, T.; Walter, H.; Haider, M. Biomass Steam Gasification for Production of SNG – Process Design and Sensitivity Analysis. *Applied Energy* **2012**, *97*, 451–461. https://doi.org/10.1016/j.apenergy.2012.01.038.
(370) *Electricity price statistics*. https://ec.europa.eu/eurostat/statistics-explained/index.php?title=Electricity_price_statistics (accessed 2023-05-16).
(371) Sultana, A.; Kumar, A. Optimal Configuration and Combination of Multiple Lignocellulosic Biomass Feedstocks Delivery to a Biorefinery. *Bioresource Technology* **2011**, *102* (21), 9947–9956. https://doi.org/10.1016/j.biortech.2011.07.119.
(372) González-Garay, A.; Frei, M. S.; Al-Qahtani, A.; Mondelli, C.; Guillén-Gosálbez, G.; Pérez-Ramírez, J. Plant-to-Planet Analysis of CO_2-Based Methanol Processes. *Energy and Environmental Science* **2019**, *12* (12), 3425–3436. https://doi.org/10.1039/c9ee01673b.
(373) D'Angelo, S. C.; Cobo, S.; Tulus, V.; Nabera, A.; Martín, A. J.; Pérez-Ramírez, J.; Guillén-Gosálbez, G. Planetary Boundaries Analysis of Low-Carbon Ammonia Production Routes. *ACS Sustainable Chem. Eng.* **2021**, *9* (29), 9740–9749. https://doi.org/10.1021/acssuschemeng.1c01915.
(374) *Soda Ash List Pricing and Energy Surcharge Program - North America*. https://www.solvay.com/en/news/soda-ash-list-pricing-and-energy-surcharge-program-north-america (accessed 2023-05-16).
(375) Boulday, D.; Marcovecchio, F. *Valorisation des cendres issues de la combustion de biomasse. Revue des gisements et des procédés associés*; RECORD. https://record-net.org/storage/etudes/14-0913-1A/rapport/Rapport_record14-0913_1A.pdf.
(376) European Commission. *Commission Recommendation of 16.12.2021 on the Use of the Environmental Footprint Methods to Measure and Communicate the Life Cycle Environmental Performance of Products and Organisations*; 2021. https://eur-lex.europa.eu/resource.html?uri=cellar:75e0de0f-5e6d-11ec-9c6c-01aa75ed71a1.0019.02/DOC_1&format=PDF (accessed 2022-08-24).
(377) Sacchi, R. Premise_gwp, 2023. https://github.com/polca/premise_gwp (accessed 2023-05-03).
(378) Peters, J. F.; Iribarren, D.; Dufour, J. Biomass Pyrolysis for Biochar or Energy Applications? A Life Cycle Assessment. *Environmental Science and Technology* **2015**, *49*, 5195–5202. https://doi.org/10.1021/ES5060786/SUPPL_FILE/ES5060786_SI_001.PDF.
(379) Smith, P.; Davis, S. J.; Creutzig, F.; Fuss, S.; Minx, J.; Gabrielle, B.; Kato, E.; Jackson, R. B.; Cowie, A.; Kriegler, E.; Van Vuuren, D. P.; Rogelj, J.; Ciais, P.; Milne, J.; Canadell, J. G.; McCollum, D.; Peters, G.; Andrew, R.; Krey, V.; Shrestha, G.; Friedlingstein, P.; Gasser, T.; Grübler, A.; Heidug, W. K.; Jonas, M.; Jones, C. D.; Kraxner, F.; Littleton, E.; Lowe, J.; Moreira, J. R.; Nakicenovic, N.; Obersteiner, M.; Patwardhan, A.; Rogner, M.; Rubin, E.; Sharifi, A.; Torvanger, A.; Yamagata, Y.; Edmonds, J.; Yongsung, C. Biophysical and Economic Limits to Negative CO_2

Emissions. *Nature Climate Change* **2016**, *6* (1), 42–50. https://doi.org/10.1038/nclimate2870.
(380) World Bank Group. *Commodity Markets Outlook: The Impact of the War in Ukraine on Commodity Markets*; World Bank Group: Washington, DC, 2022. https://openknowledge.worldbank.org/server/api/core/bitstreams/da0196b9-6f9c-5d28-b77c-31a936d5098f/content.
(381) The World Bank. *Commodity Markets*. World Bank. https://www.worldbank.org/en/research/commodity-markets (accessed 2023-05-10).
(382) *Phyllis2 - Database for the physico-chemical composition of (treated) lignocellulosic biomass, micro- and macroalgae, various feedstocks for biogas production and biochar*. https://phyllis.nl/ (accessed 2020-07-10).
(383) Fajardy, M.; Chiquier, S.; Mac Dowell, N. Investigating the BECCS Resource Nexus: Delivering Sustainable Negative Emissions. *Energy and Environmental Science* **2018**, *11* (12), 3408–3430. https://doi.org/10.1039/c8ee01676c.
(384) Cai, X.; Zhang, X.; Wang, D. Land Availability for Biofuel Production. *Environmental Science and Technology* **2011**, *45* (1), 334–339. https://doi.org/10.1021/es103338e.
(385) Fritz, S.; See, L.; Van Der Velde, M.; Nalepa, R. A.; Perger, C.; Schill, C.; McCallum, I.; Schepaschenko, D.; Kraxner, F.; Cai, X.; Zhang, X.; Ortner, S.; Hazarika, R.; Cipriani, A.; Di Bella, C.; Rabia, A. H.; Garcia, A.; Vakolyuk, M.; Singha, K.; Beget, M. E.; Erasmi, S.; Albrecht, F.; Shaw, B.; Obersteiner, M. Downgrading Recent Estimates of Land Available for Biofuel Production. *Environmental Science and Technology* **2013**, *47* (3), 1688–1694. https://doi.org/10.1021/es303141h.
(386) Elbersen, B.; Startisky, I.; Hengeveld, G.; Schelhaas, M.-J.; Naeff, H.; Böttcher, H. *Atlas of EU Biomass Potentials Deliverable 3.3: Spatially Detailed and Quantified Overview of EU Biomass Potential Taking into Account the Main Criteria Determining Biomass Availability from Different Sources*; 2012.
(387) IINAS; EFI; JR. *Forest Biomass for Energy in the EU: Current Trends, Carbon Balance and Sustainable Potential*; 2014.
(388) *Distance calculator between cities*. https://www.distancecalculator.net/ (accessed 2020-07-24).
(389) *Driving distance between European cities*. https://www.engineeringtoolbox.com/driving-distances-d_1029.html (accessed 2020-07-24).
(390) EUBIA – European Biomass Industry Association; Sénéchal, S.; Grassi, G. *Logistic Management of Wood Pellets: Data Collection on Transportation, Storage and Delivery Management*; EUBIA – European Biomass Industry Association, 2009. www.pelletsatlas.info (accessed 2020-07-28).
(391) *ISO 14040:2006(en), Environmental management — Life cycle assessment — Principles and framework*. https://www.iso.org/obp/ui/#iso:std:iso:14040:ed-2:v1:en (accessed 2020-07-07).
(392) *ISO - ISO 14044:2006 - Environmental management — Life cycle assessment — Requirements and guidelines*. https://www.iso.org/standard/38498.html (accessed 2020-07-07).
(393) *FEAT*. http://www.ecologicalmodels.psu.edu/agroecology/feat/ (accessed 2020-07-27).
(394) Hanssen, S. V.; Daioglou, V.; Steinmann, Z. J. N.; Doelman, J. C.; Van Vuuren, D. P.; Huijbregts, M. A. J. The Climate Change Mitigation Potential of Bioenergy with Carbon Capture and Storage. *Nature Climate Change* **2020**, 1–7. https://doi.org/10.1038/s41558-020-0885-y.
(395) Don, A.; Osborne, B.; Hastings, A.; Skiba, U.; Carter, M. S.; Drewer, J.; Flessa, H.; Freibauer, A.; Hyvönen, N.; Jones, M. B.; Lanigan, G. J.; Mander, Ü.; Monti, A.; Djomo,

S. N.; Valentine, J.; Walter, K.; Zegada-Lizarazu, W.; Zenone, T. Land-Use Change to Bioenergy Production in Europe: Implications for the Greenhouse Gas Balance and Soil Carbon. *GCB Bioenergy* **2012**, *4* (4), 372–391. https://doi.org/10.1111/j.1757-1707.2011.01116.x.

(396) Kang, S.; Nair, S. S.; Kline, K. L.; Nichols, J. A.; Wang, D.; Post, W. M.; Brandt, C. C.; Wullschleger, S. D.; Singh, N.; Wei, Y. Global Simulation of Bioenergy Crop Productivity: Analytical Framework and Case Study for Switchgrass. *GCB Bioenergy* **2014**, *6* (1), 14–25. https://doi.org/10.1111/gcbb.12047.

(397) Cai, X.; Zhang, X.; Wang, D. Land Availability for Biofuel Production. *Environmental Science and Technology* **2011**, *45* (1), 334–339. https://doi.org/10.1021/es103338e.

(398) Koornneef, J.; van Keulen, T.; Faaij, A.; Turkenburg, W. Life Cycle Assessment of a Pulverized Coal Power Plant with Post-Combustion Capture, Transport and Storage of CO_2. *International Journal of Greenhouse Gas Control* **2008**, *2* (4), 448–467. https://doi.org/10.1016/j.ijggc.2008.06.008.

(399) Gough, C.; Thornley, P.; Mander, S.; Vaughan, N.; Lea-Langton, A. *Biomass Energy with Carbon Capture and Storage (BECCS): Unlocking Negative Emissions*; Gough, C., Thornley, P., Mander, S., Vaughan, N., Lea-Langton, A., Eds.; John Wiley & Sons, Ltd.

(400) Ali, U.; Font-Palma, C.; Akram, M.; Agbonghae, E. O.; Ingham, D. B.; Pourkashanian, M. Comparative Potential of Natural Gas, Coal and Biomass Fired Power Plant with Post - Combustion CO_2 Capture and Compression. *International Journal of Greenhouse Gas Control* **2017**, *63*, 184–193. https://doi.org/10.1016/j.ijggc.2017.05.022.

(401) Christopher Consoli. *Bioenergy and Carbon Capture and Storage*; Global CCS Institute, 2019; pp 1–14.

(402) Vangkilde-Pedersen, T.; Anthonsen, K. L.; Smith, N.; Kirk, K.; Neele, F.; van der Meer, B.; Le Gallo, Y.; Bossie-Codreanu, D.; Wojcicki, A.; Le Nindre, Y. M.; Hendriks, C.; Dalhoff, F.; Peter Christensen, N. Assessing European Capacity for Geological Storage of Carbon Dioxide-the EU GeoCapacity Project. In *Energy Procedia*; Elsevier, 2009; Vol. 1, pp 2663–2670. https://doi.org/10.1016/j.egypro.2009.02.034.

(403) Consoli, C. P. *Global Storage Readiness Assessment*; Global CCS Institute, 2015.

(404) Turconi, R.; Boldrin, A.; Astrup, T. Life Cycle Assessment (LCA) of Electricity Generation Technologies: Overview, Comparability and Limitations. *Renewable and Sustainable Energy Reviews* **2013**, *28*, 555–565. https://doi.org/10.1016/j.rser.2013.08.013.

(405) Sokhansanj, S.; Hess, J. R. Biomass Supply Logistics and Infrastructure. *Methods in molecular biology (Clifton, N.J.)* **2009**, *581*, 1–25. https://doi.org/10.1007/978-1-60761-214-8_1.

(406) Giuntoli, J.; Boulamanti, A. K.; Corrado, S.; Motegh, M.; Agostini, A.; Baxter, D. Environmental Impacts of Future Bioenergy Pathways: The Case of Electricity from Wheat Straw Bales and Pellets. *GCB Bioenergy* **2013**, *5* (5), 497–512. https://doi.org/10.1111/gcbb.12012.

(407) Volkart, K.; Bauer, C.; Boulet, C. Life Cycle Assessment of Carbon Capture and Storage in Power Generation and Industry in Europe. *International Journal of Greenhouse Gas Control* **2013**, *16*, 91–106. https://doi.org/10.1016/j.ijggc.2013.03.003.

(408) Joseph Fargione, Jason Hill, David Tilman, Stephen Polasky, P. H. Land Clearing and the Biofuel Carbon Debt. *Science* **2008**, *319* (February), 1235–1239.

(409) *Sea distances*. https://sea-distances.org/ (accessed 2020-07-24).

(410) Ortiz-Ospina, E.; Molteni, M. *What are PPP adjustments and why do we need them?* https://ourworldindata.org/what-are-ppps (accessed 2020-07-13).

(411) de Wit, M.; Faaij, A. European Biomass Resource Potential and Costs. *Biomass and Bioenergy* **2010**, *34* (2), 188–202. https://doi.org/10.1016/j.biombioe.2009.07.011.

(412) Searcy, E.; Flynn, P.; Ghafoori, E.; Kumar, A. The Relative Cost of Biomass Energy Transport. *Applied Biochemistry and Biotechnology* **2007**, *136–140*, 639–652. https://doi.org/10.1007/s12010-007-9085-8.
(413) Duxbury, P.; Samson, R. *Assessment of Pelletized Biofuels*; 2000.
(414) Oliveira, F.; Gupta, V.; Hamacher, S.; Grossmann, I. E. A Lagrangean Decomposition Approach for Oil Supply Chain Investment Planning under Uncertainty with Risk Considerations. *Computers & Chemical Engineering* **2013**, *50*, 184–195. https://doi.org/10.1016/J.COMPCHEMENG.2012.10.012.
(415) Barbaro, A.; Bagajewicz, M. J. Managing Financial Risk in Planning under Uncertainty. *AIChE Journal* **2004**, *50* (5), 963–989. https://doi.org/10.1002/aic.10094.
(416) Vespucci, M. T.; Bertocchi, M.; Zigrino, S.; Escudero, L. F. Stochastic Optimization Models for Power Generation Capacity Expansion with Risk Management. In *International Conference on the European Energy Market*; IEEE, 2013. https://doi.org/10.1109/EEM.2013.6607352.